Jagiellonian University
Faculty of Physics, Astronomy and Applied Computer Science
Department of Organic Materials Physics

^{1}H Relaxation Processes in Solutions of Nitroxide Radicals – ^{14}N/^{15}N Isotope Effect

Author:
mgr Agnieszka Korpała

Supervisor:
dr hab. Danuta Kruk, prof. UWM

Kraków, 2016

Abstract

The thesis is focused on proton (^{1}H) spin relaxation processes in solutions of nitroxide radicals. The presented studies include experimental and theoretical parts. ^{1}H spin-lattice relaxation measurements have been performed for decalin (decahydronaphtalene), glycerol (propane-1,2,3-triol) and propylene glycol (propane-1,2-diol) solutions of 4-oxo-TEMPO-d_{16} (4-oxo-2,2,6,6-tetramethyl-1-piperidinyloxyl) containing ^{14}N and ^{15}N isotopes, by means of Nuclear Magnetic Resonance (NMR) Field Cycling (FC) relaxometry. The Nuclear Magnetic Resonance Dispersion (NMRD) experiments have been collected in a broad frequency range (10 kHz – 20 MHz) and in a broad range of temperatures dependent on viscosity of the solvent.

The NMRD data are interpreted in terms of the theory of paramagnetic relaxation enhancement (PRE) in solutions of nitroxide radicals [E. Belorizky et al. 1998, D. Kruk et al. 2012, D. Kruk et al. 2013]. The theory includes the influence of the hyperfine coupling (isotropic and anisotropic parts) between the spin of nitrogen (^{14}N and ^{15}N) and the unpaired electron spin on the ^{1}H relaxation. ^{1}H relaxation in solutions of nitroxide radicals is caused by dipole-dipole interactions between the electron spin of the radical and proton spins belonging to the solvent molecules. The dipolar interactions are modulated by three processes: translational movement of the solvent and solute molecules, their rotational dynamics and electron spin dynamics. The rotational motion plays a twofold role. First, it acts as a direct source (besides the translational motion) of fluctuations of the proton spin – electron spin dipolar coupling due to non – central positions of the interacting spins in the solvent and radical molecules (this effect is referred to as 'eccentricity effect'). Second, the anisotropic part of the hyperfine coupling (between nitrogen and electron spins) modulated by the rotational dynamics of the paramagnetic molecules gives rise to the electron spin relaxation being the source of modulations of the proton-electron dipole-dipole coupling, and thus affecting also, in this indirect way, the ^{1}H relaxation. The electron spin relaxation has been described in terms of the Redfield relaxation theory. As far as the role of the hyperfine interaction is concerned, its isotropic part affects the electron spin energy level structure and, in consequence, the ^{1}H relaxation.

The described effects and their influence on the ^{1}H relaxation are, in the thesis, thoroughly discussed and simulated. It is demonstrated that the role of the hyperfine coupling (isotropic and anisotropic) increases when the dynamics of the system slows down (the isotropic part of the hyperfine coupling is of importance already for rather fast dynamics - $D_{12} \approx 10^{-9}$ m^{2}/s while the influence of the anisotropic part becomes visible when the diffusion coefficient decreases below $D_{12} \approx 5*10^{-11}$ m^{2}/s).

The outlined theory is applied to the large set of experimental data. The data serve as a very demanding test of the theory which has to explain different ^{1}H spin-lattice relaxation for the cases of ^{14}N and ^{15}N containing nitroxide radicals, assuming the same motional conditions. The analysis reveals parameters characterizing translational and rotational dynamics of the solutions (relative translational diffusion coefficient of the solvent and solute molecules and rotational correlation times). It is demonstrated that NMR relaxometry studies performed on liquids containing paramagnetic centers give access to very fast dynamics, not accessible for diamagnetic liquids (*i.e.* in the absence of paramagnetic molecules).

Streszczenie

Przedstawiona praca dotyczy procesów relaksacji protonowej (^{1}H) w roztworach rodników nitroksylowych. Prezentowane badania zawierają cześć eksperymentalną i teoretyczną. Przeprowadzono pomiary szybkości relaksacji protonowej spin – sieć dla roztworów 4-oxo-TEMPO-d$_{16}$ (4-oxo-2,2,6,6-tetramethyl-1-piperidinyloxyl) zawierającego izotopy ^{14}N i ^{15}N w dekalinie (decahydronaphtalene), glicerolu (propane-1,2,3-triol) i glikolu propylenowym (propane-1,2-diol) wykorzystując relaksometrię Magnetycznego Rezonansu Jądrowego (MRJ) opartą na technice Field Cycling (FC). Pomiary dyspersji szybkości relaksacji przeprowadzone zostały w szerokim przedziale częstości (10 kHz – 20 MHz) i temperatur.

Zebrane dane analizowane są w oparciu o teorię paramagnetycznego wzmocnienia szybkości relaksacji (Paramagnetic Relaxation Enhancement – PRE) w roztworach rodników nitroksylowych [E. Belorizky et al. 1998, D. Kruk et al. 2012, D. Kruk et al. 2013]. Teoria ta uwzględnia wpływ oddziaływania nadsubtelnego (jego części izotropowej i anizotropowej) pomiędzy spinem jądra azotu (^{14}N i ^{15}N) i niesparowanym spinem elektronowym na relaksacje protonową. Proces relaksacji protonowej w roztworach rodników nitroksylowych jest wywołany oddziaływaniem dipolowym pomiędzy spinem elektronowym rodnika i spinami protonów należących do molekuł rozpuszczalnika. Oddziaływania te są modulowane przez trzy procesy: dyfuzja translacyjna molekuł rozpuszczalnika i molekuł substancji rozpuszczonej, ich dynamika rotacyjna i dynamika spinu elektronowego. Dynamika rotacyjna pełni podwójną rolę. Po pierwsze, jest ona bezpośrednim źródłem (poza dyfuzją translacyjną) fluktuacji odziaływań dipolowych proton-elektron wskutek ich niecentralnej pozycji (tzw. 'eccentricity effect'). Po drugie, anizotropowa część oddziaływania nadsubtelnego, która fluktuuje w czasie wskutek rotacji molekuły rodnika, prowadzi do relaksacji elektronowej, która jest czynnikiem modulującym oddziaływania dipolowe proton-elektron, wpływając w ten pośredni sposób na relaksacje protonową. Relaksacja elektronowa została opisana przy użyciu teorii Redfielda. Izotropowa część oddziaływania nadsubtelnego zmienia układ poziomów energetycznych spinu elektronowego, co w konsekwencji wpływa na proces relaksacji protonowej molekuł rozpuszczalnika. Opisane efekty i ich wpływ na szybkość relaksacji protonowej są w przedstawionej pracy szczegółowo dyskutowane w oparciu o liczne symulacje. Pokazano, że wpływ oddziaływania nadsubtelnego (izotropowego oraz anizotropowego) wzrasta, kiedy dynamika systemu zwalnia. Część izotropowa oddziaływania staje się istotnym czynnikiem gdy współczynnik dyfuzji jest rzędu $D_{12}\approx 10^{-9}$ m^2/s, a część anizotropowa – gdy współczynnik dyfuzji zmaleje do $D_{12}\approx 5*10^{-11}$ m^2/s.

Przedstawiona teoria została wykorzystana do analizy obszernego zestawu danych eksperymentalnych. Dane te stanowią wymagający test weryfikujący teorię, która w szczególności powinna prowadzić do konsystentnej interpretacji danych dla przypadków gdy rodniki nitroksylowe zawierają różne izotopy ^{14}N i ^{15}N, dla niezmienionych parametrów dynamicznych. Przeprowadzona analiza umożliwia wyznaczenie parametrów charakteryzujących dynamikę translacyjna oraz rotacyjną roztworów (względny współczynnik dyfuzji translacyjnej molekuł rozpuszczalnika i substancji rozpuszczonej oraz rotacyjne czasy korelacji). Pokazano, że relaksometria MRJ zastosowana do cieczy zawierających centra paramagnetyczne pozwala na analizę szybkich procesów dynamicznych nieosiągalnych dla cieczy diamagnetycznych (bez wprowadzonych molekuł pramagnetycznych).

Acknowledgements

I would like to thank several people who helped me and made it possible to finish this Thesis:

- My supervisor dr hab. Danuta Kruk, prof. UWM, for her assistance, support and guidance, whose permanent attention to detail drove me to finally learn how to keep everything consistent.
- Prof. dr hab. Józef Mościcki for his advice and support.
- My friends: Natalia Tomaszewska, Anna Majcher, Aleksandra Kubica-Misztal, Magdalena Nizińska, Ewa Szczęsny-Małysiak and Paula Kasza for their constant support and humor.
- My parents and my brother for their unconditional love and care.
- My husband Jakub Korpała for the love, careful listening, understanding and support in the fight with programming, calculating and writing.
- My son Ignacy simply for his presence and smile.

Contents:

Introduction

This thesis is focused on proton relaxation processes in solutions of nitroxide radicals containing ^{14}N and ^{15}N isotopes. Proton relaxation in the paramagnetic solutions is caused by dipole – dipole interactions between proton spins belonging to solvent molecules and electron spins of the radical molecules. Stochastic fluctuations of these interactions are caused by translational dynamics of the interacting molecules, molecular rotation and electron spin relaxation (attributed to the anisotropic part of the electron spin – nitrogen spin hyperfine interaction). The studies presented in the thesis have two aspects. The first one is a development of an advanced theory of proton spin relaxation in solutions of nitroxide radicals, valid for an arbitrary resonance frequency, taking into account complicated effects of spin interactions mediated by translational and rotational dynamics of the solvent and solute molecules. This theory predicts peculiar proton relaxation effects which depend on the isotope $^{14}N/^{15}N$ incorporated into the radical molecules. The isotope effect influences the proton relaxation by affecting the energy level structure of the electron spin (which is coupled by hyperfine interactions with the nitrogen spin) and by electron spin relaxation (caused by the anisotropic part of the hyperfine coupling), which acts as a source of modulations (besides the translational and rotational dynamics) of the proton spin – electron spin dipole-dipole coupling. In this thesis the theory has been thoroughly tested against ^{1}H spin-lattice relaxation experimental data collected for decalin, glycerol and propylene-glycol solutions of 4-oxo-TEMPO-d_{16}-$^{15(14)}N$. In contrary to "classical" relaxation experiments, which are performed at a single magnetic field (resonance frequency) the studies have been carried out in a very broad range of frequencies (10kHz – 20MHz) by employing the Fast Field Cycling technique, which introduces a "new dimension" to NMR relaxation experiments – the strength of the magnetic field (resonance frequency). The second aspect of the presented studies is the opportunity to investigate translational and rotational dynamics of liquids offered by NMR relaxometry, demonstrated here for numerous examples.

As the studies have been carried out with close collaboration with the supervisor, it is important to clearly describe the contribution of the author to the work:

- almost all experimental data presented in the thesis have been collected by the author,
- the author has participated in the calculations needed for the theory presented in Chapter 5 (not taking into account the electron spin relaxation),

- the numerical implementation of the theory (complemented by data fitting tools) and numerous simulations presented in the thesis have been done by the author,
- analogously, the analysis of the proton relaxation data which did not require including the electron spin relaxation has been performed by the author,
- the more advanced analysis of the proton relaxation data for slower dynamics, when the electron spin relaxation is relevant, has been performed by the author in cooperation with the supervisor.

The structure of this thesis is as follows:

- **Chapter 1** contains theoretical basics of Nuclear Magnetic Resonance (NMR) effect, including a phenomenological description of the motion of magnetization vector.
- In **Chapter 2** the Hamiltonians of the interactions present in the considered spin systems are described. The chapter also contains basic definitions of correlation functions and spectral densities including examples of these functions for different motional models.
- **Chapter 3** presents a description of relaxation theory for a two-spin system coupled by dipolar interactions. The cases of equivalent (two protons) and non-equivalent (electron – proton) spins are considered.
- The literature review on NMR relaxation studies on systems including nitroxide radicals being most relevant for the thesis is presented in **Chapter 4**.
- **Chapter 5** presents the theory of proton relaxation in solutions of nitroxide radicals.
- **Chapter 6** gives a description of the Fast Field Cycling NMR relaxation experiments and details of sample preparation.
- **Chapter 7** presents the data analysis, while **Chapter 8** contains summary and discussion of the obtained results.
- Eventually, in **Chapter 9** further perspectives of the studies are outlined.

1. Principles of Nuclear Magnetic Resonance

1.1. Nuclear spin in external magnetic field

Nuclei and electrons are characterized by spin quantum numbers, I and S respectively. The spin determines nuclear and electron magnetic moments: μ_I and μ_S [1,2]:

$$\mu_I = g_I \frac{e\hbar}{2m_p}\sqrt{I(I+1)} \tag{1}$$

$$\mu_S = g_e \frac{e\hbar}{2m_e}\sqrt{S(S+1)} \tag{2}$$

where m_p and m_e are proton and electron masses, g_e and g_I are electron and nuclear g-factors, respectively, while e is the elementary electron charge. The quantities $\mu_p = \frac{e\hbar}{2m_p}$ and $\mu_B = \frac{e\hbar}{2m_e}$ are proton and electron Bohr magnetons, while $\gamma_I = g_I\mu_P/\hbar$ is a characteristic constant of a nucleus called gyromagnetic ratio, analogously $\gamma_S = g_e\mu_B/\hbar$ is referred to as electronic gyromagnetic ratio.

In an external magnetic field, $\vec{B}_0$, the orientation of the magnetic moment is quantized. For a nucleus of spin quantum number I there are $(2I+1)$ states described by magnetic quantum numbers $m_I = -I, -I+1, ..., I-1, I$. The m_I state is associated with the energy [1-4]:

$$E_{m_I} = -\vec{\mu}_I \circ \vec{B}_0 = -m_I\gamma_I B_z \tag{3}$$

where it is assumed that the direction of the $\vec{B}_0$ field defines the z-axis of a reference system (referred to as laboratory frame), *i.e.*: $B_z = B_0$. The energy levels are equally distant and the energy difference yields:

$$\Delta E_I = E_{m_I} - E_{m_I - 1} = \gamma_I B_z \tag{4}$$

Analogous expressions describe the electron spin S, *i.e.*: $E_{m_S} = -\vec{\mu}_S \circ \vec{B}_0 = -m_S\gamma_S B_z$ and $\Delta E_S = E_{m_S} - E_{m_S - 1} = \gamma_S B_z$.

From now on I shall focus on nuclei. Populations of the energy levels are described by Boltzmann distribution. For $I = 1/2$ one obtains [1,3,4]:

$$\frac{N_+}{N_-} = e^{\frac{\Delta E}{k_B T}} = e^{\frac{\hbar \gamma_I B_0}{k_B T}} \tag{5}$$

where N_+ and N_- are populations of the energy levels corresponding to $m_I = -1/2$ and $m_I = 1/2$ (parallel and antiparallel orientation of the magnetic moment with respect to the external magnetic field), k_B denotes the Boltzmann constant. The resultant nuclear magnetization, M_I, is a sum of magnetic moments, μ_I, of N ($N = N_+ + N_-$) nuclei present in a sample [1,3,4]:

$$M_I = \sum \mu_I = \frac{\gamma_I^2 \hbar^2 B_0 N}{3 k_B T} I(I+1) \tag{6}$$

1.2. Motion of the magnetization vector and Bloch equation

The motion of the magnetization vector $\vec{M}_I(t)$ in a magnetic field $\vec{B}(t)$ is described by the Bloch equation [1,3,4]:

$$\frac{d\vec{M}_I}{dt} = \gamma_I \left(\vec{M}_I \times \vec{B} \right) \tag{7}$$

For a static magnetic field, $\vec{B}(t) = \left[0,0,B_0\right]$, the solution of Eq. 7 for the magnetization components M_{Ix}, M_{Iy} and M_{Iz} yields [1,4]:

$$M_{Ix} = M_{I\perp} \cos\left(\gamma_I B_0 t\right) \tag{8}$$

$$M_{Iy} = -M_{I\perp} \sin\left(\gamma_I B_0 t\right) \tag{9}$$

$$M_{Iz} = M_{I\parallel} \tag{10}$$

where $M_{I\perp}$ and $M_{I\parallel}$ denote the initial magnetization components in a plane perpendicular to $\vec{B}_0$ and along $\vec{B}_0$ (z-axis), respectively. This set of equations describes precession of the magnetization vector $\vec{M}_I$ around the direction of the applied magnetic field with the angular frequency $\omega_L = \gamma_I B_0$ (referred to as Larmor frequency). The solution of the Bloch equation changes when an additional magnetic field $B_1 << B_0$ rotating with an angular frequency ω in a plane perpendicular to $\vec{B}_0$ is applied: $\vec{B}_1 = [B_1 \cos(\omega t), -B_1 \sin(\omega t), 0]$. In this case it is convenient to express the solution of the Bloch equation in a coordinate system rotating around the z axis (direction of $\vec{B}_0$) with the frequency ω [1]:

$$\frac{dM'_{Ix}}{dt} = (\omega_L - \omega)M'_{Iy} \tag{11}$$

$$\frac{dM'_{Iy}}{dt} = -(\omega_L - \omega)M'_{Ix} + \gamma B_1 M_{Iz} \tag{12}$$

$$\frac{dM_{Iz}}{dt} = \gamma_I B_1 M'_{Iy} \tag{13}$$

where the index "'" refers to the rotating frame. For $\omega_L = \omega$ the equations reduce to the form [1]:

$$\frac{d\vec{M}'_I}{dt} = \gamma_I \vec{M}'_I \times \vec{B}_1 \tag{14}$$

which describes a precession in the magnetic field $\vec{B}_1$ (the $\vec{B}_1$ field is constant in the rotating frame).

The magnetic field $\vec{B}_1$ applied for a time t_θ (radio-frequency, RF, pulse) can change the orientation of the magnetization vector by the angle:

$$\theta = \gamma_I B_1 t_\theta \tag{15}$$

In NMR experiments a $\pi/2$ pulse refers to $\theta = \pi/2$, analogously a π pulse means $\theta = \pi$. This description should be extended by taking into account that the nuclear magnetic moments interact not only with the external magnetic field but also with each other. Molecules, ions and molecular units undergo stochastic motions causing time fluctuations of the interactions between the magnetic moments. As a result, transitions between the energy levels E_{m_I} are induced, leading to changes in the magnetization M_I that are referred to as relaxation processes. The Bloch equation including terms describing the relaxation processes takes the form [1,4,5]:

$$\frac{d\vec{M}_I}{dt} = \gamma_I\left(\vec{M}_I \times \vec{B}\right) - \frac{M_{Iz} - M_{I0}}{T_1}\vec{k} - \frac{M_{Ix}\vec{i} + M_{Iy}\vec{j}}{T_2} \tag{16}$$

where M_{I0} denotes equilibrium magnetization. The time constants T_1 and T_2 denote longitudinal and transverse relaxation times describing the evolution of the parallel and perpendicular magnetization components, respectively. Thus the T_1 parameter is called longitudinal (spin-lattice) relaxation time, while T_2 is referred to as transverse (spin-spin) relaxation time. The relaxation time T_2 describes how fast the collective movement of individual magnetic moments in the $x-y$ plane becomes incoherent.

In NMR experiments one can apply various pulse sequencies. To measure the spin-lattice relaxation time commonly the inversion-recovery sequence: $\pi-\tau-\pi/2$ is used (τ denotes here the evolution time between the two pulses and can be varied). At $t=0$ the magnetization M_{I0} is directed along the direction of the static magnetic field $\vec{B}_0$. After applying a π pulse the magnetization vector is inverted and starts to return to the initial state. After time τ (the relaxation period) a $\pi/2$ pulse is applied so the magnetization vector rotates in the $x-y$ plane and can be detected. Such experiment is repeated for different values of τ. A schematic picture of the inversion recovery experiment is shown in Fig. 1.1. The evolution of the longitudinal component of the magnetization vector is then described by the equation [3,5]:

$$M_{Iz}(t)=M_{I0}\left(1-2e^{-\tau/T_1}\right) \tag{17}$$

The experiment (pulse sequence) may be repeated after a time RD (Recycle Delay) long enough for the system to return to the initial state. It is recommended to apply $RD=5T_1$.

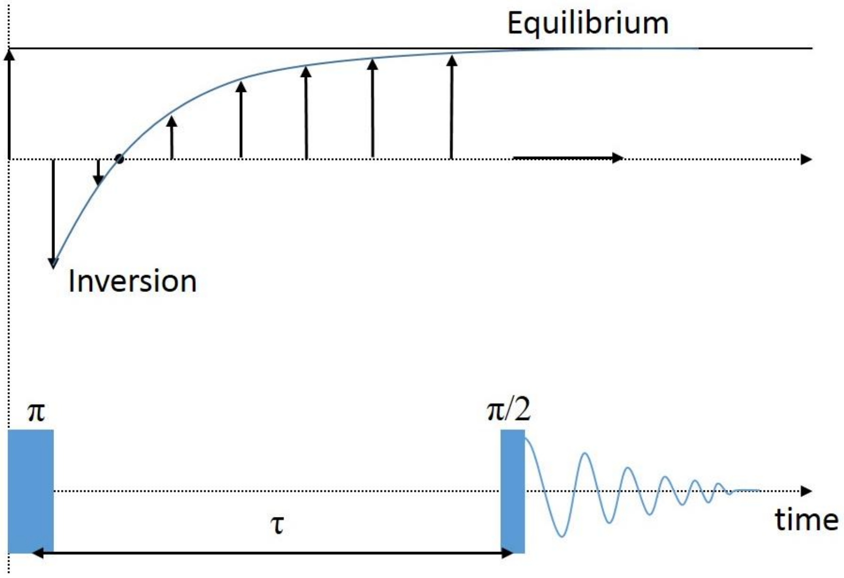

Figure 1.1. Schematic picture of inversion recovery sequence.

The relaxation time T_2 can be measured by applying, for instance, the Hahn sequence [6]. First, a transverse magnetization is created by applying a $\pi/2$ pulse. After a time τ the movement of the individual spins loses its coherence due to local field inhomogeneities. Then a π pulse is applied and the precession is reversed. This implies that after time τ (after the π pulse) the decoherence disappears and the magnetization gives rise to an echo.

2. Spin interactions

2.1. The spin Hamiltonian

As already anticipated, spin-lattice relaxation is a result of transitions between spin energy levels. The energy required for the transitions is provided by fluctuating local magnetic fields. Thus the total Hamiltonian describing a spin system has two parts: a time-independent part (main Hamiltonian) H_0, which defines the energy level structure, and a time-dependent part (perturbing Hamiltonian) $\mathrm{H}_1(t)$ describing the interactions fluctuating in time:

$$\mathrm{H}(t) = \mathrm{H}_0 + \mathrm{H}_1(t) \tag{18}$$

This work is focused on proton relaxation in solutions of paramagnetic molecules (nitroxide radicals). Several interactions between protons and electrons have to be considered. They are described below.

2.2. Zeeman and dipolar interactions

The most common ^{1}H relaxation mechanism is provided by magnetic dipolar interactions. For a proton (I) – electron (S) spin system the total Hamiltonian takes the form:

$$\mathrm{H} = \underbrace{\mathrm{H}_Z(I) + \mathrm{H}_Z(S)}_{\mathrm{H}_0} + \underbrace{\mathrm{H}_{DD}(I,S)(t)}_{\mathrm{H}_1} \tag{19}$$

where $\mathrm{H}_Z(I)$ and $\mathrm{H}_Z(S)$ are Hamiltonians of proton and electron Zeeman interactions (i.e. interactions with an external magnetic field $\vec{B}_0$), respectively, while $\mathrm{H}_{DD}(I,S)(t)$ denotes the Hamiltonian of the proton-electron dipole-dipole interaction. In the laboratory frame the Zeeman Hamiltonians are expressed as [1,2,4,5]:

$$\mathrm{H}_Z(I) = \gamma_I B_0 I_Z, \quad \mathrm{H}_Z(S) = \gamma_S B_0 S_Z \tag{20}$$

They form the main, unperturbed part of the total Hamiltonian, denoted as H_0. The $I - S$ dipole-dipole Hamiltonian, $\mathrm{H}_{DD}(I,S)(t)$, fluctuates in time due to stochastic motion of molecules carrying the spins of interest and hence $\mathrm{H}_{DD}(I,S)(t)$ belongs to the time dependent (perturbing) part of the Hamiltonian denoted as H_1.

Dipole-dipole interactions between two magnetic moments $\vec{\mu}$ and $\vec{\mu}'$ are characterized by the energy [1,4,7,8]:

$$E = \frac{\vec{\mu} \circ \vec{\mu}'}{r^3} - \frac{3(\vec{\mu} \circ \vec{r})(\vec{\mu}' \circ \vec{r})}{r^5} \tag{21}$$

where $\vec{r}$ is a vector between the interacting moments. If these magnetic moments (spins) belong to the same molecule (intra-molecular coupling), the dipole-dipole interaction fluctuates in time only due to the rotational motion of the molecule (provided the molecule does not show internal dynamics). For dipoles placed in different molecules (inter-molecular coupling), time fluctuations of the interaction are dominated by the relative translational motion of both molecules. A schematic view of intra- and inter-molecular dipolar interactions is presented in Fig. 2.1 for glycerol molecules.

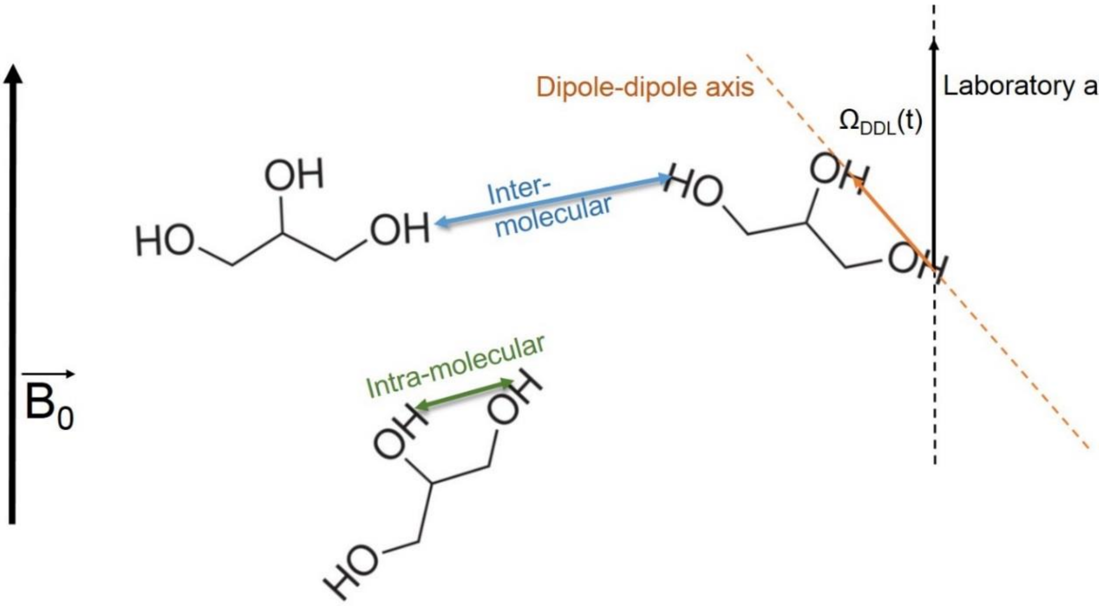

Figure 2.1. A schematic view of the inter- and intra-molecular dipole-dipole interactions.

In the laboratory frame the dipole-dipole Hamiltonian has the form [1,2,4,5,9-11]:

$$\mathrm{H}_{DD}(I,S)(t) = a_{DD}^{IS} \sum_{m=-2}^{2} (-1)^m F_{-m}^2(t) T_m^2(I,S) \tag{22}$$

where the two-spin tensor operators $T_m^2(I,S)$ are defined as [1,2,4,5,9-11]:

$$T_0^2(I,S) = \frac{1}{\sqrt{6}}\left[2I_z S_z - \frac{1}{2}(I_+ S_- + I_- S_+)\right] \tag{23a}$$

$$T_{\pm 1}^2(I,S) = \mp \frac{1}{2}[I_z S_\pm + I_\pm S_z] \tag{23b}$$

$$T_{\pm 2}^2(I,S) = \frac{1}{2} I_\pm I_\pm . \tag{23c}$$

The dipole-dipole coupling constant, a_{DD}^{IS}, is defined as:

$$a_{DD}^{IS} = \sqrt{6}\,\frac{\mu_0}{4\pi}\,\frac{\gamma_I \gamma_S \hbar^2}{r_{IS}^3} \tag{24}$$

where r_{IS} is the distance between the interacting spins, I and S ($r_{IS} = r$ in Eq. 21).

For intra-molecular couplings the r_{IS} distance does not change in time, but it does for inter-molecular interactions. The functions $F_{-m}^2(t)$ are expressed in the laboratory frame by Wigner rotation matrices [2], $D_{0,-m}^2(\Omega_{DDL}(t))$, dependent on a set of Euler angles, Ω_{DDL}, describing the orientation of the dipole-dipole (DD) axis with respect to the laboratory (L) frame (see Fig. 2.1) [2,12]:

$$F_{-m}^2 = D_{0,-m}^2(\Omega_{DDL}) = D_{0,-m}^2(0, \beta_{DDL}(t), \gamma_{DDL}(t)) \tag{25}$$

where the Wigner rotation matrices are defined as follows [12-14]:

$$D_{0,0}^2(0, \beta_{DDL}(t), \gamma_{DDL}(t)) = 2^{-1}\left[3\cos^2(\beta_{DDL}(t)) - 1\right] \tag{26a}$$

$$D_{0,\pm 1}^2(0, \beta_{DDL}(t), \gamma_{DDL}(t)) = \mp 2^{-1} 6^{1/2} \sin(\beta_{DDL}(t)) \cos(\beta_{DDL}(t)) \tag{26b}$$

$$D_{0,\pm 2}^2(0, \beta_{DDL}(t), \gamma_{DDL}(t)) = \mp 2^{-1} 6^{1/2} \sin^2(\beta_{DDL}(t)). \tag{26c}$$

For two nuclear spins (e.g. two protons: I_1 and I_2) the tensor operators of Eq. 22 are obtained by replacing I by I_1 and S by I_2, γ_S in Eqs. 23a-c has to be replaced by γ_I and the inter-spin distance refers to the two nuclei. However, it should be kept in mind that due to the ratio between the electron and proton gyromagnetic ratios, $\gamma_S / \gamma_I = 657$, the dipole-dipole coupling constant for a system of proton and electron is much larger than for two protons.

2.4. Hyperfine interactions in nitroxide radicals

In nitroxide radical molecules the unpaired electron is located between oxygen and nitrogen nuclei as shown in Fig. 2.2.

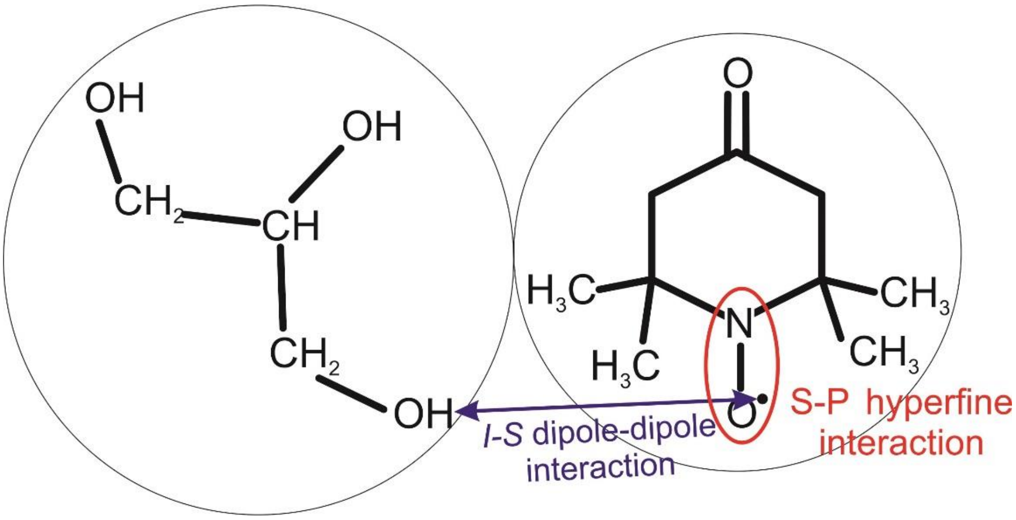

Figure 2.2. A schematic view of spin interactions for glycerol and 4-oxo-TEMPO molecules.

The electron spin S and the nitrogen spin P are coupled by hyperfine interactions. The hyperfine coupling is a result of two interactions: Fermi contact interaction and dipolar coupling. The first mechanism is important when the spin density of the electron is nonzero at the position of the nucleus. The isotropic (scalar) part of the hyperfine coupling, influences the electron spin energy level structure. The Hamiltonian of the isotropic scalar coupling has the form [15-18]:

$$\mathrm{H}_{iso}(S,P) = A_{iso}\left[S_z P_z + \frac{1}{2}(S_+ P_- + S_- P_+)\right] \tag{27}$$

where A_{iso} denotes the amplitude of the coupling.

The anisotropic part of the hyperfine coupling ($\mathrm{H}_{aniso}(S,P)$) is dependent on the orientation of the molecule and hence it becomes time dependent as a result of molecular rotation. Thus, the total Hamiltonian including all interactions present in the system shown in Fig. 2.2 consists of five terms [1,2,4,5,9-11,15-18]:

$$\mathrm{H}_0(I,S) = \underbrace{\mathrm{H}_Z(I) + \mathrm{H}_Z(S) + \mathrm{H}_{iso}(S,P)}_{\mathrm{H}_0} + \underbrace{\mathrm{H}_{DD}(I,S) + \mathrm{H}_{aniso}(S,P)}_{\mathrm{H}_1} \tag{28}$$

when one neglects the weak Zeeman interaction of nitrogen. In solutions of nitroxide radicals the $I-S$ (proton-electron) dipole-dipole interaction is modulated by the relative translational dynamics of the solvent molecule and the nitroxide radical molecule, while the anisotropic hyperfine interaction is modulated (as already mentioned) by rotation of the nitroxide radical.

2.5. Correlation function and spectral density

Stochastic processes (like movement of molecules in liquids) are characterized by time dependent correlation functions which are defined as [1,2,5,9,19,20]:

$$C(t) = \left\langle A^*(t)A(0)\right\rangle = \iint A(x)A(x_0)P(x,x_0,t)P(x_0)dx_0dx \qquad (29)$$

where $A(t)$ is a quantity of interest dependent on a variable $x(t)$ describing the states of the system (x and x_0 denote the variable at times t and t_0, respectively). $P(x,x_0,t)$ is the conditional probability that the system is in the state x at time t provided that at time zero it has been in the state x_0.

Probabilities of transitions between spin states and hence the relaxation times depend on spectral densities, $J(\omega)$, which are defined as a Fourier transform of corresponding correlation functions [1,5,19]:

$$J(\omega) = \int_0^\infty C(t)e^{-i\omega t}dt \qquad (30)$$

2.6. Spectral densities for different motional models

The exact formula of the correlation function depends on the kind of motion (for instance rotational or translational diffusion) and the model which is chosen to describe the motion. In the simplest case of isotropic rotation the correlation function is exponential [21]:

$$C(t) = \left\langle D^{2*}_{0,-m}\left(0,\beta_{DDL}(t),\gamma_{DDL}(t)\right)D^{2}_{0,-m}\left(0,\beta_{DDL}(0),\gamma_{DDL}(0)\right)\right\rangle = \frac{1}{5}\exp\left(-\frac{t}{\tau_R}\right) \qquad (31)$$

where τ_R is a characteristic time constant referred to as rotational correlation time. Thus, the corresponding spectral density has a Lorentzian form (the factor 1/5 has been omitted) [2,21]:

$$J(\omega) = \frac{\tau_R}{1+(\omega\tau_R)^2}. \qquad (32)$$

For heterogenous systems (characterized by a distribution of correlation times) the rotational correlation function is often streched [22]:

$$C(t) = \exp\left[-\left(\frac{t}{\tau_R}\right)^\beta\right] \qquad (33)$$

The phenomenological parameter $\beta \in \langle 0,1\rangle$ reflects the distribution of the correlation times. Fourier transform of streched exponential function can be approximated by the Cole-

Davidson spectral density [23]:

$$J(\omega) = \frac{\sin\left[\beta \arctan\left(\omega\tau_{CD}\right)\right]}{\omega\left[1+\left(\omega\tau_{CD}\right)^2\right]^{\beta/2}}. \tag{34}$$

The time constant τ_{CD} is related to the rotational correlation time τ_R as: $\tau_R = \tau_{CD}\beta$. For $\beta = 1$ the spectral density of Eq. 34 becomes Lorentzian. The deviations of the Cole-Davidson spectral density from the Lorentzian shape for different values of β versus frequency and versus reciprocal temperature are shown in Fig. 2.3 a) and 2.3 b), respectively. The values of the spectral density in Fig. 2.3 a) have been normalized in the low field limit to unity (divided by β) to make the differencies at the inflection point more visible. In Fig. 2.3 b) the Vogel-Fulcher-Tamman (VFT) equation has been used to simulate the temperature dependence of the rotational correlation time τ_R on temperature T [24]:

$$\tau_R = \tau_0 \exp\left(\frac{B}{T-T_0}\right) \tag{35}$$

where τ_0, B and T_0 are phenomenological parameters.

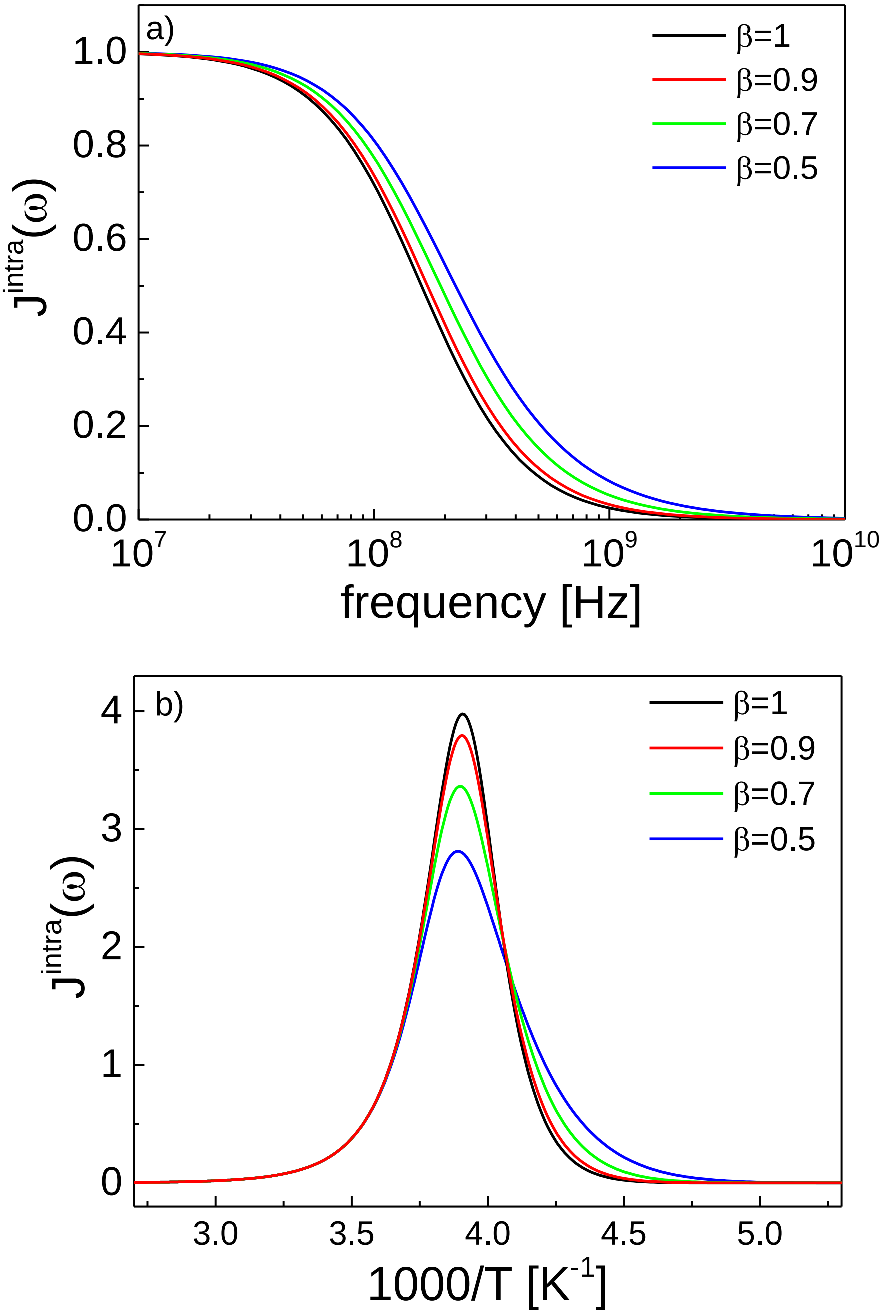

Figure 2.3. Spectral densities versus a) frequency and b) reciprocal temperature for different values of β *parameter. Parameters used for the simulations are: a)* $\tau_R = 1*10^{-9}\,s$ *and b)* $\tau_0 = 1*10^{-15}\,s$, $B = 2000\,K$, $T_0 = 130\,K$, $\omega = 20\,MHz$. *The maximum is reached at a temperature for which* $\omega\tau_R = 1$.

As already mentioned, when the interacting spins belong to different molecules, translational diffusion is the main process which causes the fluctuations of the dipole-dipole interactions. As a result of translational dynamics the inter-spin distance r_{IS} as well as the orientation of the $I-S$ dipole-dipole axis vary in time. Thus the correlation function includes the Euler angles encoded in the Wigner rotation matrices $D^2_{0,m}(\Omega(t))$ as well as in the inter-spin distance $r_{IS}(t)$ [2,5,25-29]:

$$C_{inter}(t) = \left\langle \frac{D^{2*}_{0,m}(\Omega(t))}{r^3_{IS}(t)} \frac{D^2_{0,m}(\Omega(0))}{r^3_{IS}(0)} \right\rangle \tag{36}$$

The commonly used models describing translational dynamics of molecules is referred to as force-free hard-sphere model [26,27]. It assumes that molecules can be treated as hard spheres uniformly distributed beyond their distance of the closest approach, d_{IS}, and the interacting spins are placed in their centers. In that case the closest distance is given by a sum of the radii of the molecules carrying the nuclear and electron spins, r_I and r_S, respectively [30]: $d_{IS} = r_I + r_S$ (blue line in Fig. 2.4).

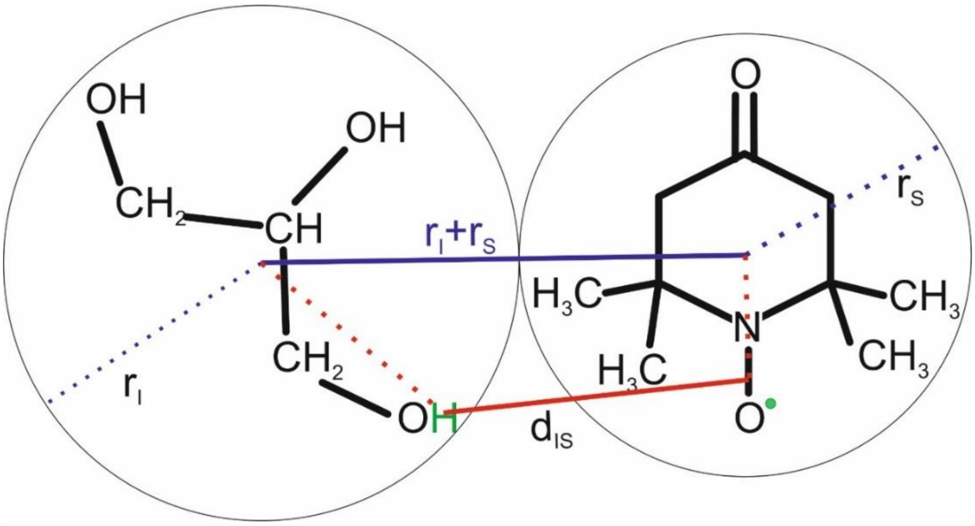

Figure 2.4. Schematic view of two interacting molecules (glycerol and nitroxide radical 4-oxo-TEMPO) with inter-spin distances marked by blue line - for the force-free hard-sphere model, and by red line - when the eccentricity effect is considered.

The inter-molecular (translational) correlation function resulted from this model is described by the formula [27,29,31-33]:

$$C_{trans}(t) = 72\frac{N_S}{d^3_{IS}}\int_0^{\infty} \frac{u^2}{81+9u^2-2u^4+u^6}\exp\left(-\frac{u^2 t}{\tau_{trans}}\right)du \tag{37}$$

where N_S denotes the number of electron spins per unit volume. Since the nitroxide radical molecule contains one unpaired electron (spin S), N_S is equivalent to the molar concentration multiplied by Avogadro number, A_V: $N_S = 1000[M]A_V$; the factor 1000 results from the relationship between dm^3 and m^3. The translational correlation time τ_{trans} appearing in the formula is defined as $\tau_{trans} = d_{IS}^2 / D_{12}$, where D_{12} is the relative translational diffusion coefficient defined as a sum of self-diffusion coefficients of the interacting molecules. For identical molecules the relative diffusion coefficient is twice as large as the self-diffusion coefficient, and the distance of closest approach is given by the diameter of the molecule. The corresponding spectral density is given as [2,27,29,31-34]:

$$J_{trans}(\omega) = 72\frac{N_S}{d_{IS}^3}\int_0^\infty \frac{u^2}{81+9u^2-2u^4+u^6}\,\frac{u^2\tau_{trans}}{u^4+(\omega\tau_{trans})^2}\,du. \tag{38}$$

It is worth to notice that the spectral density is a superposition of Lorentzian functions multiplied by the weight factors $\frac{u^2}{81+9u^2-2u^4+u^6}$.

The presented force-free hard-sphere model is not always sufficient. The assumption that the interacting spins are placed in the centers of the molecules can turn out to be an oversimplification. As in real molecules they occupy non-central positions the inter-molecular dipole-dipole interactions are modulated not only by translational dynamics, but also the rotational motion contributes to the fluctuations of the inter-spin vector ('eccentricity effects') [25,26,31-33,27,35] as shown in Fig. 2.4. A rigorous mathematical description of the combined translational-rotational effect on the dipole-dipole coupling gives complex solutions with additional distances between the molecular center and the positions of the nuclei [25-27]. A compromise between the accuracy of the description and its mathematical complexity can be achieved by adding a rotational contribution to the translational spectral density [31-33,35]:

$$\begin{aligned} J_{\mathrm{inter}}(\omega) = {} & \frac{N_s}{d_{IS}^3}\times\left[\tilde{J}_{trans}(\omega) + fJ_{rot}(\omega)\right] = \\ & \frac{N_s}{d_{IS}^3}\times\left\{72\int_0^\infty \frac{u^2}{81+9u^2-2u^4+u^6}\,\frac{u^2\tau_{trans}}{u^4+(\omega\tau_{trans})^2}\,du + f\,\frac{4\pi}{3}\,\frac{\sin\left[\beta\arctan(\omega\tau_{CD})\right]}{\omega\left[1+(\omega\tau_{CD})^2\right]^{\frac{\beta}{2}}}\right\} \end{aligned} \tag{39}$$

where the factor f reflects the role of the 'eccentricity effects'. When the spins are placed in the center of molecules, $f = 0$. The factor $4\pi/3$ in Eq. 39 has its source in normalization of the spectral densities: $\int J_{rot}(\omega)d\omega = \int \tilde{J}_{trans}(\omega)d\omega$.

According to the hydrodynamic model of a molecule considered as a sphere undergoing rotational and translational movement in a viscous medium, the ratio of the translational and rotational correlation time is: $\tau_{trans}/\tau_{rot} = 9$ [9]. In real systems the ratio is even larger, for example for glycerol it was obtained: $\tau_{trans}/\tau_{rot} = 40-50$ [34].

To estimate the influence of rotational dynamics on ^{1}H spin-latice relaxation of solvent, the ratio between spectral densities describing rotational and translational dynamics ($J_{rot}(\omega)$ and $\tilde{J}_{trans}(\omega)$ of Eq. 39) is shown versus frequency Fig. 2.5. For the frequency dependent simulations, the rotational correlation times have been chosen in a wide range starting from very short values (characteristic for water) up to long correlation times (characteristic for viscous solvents near their glass transition temperature). The ratio between translational and rotational correlation times yields $\tau_{trans}/\tau_{rot} = 40$.

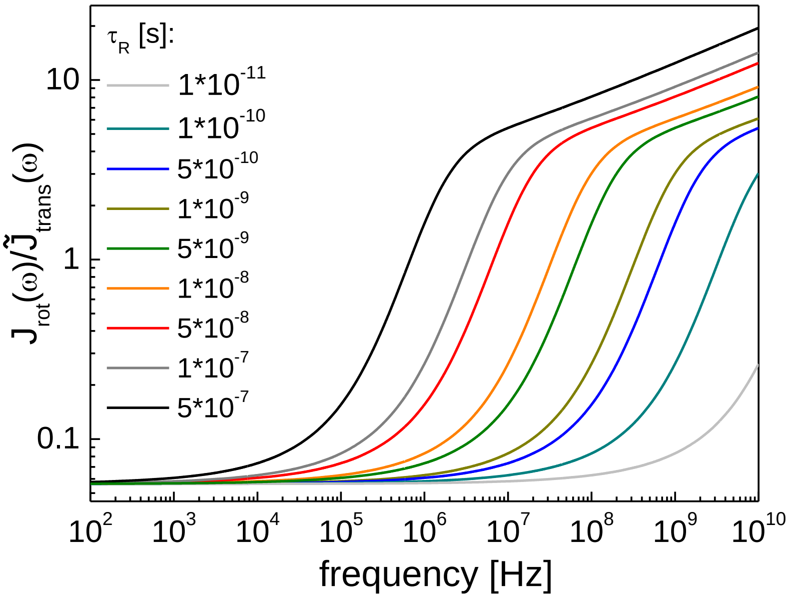

Figure 2.5. Ratio between spectral densities characterizing rotational and translational dynamics: $J_{rot}(\omega)/\tilde{J}_{trans}(\omega)$ *versus frequency for* $\beta = 0.8$.

The temperature dependence of the rotational correlation time has been simulated according to Eq. 35 with following parameters: $\tau_0 = 1.4*10^{-14}$ s, $B = 1.84*10^{-3}$ K, $T_0 = 132$ K (such parameters have been obtained for glycerol solutions of different nitroxide radicals [33]).

Due to the fact that $\tau_{trans} >> \tau_R$ at higher frequencies the role of the rotational spectral density increases and the ratio $J_{rot}(\omega)/\tilde{J}_{trans}(\omega)$ exceeds at some frequency the value of one (Fig. 2.5).

The time scale separation of the translational and rotational dynamics allows to decompose the overall ^{1}H relaxation dispersion profile (relaxation rate versus frequency) into translational and rotational part.

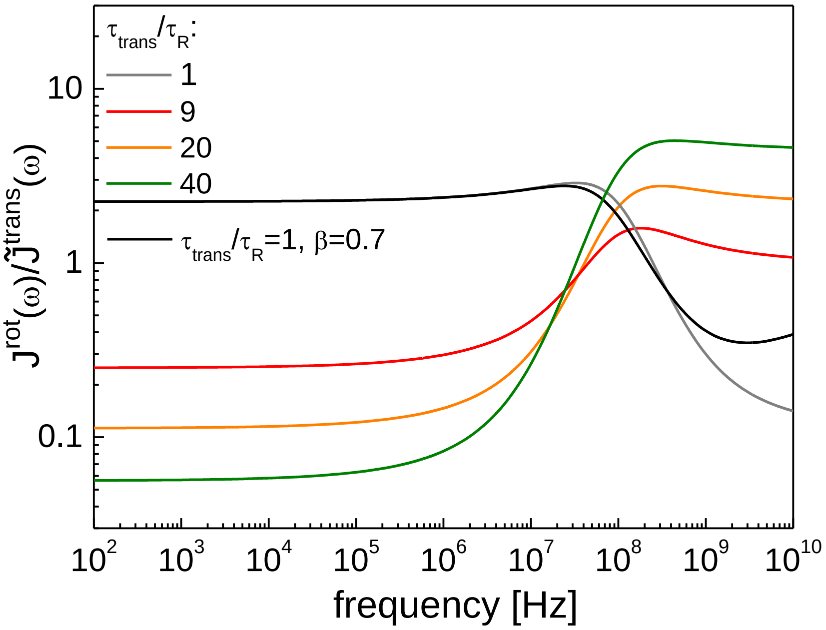

Figure 2.6. Ratio between spectral densities describing rotational and translational dynamics of the solvent molecules - $J_{rot}(\omega)/\tilde{J}_{trans}(\omega)$ *versus frequency for different values of the ratio between translational and rotational correlation times,* τ_{trans}/τ_R *for* $\beta = 1$*. As a comparison the results obtained for* $\beta = 0.7$ *and* $\tau_{trans}/\tau_R = 1$ *are shown.*

To finish this section it is worth to compare the frequency dependence of $J_{rot}(\omega)/\tilde{J}_{trans}(\omega)$ calculated for different values of the ratio between the translational and rotational correlation times $x = \tau_{trans}/\tau_R$. Such comparison is presented in Figure 2.6. The figure includes the case of $x = 1$ to clearly show that it differs from those for which $\tau_{trans} >> \tau_R$.

3. Relaxation in different systems

3.1. Density matrix and its evolution in time

A spin system can be characterized by a Hamiltonian. Eigenfunctions of the Hamiltonian form a complete basis $\{|\alpha\rangle\}$, i.e. every state of the spin system can be described as their superposition [1,2]:

$$\Psi(t) = \sum_{\alpha} c_{\alpha}(t)\,|\,\alpha\rangle \tag{40}$$

It is convenient to describe a spin state using the concept of density matrix (operator) [1-4]. Density matrix is a matrix representation of the density operator in a basis formed from pairs of the eigenfunctions $\{|\alpha\rangle\langle\beta|\}$ referred to as Liouville space [1,2]. The density matrix elements are defined as:

$$\rho_{\alpha\beta}(t) = \langle\alpha\,|\,\rho(t)\,|\,\beta\rangle, \tag{41}$$

and they can be calculated from the expression [1,2]:

$$\rho_{\alpha\beta}(t) = \langle c_{\alpha}(t) c_{\beta}^{*}(t)\rangle \tag{42}$$

where the star denotes complex conjugation.

Time evolution of the density operator $\rho(t)$ (i.e. evolution of the spin system under a given Hamiltonian H) is described by the Liouville-von Neumann equation [1,2,4]:

$$\frac{d}{dt}\rho(t) = -i\left[\mathrm{H}, \rho(t)\right] \tag{43}$$

The equation can be presented as a set of coupled differential equations for individual density matrix elements (referred to as the Redfield relaxation equation) [1,2,36-38]:

$$\frac{d\rho_{\alpha\alpha'}(t)}{dt} = -i\omega_{\alpha\alpha'}\rho_{\alpha\alpha'}(t) + \sum_{\beta\beta'}\Gamma_{\alpha\alpha'\beta\beta'}\rho_{\beta\beta'}(t) \tag{44}$$

where $\omega_{\alpha\alpha'} = \omega_{\alpha} - \omega_{\alpha'}$ denotes the transition frequency between the eigenstates $|\,\alpha\rangle$ and $|\,\alpha'\rangle$ of the spin system. The summation is restricted to the terms for which $\omega_{\alpha\alpha'} = \omega_{\beta\beta'}$. The coefficients $\Gamma_{\alpha\alpha'\beta\beta'}$ also form a matrix (its real part is referred to as Redfield relaxation matrix) and are given as a combination of spectral densities [2,4,5,9]:

$$\begin{aligned}&\mathrm{Re}\left(\Gamma_{\alpha\alpha'\beta\beta'}\right) = R_{\alpha\alpha'\beta\beta'} = \\ &= J_{\alpha\beta\alpha'\beta'}(\omega_{\alpha\beta}) + J_{\alpha\beta\alpha'\beta'}(\omega_{\beta'\alpha'}) - \delta_{\alpha'\beta'}\sum_{\gamma} J_{\alpha\gamma\beta\gamma}(\omega_{\gamma\beta}) - \delta_{\alpha\beta}\sum_{\gamma} J_{\beta'\gamma\alpha'\gamma}(\omega_{\beta'\gamma}).\end{aligned} \tag{45}$$

The spectral densities $J_{\alpha\alpha'\beta\beta'}(\omega)$ are defined as:

$$J_{\alpha\alpha'\beta\beta'}(\omega) = \mathrm{Re}\int_0^\infty \langle\langle\alpha\,|\,\mathrm{H}_1(t)\,|\,\alpha'\rangle\langle\beta\,|\,\mathrm{H}_1(t-\tau)\,|\,\beta'\rangle\rangle \exp(-i\omega\tau)d\tau \qquad (46)$$

where H_1 denotes the time dependent part of the spin Hamiltonian, (Eq. 22).

3.2. Diamagnetic systems

For a diamagnetic liquid (no unpaired electron spins) the total Hamiltonian includes Zeeman couplings for nuclei of spins I_1 and I_2 and a dipole-dipole interaction between them (see Section 2):

$$\mathrm{H} = \mathrm{H}_Z(I_1) + \mathrm{H}_Z(I_2) + \mathrm{H}_{DD}(I_1, I_2)(t) \qquad (47)$$

The eigenbasis of the main (unperturbed) part of the Hamiltonian ($\mathrm{H}_0 = \mathrm{H}_Z(I_1) + \mathrm{H}_Z(I_2)$) contains four functions $|\,n\rangle = |\,m_1, m_2\rangle$ where m_1 and m_2 are the magnetic quantum numbers for spins I_1 and I_2. A schematic view of the energy levels structure for such system is shown in Fig. 3.1 under the assumption that the two spins are equivalent (i.e. they have the same resonance frequency, ω_I).

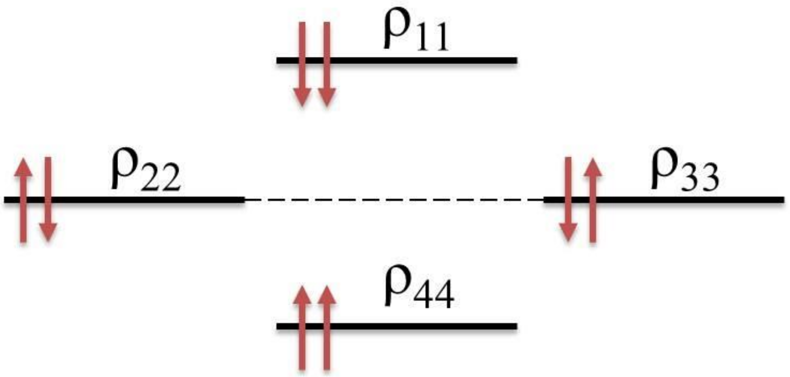

Figure 3.1. Schematic view of the energy levels structure for two equivalent spins $I = 1/2$.

To obtain an expression for the spin-lattice relaxation rate (reciprocal relaxation time), $R_1^{diam}(\omega_I)$, for a system of two equivalent spins $I = 1/2$ the relaxation matrix elements have to be calculated by means of Eq. 45. The dimension of the relaxation matrix is 16x16, but the spin-lattice relaxation is described by the population block (only for the elements $\rho_{\alpha\alpha}$) of dimension 4x4. The expressions for the relaxation matrix elements $R_{\alpha\alpha\beta\beta}$ are given below [2]:

$$\frac{d}{dt}\begin{bmatrix}\rho_{11}\\ \rho_{22}\\ \rho_{33}\\ \rho_{44}\end{bmatrix}=$$

$$\begin{bmatrix} -\frac{1}{4}J_1(\omega_I)-\frac{1}{2}J_2(2\omega_I) & \frac{1}{8}J_1(\omega_I) & \frac{1}{8}J_1(\omega_I) & \frac{1}{2}J_2(2\omega_I) \\ \frac{1}{8}J_1(\omega_I) & -\frac{1}{12}J_0(0)-\frac{1}{4}J_1(\omega_I) & \frac{1}{12}J_0(0) & \frac{1}{8}J_1(\omega_I) \\ \frac{1}{8}J_1(\omega_I) & \frac{1}{12}J_0(0) & -\frac{1}{12}J_0(\omega_I)-\frac{1}{4}J_1(\omega_I) & \frac{1}{8}J_1(\omega_I) \\ \frac{1}{2}J_2(2\omega_I) & \frac{1}{8}J_1(\omega_I) & \frac{1}{8}J_1(\omega_I) & -\frac{1}{4}J_1(\omega_I)-\frac{1}{2}J_2(2\omega_I) \end{bmatrix} \times \begin{bmatrix}\rho_{11}\\ \rho_{22}\\ \rho_{33}\\ \rho_{44}\end{bmatrix} \tag{48}$$

The longitudinal magnetization is proportional to the expectation value of the z-component of the spin operator $\langle I_z \rangle$ ($I_z = I_{1z} + I_{2z}$) that can be expressed by the linear combination of the density matrix elements ρ_{11} and ρ_{44} [2,10]:

$$\langle I_z \rangle = \frac{1}{2}(\rho_{11}-\rho_{44}) \tag{49}$$

The elements follow the set of equations [2] as a consequence of the formula of Eq. 44:

$$\frac{d\rho_{11}}{dt} = -R_{1111}\rho_{11} - R_{1122}\rho_{22} - R_{1133}\rho_{33} - R_{1144}\rho_{44} - R_{1123}\rho_{23} - R_{1132}\rho_{32} \tag{50a}$$

$$\frac{d\rho_{44}}{dt} = -R_{1144}\rho_{11} - R_{2244}\rho_{22} - R_{3344}\rho_{33} - R_{4444}\rho_{44} - R_{2344}\rho_{23} - R_{3244}\rho_{32} \tag{50b}$$

These equations do not include couplings with the coherences ρ_{23} and ρ_{32} ($\omega_{23}=0$ as a result of the degenerated energy levels shown in Fig. 3.1). Moreover, due to the fact that $R_{1123} = R_{2344}$ and $R_{3211} = R_{3244}$, contributions of these terms cancel anyway. The resulted expression for $(\rho_{11}-\rho_{44})$:

$$\begin{aligned}\frac{d}{dt}(\rho_{11}-\rho_{44}) = (-R_{1111}+R_{1144})\rho_{11} + (-R_{1122}+R_{2244})\rho_{22} + \\ + (-R_{1133}+R_{3344})\rho_{33} + (-R_{1144}+R_{4444})\rho_{44}\end{aligned} \tag{51}$$

combined with Eq. 48 gives the well-known expression for the spin-lattice relaxation rate $R_1^{diam}(\omega_I)$ [1-5,7,9-11]:

$$R_1^{diam}(\omega_I) = \frac{2}{5}\left(\frac{\mu_0}{4\pi}\frac{\gamma_I^2\hbar}{r_{II}^3}\right)^2 I(I+1)\left[J(\omega_I)+4J(2\omega_I)\right] \tag{52}$$

where r_{II} is the interspin distance.

3.3. Paramagnetic systems

In liquids with paramagnetic centres the dipole-dipole interaction is between two non-equivalent spins (a proton spin I and an electron spin S). For $S = 1/2$ and assuming that the relaxation is caused by dipole-dipole interactions between the proton and electron spins, while the energy level structure is determined solely by their Zeeman couplings (Eq. 19), the nuclear spin-lattice relaxation rate $R_1^{par}(\omega_I)$ is given by the Solomon-Bloembergen-Morgan (SBM) formula [1,2,5,20,25,39-41].

The eigenbasis of the unperturbed part of the Hamiltonian consists of functions $|n\rangle = |m_I, m_S\rangle$ where m_I and m_S are the magnetic quantum numbers of proton and electron, respectively. As the nuclear and electron resonance frequencies, ω_I and ω_S, respectively, are much different, the degeneracy of the energy levels is removed. As a result of Eq. 45, the population block of the relaxation matrix contains now the elements [2]:

$$\frac{d}{dt}\begin{bmatrix}\rho_{11}\\ \rho_{22}\\ \rho_{33}\\ \rho_{44}\end{bmatrix} = \begin{bmatrix} \Lambda & \frac{1}{8}J_1(\omega_S) & \frac{1}{8}J_1(\omega_I) & \frac{1}{2}J_2(\omega_I+\omega_S) \\ \frac{1}{8}J_1(\omega_S) & \Lambda & \frac{1}{12}J_0(\omega_I-\omega_S) & \frac{1}{8}J_1(\omega_I) \\ \frac{1}{8}J_1(\omega_I) & \frac{1}{12}J_0(\omega_I-\omega_S) & \Lambda & \frac{1}{8}J_1(\omega_S) \\ \frac{1}{2}J_2(\omega_I+\omega_S) & \frac{1}{8}J_1(\omega_I) & \frac{1}{8}J_1(\omega_S) & \Lambda \end{bmatrix} \times \begin{bmatrix}\rho_{11}\\ \rho_{22}\\ \rho_{33}\\ \rho_{44}\end{bmatrix} \tag{53}$$

where $\Lambda = -\frac{1}{8}J_1(\omega_I) - \frac{1}{8}J_1(\omega_S) - \frac{1}{2}J_2(\omega_I+\omega_S)$. Then the evolution of the nuclear magnetization (the expectation value of $\langle I_z\rangle$) is described by the expression [2]:

$$\begin{aligned} \frac{d\langle I_z\rangle}{dt} &= \frac{d}{dt}\left(\rho_{11}+\rho_{22}-\rho_{33}-\rho_{44}\right) = \\ &= -\underbrace{\left[\frac{1}{12}J(\omega_I-\omega_S)+\frac{1}{4}J(\omega_I)+\frac{1}{2}J(\omega_I+\omega_S)\right]}_{R_{II}(\omega_I)}\underbrace{\left(\rho_{11}+\rho_{22}-\rho_{33}-\rho_{44}\right)}_{\langle I_z\rangle-\langle I_z\rangle_{eq}} \\ &+ \underbrace{\left[\frac{1}{2}J(\omega_I+\omega_S)-\frac{1}{12}J(\omega_I-\omega_S)\right]}_{R_{IS}(\omega_I)}\underbrace{\left(\rho_{11}+\rho_{33}-\rho_{22}-\rho_{44}\right)}_{\langle S_z\rangle-\langle S_z\rangle_{eq}} \end{aligned} \tag{54}$$

where R_{IS} is a cross-relaxation rate and the quantities $\langle I_z\rangle_{eq}$ and $\langle S_z\rangle_{eq}$ denote the expectation values of the spins I_z and S_z in the equilibrium state. When the electron spin relaxation is very fast, the term $\langle S_z\rangle - \langle S_z\rangle_{eq}$ becomes zero very quickly and the nuclear spin relaxation is single exponential with the relaxation rate [1-3,5,11,19,20,25,39-41]:

$$R_1^{par}(\omega_I) = R_{II}(\omega_I) = \frac{2}{15}\left(\frac{\mu_0}{4\pi}\frac{\gamma_I\gamma_S\hbar}{r_{IS}}\right)^2 S(S+1)\left[J(\omega_I-\omega_S)+3J(\omega_I)+6J(\omega_I+\omega_S)\right] \quad (55)$$

Taking into account that $\omega_S = 657\omega_I$, the sum and the difference of the two Larmor frequencies can be approximated by electron Larmor frequency and the above formula reduces to the form:

$$R_1^{par}(\omega_I) = R_{II}(\omega_I) = \frac{2}{15}\left(\frac{\mu_0}{4\pi}\frac{\gamma_I\gamma_S\hbar}{r_{IS}}\right)^2 S(S+1)\left[3J(\omega_I)+7J(\omega_S)\right] \quad (56)$$

In a more elaborated form this equation includes electron spin relaxation rates [2,40]. Electron spin relaxation acts as an additional source of modulations of the $I-S$ dipole-dipole interaction and this is reflected by the form of the spectral densities. Assuming that the original source of the modulations of the dipolar coupling is rotation and that the spectral densities are Lorentzian, one obtains:

$$J(\omega) = \frac{\tau_{c,eff}}{1+\left(\omega\tau_{c,eff}\right)^2} \quad (57)$$

The effective correlation time is defined as: $\tau_{c,eff}^{-1} = \tau_R^{-1} + R_1^e$ for $J(\omega_I)$ and $\tau_{c,eff}^{-1} = \tau_R^{-1} + R_2^e$ for $J(\omega_S)$, where R_1^e and R_2^e denote the electronic spin-lattice and spin-spin relaxation rates, respectively [1,2,4,9,40,41].

3.4. General approach to relaxaton in paramagnetic systems

When there are other spin interactions (besides the Zeeman couplings) contributing to the energy level structure of the spin system (for instance the isotropic part of the hyperfine interaction – Eq. 27), Eq. 55 describing the nuclear spin-lattice relaxation caused by a nuclear spin – electron spin dipole – dipole interaction has to be replaced by a more general expression [2,43,49]:

$$R_1^{par}(\omega_I) = \frac{1}{10}\left(\frac{\mu_0}{4\pi}\frac{\gamma_I\gamma_S\hbar}{r_{IS}}\right)^2 \left(s_{1,1}(\omega_I)+3s_{0,0}(\omega_I)+6s_{-1,-1}(\omega_I)\right). \quad (58)$$

The quantities $s_{q,q}(\omega_I)$ are referred to as generalized spectral densities, which for isotropic rotational dynamics are characterized by a single correlation time, τ_R. They can be obtained as a matrix product [2,21,39,43,44,49]:

$$s_{q,q}(\omega_I) = \frac{1}{2S+1}\mathrm{Re}\left\{\left[S_q^1\right]^{+}\left[M\right]^{-1}\left[S_q^1\right]\right\} \tag{59}$$

The matrices of Eq. 59 are defined in a basis formed by pairs of the eigenstates of the spin system (+ denotes matrix transposition). For $I = S = 1/2$ its dimension is 16. The diagonal elements of the matrix $[M]$ are defined as [2,32]:

$$[M]_{\alpha\alpha'\alpha\alpha'} = i(\omega_I - \omega_{\alpha\alpha'}) + R^e_{\alpha\alpha'\alpha\alpha'} + \tau_R^{-1} \tag{60}$$

where $R^e_{\alpha\alpha'\alpha\alpha'}$ are electron spin relaxation rates. The off-diagonal elements are given as:

$$[M]_{\alpha\alpha'\beta\beta'} = R^e_{\alpha\alpha'\beta\beta'} \tag{61}$$

The matrix $\left[S_q^1\right]$ is a representation of the operators:

$$S_0^1 = S_z \tag{62a}$$

$$S_{\pm 1}^1 = \frac{1}{\sqrt{2}} S_{\pm} \tag{62b}$$

in the same basis [21,32,37,44-46].

3.5. Relaxation in diamagnetic and paramagnetic systems - a comparison

The relaxation rate $R_1^{diam}(\omega_I)$ for short correlation times (fast motion of the interacting molecules) is almost field (frequency) independent as shown in Fig. 3.2 a) for $\tau_R = 1*10^{-11}s$ (characteristic of water; simulations have been calculated for ^{1}H relaxation therefore $\omega_I = \omega_H$). For more viscous liquids (longer correlation times) one observes a dispersion of relaxation at high frequencies (Fig. 3.2 b)). The value of the distance of closest approach was set to $d_{II} = 3\text{Å}$ that is between the values presented in literature for water [47] and for glycerol [31-34]. The rotational spectral densities were described as Lorentzian functions.

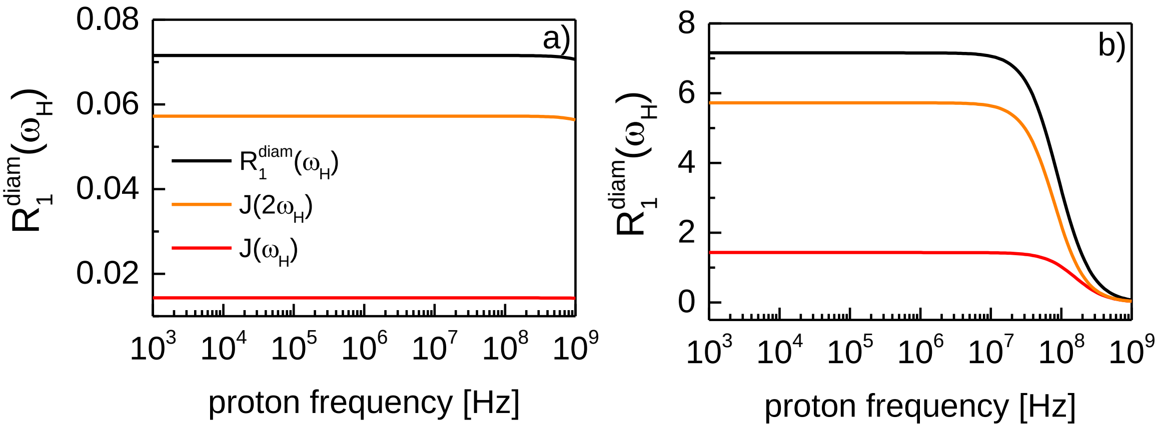

Figure 3.2. $R_1^{diam}(\omega_H)$ *versus proton frequency simulated according to Eq. 52 for a)* $\tau_R = 1*10^{-11}s$ *and b)* $\tau_R = 1*10^{-9}s$*;* $d_{II} = 3Å$*. Decomposition of the relaxation dispersion profile into the* $J(\omega_H)$ *and* $J(2\omega_H)$ *contributions is shown.*

In Fig. 3.3 a), b) simulations of $R_1^{par}(\omega_H)$ are presented for the same values of the rotational correlation time.

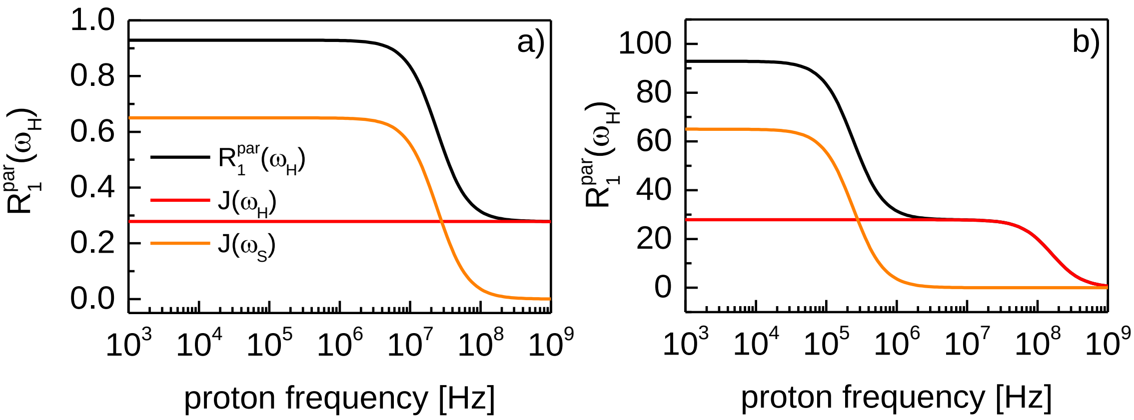

Figure 3.3. $R_1^{par}(\omega_H)$ *versus proton frequency simulated according to Eq. 56 for a)* $\tau_R = 1*10^{-11}s$ *and b)* $\tau_R = 1*10^{-9}s$*;* $d_{IS} = 3Å$*. Decomposition of the relaxation dispersion profile into the* $3J(\omega_H)$ *and* $7J(\omega_S)$ *contributions is shown.*

$R_1^{par}(\omega_H)$ shows a strong dispersion even for the shorter correlation time. It is caused by the term $7J(\omega_S)$ present in Eq. 56. The electron Larmor frequency, ω_S, is 657 times larger than proton Larmor frequency due to the ratio between the proton and electron gyromagnetic factors and therefore it leads to a considerable nuclear relaxation dispersion for paramagnetic liquids even though the dynamics is pretty fast. In consequence, NMR relaxation studies for liquids containing paramagnetic centres provide information about fast dynamics of the solvent which is not accesible otherwise.

In solutions of paramagnetic species two kinds of dipole-dipole interaction involving the solvent protons should be distinguished: the proton-proton ($I-I$) interactions between solvent molecules and proton-electron ($I-S$) dipole-dipole interactions between the solvent and solute (carrying the electron spin) molecules. As a result the overall nuclear (proton) relaxation rate $R_1(\omega_H)$ meassured in the experiment is a sum of two contributions:

$$R_1(\omega_H) = R_1^{diam}(\omega_H) + R_1^{par}(\omega_H) \tag{63}$$

Therefore to obtain the $R_1^{par}(\omega_H)$ relaxation part, the relaxation rate $R_1^{diam}(\omega_H)$ for pure solvents should also be measured and then subtracted from $R_1(\omega_H)$. The value of $R_1^{par}(\omega_H)$ is proportional to the concentration of the paramagnetic centres [20,26,31]. Thus, it is convenient to normalize the obtained $R_1^{par}(\omega_H)$ data to unit concentration (1 mM). The normalized relaxation rates are referred to as relaxivity [20,31].

4. Literature review

The subject of nuclear spin relaxation in the presence of paramagnetic centres begins with the pioniering work of Solomon, Bloembergen and Morgan [39,40], referred to as the SBM theory. The authors developed the first theory of Paramagnetic Relaxation Enhancement, PRE, (enhancement of the nuclear spin relaxation caused by strong dipole-dipole interactions with the electron spin of the paramagnetic molecule) pointing out the possibility of two-exponential relaxation in systems containing so-called non-equivalent spins and introducing the concept of electron spin relaxation acting as an additional (besides the molecular dynamics) source of stochastic fluctuations of the nuclear spin-electron spin interactions. The electron spin relaxation is treated in the theory as a phenomenological parameter. The most serious limitation of this description is that it is valid only at high magnetic fields when all other spin interactions are negligible compared to the Zeeman coupling.

As for long time the only way to study NMR relaxation was performing relaxation experiments at a single, rather high frequency versus temperature, there was no need for developing more general approaches. The situation has drastically changed with the emergence of FFC relaxometers [48] that has opened the possibility to perform frequency dependent relaxation experiments going down to low frequencies where the spin interactions neglected by the SBM approach are of primary importance. The development of the FFC technology was accompanied by rapidly growing interest in the development of paramagnetic contrast agents for Magnetic Resonance Imaging and FFC relaxation experiments have become a tool to probe the efficiency of new candidates for MRI contrast agents. These studies have revealed the inaccuracy and the insufficiency of the SBM approach – the theory is not even able to explain the appearance of frequency specific relaxation maxima beeing the basis of the paramagnetic contrast mechanism, not talking about their shapes and properties. This situation has stimulated the development of theories of PRE effects in solutions of transition and rare earth metal complexes. The development has started from introducing to the SBM theory the concept of frequency dependent electron spin relaxation calculated by means of simplified (oversimplified) approaches, but explicitly involving zero field splitting interactions (characteristic of paramagnetic systems of the electron spin of one or higher) and the time scale of their fluctuations. This was the first attempt to go beyond the purely phenomenological treatment of the electron spin relaxation used in the SBM equations.

Further theoretical development went through several steps, aiming at obtaing a theory of PRE which is valid for an arbitrary magnetic field, includes relevant spin interactions and can be used for arbitrary motional condition. The theories available at present can be divided into two groups: 1) approaches based on the second rank perturbation theory [49,50] and approaches using a full solution of the stochastic Liouville equation [51-56]. The perturbation approaches are very advanced – they include complex models of zero field splitting interactions, but as far as the motional conditions are concerned their validity is restricted to the limiting cases of slow and fast dynamics. The expectations of generality are fulfilled by the approach based on the Liouville equations, but for the price of high conceptual and computational effort.

Another group of chemical compounds that gained a lot of interest due to their applications are nitroxide radicals. The enhancement induced in such systems is smaller in comparison to the PRE obtained for systems with transition and rare-earth metal complexes, but by introducing nitroxide radicals to liquids, the dynamics of the solvent can be investigated provided an appropriate relaxation theory is available.

The overall proton relaxation rate is a sum of spectral densities being the Fourier transform of the correlation functions describing the dynamics of the system. Therefore, to form theory of PRE for nitroxide radicals valid for an arbitrary magnetic field, the spectral densities describing the translational dynamics of spin bearing molecules had to be calculated. It has been done in seminal works of Hwang and Freed [29] and Ayant et al. [28]. The dynamical model presented in their works is based on the assumptions that the interacting spins are placed in the centers of molecules which are treated as hard spheres. In reality, this assumption is not fulfilled. It implies that rotational motion also contributes to the modulations of the inter-molecular dipole-dipole interaction. Therefore, the definition of the translational spectral density presented in Refs. [28,29] has been extended by including the translation – rotation coupling referred to as ‘eccentricity effect’, [25-27]. It was experimentally confirmed for many different systems (either in diamagnetic liquids [34,35] and in solutions of nitroxide radicals [31-33]). In consequence the PRE effect occuring for solutions of nitroxide radicals can be used to study both: the translational as well as the rotational dynamics of the system.

The applicability of the above approach is limited to the high values of the magnetic field (like it was for the SBM theory). The low field features of nuclear relaxation resulting from interactions with nitroxide radicals have been less intensively investigated and an appropriate description of the PRE effect valid for an arbitrary magnetic field was not available for a long time.

First attempts to face this problem have been made by Belorizky et al. in Ref. [15]. A description of PRE effects for solutions of ^{15}N containing radicals taking into account the influence of the isotropic hyperfine coupling on the electron spin energy level structure has been presented neglecting the electron spin relaxation. Additionally the theory has been combined with the low frequency expansion of the translational spectral density into an expression linking the relative diffusion coefficient of the solvent and solute molecules to a linear slope of the dependence of the proton relaxation rate on square root of frequency, observed at low frequencies.

A more complex description of PRE effects for ^{14}N containing radicals taking into account the isotropic part of the hyperfine coupling has been developed by D. Kruk et al. in Ref. [32]. In further works of the authors the PRE theory (both for ^{15}N from Ref. [15] and ^{14}N from Ref. [32]) has been generalized including the influence of the electron spin relaxation on the modulations of the electron spin – proton spin dipole – dipole interaction [31,57]. The dominating electron spin relaxation mechanism for nitroxide radicals has been provided by the anisotropic part of the electron spin – nitrogen spin hyperfine coupling. The modulations of this interaction caused by the overall tumbling of the paramagnetic molecule has been considered in Refs. [31,57]. This extended approach has been carefully tested against the experimental data. The detailed analysis of ^{1}H NMRD data for several solutions differing in dynamic parameters over a broad temperature range has been presented in Refs. [31,32,57].

5. Proton relaxation in paramagnetic system with hyperfine coupling

5.1. Influence of isotropic hyperfine coupling on proton relaxation

As described in section 3, for proton relaxation caused by the proton spin I - electron spin S dipole-dipole coupling, the relaxation rate $R_1^{par}(\omega_H)$ is given by the Solomon – Bloembergen – Morgan formula (Eq. 56) [1-3,5,11]. This description is valid at high magnetic fields when the condition $\omega_S >> A_{iso}$ is fulfilled. In this range the energy levels of the electron spin S are determined only by the electron Zeeman interaction.

solvent	A_{xx} [MHz]	A_{yy} [MHz]	A_{zz} [MHz]	$A_{iso} = \frac{A_{xx}+A_{yy}+A_{zz}}{3}$ [MHz]
toluene-d8 [58]	11.49	17.10	93.60	40.64
glycerol-d3-D2O [58]	15.41	15.97	100.33	44.00
acetone-d6 [58]	13.45	15.13	95.28	41.20
propylene glycol [57]	10.6	10.6	107.3	42.83

Table 5.1. Components of hyperfine coupling for deuterated 4-oxo-TEMPO determined from ESR experiments [57,58].

Values of the isotropic part of the hyperfine coupling, A_{iso}, obtained from ESR experiments for solutions of nitroxide radicals (deuterated 4-oxo-TEMPO) are of the order of 50 MHz (some of them are shown as an example in Table 5.1) [57,58]. Conventional Field Cycling experiments are performed in the frequency range of 10 kHz – 20 MHz for protons. Due to the value of the ratio between electron and proton gyromagnetic factors ($\gamma_S / \gamma_H = 657$) it corresponds to the range of 6.5 MHz - 13 GHz for electrons. This means that for a significant part of the frequency range the hyperfine coupling of the electron spin S with nitrogen spin P has to be taken into account.

As explained in section 2 the unperturbed Hamiltonian of the pair of electron and nitrogen spins $S-P$ consists of two parts [15-18]:

$$\mathrm{H}_0(S,P)=\mathrm{H}_Z(S)+\mathrm{H}_{iso}(S,P) \tag{64}$$

The Zeeman functions $\left|n\right\rangle=\left|m_S,m_P\right\rangle$ for the $S-P$ system are determined by the electron spin and nitrogen spin magnetic quantum numbers, m_S and m_P, respectively. For $P=1/2$ (^{15}N) it gives: $|1\rangle=|+,+\rangle$, $|2\rangle=|+,-\rangle$, $|3\rangle=|-,+\rangle$, $|4\rangle=|-,-\rangle$ (the abbreviation ± instead of the $1/2$ and $-1/2$ magnetic quantum numbers is used). For $P=1$ (^{14}N) the system is described by 6 Zeeman functions: $|1\rangle=|+,1\rangle$, $|2\rangle=|+,0\rangle$, $|3\rangle=|+,-1\rangle$, $|4\rangle=|-,1\rangle$, $|5\rangle=|-,0\rangle$, $|6\rangle=|-,-1\rangle$. The eigenfunctions $|\Psi_i\rangle$ of the system resulting from diagonalization of the Hamiltonian of Eq. 64 are given as linear combination of the Zeeman functions $\left|n\right\rangle=\left|m_S,m_P\right\rangle$. For the simpler case of ^{15}N ($P=1/2$) there are four energy levels [15,31,32]:

$$\begin{aligned}
E_1 &= \frac{\omega_s}{2}+\frac{A_{iso}}{4} & |\Psi_1\rangle &= |+,+\rangle \\
E_2 &= \frac{1}{2}\sqrt{\omega_S^2+A_{iso}^2}-\frac{A_{iso}}{4} & |\Psi_2\rangle &= a\,|+,-\rangle+b\,|-,+\rangle \\
E_3 &= -\frac{1}{2}\sqrt{\omega_S^2+A_{iso}^2}-\frac{A_{iso}}{4} & |\Psi_3\rangle &= -b\,|+,-\rangle+a\,|-,+\rangle \\
E_4 &= -\frac{\omega_s}{2}+\frac{A_{iso}}{4} & |\Psi_4\rangle &= |-,-\rangle
\end{aligned} \tag{65}$$

where

$$a=\left\{\frac{1}{2}\left[1+\frac{\omega_S}{\sqrt{\omega_S^2+A_{iso}^2}}\right]\right\}^{\frac{1}{2}} \quad \text{and} \quad b=\left\{\frac{1}{2}\left[1-\frac{\omega_S}{\sqrt{\omega_S^2+A_{iso}^2}}\right]\right\}^{\frac{1}{2}} \tag{66}$$

For the case of ^{14}N ($P=1$) the system is characterized by six energy levels [31,32]:

$$\begin{aligned}
E_1 &= \frac{\omega_s}{2} + \frac{A_{iso}}{2} && |\Psi_1\rangle = |+,1\rangle \\
E_2 &= \frac{1}{2}\sqrt{\frac{9A_{iso}^2}{4} + \omega_S^2 + \omega_S A_{iso}} - \frac{A_{iso}}{4} && |\Psi_2\rangle = a\,|+,0\rangle + b\,|-,1\rangle \\
E_3 &= -\frac{1}{2}\sqrt{\frac{9A_{iso}^2}{4} + \omega_S^2 + \omega_S A_{iso}} - \frac{A_{iso}}{4} && |\Psi_3\rangle = c\,|+,0\rangle + d\,|-,1\rangle \\
E_4 &= \frac{1}{2}\sqrt{\frac{9A_{iso}^2}{4} + \omega_S^2 - \omega_S A_{iso}} - \frac{A_{iso}}{4} && |\Psi_4\rangle = e\,|+,-1\rangle + f\,|-,0\rangle \\
E_5 &= -\frac{1}{2}\sqrt{\frac{9A_{iso}^2}{4} + \omega_S^2 - \omega_S A_{iso}} - \frac{A_{iso}}{4} && |\Psi_5\rangle = g\,|+,-1\rangle + d\,|-,0\rangle \\
E_6 &= -\frac{\omega_s}{2} + \frac{A_{iso}}{2} && |\Psi_6\rangle = |-,-1\rangle
\end{aligned} \tag{67}$$

with the a,b,c,d,e,f,g,h coefficients given as:

$$\begin{aligned}
&a = (1+\alpha^2)^{(-1/2)} \quad b = \alpha a \quad c = (1+\beta^2)^{(-1/2)} \quad d = \beta c \\
&e = (1+\gamma^2)^{(-1/2)} \quad f = \gamma e \quad g = (1+\delta^2)^{(-1/2)} \quad h = \delta g
\end{aligned} \tag{68}$$

where

$$\begin{aligned}
\alpha &= \frac{A_{iso} + 2\omega_S - \sqrt{9A_{iso}^2 + 4A_{iso}\omega_S + 4\omega_S^2}}{2\sqrt{2}A_{iso}} \qquad \beta = \frac{A_{iso} + 2\omega_S + \sqrt{9A_{iso}^2 + 4A_{iso}\omega_S + 4\omega_S^2}}{2\sqrt{2}A_{iso}} \\
\gamma &= \frac{A_{iso} - 2\omega_S + \sqrt{9A_{iso}^2 - 4A_{iso}\omega_S + 4\omega_S^2}}{2\sqrt{2}A_{iso}} \qquad \delta = \frac{A_{iso} - 2\omega_S - \sqrt{9A_{iso}^2 - 4A_{iso}\omega_S + 4\omega_S^2}}{2\sqrt{2}A_{iso}}
\end{aligned} \tag{69}$$

Diagrams of the electron energy levels as a function of ^{1}H frequency for the case of ^{15}N (A_{iso} = 63 MHz) and ^{14}N (A_{iso} = 45 MHz) are shown in Fig. 5.1. From now on the frequency axis corresponds to proton frequency, so the term “proton” is omitted.

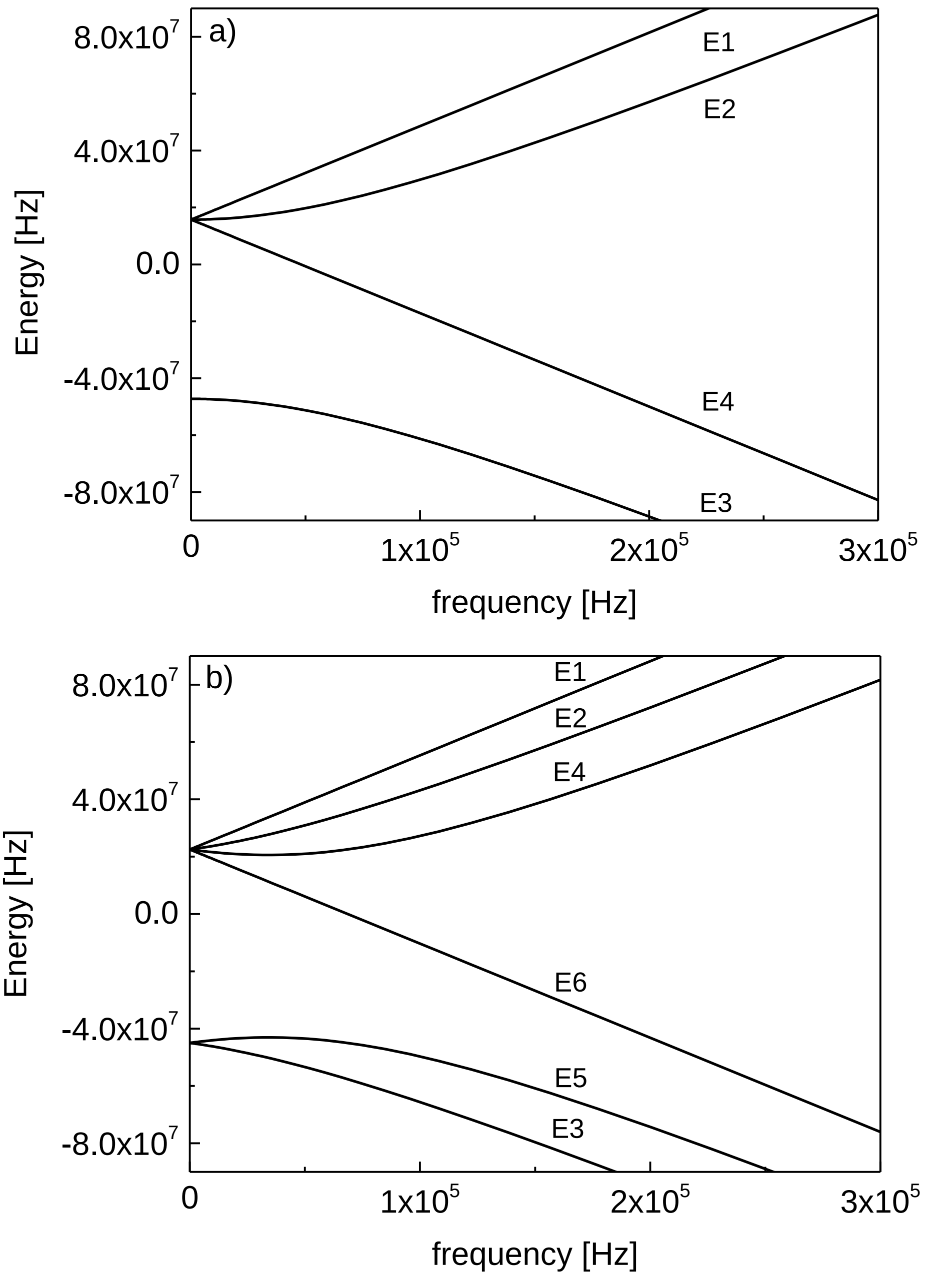

Figure 5.1. Energy levels diagrams for a system of electron spin S *coupled by hyperfine interaction with a)* ^{15}N *and b)* ^{14}N *spin* P *versus proton frequency. The values of hyperfine isotropic (scalar) coupling are: for* ^{15}N: $A_{iso} = 63\,MHz$ *and for* ^{14}N: $A_{iso} = 45\,MHz$.

Proton spin-lattice relaxation rate in solutions of paramagnetic molecules is described by a combination of generalized spectral densities defined by Eq. 58. The spectral densities $s_{m,m}(\omega_H)$ for translational dynamics are defined in analogy to Eq. 59 as [2,31,51,55,59]:

$$s_{m,m}(\omega_H) = 36\frac{N_S}{d_{IS}^3} Re\int_0^\infty \frac{u^2}{81+9u^2-2u^4+u^6}\left\{\left[S_m^1\right]^+\left[M\right]^{-1}\left[S_m^1\right]\right\}du \qquad (70)$$

where $\left[S^1_m\right]$ are matrix representations of the operators S^1_m: $S^1_0 = S_Z$, $S^1_{\pm 1} = 1/\sqrt{2}S_{\pm}$, in the eigenbasis of the $S - P$ system, $\left|\Psi_i\right\rangle$. This representation can be derived using the following expressions [2,31]:

$$\begin{aligned}
S^1_0 &= \sum_{m_S > 0} (| m_S, m_P\rangle\langle m_S, m_P | - | -m_S, m_P\rangle\langle -m_S, m_P |) \\
S^1_1 &= -\sum_{m_S} | m_S, m_P\rangle\langle m_S - 1, m_P | \\
S^1_{-1} &= \sum_{m_S} | m_S - 1, m_P\rangle\langle m_S, m_P |
\end{aligned} \tag{71}$$

and the relationship between the Zeeman basis and the eigenbasis $\left\{\left|\Psi_i\right\rangle\right\}$, (Eqs. 65 and 67). The matrices $\left[M\right]$ and $\left[S^1_m\right]$ are defined in a basis constructed from pairs of the eigenfunctions $\left|\Psi_i\right\rangle\left\langle\Psi_j\right|$, referred to as a Liouville space [2,4,11,36-38,41]. The matrix $\left[M\right]$ is diagonal with the elements [2,31,49,57]:

$$\left[M\right]_{ij,ij} = i(\omega_H + \omega_{ij}) + u^2 \tau^{-1}_{trans} \tag{72}$$

where $\omega_{ij} = E_i - E_j$ are transition frequencies between the energy levels presented in Fig. 5.1. As $\omega_{ij} >> \omega_H$ the expressions $\omega_{ij} \pm \omega_H$ can be replaced by ω_{ij}. Using the outlined approach, expressions for the paramagnetically induced proton spin-lattice relaxation rate $R^{par}_1(\omega_H)$ for the systems with ^{15}N and ^{14}N have been derived. For the case of ^{15}N the expression yields [15,31,32] :

$$R^{par}_1(\omega_H) = K_{DD} \times \left\{ \begin{array}{l} \overbrace{\frac{3}{2}[1 + (a^2 - b^2)^2] J(\omega_H)}^{R^{15,I}_1(\omega_H)} + \overbrace{6(ab)^2 J(\omega_{23})}^{R^{15,II}_1(\omega_H)} \\ \\ \underbrace{+\frac{7}{2} a^2 [J(\omega_{13}) + J(\omega_{24})] + \frac{7}{2} b^2 [J(\omega_{12}) + J(\omega_{34})]}_{R^{15,III}_1(\omega_H)} \end{array} \right\} \tag{73}$$

while for the case of ^{14}N it is [31,32]:

$$R_1^{par}(\omega_H) = K_{DD} \times \left\{ \begin{array}{l} \overbrace{\left[1+\frac{(a^2-b^2)^2}{2}+\frac{(c^2-d^2)^2}{2}+\frac{(e^2-f^2)^2}{2}+\frac{(g^2-h^2)^2}{2}\right]J(\omega_H)}^{R_1^{14,I}(\omega_H)} \\ \\ +\overbrace{[(ac-bd)^2 J(\omega_{23})+(eg-fh)^2 J(\omega_{45})]}^{R_1^{14,II}(\omega_H)} \\ \\ +\overbrace{\frac{7}{3}[b^2 J(\omega_{12})+d^2 J(\omega_{13})+e^2 J(\omega_{46})+g^2 J(\omega_{56})]}^{R_1^{14,III}(\omega_H)} \\ \\ +\underbrace{\frac{7}{3}[(af)^2 J(\omega_{24})+(ah)^2 J(\omega_{25})+(cf)^2 J(\omega_{34})+(ch)^2 J(\omega_{35})]}_{R_1^{14,IV}(\omega_H)} \end{array} \right\} \tag{74}$$

where:

$$K_{DD} = \frac{2}{15} S(S+1)\left(\frac{\mu_0}{4\pi}\gamma_I \gamma_S \hbar\right)^2 \tag{75}$$

The expressions $R_1^{15(14),X}\left(\omega_H\right)$ are introduced for the clarity of descriptions of figures in this section and the next ones ($x = I, II, III, IV$).

Examples of ^{1}H relaxation dispersion profiles, $R_1^{par}(\omega_H)$, for ^{15}N and ^{14}N are shown in Fig. 5.2 a) and b), respectively; for ^{15}N: $A_{iso} = 63$ MHz and for ^{14}N: $A_{iso} = 45$ MHz and 1 mM concentration of the radical molecules.

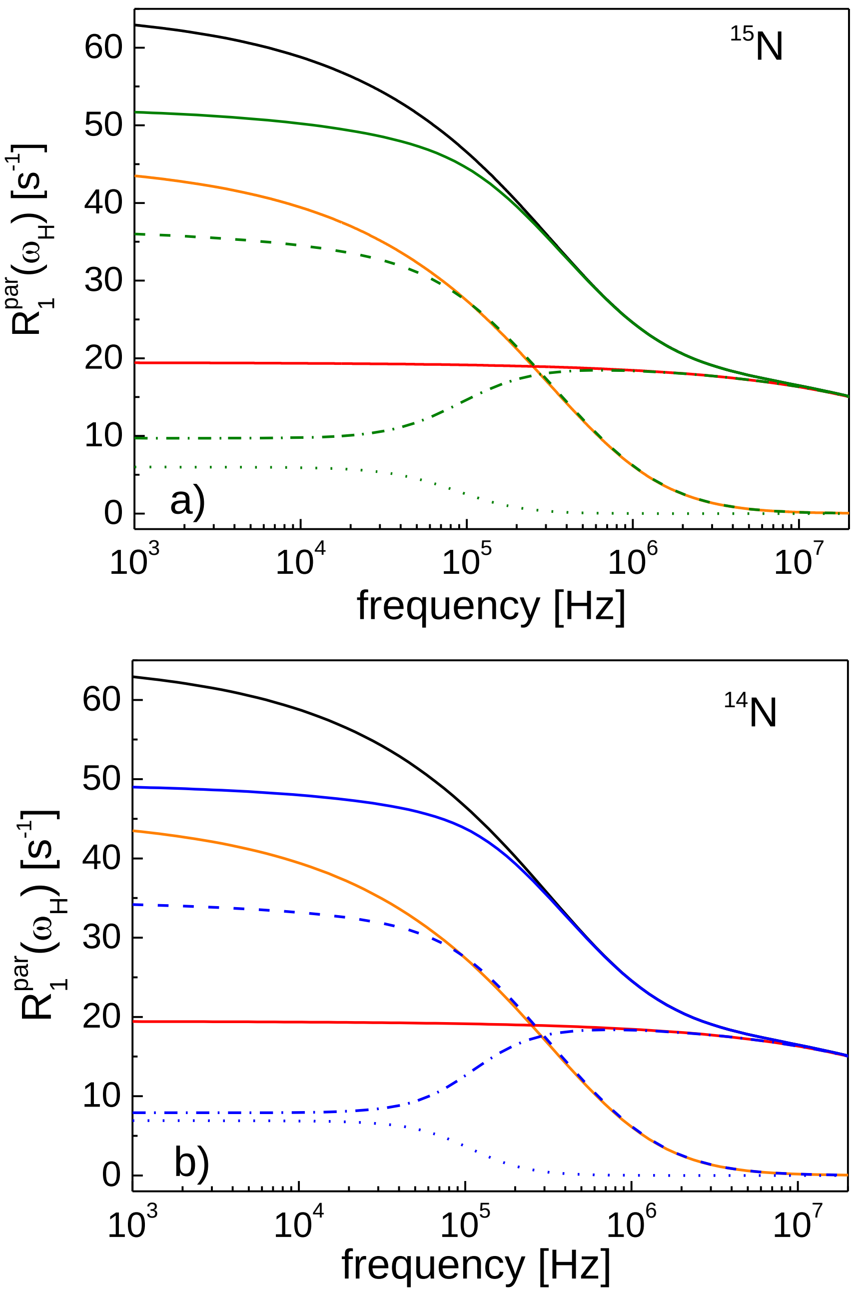

Figure 5.2. Simulations of ^1H *spin-lattice relaxation dispersion profiles,* $R_1^{par}(\omega_H)$, *for a)* ^{15}*N and b)* ^{14}*N containing nitroxide radicals. Solid black lines -* $R_1^{par}(\omega_H)$ *for* $A_{iso} = 0\,MHz$, *Eq.56; solid red lines - part of Eq. 56 dependent on* ω_H $(K_{DD}3J(\omega_H))$*; solid orange lines - part of Eq. 56 dependent on* ω_S $(K_{DD}7J(\omega_S))$*. Solid lines –* $R_1^{par}(\omega_H)$ *for* $A_{iso} = 63\,MHz$ *(green line,* ^{15}*N, Eq. 73) and for* $A_{iso} = 45\,MHz$ *(blue line,* ^{14}*N, Eq. 74); The contributions dependent on different transition frequencies are marked as follows:*

a) from Eq. 73: dashed-dotted green line – $K_{DD}R_1^{15,I}(\omega_H)$, *dotted green line –* $K_{DD}R_1^{15,II}(\omega_H)$, *dashed green line –* $K_{DD}R_1^{15,III}(\omega_H)$*;*

b) from Eq. 74: dashed-dotted blue line – $K_{DD}R_1^{14,I}(\omega_H)$, *dotted blue line –* $K_{DD}R_1^{14,II}(\omega_H)$*, dashed blue line –* $K_{DD}\left(R_1^{14,III}(\omega_H) + R_1^{14,IV}(\omega_H)\right)$*. The simulations have been performed for the following parameters:* $\tau_{trans} = 1*10^{-9}\,s$, $d_{IS} = 4\,Å$, $D_{12} = 1.6*10^{-10}\,m/s^2$.

In both figures the case of $A_{iso}=0$ MHz when Eq. 73 and Eq. 74 simplify to the SBM formula (Eq. 56) is shown with black solid line. It can be easily seen that the isotropic hyperfine coupling leads to reduction of $R_1^{par}(\omega_H)$ in the low field range (defined by the condition $\omega_S << A_{iso}$). The reduction of the $R_1^{par}(\omega_H)$ for the case of ^{14}N ($P=1$) is larger than for the case of ^{15}N ($P=1/2$) and this effect becomes more pronounced for slower dynamics as shown in Fig. 5.3.

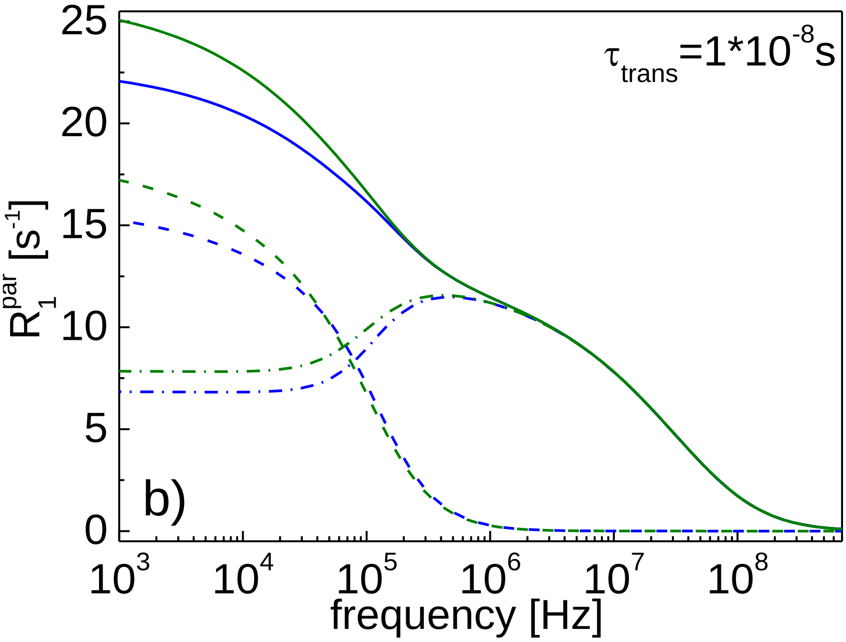

Figure 5.3. Simulations of ^{1}*H spin-lattice relaxation dispersion profile,* $R_1^{par}(\omega_H)$*, for slow dynamics (*$\tau_{trans}=1*10^{-8}$ *s,* $d_{IS}=4$ *Å,* $D_{12}=1.6*10^{-11}$ *m/s*^{2}*); blue lines – case of* ^{14}*N (Eq. 74); green lines – case of* ^{15}*N (Eq. 73); dashed lines – the terms:* $K_{DD}\left(R_1^{15,II}(\omega_H)+R_1^{15,III}(\omega_H)\right)$ *for* ^{15}*N and* $K_{DD}\left(R_1^{14,II}(\omega_H)+R_1^{14,III}(\omega_H)+R_1^{14,IV}(\omega_H)\right)$ *for* ^{14}*N; dashed-dotted lines – the terms:* $K_{DD}R_1^{15,I}(\omega_H)$ *for* ^{15}*N and* $K_{DD}R_1^{14,I}(\omega_H)$ *for* ^{14}*N.*

5.2. High and low field limits

Taking into account the values of the isotropic hyperfine coupling constant, A_{iso}, two limiting cases can be distinguished: the low field regime in which the amplitude of the scalar hyperfine coupling is much larger than the electron Larmor frequency, ω_S

($A_{iso} >> \omega_S$), and the high field regime when the scalar hyperfine coupling is much smaller than ω_S ($A_{iso} << \omega_S$). The dependencies of the a, b coefficients of Eq. 73 (the case of ^{15}N) on the ^{1}H frequency are presented in Fig. 5.4 a), analogous dependencies of the coefficients $a-h$ (the case of ^{14}N) are shown in Fig. 5.4 b).

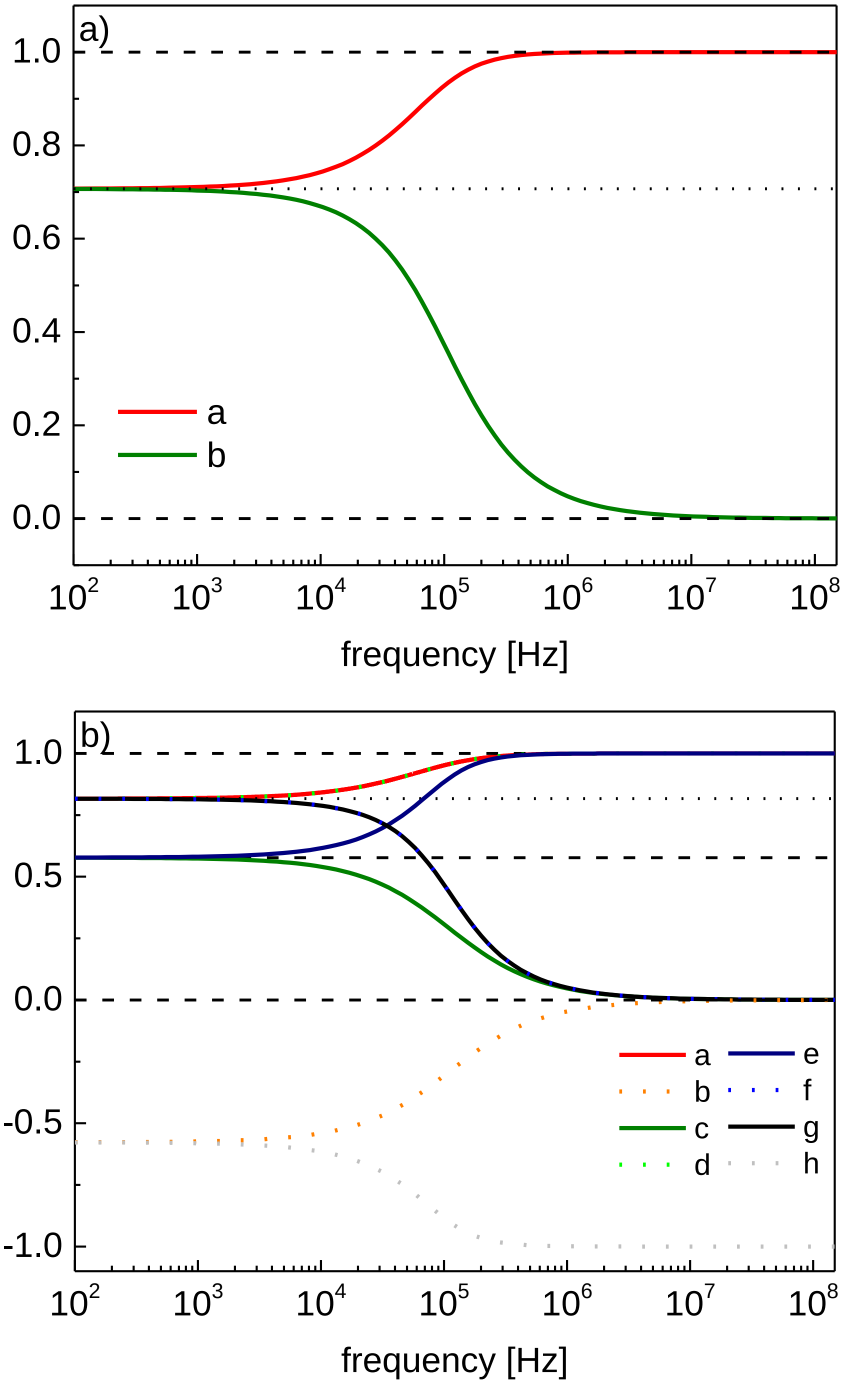

Figure 5.4. a) The coefficients a and b from Eq. 73 b) $a-h$ *from Eq. 74 (*$A_{iso} = 63$ *MHz for* ^{15}*N and* $A_{iso} = 45$ *MHz for* ^{14}*N) versus* ^{1}*H frequency.*

The coefficients reach in the low and high field limits the following values:

low field value	coefficients	high field value
	^{15}N	
$1/\sqrt{2}$	a	1
$1/\sqrt{2}$	b	0
	^{14}N	
$2/\sqrt{3}$	a	1
$-1/\sqrt{3}$	b	0
$1/\sqrt{3}$	c	0
$2/\sqrt{3}$	d	1
$1/\sqrt{3}$	e	1
$2/\sqrt{3}$	f	0
$2/\sqrt{3}$	g	0
$-1/\sqrt{3}$	h	1

Table 5.2. Values of the coefficients: a, b from Eq. 73 and $a-h$ from Eq. 74 in the low and high field limits.

Analogously, for the transition frequencies one obtains:

low field value	transition frequencies, ω_{ij}	high field value
	^{15}N	
A_{iso}	ω_{13}	ω_S
A_{iso}	ω_{23}	ω_S
A_{iso}	ω_{34}	0
0	ω_{12}	0
0	ω_{24}	ω_S
	^{14}N	
$3A_{iso}/2$	ω_{23}	ω_S
$3A_{iso}/2$	ω_{45}	ω_S
$3A_{iso}/2$	ω_{13}	ω_S
$3A_{iso}/2$	ω_{56}	0

$3A_{iso}/2$	ω_{25}	ω_S
$3A_{iso}/2$	ω_{34}	0
0	ω_{12}	0
0	ω_{46}	ω_S
0	ω_{24}	0
0	ω_{35}	0

Table 5.3. Values of the transition frequencies, ω_{ij}, from Eqs. 73 and 74 in the low and high field limits.

In consequence, the proton spin relaxation rate, $R_1^{par}(\omega_H)$, for the case of ^{15}N is given in the low field range by the expression [15,32]:

$$R_1^{par}(\omega_H \to 0) \cong K_{DD}[5J(0) + 5J(A_{iso})] \tag{76}$$

while for the case of ^{14}N one gets [32]:

$$R_1^{par}(\omega_H \to 0) \cong K_{DD}\left[\frac{110}{27}J(0) + \frac{160}{27}J\left(\frac{3A_{iso}}{2}\right)\right]. \tag{78}$$

In the high field range, the expressions of Eqs. 73 and 74 for the cases of ^{15}N and ^{14}N, respectively, converge to the well-known Solomon-Bloembergen-Morgan equation [15,32]:

$$R_1^{par}(\omega_H \to \infty) \cong K_{DD}[3J(\omega_H) + 7J(\omega_S)] \tag{77}$$

5.3. Origin of local relaxation enhancement

One can see in Fig. 5.3 that for slow dynamics the relaxation rate, $R_1^{par}(\omega_H)$, tends to form a maximum (a local relaxation enhancement) that is associated with the terms represented by the dashed-dotted lines. The apperance of the maximum is a result of an interplay between the spectral densities, $J(\omega_H)$, decreasing with increasing frequency and the corresponding prefactors that increase with increasing frequency. The effect is shown in Fig 5.5 a), b) for the cases of ^{15}N and ^{14}N, respectively (the values of the spectral density have been normalized to 1 in the low field limit).

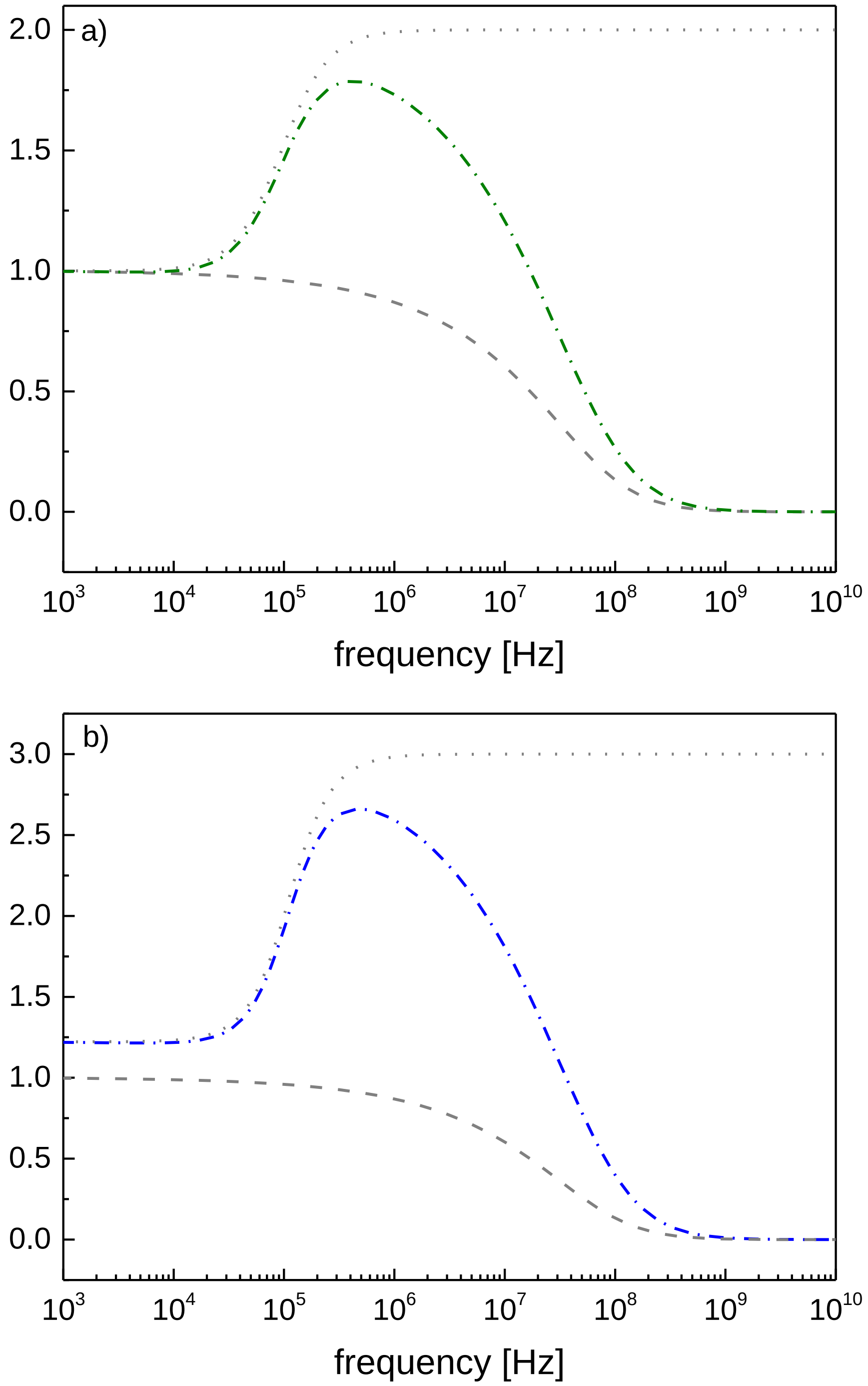

Figure 5.5. a) Dashed-dotted green line - $\left[1+\left(a^2-b^2\right)^2\right]J\left(\omega_H\right)$*; dashed grey line - spectral density* $J\left(\omega_H\right)$*; dotted grey line - weight factor of the spectral density* $\left[1+\left(a^2-b^2\right)^2\right]$*; b) dashed-dotted blue line* $\left[1+\frac{\left(a^2-b^2\right)^2}{2}+\frac{\left(c^2-d^2\right)^2}{2}+\frac{\left(e^2-f^2\right)^2}{2}+\frac{\left(g^2-h^2\right)^2}{2}\right]J\left(\omega_H\right)$*; dashed grey line – spectral density* $J\left(\omega_H\right)$*; dotted grey line – weight factor of the spectral density* $\left[\frac{1+\left(a^2-b^2\right)^2}{2}+\frac{\left(c^2-d^2\right)^2}{2}+\frac{\left(e^2-f^2\right)^2}{2}+\frac{\left(g^2-h^2\right)^2}{2}\right]$*;* $\tau_{trans}=4*10^{-8}\,s$*,* $d_{IS}=4\,Å$*,* $D_{12}=4.0*10^{-12}\ m/s^2$*.*

The relaxation dispersion profile, $R_1^{par}(\omega_H)$, being a sum of the term shown in Fig. 5.5 and the other terms present in Eqs. 73 and 74 (^{15}N and ^{14}N cases, respectively) takes the shape presented in Fig. 5.6 a), b) for the cases of ^{15}N and ^{14}N containing radicals, respectively. The relaxation maxima are well pronounced.

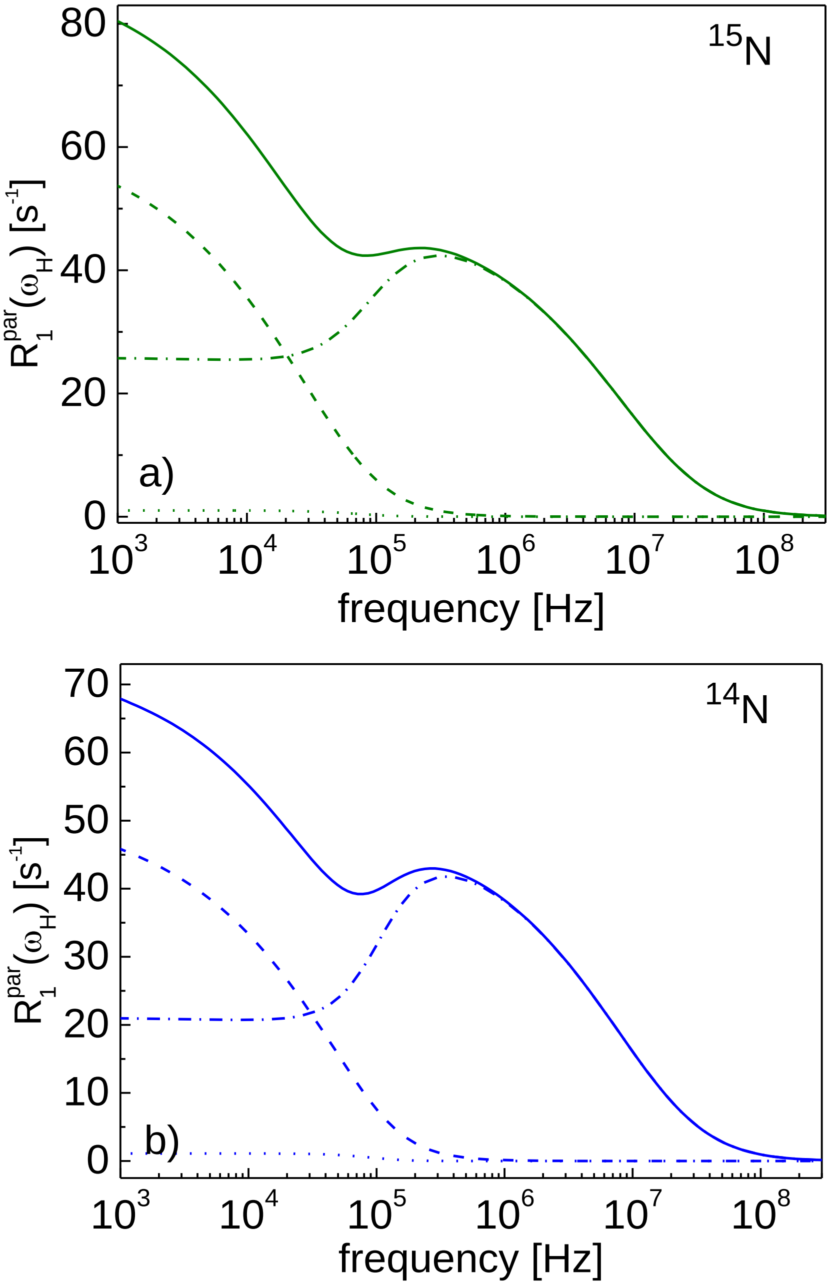

Figure 5.6. ^{1}H relaxation dispersion, $R_1^{par}(\omega_H)$, for a) ^{15}N and b) ^{14}N. Solid green and blue lines - $R_1^{par}(\omega_H)$ according to Eqs. 73 and 74, respectively. Dashed-dotted lines – the terms: $K_{DD}R_1^{15,I}(\omega_H)$ for ^{15}N and $K_{DD}R_1^{14,I}(\omega_H)$ for ^{14}N; dashed lines - $K_{DD}R_1^{15,III}(\omega_H)$ for ^{15}N and $K_{DD}\left(R_1^{14,III}(\omega_H)+R_1^{14,IV}(\omega_H)\right)$ for ^{14}N; dotted lines - $K_{DD}R_1^{15,II}(\omega_H)$ for ^{15}N and $K_{DD}R_1^{14,II}(\omega_H)$ for ^{14}N. ($\tau_{trans}=4*10^{-8}\,s$, $d_{IS}=4\text{Å}$, $D_{12}=4.0*10^{-12}$ m/s^2).

5.4. Comparison with “classical” relaxation theory

It is interesting to discuss in more details the influence of the hyperfine coupling between the electron and nitrogen spins on the ^{1}H relaxation.

In Fig. 5.7 a), b) the ratio between the relaxation rates $R_1^{par}(\omega_H)$ calculated according to Eqs. 73 and 74 (i.e. including the isotropic hyperfine coupling) and the relaxation rates $R_1^{par,SBM}(\omega_H)$ calculated using the SBM formula (Eq. 56, here the superscript “SBM” is added to distinguish it from the results obtained by Eqs. 73 and 74) is shown for the cases of ^{15}N and ^{14}N containing radicals.

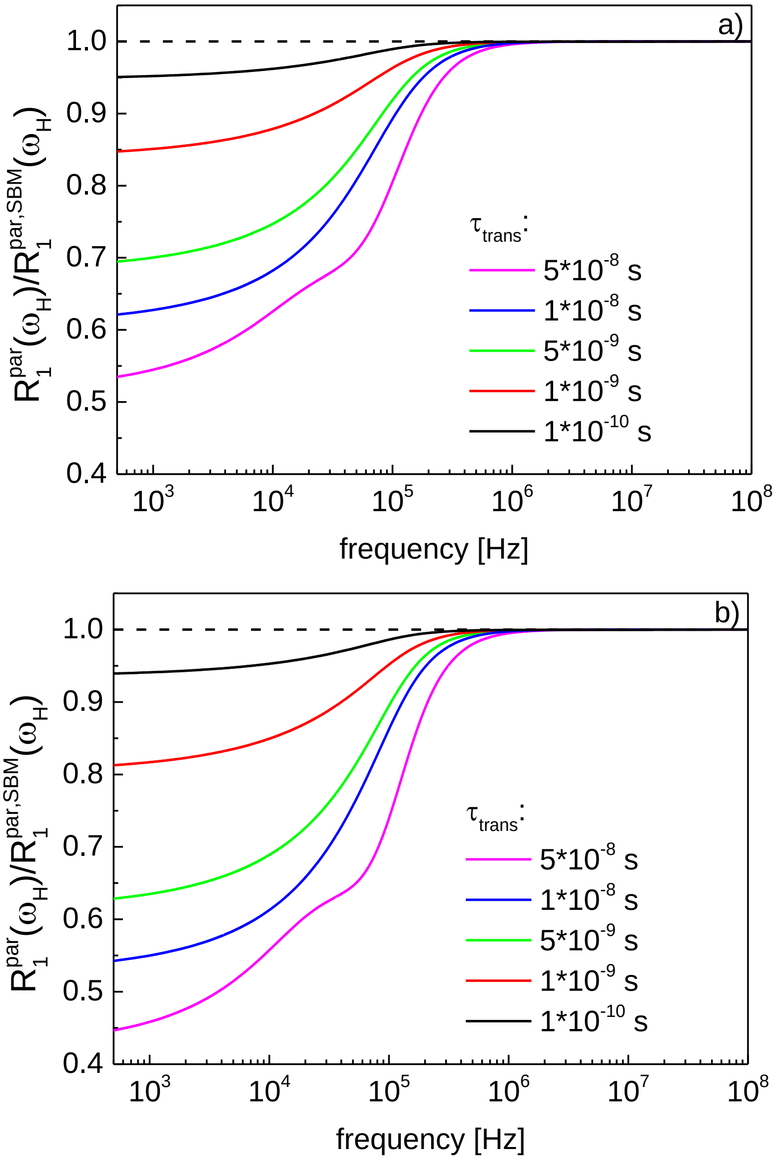

Figure 5.7. Ratio between $R_1^{par}(\omega_H)$ *calculated according to Eq. 73 and 74 and predictions of the SBM theory (*$R_1^{par,SBM}(\omega_H)$ *given by Eq. 56) for a)* ^{15}*N and b)* ^{14}*N (the value of 1 is marked with dashed black horizontal line).*

As at higher frequencies the energy level structure is mostly defined by the Zeeman interaction, the influence of the hyperfine coupling is less important and eventually the ratio reaches one (i.e. Eqs. 73 and 74 converge to the SBM expression). At low frequencies the relaxation rates calculated according to Eqs. 73 and 74 are smaler than those predicted by the SBM formula. This is a consequence of the energy level structure of the electron spin beeing affected (even determined at very low frequencies) by the isotropic hyperfine coupling. This effect is more pronounced for slower dynamics when the details of the energy level structure are more visible (in the extreme narrowing condition $\omega\tau_c << 1$ the role of the isotropic hyperfine coupling is minor).

To illustrate the differences in the effects of the hyperfine coupling for ^{15}N and ^{14}N isotopes, the ratio $R_1^{par,{}^{14}\mathrm{N}}(\omega_H)/R_1^{par,{}^{15}\mathrm{N}}(\omega_H)$ versus frequency is shown in Fig. 5.8 for different translational correlation times, τ_{trans}. The ratio is smaller than one – i.e. the ^{1}H relaxation in solutions of ^{14}N containing radicals is slower, except for the high frequency range when the relaxation rates become equal (and described by the SBM expression, Eq. 56).

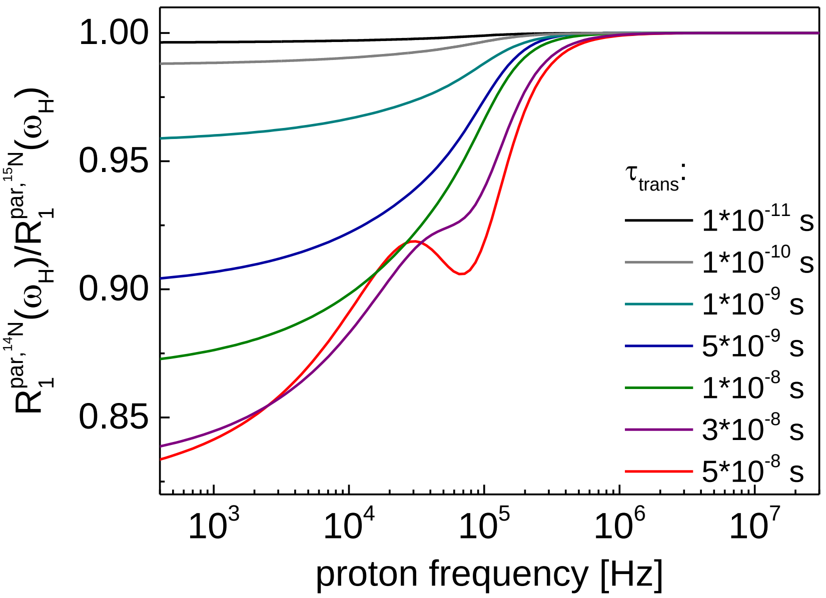

Figure 5.8. Ratio between $R_1^{par,{}^{14}\mathrm{N}}(\omega_H)/R_1^{par,{}^{15}\mathrm{N}}(\omega_H)$ *versus proton frequency for different values of the translational correlation time,* τ_{trans}.

The correlation times are in the range from water translational correlation time ($\tau_{trans} \approx 1*10^{-11}$s, [47]) to values somewhat longer than those characteristic of solvents of high viscosity (like glycerol or propylene glycol at low temperatures, [31-34,57]). For shorter correlation time the difference between the ^{1}H relaxation in the case of nitrogen isotopes is negligible. For longer correlation times the effect is clearly seen.

5.5. Electron spin relaxation

Electron spin relaxation acts as an additional source of modulations of the electron spin-proton spin dipole-dipole interaction. In the SBM expression (Eq. 56), the correlation time τ_c is replaced by the effective correlation time: $\tau_{c,eff}^{-1} = \tau_c^{-1} + R_i^e$.

The intermolecular spectral density can be modified in a similar way by replacing the factor $u^2\tau_{trans}^{-1}$ by $(u^2\tau_{trans}^{-1} + R_i^e)$ ($i = 1$ for $J(\omega_H)$ and $i = 2$ for $J(\omega_S)$) as follows [2,31-33] (the index ^{R} is added to distinguish from the spectral density presented in chapter 2, not including the electron spin relaxation):

$$J^R(\omega_H,\tau_{trans},R_1^e) = 72\frac{N_S}{d_{IS}^3}\int_0^\infty \frac{u^2}{81+9u^2-2u^4+u^6}\,\frac{(u^2+\tau_{trans}R_1^e)\tau_{trans}}{(u^2+\tau_{trans}R_1^e)^2+(\omega_H\tau_{trans})^2}\,du \qquad (79)$$

$$J^R(\omega_S,\tau_{trans},R_2^e) = 72\frac{N_S}{d_{IS}^3}\int_0^\infty \frac{u^2}{81+9u^2-2u^4+u^6}\,\frac{(u^2+\tau_{trans}R_2^e)\tau_{trans}}{(u^2+\tau_{trans}R_2^e)^2+(\omega_S\tau_{trans})^2}\,du \qquad (80)$$

The description of the electron spin relaxation becomes more complicated at lower fields when the SBM approach breaks down [2,31-33]. Here only the main concept of introducing the electron spin relaxation into the theory of the ^{1}H spin-lattice relaxation is briefly outlined. For the diagonal part of the matrix $[M]$ (except of the population block of the matrix), the following generalisation of the spectral densities has to be applied [2,31-33]:

$$J^R(\omega_{\alpha\alpha'},\tau_{trans},R^e_{\alpha\alpha'\alpha\alpha'}) = 72\frac{N_S}{d_{IS}^3}\int_0^\infty \frac{u^2}{81+9u^2-2u^4+u^6}\,\frac{(u^2+\tau_{trans}R^e_{\alpha\alpha'\alpha\alpha'})\tau_{trans}}{(u^2+\tau_{trans}R^e_{\alpha\alpha'\alpha\alpha'})^2+(\omega_H\tau_{trans})^2}\,du \qquad (81)$$

In Eq. 81 its is assumed that $\alpha = \alpha'$. For the population block of the matrix $[M]$ one obtains for the case of ^{15}N [31]:

$$\left[1+\left(a^2-b^2\right)^2\right]J^R(\omega_H,\tau_{trans}) = 72\frac{N_S}{d_{IS}^3}\int_0^\infty \frac{u^2}{81+9u^2-2u^4+u^6}\,\tilde{s}^R(u,\tau_{trans},\omega_H,R^e)\,du \qquad (82)$$

where $\tilde{s}^R(u,\tau_{trans},\omega_H,R^e)$ is given as a matrix product:

$$\tilde{s}^{R}(u,\tau_{trans},\omega_H,R^e)=\frac{1}{2}Re\left\{\left[S_0^1\right]^{+}\begin{bmatrix}\Lambda+R^e_{1111} & R^e_{1122} & R^e_{1133} & R^e_{1144}\\ R^e_{1122} & \Lambda+R^e_{2222} & R^e_{2233} & R^e_{2244}\\ R^e_{1133} & R^e_{2233} & \Lambda+R^e_{3333} & R^e_{3344}\\ R^e_{1144} & R^e_{2244} & R^e_{3344} & \Lambda+R^e_{4444}\end{bmatrix}^{-1}\left[S_0^1\right]\right\} \qquad (83)$$

R^e represents here a set of the electron spin relaxation rates $R^e_{\alpha\alpha'\alpha'}$; $\Lambda = i\omega_H + u^2/\tau_{trans}$. Analogously for the case of ^{14}N the equations take the form [31]:

$$\left[1+\frac{(a^2-b^2)^2}{2}+\frac{(c^2-d^2)^2}{2}+\frac{(e^2-f^2)^2}{2}+\frac{(g^2-h^2)^2}{2}\right]J^{R}(\omega_H,\tau_{trans})= \\ =72\frac{N_S}{d_{IS}^3}\int_0^{\infty}\frac{u^2}{81+9u^2-2u^4+u^6}\tilde{s}^{R}(u,\tau_{trans},\omega_H,R^e)du \qquad (84)$$

where:

$$\tilde{s}^{R}(u,\tau_{trans},\omega_I,R^e)=$$

$$\frac{1}{2}Re\left\{\left[S_0^1\right]^{+}\begin{bmatrix}\Lambda+R^e_{1111} & R^e_{1122} & R^e_{1133} & R^e_{1144} & R^e_{1155} & R^e_{1166}\\ R^e_{1122} & \Lambda+R^e_{2222} & R^e_{2233} & R^e_{2244} & R^e_{2255} & R^e_{2266}\\ R^e_{1133} & R^e_{2233} & \Lambda+R^e_{3333} & R^e_{3344} & R^e_{3355} & R^e_{3366}\\ R^e_{1144} & R^e_{2244} & R^e_{3344} & \Lambda+R^e_{4444} & R^e_{4455} & R^e_{4466}\\ R^e_{1155} & R^e_{2255} & R^e_{3355} & R^e_{4455} & \Lambda+R^e_{5555} & R^e_{5566}\\ R^e_{1166} & R^e_{2266} & R^e_{3366} & R^e_{4466} & R^e_{5566} & \Lambda+R^e_{6666}\end{bmatrix}^{-1}\left[S_0^1\right]\right\}. \qquad (85)$$

The electron spin relaxation is primarily caused by the anisotropic part of the electron spin - nitrogen spin hyperfine coupling modulated by the rotation of the paramagnetic molecule [17]. The individual relaxation rates $R^e_{\alpha\alpha'\alpha'}$ are calculated in terms of the Redfield relaxation formula, presented in Section 3.1, Eq. 45 [2,4,5,9]. The explicit expressions for the electron spin relaxation rates as linear combinations of the electron spin spectral densities are given in Ref. [31].

The electron spin spectral densities $J^A(\omega)$ are given as [31,57]:

$$J^A(\omega)=\left\{\frac{2}{3}\left[A_{zz}-\frac{1}{2}(A_{xx}+A_{yy})\right]^2+\frac{1}{2}(A_{xx}-A_{yy})^2\right\}\times J(\omega) \qquad (91)$$

where $J(\omega)$ is a spectral density describing the rotational motion of the radical molecule (it can be the Cole-Davidson spectral density, $J_{CD}(\omega)$, defined by Eq. 34 or simple Lorentz function, Eq. 32).

Fig. 5.9 shows a comparison of the ^{1}H spin-lattice relaxation dispersion profiles predicted by the SBM theory (Eq. 56), Eqs. 73 and 74 (for the ^{15}N and ^{14}N cases, respectively) taking into account the contribution of the isotropic part of the hyperfine coupling to the energy level structure of the electron spin, and predictions of the theory including both the isotropic and anisotropic part of the hyperfine coupling (i.e. the electron spin relaxation).

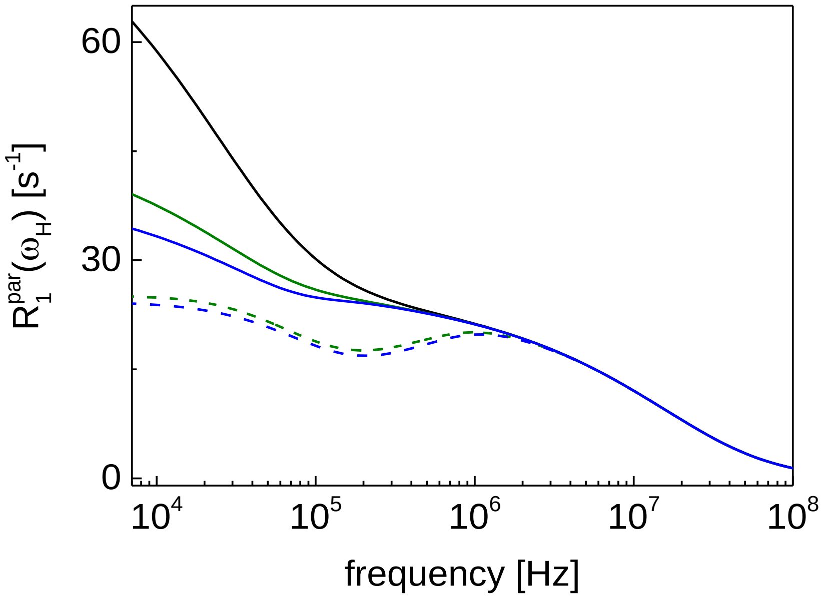

Figure 5.9. ^{1}H spin-lattice relaxation dispersion profiles predicted by the SBM theory (Eq. 56, solid black line), the theory including the isotropic part of the hyperfine coupling (solid green and blue line, Eq. 73 and 74, respectively) and the extended theory including the electron spin relaxation (dashed green and blue lines). $\tau_{trans} = 1*10^{-8}$ *s,* $d_{IS} = 4\,Å$, $D_{12} = 1.6*10^{-11}$ *m/s^2.*

The figure demonstrates that the electron spin relaxation leads to a further decrease of the ^{1}H spin-lattice relaxation in the low frequency range due to faster modulations of the proton spin-electron spin dipole-dipole coupling.

Fig. 5.10 shows the ratio between the predictions including the electron spin relaxation, and the effect of the isotropic part of the hyperfine coupling and the predictions neglecting the electron spin relaxation for different translational correlation times (the ratio between τ_{trans} and τ_R was set to 30, the tensor components of the hyperfine coupling yield $A_{xx} = 22.0\,\mathrm{MHz}$, $A_{yy} = 23.0\,\mathrm{MHz}$ and $A_{zz} = 142.0\,\mathrm{MHz}$ for ^{15}N and $A_{xx} = 15.4\,\mathrm{MHz}$, $A_{yy} = 16.1\,\mathrm{MHz}$ and $A_{zz} = 99.5\,\mathrm{MHz}$ for ^{14}N).

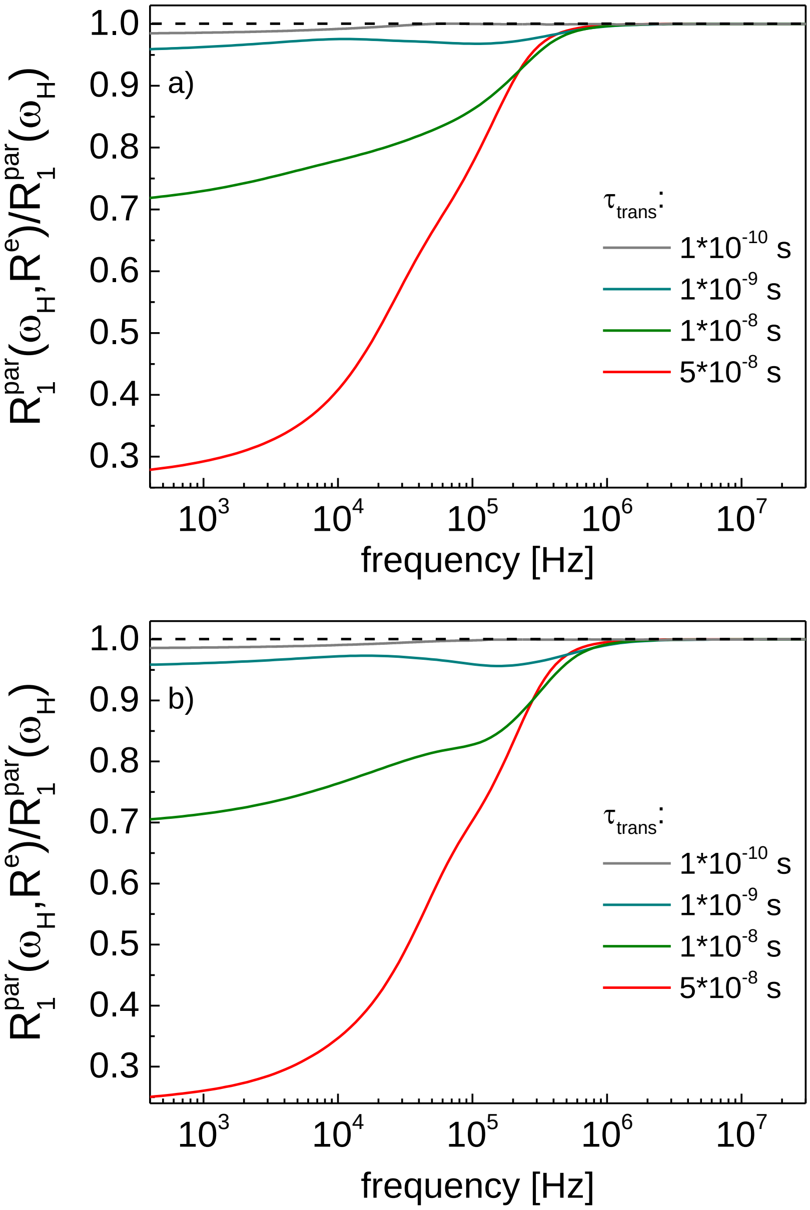

Figure 5.10. Ratio between $R_1^{par}(\omega_H)$ *obtained for a)* ^{15}N *and b)* ^{14}N *after including the influence of electron spin relaxation and obtained including only the effect of the isotropic part of the hyperfine coupling (the value of 1 is marked with black dashed horizontal line).*

The role of the electron spin relaxation is important when the electron spin relaxation time becomes of the same order as the translational correlation time. When the rotational (and hence translational) dynamics is fast, the electron spin relaxation is slow and then it can be neglected. For slower dynamics the electron spin relaxation is faster and then it becomes an important component of the fluctuations of the proton spin-electron spin dipole-dipole coupling (especially as the dynamics itself becomes slower).

Eventually, in Fig. 5.11 the ratio between the predictions including both the isotropic and anisotropic parts of the hyperfine coupling and the SBM theory is shown to demonstrate the inaccuracy of the latter approach.

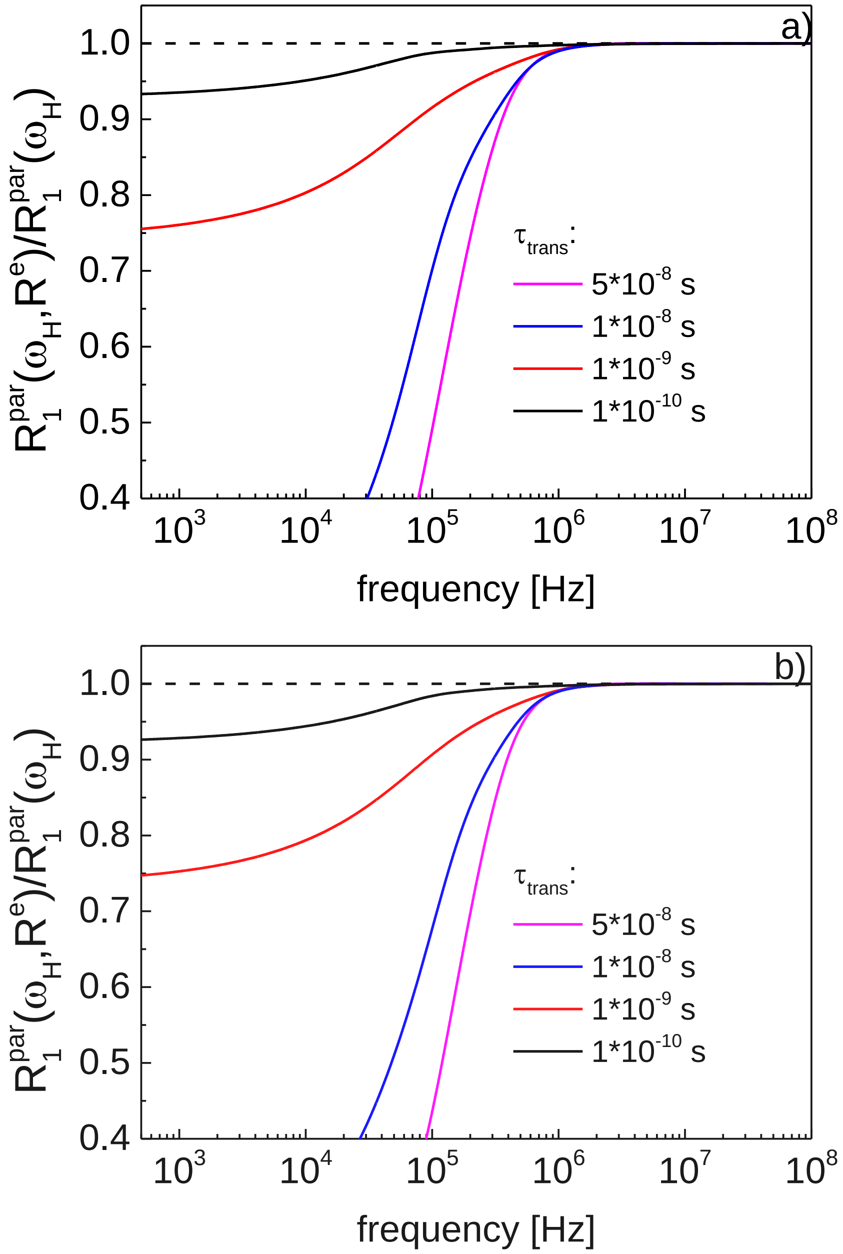

Figure 5.11. Ratio between $R_1^{par}(\omega_H, R^e)$ *including both the isotropic and anisotropic parts of the hyperfine interaction and values of* $R_1^{par}(\omega_H)$ *given by SBM formula (Eq.56) for a)* ^{15}*N and b)* ^{14}*N (the value of 1 is marked with black dashed horizontal line).*

At the end of this section, the ratio $R_1^{par,{}^{14}\mathrm{N}}(\omega_H)/R_1^{par,{}^{15}\mathrm{N}}(\omega_H)$ versus translational correlation time, τ_{trans}, and versus proton frequency is shown in Fig. 5.12 a) and b), respectively, to illustrate the differences in the influence of the isotropic hyperfine coupling resulting from ^{14}N and ^{15}N. The first simulations have been performed for several values of frequency. For 1 MHz the ratio is close to one even for very long correlation times. For progressively lower frequencies the deviations from unity increase especially for long correlation times. The changes are monotonic only for higher frequencies, but the ratio is always smaller than one. Also the ratio plotted versus frequency shows a non-monotonic behaviour at low and intermediate frequencies for longer τ_{trans}.

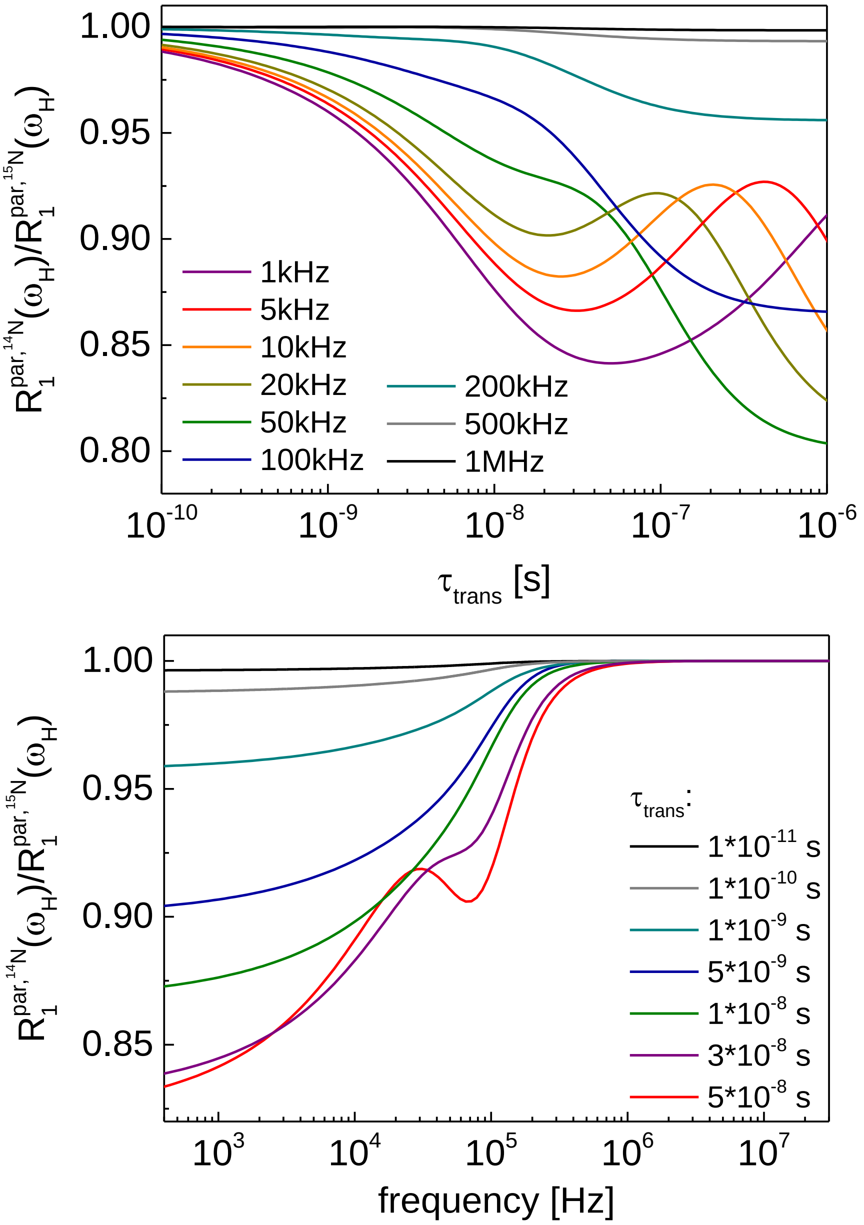

Figure 5.12. Ratio $R_1^{par,{}^{14}\mathrm{N}}(\omega_H)/R_1^{par,{}^{15}\mathrm{N}}(\omega_H)$ *versus a) translational correlation time,* τ_{trans} *and b) versus frequency;* $\tau_{trans}/\tau_R = 30$.

Similar comparison is presented in Fig. 5.13. The ratio $R_1^{par,{}^{14}\mathrm{N}}(\omega_H, R^e)/R_1^{par,{}^{15}\mathrm{N}}(\omega_H, R^e)$ after including the influence of the electron spin relaxation versus translational correlation time, τ_{trans}, and versus frequency is shown in Fig. 5.13 a) and b), respectively. The ratio does not change monotically over the entire range of correlation times and frequencies and it is always smaller than 1.

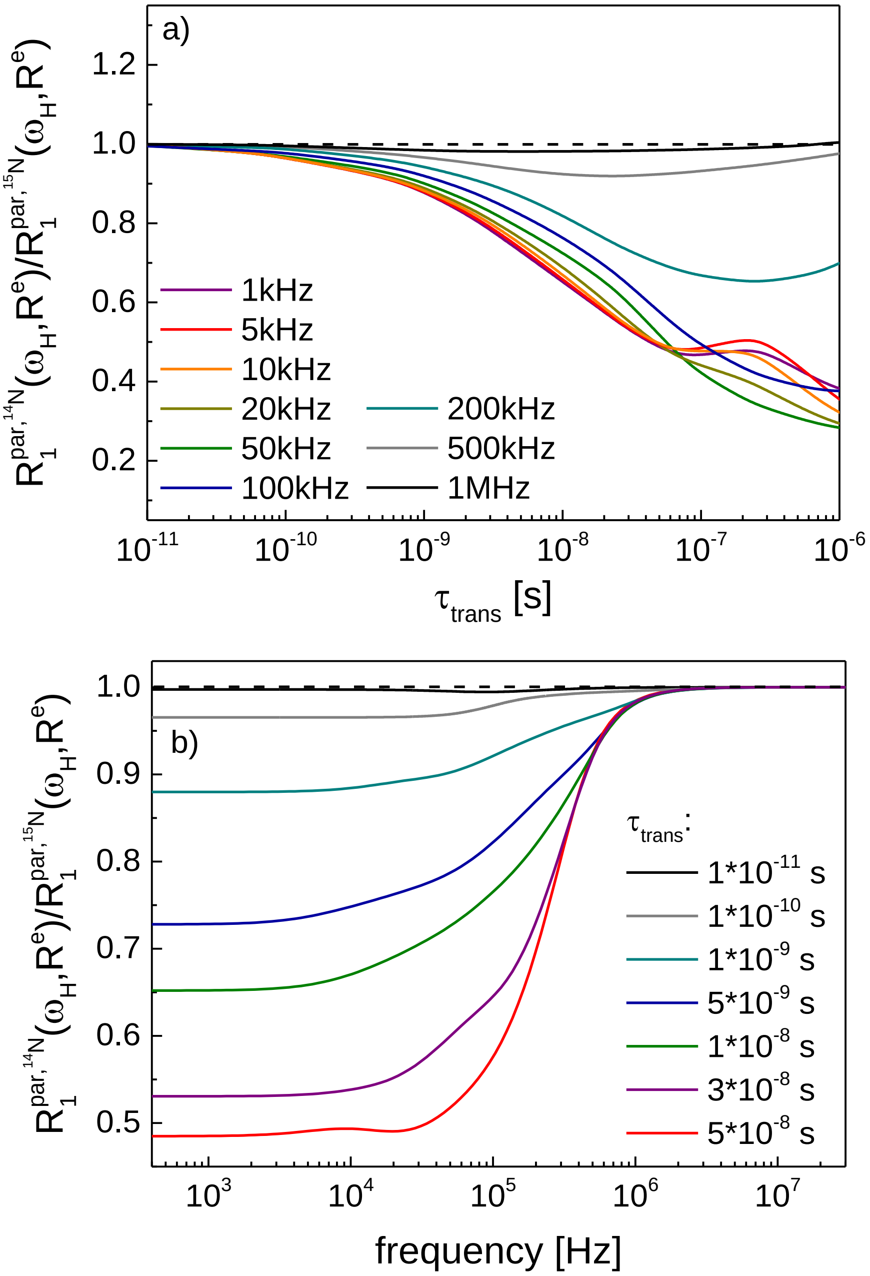

Figure 5.13. Ratio $R_1^{par,{}^{14}\mathrm{N}}(\omega_H, R^e)/R_1^{par,{}^{15}\mathrm{N}}(\omega_H, R^e)$ obtained after including the influence of electron spin relaxation: a) versus correlation time, τ_R, and b) versus frequency; the value of 1 is marked with black dashed horizontal line;

6. Experimental details

6.1. Principles of NMR Field Cycling relaxation experiments

Standard NMR relaxation experiments are performed at a single frequency. Fast Field Cycling (FFC) technology opens the possibility to perform relaxation experiments in a broad frequency (magnetic field) range, typically 10 kHz – 20 MHz (for ^{1}H). In consequence, by FFC NMR relaxometry one can detect motional processes across a huge range of time scales (from ms to ps) [48]. As already explained, frequency dependent relaxation studies have the potential to reveal the underlying mechanisms of molecular motion (not only its time scale). The dependence of spin-lattice relaxation rate on the resonance frequency is referred to as a relaxation dispersion profile.

A schematic representation of spin-lattice FFC experiments is shown in Fig. 6.1. Two sequences can be used: prepolarized sequence (*PP*) at low and intermediate magnetic field and non-polarized (*NP*) sequence at high magnetic field.

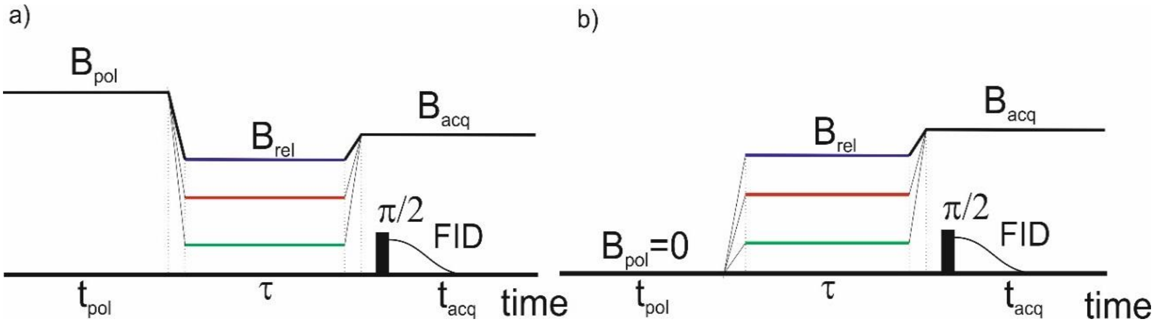

Figure 6.1. Schematic view of sequences used in spin-lattice relaxation FFC experiments: a) prepolarized (PP) sequence, b) non-polarized (NP)sequence.

The *PP* sequence consists of three steps:

1. **Polarization:** a relatively strong magnetic field, B_{pol}, (about 0.5 T) is applied for a time $t_{pol} \cong 5T_1$, i.e. until the magnetization reaches its equilibrium, M_{I0} (a value predicted by Boltzmann distribution at the field B_{pol}, Eq. 6).
2. **Relaxation:** the magnetic field is reduced to a lower value B_{rel} that is kept for a time τ. During the time τ the initial magnetization evolves (decreases) towards the new equilibrium. The decreasing is characterized by a spin-lattice relaxation time, T_1.

3. **Acquisition**: to meassure the value of the magnetization after time τ, $M_{Iz}(\tau)$, a $\pi/2$ pulse is applied and the amplitude of the resulting FID (Free Induction Decay) signal at the acquisition time, t_{acq}, is registered at a detection (acquisition) field, B_{acq}.

For every relaxation field, B_{rel}, this sequence is repeated with varying τ, leading to a magnetization curve, $M_{Iz}(\tau)$, schematically shown in Fig. 6.2.

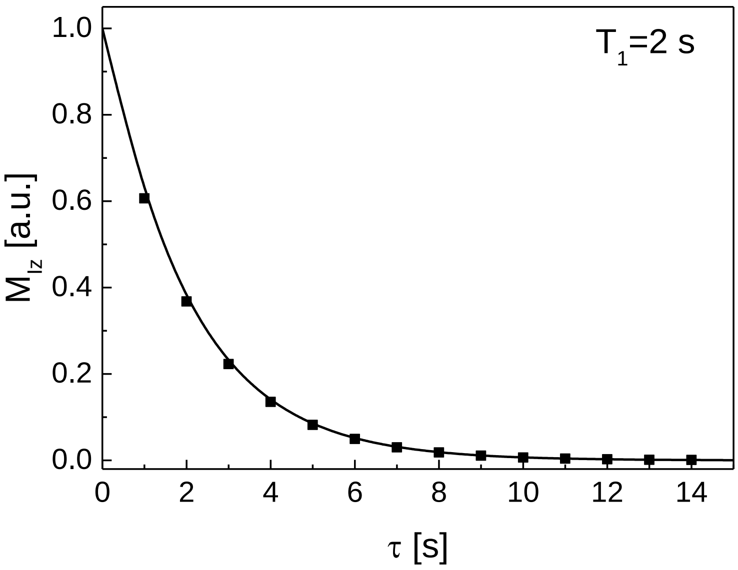

Figure 6.2. Schematic view of a magnetization curve $M_{Iz}(\tau)$ *obtained using PP sequence. The initial magnetization has been set to* $M_{I0}=1$.

When the magnetization curve turns out to be single-exponential (as the symulated curve shown in Fig.6.2), the spin-lattice relaxation time, T_1, can be obtained from the formula:

$$M_{Iz}(\tau)=M_{I0}e^{-\frac{\tau}{T_1}} \tag{121}$$

At a high relaxation field, *PP* sequence is replaced by *NP* sequence. The field at which this switching takes place depends on some technical parameters of the spectrometer. For *NP* sequence $B_{pol}=0$ (as indicated by the name) as shown in Fig. 6.1. b). This implies that the magnetization, M_{Iz}, increases from almost zero (at Earth magnetic field) to the equilibrium at B_{rel} (Fig. 6.3).

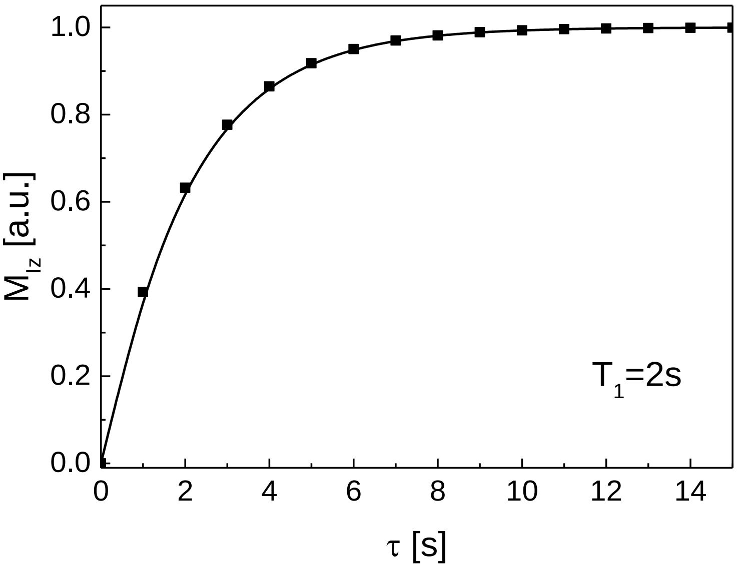

Figure 6.3. Schematic view of a magnetization curve $M_{Iz}(\tau)$ *obtained using NP sequence. The final magnetization has been set to* $M_{Iz}^{\infty}=1$.

In this case the evolution of the magnetization is described, provided it is single-exponential, by the expression:

$$M_{Iz}(\tau)=M_{Iz}^{\infty}-M_{I0}e^{-\frac{\tau}{T_1}} \tag{122}$$

6.2. Materials and sample preparation

^{1}H spin-lattice relaxation dispersion experiments have been performed for solutions of deuterated nitroxide radicals 4-oxo-TEMPO-d$_{16}$ (TEMPONE, 4-oxo-2,2,6,6-tetramethyl-1-piperidinyloxyl) containing ^{15}N and ^{14}N isotopes. The structure of the nitroxide radical molecule is shown in Fig. 6.4.

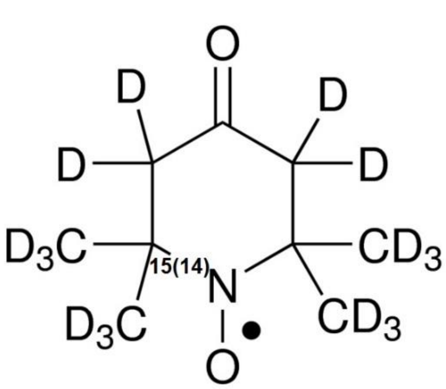

Figure 6.4. Sructure of 4-oxo-TEMPO-d$_{16}$*-*$^{15(14)}$*N. The unpaired electron is marked with a black dot.*

Deuterated compounds have been used to eliminate influence of methyl groups of the radicals on ^{1}H relaxation. As solvents decalin (decahydronaphtalene, mixture of *cis*- and *trans*-decalin isomers), glycerol (propane-1,2,3-triol) and propylene glycol (propane-1,2-diol) have been used. Structures of these compounds are shown in Fig. 6.5.

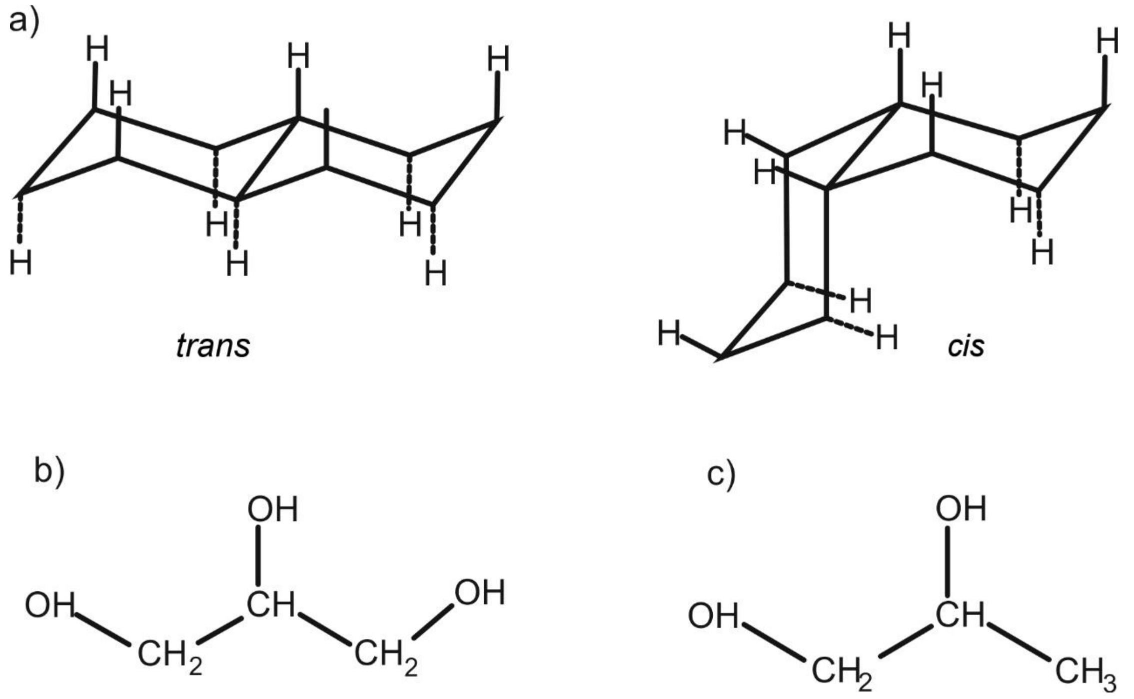

Figure 6.5. Structures of solvents molecules: a) decalin (cis- and trans- isomers) b) glycerol and c) propylene glycol.

These liquids undergo glass transition. The melting temperature of decalin is $T_m = 240\,\mathrm{K}$ for *cis* isomer and $T_m = 243\,\mathrm{K}$ for *trans* isomer [60]. The melting point of glycerol is $T_m = 290.9\,\mathrm{K}$ however one can cool it down to even lower temperatures avoiding freezing [61]. Propylene glycol melts at $T_m = 214\,\mathrm{K}$ [60].

All three liquids show considerably different viscosity: at 298 K the viscosities yields (3.355/2.107 mPa*s [62], 1412 mPa*s [63], 57.571 mPa*s [64] for decalin, glycerol and propylene glycol, respectively. That implies different time-scales of translational diffusion.

^{1}H spin – lattice relaxation rates have been measured for 4-oxo-TEMPO-d_{16}-^{15}N and 4-oxo-TEMPO-d_{16}-^{14}N dissolved in decalin, glycerol and propylene glycol in the temperature range 244 K - 308 K, 290 K - 363 K, 253 K - 298 K, respectively. The lowest temperature is limited by the melting points of the solvents and by the largest relaxation rate accesible to the spectrometer. The highest temperature is limited by the lack of the relaxation dispersion. ^{1}H relaxation dispersion profiles for pure solvents have been collected for the corresponding temperatures, if not available in the literature. To extract the relaxation contribution associated with proton-electron interactions the relaxation rates of the pure solvents were subtracted from the relaxation rates obtained for the corresponding solution. The following concentrations of the radicals have been used: 20 mM, 2.7 mM, 5 mM for decalin, glycerol and propylene glycol solutions, respectively.

Eventually, to confirm that the rates of the paramagnetically induced relaxation are proportional to the concentration of the radicals, additional measurements for 1 mM and 5 mM decalin solutions were performed.

To avoid oxidation and absorption of water all samples have been degassed and sealed in glass tubes. All chemicals (radicals and solvents) were purchased from Sigma-Aldrich.

7. Results and analysis

In this section ^{1}H spin-lattice relaxation data for the solutions (and pure solvents for comparison) listed in Section 6 are presented and quantitatively analized. A MATLAB software is used for the analysis; the source code is included in Appendix A.1.

7.1. Decalin solutions of 4-oxo-TEMPO-d$_{16}$-$^{15(14)}$N

^{1}H spin-lattice relaxation dispersion profiles for pure decalin are shown in Fig. 7.1 [65]. Frequncy in the axis description refers to ^{1}H resonance frequency ($\omega_H / 2\pi$) and it has this meaning for all figures in this section.

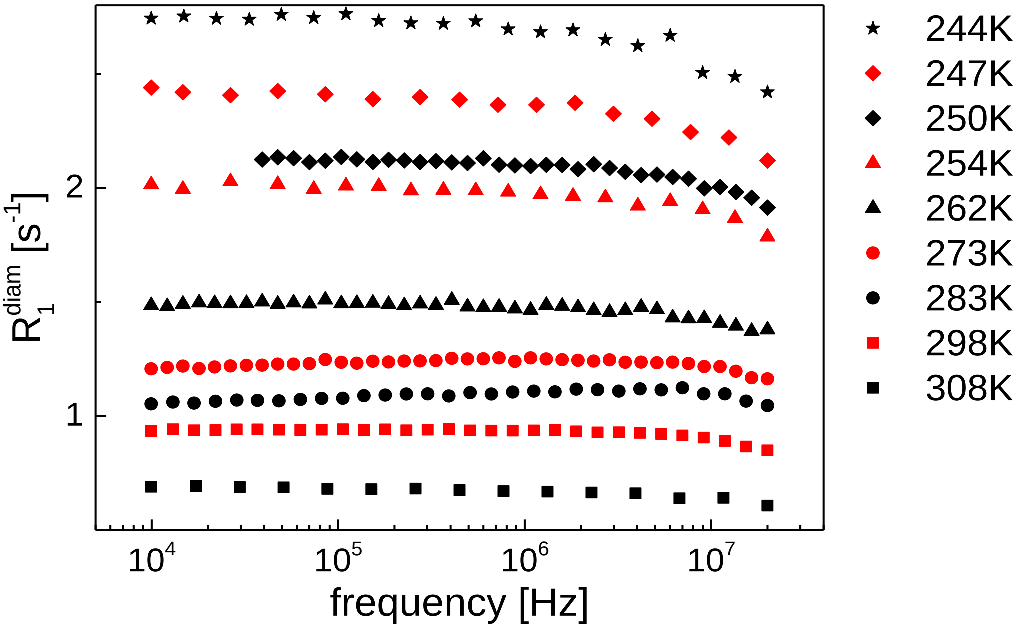

Figure 7.1. ^{1}H spin-lattice relaxation dispersion, $R_1^{diam}(\omega_H)$, for pure decalin (Ref. [65]). Reprinted with permission from D. Kruk et al., J. Chem. Phys. 140, 174504 (2014). Copyright 2014, AIP Publishing LLC.

The dispersion of the ^{1}H spin-lattice relaxation rates, $R_1^{diam}(\omega_H)$, is small due to fast dynamics of decalin. The relaxation is single exponential. Fig. 7.2 a) and b) shows time dependences of the proton magnetization in arbitrary units measured at 244 K and 308 K for the highest and lowest frequencies (20 MHz and 10 kHz, respectively).

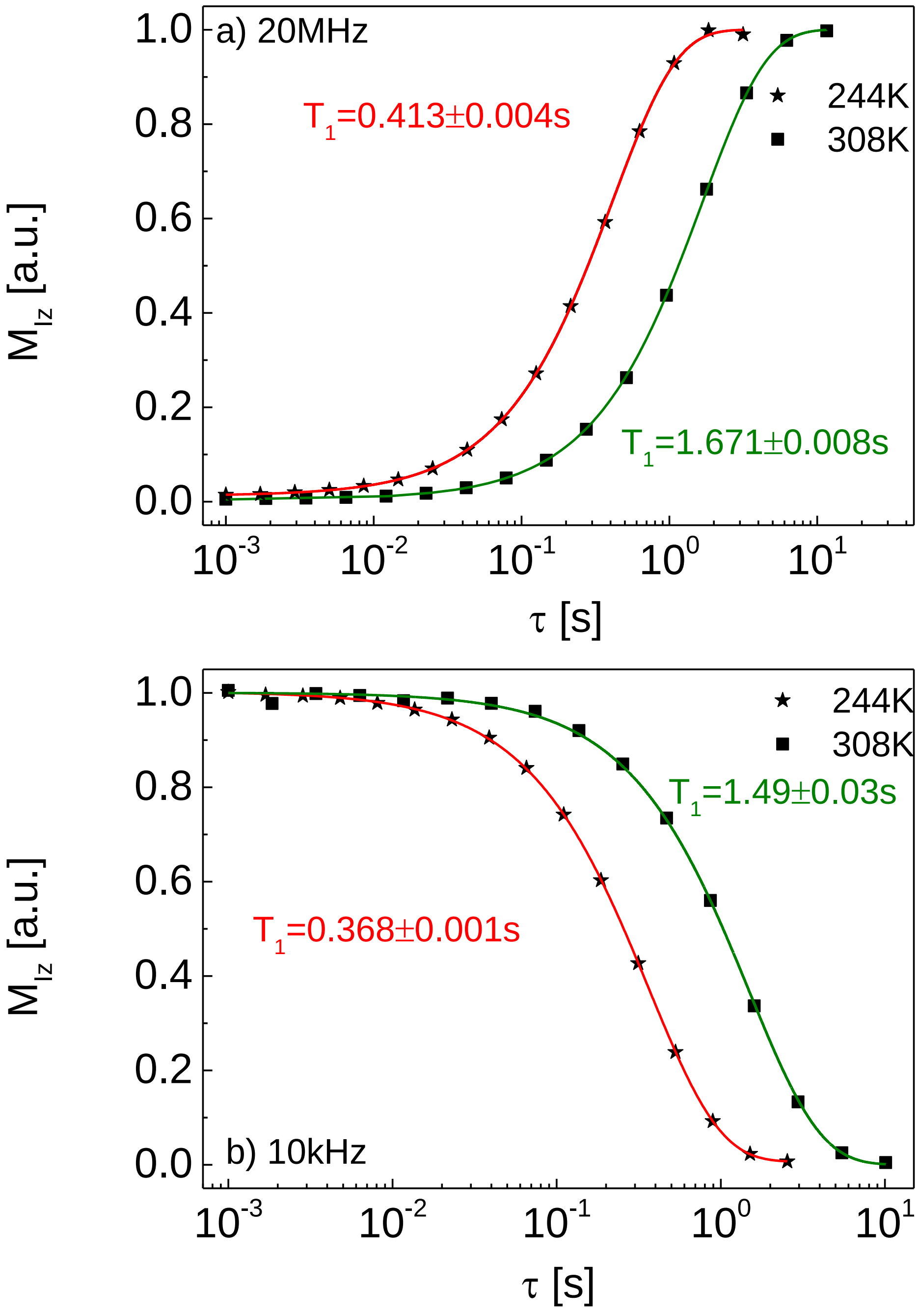

Figure 7.2. ^{1}H magnetization versus time for pure decalin obtained applying a) NP sequence at 20 MHz and by b) PP sequence at 10 kHz. Solid lines show single-exponential fits.

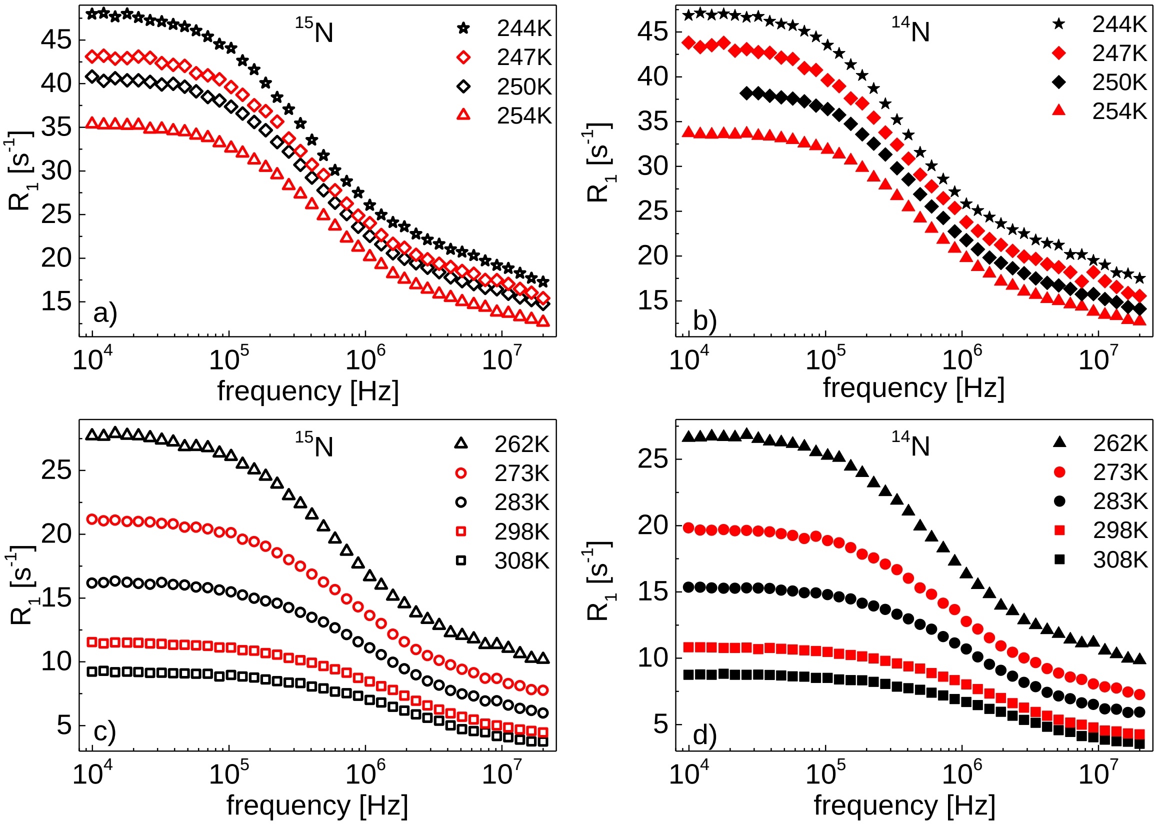

Figure 7.3. ^{1}H spin-lattice relaxation dispersion profiles, $R_1(\omega_H)$, for decalin solutions of a), c) 4-oxo-TEMPO-d_{16}-^{15}N and b), d) 4-oxo-TEMPO-d_{16}-^{14}N for 20 mM concentration of radicals.

In Fig. 7.3 ^{1}H spin-lattice relaxation dispersion profiles for decalin solutions of 4-oxo-TEMPO-d_{16}-^{15}N (left part) and 4-oxo-TEMPO-d_{16}-^{14}N (right part) are shown [32]. The relaxation is single exponential also for the paramagnetic solutions (see Fig. 7.4 a), b), c) and d)). Comparing Fig. 7.1 and Fig. 7.3 one can clearly see that the relaxation rates for the paramagnetic solutions are much larger (the relaxation is much faster).

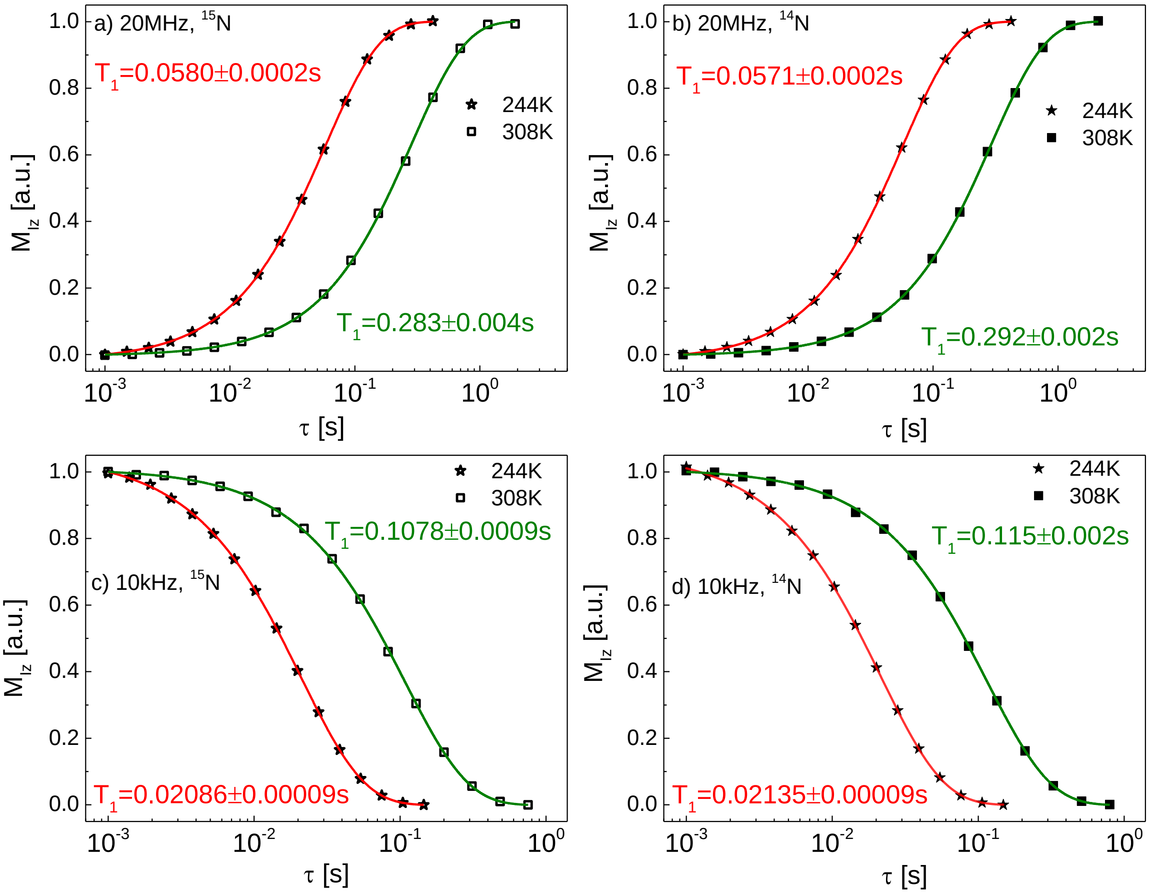

Figure 7.4. ^{1}H magnetization (in arbitrary units) versus time for 20 mM decalin solutions of 4-oxo-TEMPO-d$_{16}$-^{15}N (left) and 4-oxo-TEMPO-d$_{16}$-^{14}N (right) obtained by a), b) NP sequence at 20 MHz and c), d) PP sequence at 10 kHz. Solid red and green lines show single-exponential fits for the lowest and highest temperatures, respectively.

The relaxation rates $R_1^{par}(\omega_H)$ have been determined by subtracting the diamagnetic contribution $R_1^{diam}(\omega_H)$ (shown in Fig. 7.1) from the total relaxation rate, $R_1(\omega_H)$ (Fig. 7.3, Eq. 63). According to the theory (Eqs. 73 and 74), the rates of the ^{1}H spin-lattice relaxation induced by dipolar couplings of protons with paramagnetic molecules are proportional to the concentration, N_S, of the last species. This has been experimentally confirmed. As said in Section 6, ^{1}H spin-lattice relaxation rates at 20 MHz and 6 MHz have been measured for three different concentrations of 4-oxo-TEMPO-d$_{16}$-^{14}N in decalin (the full relaxation dispersion profile was not collected due to long relaxation times for the low concentration of the paramagnetic molecules). The values obtained after subtracting the diamagnetic contribution are presented in Fig. 7.5. It is clearly seen that the relaxation rates $R_1^{par}(\omega_H)$ linearly change with the concentration of the radical.

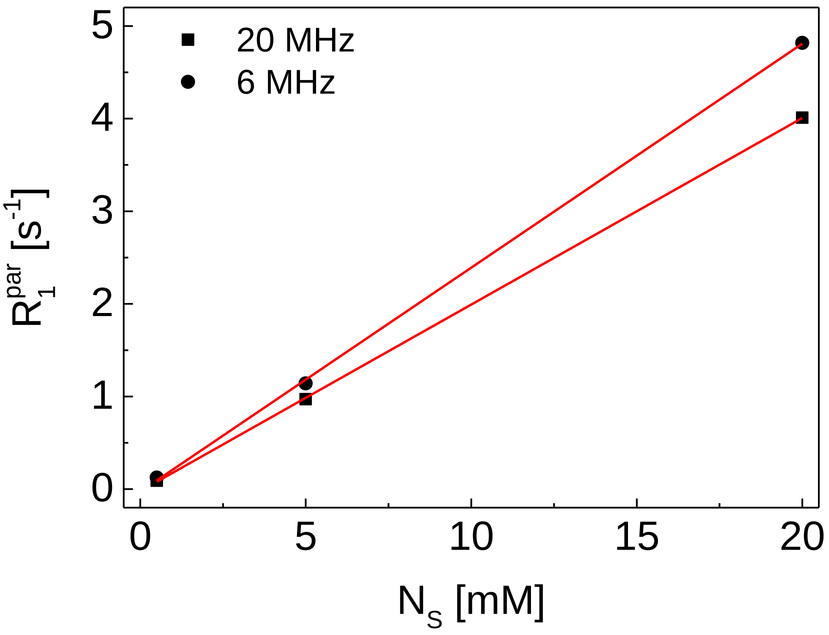

Figure 7.5. Experimental values of ^{1}H relaxation rates originating from proton-electron dipolar interactions, $R_1^{par}(\omega_H)$, in decalin solutions of 4-oxo-TEMPO-d_{16}-^{14}N versus the number N_S of the radical molecules per unit volume.

Then the $R_1^{par}(\omega_H)$ relaxation rates were normalized to 1 mM concentration of the radicals. The normalized relaxation rates, $R_1^{norm}(\omega_H)$, are shown in Fig. 7.6 a)-d). From now on, when reffering to the equations presented in previous sections it is assumed that the concentration of the electron spins is 1 mM.

The figures contain corresponding theoretical fits. Before explaining the fitting strategy one should notice that for decalin the ^{1}H spin-lattice relaxation dispersion profiles for the cases of ^{15}N and ^{14}N containing radicals almost coincide as predicted for fast dynamics by the theory (Eq. 73 and 74).

The relaxation rate, $R_1^{norm}(\omega_H)$, depends on six parameters: the distance of closest approach, d_{IS}, translational correlation, τ_{trans}, the parameter f describing the 'effective' influence of the rotational motion on the modulations of the proton spin-electron spin dipolar interactons, the rotational correlation time, τ_R, the stretching parameter, β, and the isotropic hyperfine coupling, A_{iso} (see Eqs. 73 and 74 for ^{15}N and ^{14}N cases, respectively).

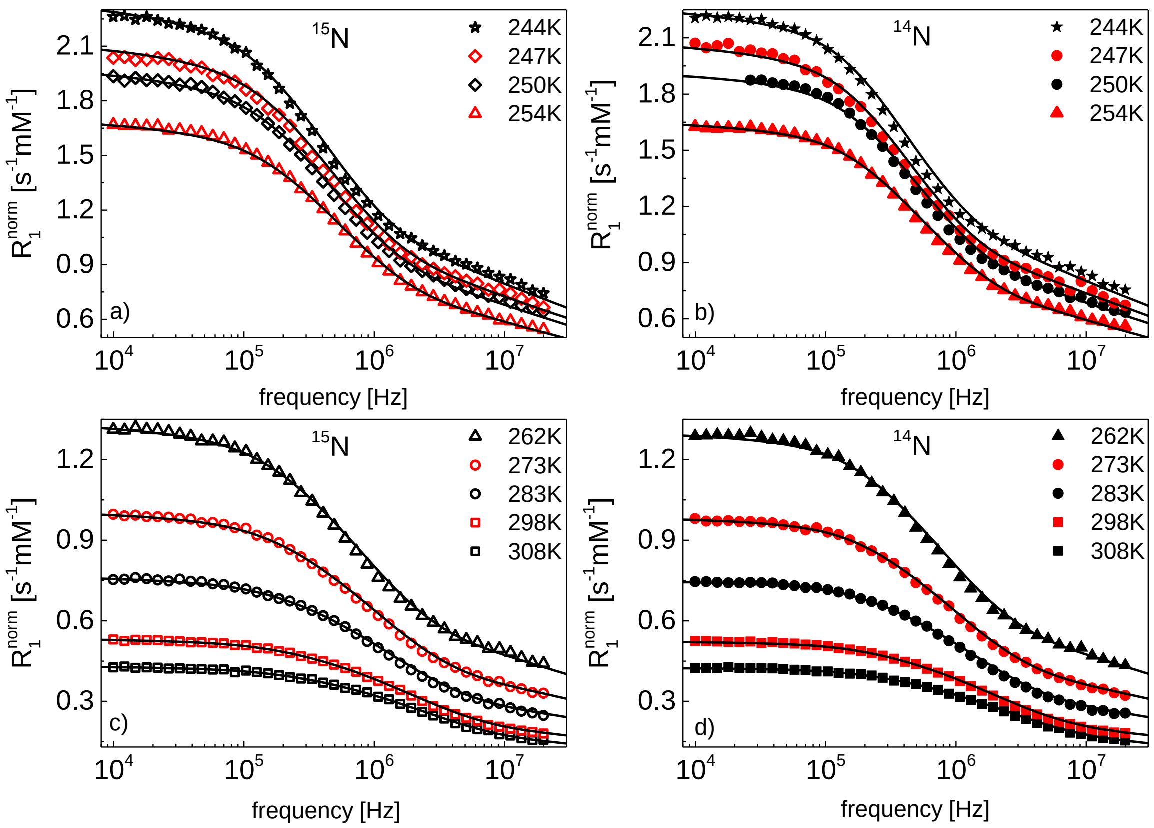

Figure 7.6. Normalized (to 1 mM concentration) ^{1}*H spin-lattice relaxation dispersion profiles,* $R_1^{norm}(\omega_H)$*, for decalin solutions of a), c) 4-oxo-TEMPO-d*$_{16}$*-*^{15}*N and b), d) 4-oxo-TEMPO-d*$_{16}$*-*^{14}*N with corresponding fits in terms of Eqs. 73 and 74, respectively (Ref. [32]). Adopted with permission from D. Kruk et al., J. Chem. Phys. 137, 044512 (2012). Copyright 2012, AIP Publishing LLC.*

The isotropic hyperfine coupling constant, A_{iso}, has been set to the value of $A_{iso} = 44\,\mathrm{MHz}$ (^{14}N) and $A_{iso} = 62\,\mathrm{MHz}$ (^{15}N) taken from literature [58]. In [58] the A_{iso} values have been determined by means of ESR (Electron Spin Resonance) experiments for 4-oxo-TEMPO-d$_{16}$ diluted in a mixture of glycerol and water. The ratio $A_{iso}(^{15}\mathrm{N})/A_{iso}(^{14}\mathrm{N})$ corresponds to the ratio between gyromagnetic factors $\gamma(^{15}\mathrm{N})/\gamma(^{14}\mathrm{N})$ that yields 1.4. The value of the stretching parameter, β, has been fixed to the literature value of 0.53 for pure decalin [66]. This reduces the number of the adjustable parameters to four: d_{IS}, τ_{trans}, f and τ_R.

The rotational motion of the paramagnetic molecules influences the proton spin relaxation when the dynamics of the system is relatively slow. Therefore, the rotational contribution to the modulations of the proton spin-electron spin dipole-dipole coupling (Eq. 39) has only been taken into account for the four lowest temperatures (244 K, 247 K, 250 K and 254 K). The proton relaxation data for both cases (^{15}N and ^{14}N containing radicals) have been fitted simultaneously for each temperature using Eqs. 73 and 74, respectively, in terms of the same parameters (the dynamics does not depend on the nitrogen isotope). The value of the distance of closest approach, d_{IS}, obtained for the individual teperatures has varied between 4.97 Å – 5.09 Å. As this range is quite narrow it has been fixed to $d_{IS} = 5.05$ Å and kept temperature independent. The f value has been ranging from 1.77 to 1.82 and finally it has been fixed to $f = 1.8$ for 244 K, 247 K, 250 K and 254 K; at higher temperatures $f = 0$ (the rotational contribution is neglected). With this assumptions the analysis has been repeated with only two adjustable parameters: τ_R and τ_{trans} (the same for ^{15}N and ^{14}N cases) at the lower temperatures. For the higher temperatures only the translational correlation time has been fitted. This fitting strategy is described in [32].

The rotational correlation times obtained from the current analysis are included into Table 7.1. and compared in Fig. 7.7 with literature values from ESR studies [66,67]. They stay in good agreement, however one should remember that the rotational correlation time, τ_R, obtained from the current analysis describes the combined effect of the rotational dynamics of the solvent and radical molecules (both interacting spins: the electron - S and nuclear - I are not placed in the center of the molecule), while the correlation time obtained from ESR experiments describes the rotational motion of only the radical molecule. The ratio of τ_{trans}/τ_R is much higher than theoretically predicted by the hydrodynamic model: $\tau_{trans}/\tau_R = 9$ [9] and it yields about $\tau_{trans}/\tau_R \approx 70$. This effect has also been reported for other liquids [34].

T [K]	τ_R [s]	τ_{trans} [s]	d_{IS} [Å]	f	$x = \frac{\tau_{trans}}{\tau_R}$	D_{12} [m^2/s]
308	-	$2.01*10^{-10}$ (1.9%)	5.05	1.8	-	$1.24*10^{-9}$ (4.4%)
298	-	$2.57*10^{-10}$ (1.6%)	5.05	1.8	-	$9.86*10^{-10}$ (4.3%)
283	-	$3.70*10^{-10}$ (2.0%)	5.05	1.8	-	$6.79*10^{-10}$ (4.5%)
273	-	$5.05*10^{-10}$ (1.7%)	5.05	1.8	-	$5.04*10^{-10}$ (4.4%)
262	-	$6.41**10^{-10}$ (3.4%)	5.05	1.8	-	$3.82*10^{-10}$ (5.3%)
254	$1.30*10^{-11}$ (27%)	$9.48*10^{-10}$ (3.2%)	5.05	1.8	73	$2.79*10^{-10}$ (5.1%)
250	$1.43*10^{-11}$ (23%)	$1.06*10^{-9}$ (2.7%)	5.05	1.8	74	$2.42*10^{-10}$ (4.8%)
247	$1.66*10^{-11}$ (20%)	$1.19*10^{-9}$ (2.3%)	5.05	1.8	72	$2.20*10^{-10}$ (4.6%)
244	$1.91*10^{-11}$(18%)	$1.32*10^{-9}$ (2.3%)	5.05	1.8	69	$1.99*10^{-10}$ (4.6%)

Table 7.1. Rotational and translational diffusion parameters for decalin solutions of 4-oxo-TEMPO-d_{16} *(*^{14}*N and* ^{15}*N), Ref. [32]. The accuracy of the parameters is given in % (the error analysis is described in Appendix A.2). Results obtained neglecting the rotational contribution are separated with red horizontal line. Adopted with permission from D. Kruk et al., J. Chem. Phys. 137, 044512 (2012). Copyright 2012, AIP Publishing LLC.*

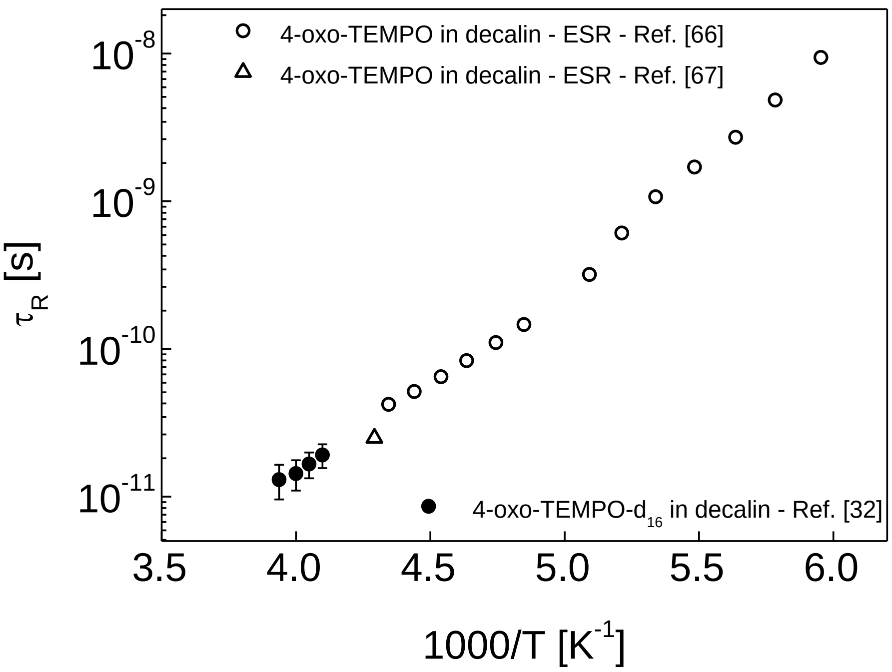

Figure 7.7. Rotational correlation times, τ_R, for solution of 4-oxo-TEMPO-d_{16} in decalin (current analysis described in Ref. [32]) compared with the literature data (Refs. [66,67]). Adopted with permission from D. Kruk et al., J. Chem. Phys. 137, 044512 (2012). Copyright 2012, AIP Publishing LLC.

In Fig. 7.8 relative diffusion coefficients, D_{12}, for decalin and radical molecules (Table 7.1) calculated from the relation $D_{12} = d_{IS}^2 / \tau_{trans}$ are compared with literature data obtained by means of Pulse Field Gradient (PFG) diffusometry [68]. As relaxation data give relative diffusion coefficients, while self-diffusion coefficients are meassured by PFG diffusometry, the results from literature were multiplied by factor 2 ($D_{12} = 2D$ for identical molecules; D - self diffusion coefficient). In the present experiments a mixture of *cis*- and *trans*-decalin isomers was used (the relative diffusion coefficients for pure *cis*- and *trans*-decalin are marked in Fig. 7.8 with full and open orange diamonds, respectively). The values of D_{12} obtained for solutions of nitroxide radicals are in good agreement with the values obtained by means of PFG diffusometry.

At this point it is worth stressing that for paramagnetic solutions the relaxation dispersion is stronger than for pure diamagnetic solvent (it is so due to the contribution of spectral densities taken at frequencies close to that of electron spin frequency, $(\omega_S \pm \omega_H) \cong \omega_S$, to $R_1^{par}(\omega_H)$ as explained in Section 3). Thus, the NMR relaxometry gives for liquids containing paramagnetic centres the possibility to investigate very fast dynamics even when the proton relaxation of the corresponding diamagnetic system is already frequency independent.

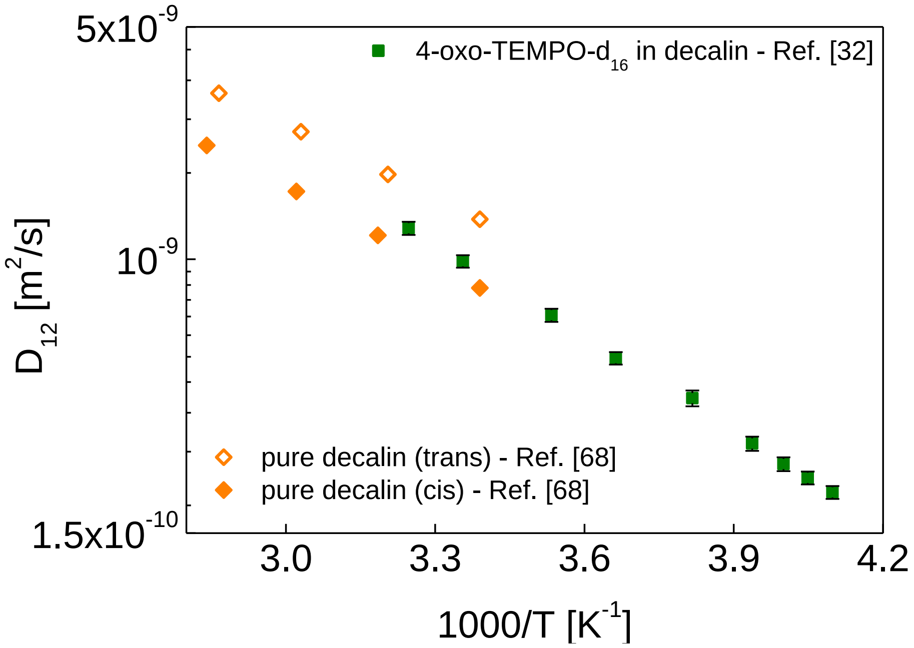

Figure 7.8. Relative translation diffusion coefficient, D_{12}*, for decalin solution of 4-oxo-TEMPO-d*$_{16}$ *(*^{15}*N,* ^{14}*N) obtained from current analysis of* ^{1}*H spin-lattice relaxation dispersion profiles (described in Ref. [32]) compared with literature values (open orange diamonds - trans-decalin, Ref. [68]; full orange diamonds – cis-decalin, Ref. [68]); Adopted with permission from D. Kruk et al., J. Chem. Phys. 137, 044512 (2012), Copyright 2012, AIP Publishing LLC and from D. Kruk et al., J. Chem. Phys. 140, 174504 (2014), Copyright 2014, AIP Publishing LLC.*

In Fig. 7.9. the relaxation dispersion data for decalin solutions of 4-oxo-TEMPO-d$_{16}$-$^{14(15)}$N at the lowest a) and the highest b) temperatures are shown in detail, including the corresponding fits. In both figures the predictions for the case of no hyperfine interaction ($A_{iso} = 0$) are also shown. It can be clearly seen that for slower dynamics the low field reduction of the relaxation rates caused by the non-zero scalar hyperfine interaction is larger. At 308 K the effect is small and the differences between the ^{15}N and ^{14}N cases almost vanish.

The reduction is caused by the fact that for $A_{iso} \neq 0$ at low frequencies the small frequency of electron Zeeman splitting is replaced in the spectral densities by the larger hyperfine splitting.

The effect vanishes at higher frequencies when the electron Zeeman interaction dominates the isotropic hyperfine coupling.

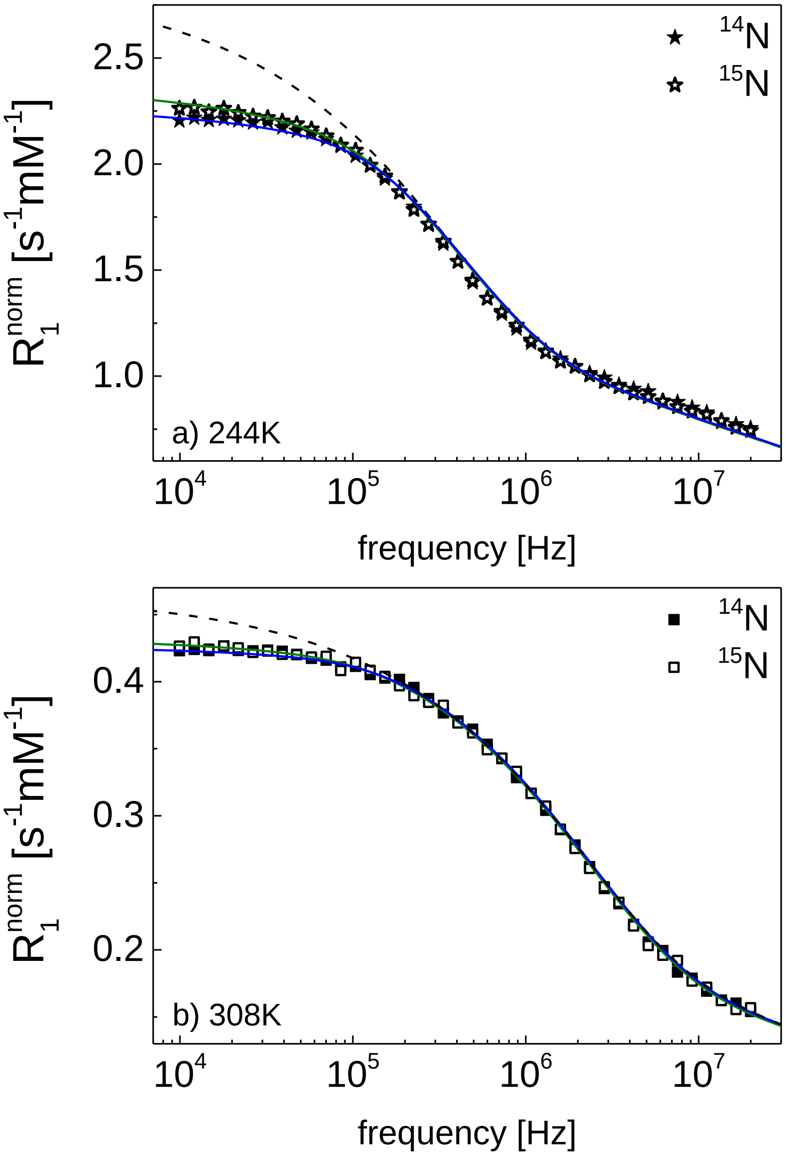

Figure 7.9. ^{1}H spin-lattice relaxation dispersion profiles, $R_1^{norm}(\omega_H)$, for decalin solution of 4-oxo-TEMPO-d_{16}-$^{14(15)}$N at a) 244 K and b) 308 K (Ref. [32]). Solid green and blue lines - fits for ^{15}N and ^{14}N according to Eqs. 73 and 74, respectively; dashed black line - the corresponding predictions for $A_{iso} = 0$. Adopted with permission from D. Kruk et al., J. Chem. Phys. 137, 044512 (2012). Copyright 2012, AIP Publishing LLC.

To illustrate how the individual terms of Eqs. 73 and 74 (for the cases of ^{15}N and ^{14}N, respectively) contribute to the overall shape of $R_1^{norm}(\omega_H)$, in Figs. 7.10 and 7.11 the $R_1^{norm}(\omega_H)$

profiles for ^{14}N and ^{15}N at 244 K and 308 K are decomposed into terms marked in Eqs. 73 and 74 by $K_{DD}R_1^{15(14),X}(\omega_H)$ (where $X = I, II, III\ or\ IV$).

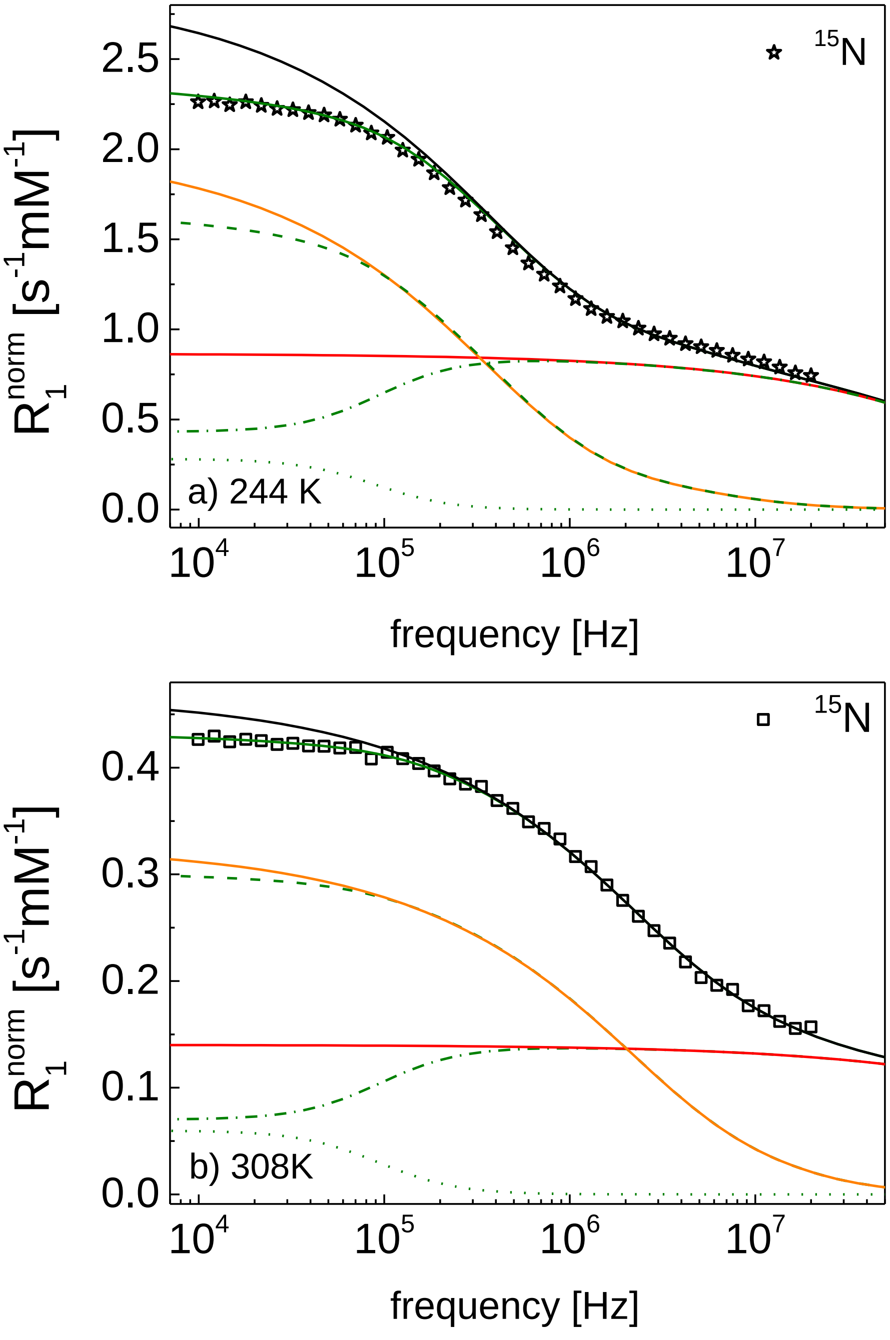

Figure 7.10. ^{1}*H spin-lattice relaxation dispersion,* $R_1^{norm}(\omega_H)$*, for decalin solution of 4-oxo-TEMPO-d*$_{16}$*-*^{15}*N at a) 244 K and b) 308 K (Ref. [32]). Solid black lines – predictions for* $A_{iso} = 0$*; solid orange lines –* $K_{DD}7J(\omega_S)$*; solid red lines –* $K_{DD}3J(\omega_H)$*; solid green lines – fits according to Eq. 73; dashed-dotted green lines –* $K_{DD}R_1^{15,I}(\omega_H)$*; dashed green lines –* $K_{DD}R_1^{15,III}(\omega_H)$*; dotted green lines –* $K_{DD}R_1^{15,II}(\omega_H)$*.*

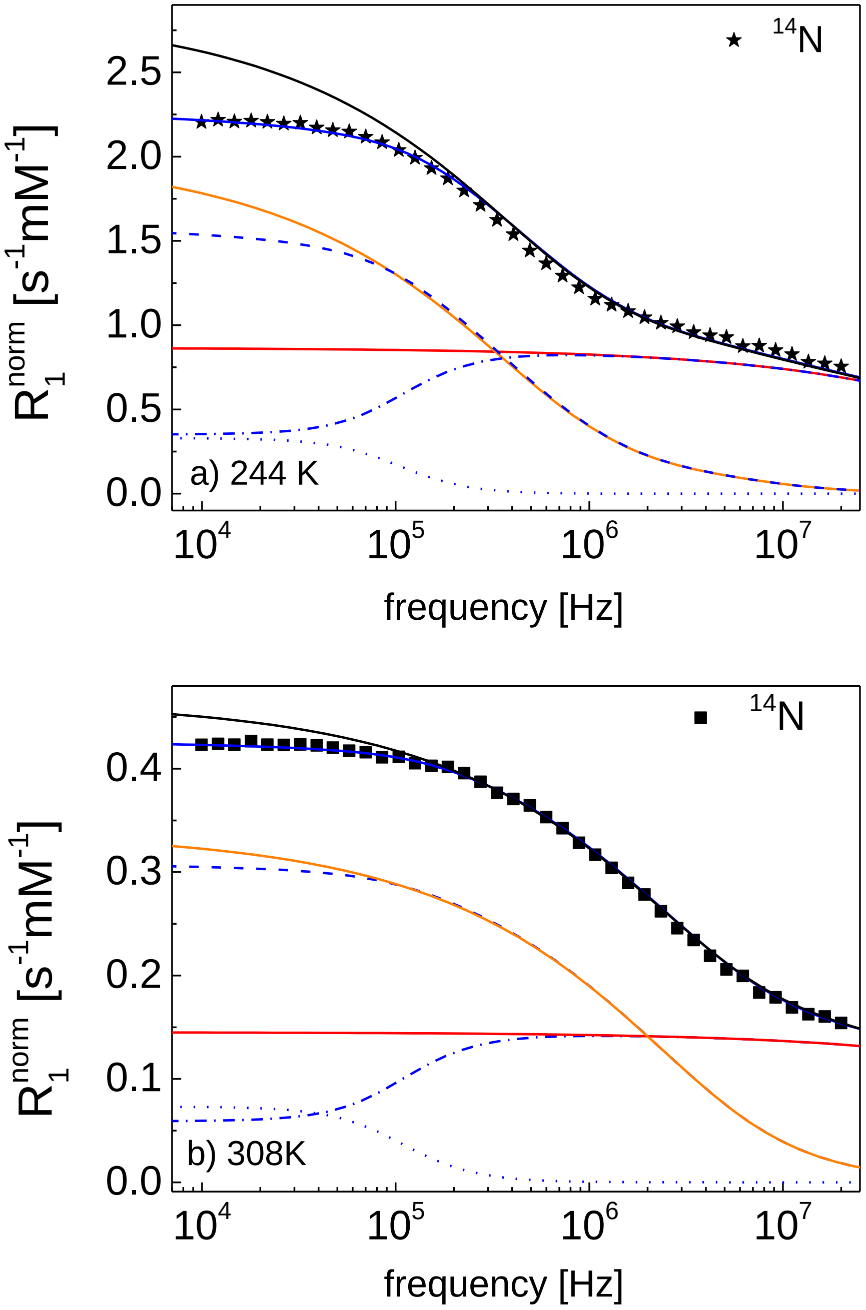

Figure 7.11. ^{1}H spin-lattice relaxation dispersion, $R_1^{norm}(\omega_H)$, for decalin solution of 4-oxo-TEMPO-d$_{16}$-^{14}N at a) 244 K and b) 308 K (Ref. [32]). Solid black lines – predictions for $A_{iso}=0$; solid orange lines - $K_{DD}7J(\omega_S)$; solid red lines – $K_{DD}3J(\omega_H)$; solid blue lines – fits according to Eq. 74; dashed-dotted blue lines - $K_{DD}R_1^{14,I}(\omega_H)$; dashed blue lines - $K_{DD}\left(R_1^{14,III}(\omega_H)+R_1^{14,IV}(\omega_H)\right)$; dotted blue lines - $K_{DD}R_1^{14,II}(\omega_H)$.

At 240 K decalin freezes. Therefore, in order to investigate the ^{1}H relaxation effects caused by nitroxide radicals in solution for slower dynamics, more viscous solvents have to be used. The results obtained for glycerol and propylene glycol solutions of 4-oxo-TEMPO-d$_{16}$-$^{14(15)}$N are presented and analyzed in the next sections.

7.2. Glycerol solutions of 4-oxo-TEMPO-d_{16}-$^{15(14)}$N

^{1}H spin-lattice relaxation dispersion profiles for pure glycerol are shown in Fig.7.12.

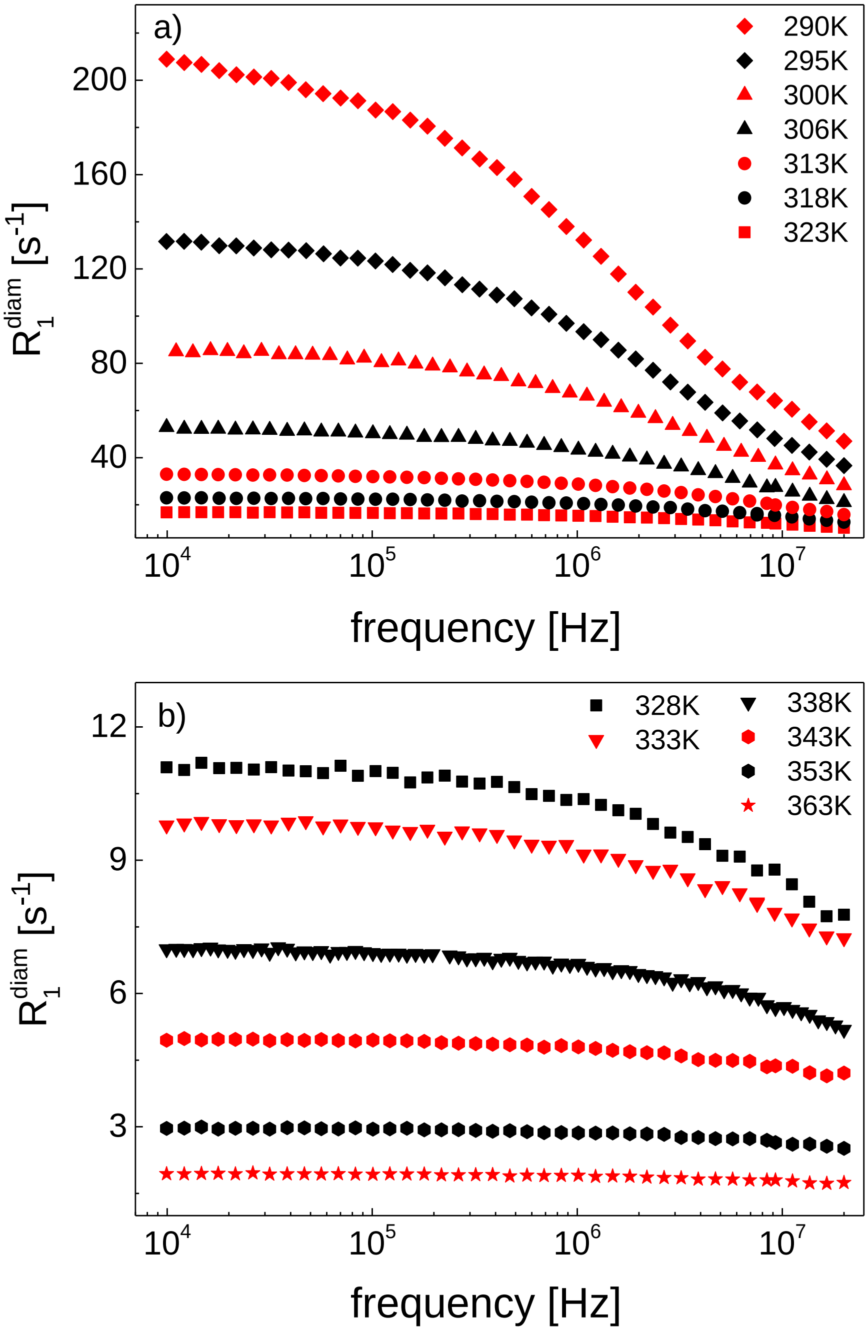

Figure 7.12. ^{1}H spin-lattice relaxation dispersion, $R_1^{diam}(\omega_H)$, for pure glycerol (Ref. [31]). Adopted with permission from D. Kruk et al., J. Chem. Phys. 138, 124506 (2013), Copyright 2013, AIP Publishing LLC.

The relaxation process is single exponential (Fig. 7.13 shows illustrative time dependences of the proton magnetization measured at 290 K and 363 K for the highest and lowest frequencies – 20 MHz and 10 kHz).

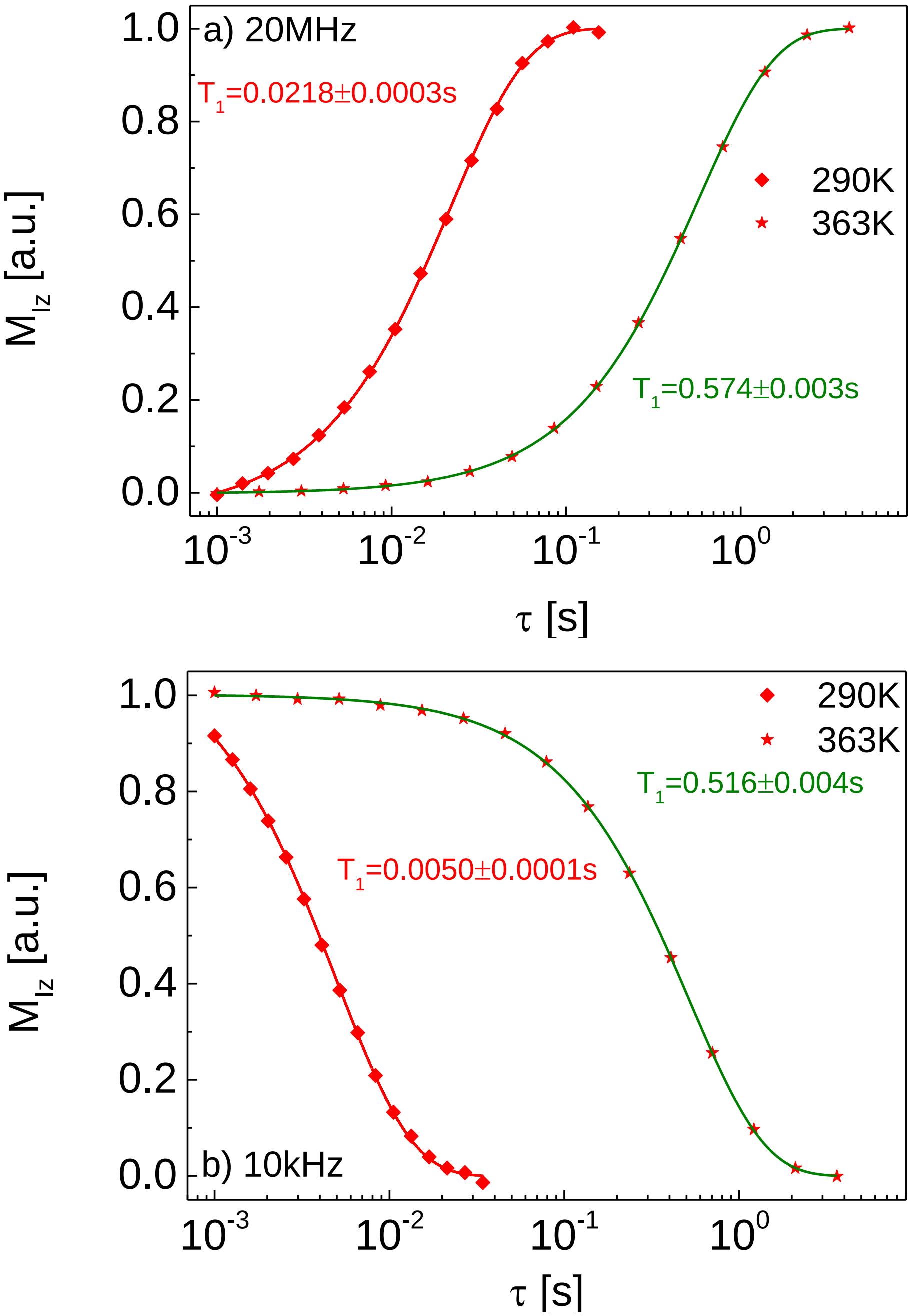

Figure 7.13. ^{1}H magnetization (in arbitrary units) versus time for pure glycerol obtained by a) NP sequence at 20 MHz and by b) PP sequence at 10 kHz. Solid lines (red and green) show single-exponential fits at 290 K and 363 K, respectively.

^{1}H relaxation dispersion profiles for pure glycerol have been measured and thoroughly analyzed in Ref. [34] (the data described in Ref. [34] have been collected at different tempratures than needed for the current analysis, therefore the ^{1}H relaxation dispersion profiles presented in this section have been measured specifically for the purpose of comparison with the coresponding results for glycerol solutions of nitroxide radicals). The rotational correlation time and the relative diffusion coefficients obtained in [34] for pure glycerol are presented in Figs. 7.14 and 7.15 (which also contain results for the paramagnetic solusions that are discussed later), respectively, and they provide a reference point for the current analysis of proton relaxation in glycerol solutions of 4-oxo-TEMPO-d$_{16}$-$^{14(15)}$N. Furthermore, as a result of the analysis described in Ref. [34] the distance of closest approach has been obtained and it yelds $d_{II} \approx 3.5\text{Å}$. The ratio between the translational and rotational correlation times varies between the values of $\tau_{trans}/\tau_R = 40$ and $\tau_{trans}/\tau_R = 62$ obtained for the highest and lowest temperatures, respectively.

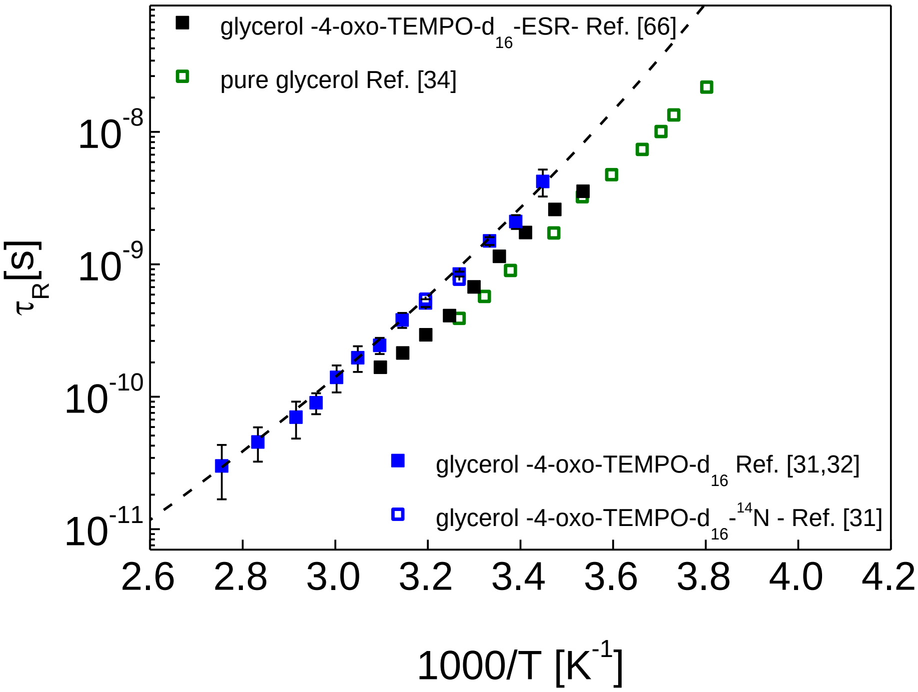

Figure 7.14. Rotational correlation times, τ_R, of 4-oxo-TEMPO-d$_{16}$ dissolved in glycerol obtained from the current analysis (blue squares, Refs. [31,32]) and compared with literature data. Dashed black line – interpolation by the Vogel-Fulcher-Tamman equation. Reprinted with permission from D. Kruk et al., J. Chem. Phys. 138, 124506 (2013), Copyright 2013, AIP Publishing LLC.

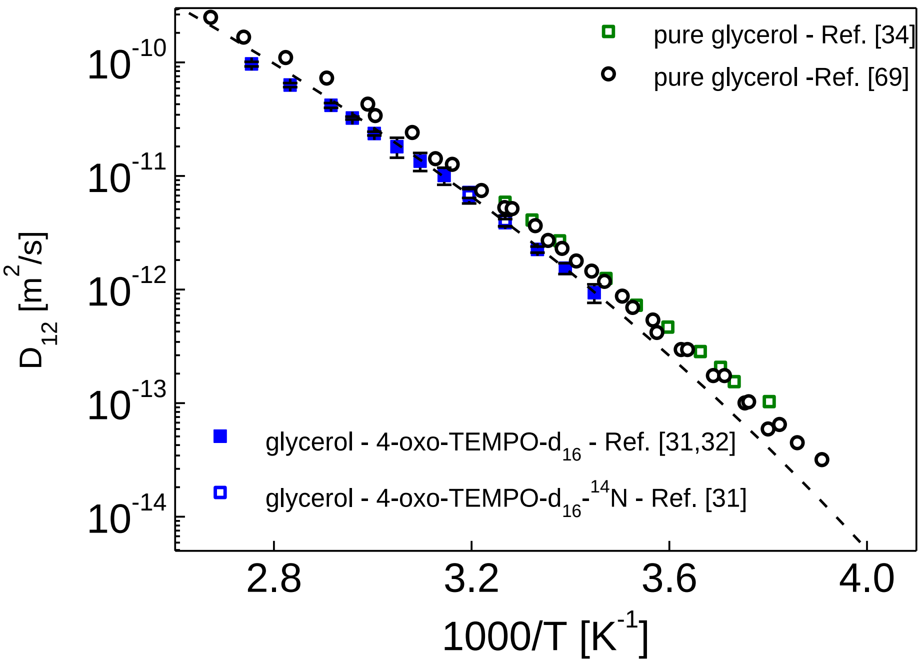

Figure 7.15. Relative diffusion coefficient, D_{12}*, for glycerol solutions of 4-oxo-TEMPO-*d_{16} *obtained from the current analysis (blue squares, described in Refs. [31,32]) and compared with literature [34,69]. Dashed black line - interpolation by the Vogel-Fulcher-Tamman equation. Reprinted with permission from D. Kruk et al., J. Chem. Phys. 138, 124506 (2013), Copyright 2013, AIP Publishing LLC.*

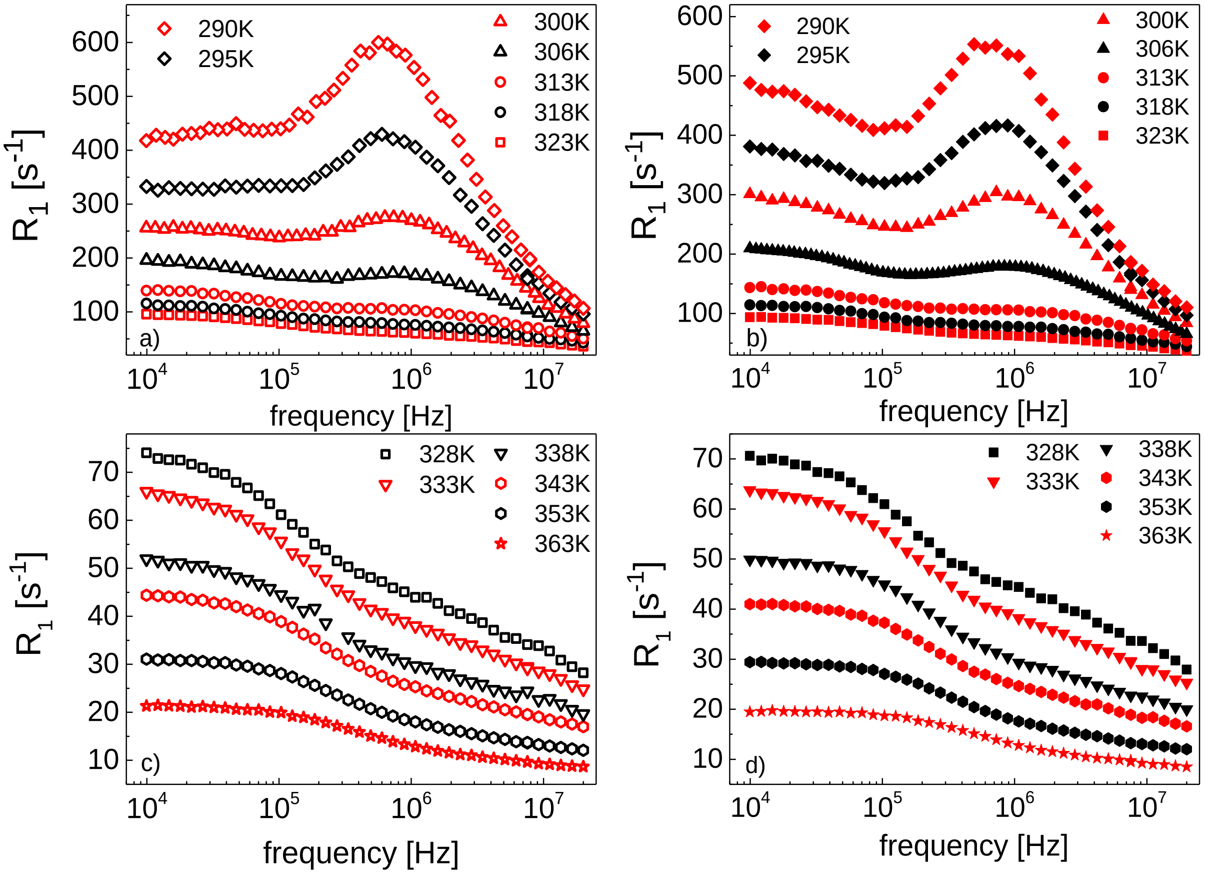

Figure 7.16. ^{1}H spin-lattice relaxation dispersion, $R_1(\omega_H)$, for glycerol solutions of a), c) 4-oxo-TEMPO-d_{16}-^{15}N and b), d) 4-oxo-TEMPO-d_{16}-^{14}N for 2.7 mM concentration of radicals (Ref. [31]). Adopted with permission from D. Kruk et al., J. Chem. Phys. 138, 124506 (2013), Copyright 2013, AIP Publishing LLC.

In Fig. 7.16 ^{1}H spin-lattice relaxation dispersion profiles collected for glycerol solutions of 4-oxo-TEMPO-d_{16}-^{15}N and 4-oxo-TEMPO-d_{16}-^{14}N are shown. Analogously to the case of decalin solutions, the ^{1}H relaxation is single exponential also when glycerol is used as the solvent (see Fig. 7.17 a), b), c) and d)).

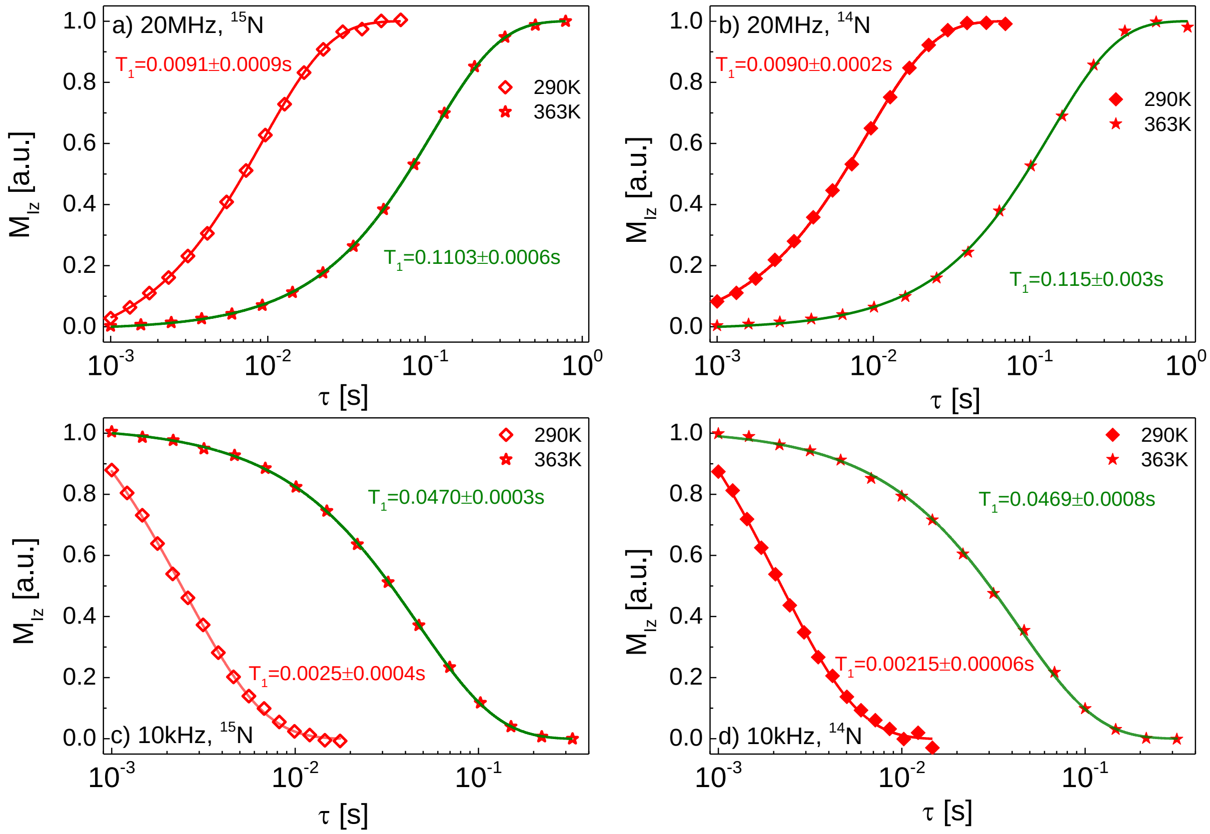

Figure 7.17. ^{1}H magnetization versus time for 2.7 mM glycerol solutions of 4-oxo-TEMPO-d_{16}-^{15}N (left) and 4-oxo-TEMPO-d_{16}-^{14}N (right) obtained by a), b) NP sequence at 20 MHz and c), d) PP sequence at 10 kHz. Solid red and green lines show single-exponential fits at 290 K and 363 K, respectively.

Comparing Fig. 7.12 and Fig. 7.16 one can clearly see that the relaxation rates for the paramagnetic solutions are much larger (the relaxation is much faster) than in pure glycerol. At lower temperatures a relaxation maximum appear in the intermediate frequency range.

Analogously to decalin the relaxation rates $R_1^{par}(\omega_H)$ for the glycerol solutions have been determined by subtracting the diamagnetic contribution $R_1^{diam}(\omega_H)$ (shown in Fig.7.12) from the overall relaxation profile, $R_1(\omega_H)$. The $R_1^{par}(\omega_H)$ relaxation rates were normalized to 1 mM concentration of the radicals. The normalized relaxation rates $R_1^{norm}(\omega_H)$ are shown in Fig. 7.18. The figures contain corresponding theoretical fits (the detailed analysis is presented further in).

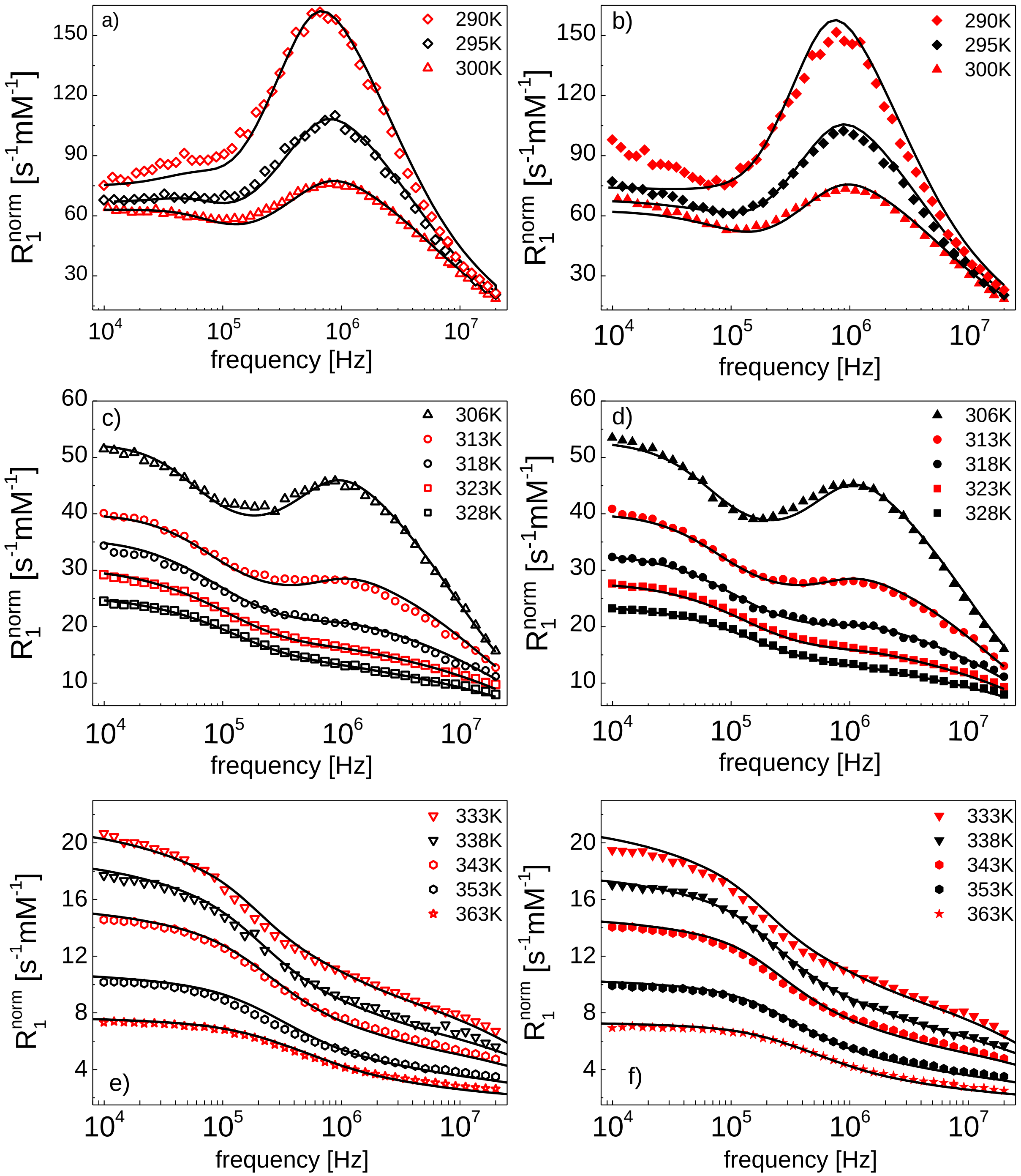

Figure 7.18. ^{1}H relaxation dispersion, $R_1^{norm}(\omega_H)$, for 1 mM glycerol solutions of a), c), e) 4-oxo-TEMPO-d$_{16}$-^{15}N and b), d), f) 4-oxo-TEMPO-d$_{16}$-^{14}N with corresponding fits in terms of Eqs. 73 and 74, respectively (Refs. [31, 32]). Adopted with permission from D. Kruk et al., J. Chem. Phys. 138, 124506 (2013), Copyright 2013, AIP Publishing LLC and from D. Kruk et al. J. Chem. Phys. 137, 044512 (2012), Copyright 2012, AIP Publishing LLC.

The analysis has been started from the highest temperature of 363 K. The isotropic hyperfine coupling constant, A_{iso}, has been set to the same value of $A_{iso} = 44$ MHz (^{14}N) and $A_{iso} = 62$ MHz (^{15}N). The value of the stretching parameter, β, has been fixed to the literature value of 0.67 [34,70]. The adjustable parameters are: d_{IS}, τ_{trans}, f and τ_R. The rotational contribution to the modulations of the proton spin-electron spin dipolar coupling has to be taken into account due to the high viscosity of glycerol. Again, in analogy to decalin, the proton relaxation data for both cases (^{14}N and ^{15}N) have been fitted simultaneously for each temperature using Eqs. 73 and 74 under the assumption that the adjustable parameters have the same values at one temperature. It was possible to keep the distance of closest approach, d_{IS}, and the f parameter temperature independent down to 333 K. The strategy of the analysis has been described in [31,32]. The obtained values are as follows: $d_{IS} = 3.4$ Å and $f = 1.2$, and they are very close to those reported in Ref. [33], for proton relaxation rates for glycerol solutions of different nitroxide radicals studied at high fields (25 MHz and 15 MHz) versus temperature. The obtained values of the fitted parameters and the relative diffusion coefficient, D_{12}, calculated from the relationship $D_{12} = d_{IS}^2 / \tau_{trans}$ are presented in Table 7.2. and compared in Fig. 7.14 and 7.15, (the rotational correlation time, τ_R, and the relative diffusion coefficient, D_{12}, respectively), with literature data.

As an illustration the individual terms of Eqs. 73 and 74 leading to the overall relaxation are presented in Fig. 7.19 for 338 K.

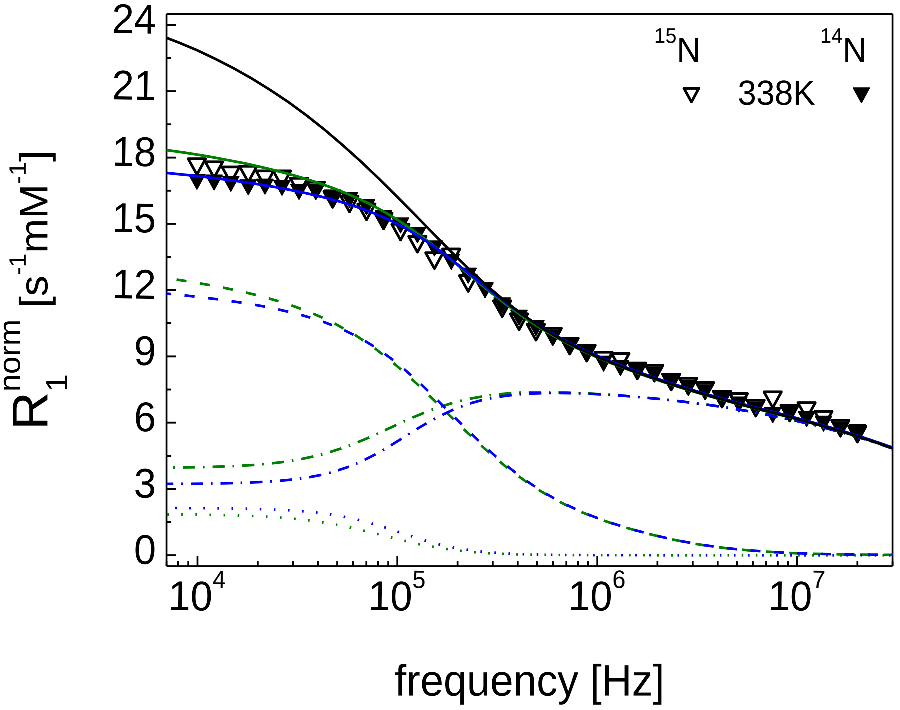

Figure 7.19. ^{1}*H spin-lattice relaxation dispersion,* $R_1^{norm}(\omega_H)$*, for 4-oxo-TEMPO-d*$_{16}$*-*^{15}*N and 4-oxo-TEMPO-d*$_{16}$*-*^{14}*N (open and solid symbols, respectively) in glycerol solution at 338 K (Ref. [32]). Solid lines (green and blue) – corresponding fits (according to Eqs. 73 and 74 for* ^{15}*N and* ^{14}*N, respectively); solid black line – prediction for* $A_{iso} = 0$*; dashed – dotted blue line -* $K_{DD}R_1^{14,I}(\omega_H)$ *from Eq. 74 for* ^{14}*N; dashed blue line -* $K_{DD}\left(R_1^{14,III}(\omega_H)+R_1^{14,IV}(\omega_H)\right)$ *from Eq. 74 for* ^{14}*N ; dotted blue line -* $K_{DD}R_1^{14,II}(\omega_H)$ *from Eq. 74 for* ^{14}*N; dashed – dotted green line -* $K_{DD}R_1^{15,I}(\omega_H)$ *from Eq. 73 for* ^{15}*N; dashed green line -* $K_{DD}R_1^{15,III}(\omega_H)$ *from Eq. 73 for* ^{15}*N; dotted green line -* $K_{DD}R_1^{15,II}(\omega_H)$ *from Eq. 73 for* ^{15}*N.*

T [K]		τ_R [s]		τ_{trans} [s]		d_{IS} [Å]		f		$\chi = \frac{\tau_{trans}}{\tau_R}$	D_{12} [m^2/s]	
363		$3.87*10^{-11}$	(34%)	$1.19*10^{-9}$	(4.6%)	3.40		1.2		31	$9.66*10^{-11}$	(4.6%)
353		$4.55*10^{-11}$	(29%)	$1.82*10^{-9}$	(4.1%)	3.40		1.2		40	$6.31*10^{-11}$	(4.1%)
343		$7.0*10^{-11}$	(31%)	$2.80*10^{-9}$	(5.0%)	3.40		1.2		40	$4.18*10^{-11}$	(5.0%)
338		$9.0*10^{-11}$	(18%)	$3.69*10^{-9}$	(3.0%)	3.40		1.2		41	$3.23*10^{-11}$	(3.0%)
333		$1.4*10^{-10}$	(23%)	$5.74*10^{-9}$	(4.5%)	3.40		1.2		41	$2.36*10^{-11}$	(4.5%)
328		$1.97*10^{-10}$	(22%)	$7.94*10^{-9}$	(21%)	3.68	(1.3%)	1.16	(11%)	40	$1.81*10^{-11}$	(21%)
323		$2.44*10^{-10}$	(13%)	$1.01*10^{-8}$	(17%)	3.69	(1.0%)	1.35	(11%)	41	$1.35*10^{-11}$	(18%)
318		$3.80*10^{-10}$	(11%)	$1.35*10^{-8}$	(16%)	3.69	(1.6%)	1.27	(11%)	35.5	$1.01*10^{-11}$	(17%)
313	^{15}N	$5.10*10^{-10}$	(6.7%)	$1.92*10^{-8}$	(10%)	3.70	(1.5%)	1.38	(14%)	38	$7.13*10^{-12}$	(10%)
	^{14}N	$5.45*10^{-10}$	(9.9%)	$2.05*10^{-8}$	(14%)		(1.6%)		(13%)		$6.68*10^{-12}$	(14%)
306	^{15}N	$8.44*10^{-10}$	(4.3%)	$3.53*10^{-8}$	(7.0%)	3.70	(1.3%)	1.44	(11%)	42	$3.88*10^{-12}$	(7.5%)
	^{14}N	$7.79*10^{-10}$	(9.2%)	$3.21*10^{-8}$	(9.8%)	3.60	(2.0%)	1.50	(15%)		$4.04*10^{-12}$	(10%)
300	^{15}N	$1.50*10^{-9}$	(4.1%)	$5.67*10^{-8}$	(5.8%)	3.57	(1.1%)	1.45	(7.5%)	38	$2.25*10^{-12}$	(6.2%)
	^{14}N		(6.7%)		(9.5%)		(1.7%)		(11%)			(10%)
295	^{15}N	$2.10*10^{-9}$	(11%)	$8.16*10^{-8}$	(10%)	3.54	(2.3%)	1.35	(14%)	39	$1.54*10^{-12}$	(11%)
	^{14}N		(12%)		(11%)		(2.7%)		(17%)			(12%)
290	^{15}N	$4.22*10^{-9}$	(17%)	$1.37*10^{-7}$	(18%)	3.58	(2.3%)	1.45	(10%)	32	$9.36*10^{-13}$	(18%)
	^{14}N		(23%)		(22%)		(4.1%)		(17%)			(23%)

Table 7.2. Rotational and translational parameters for glycerol solutions of 4-oxo-TEMPO-d_{16} (^{14}N and ^{15}N), Refs. [31,32]. The accuracy of the parameters is given in %. Red line indicates the temperature for which (and below) electron spin relaxation has been included into the analysis. With grey color the temperatures at which the data have been analyzed separately are marked. Adopted with permission from D. Kruk et al., J. Chem. Phys. 138, 124506 (2013), Copyright 2013, AIP Publishing LLC and from D. Kruk et al. J. Chem. Phys. 137, 044512 (2012), Copyright 2012, AIP Publishing LLC.

To explicitly demonstrate the role of the rotational contribution to the modulations of the intermolecular proton spin-electron spin dipole-dipole interaction reflected by the form of the spectral density of Eq. 39, in Fig. 7.20, the overall relaxation dispersion profiles have been separated into parts associated with the translational and rotational modulations of the dipolar interaction.

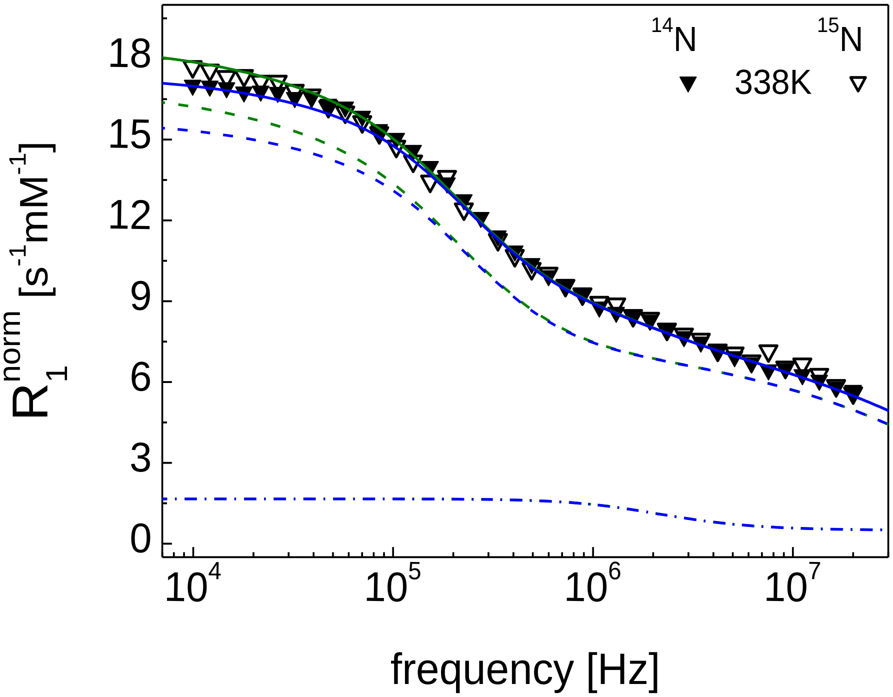

Figure 7.20. ^{1}*H spin-lattice relaxation dispersion,* $R_1^{norm}(\omega_H)$*, for 4-oxo-TEMPO-*d_{16}*-*^{15}*N and 4-oxo-TEMPO-*d_{16}*-*^{14}*N (open and solid symbols, respectively) in glycerol solution at 338 K (Ref. [32]). Solid lines (green and blue) – corresponding fits (according to Eq. 73 and 74, for* ^{15}*N and* ^{14}*N, respectively); dashed dotted lines – rotational contribution to* $R_1^{norm}(\omega_H)$*; dashed lines – translational contribution to* $R_1^{norm}(\omega_H)$*.*

For the higher temperatures the relaxation data have been reproduced quite well, but with decreasing temperature the quality of the fits gets progressively worse. For 328 K and below it was impossible to obtain the sufficient low field reduction of the relaxation rate by taking into account only the influence of the isotropic hyperfine interaction. One has to also take into account the electron spin relaxation as an additional (besides the translational and rotational dynamics) source of modulations of the proton spin-electron spin dipole-dipole interaction.

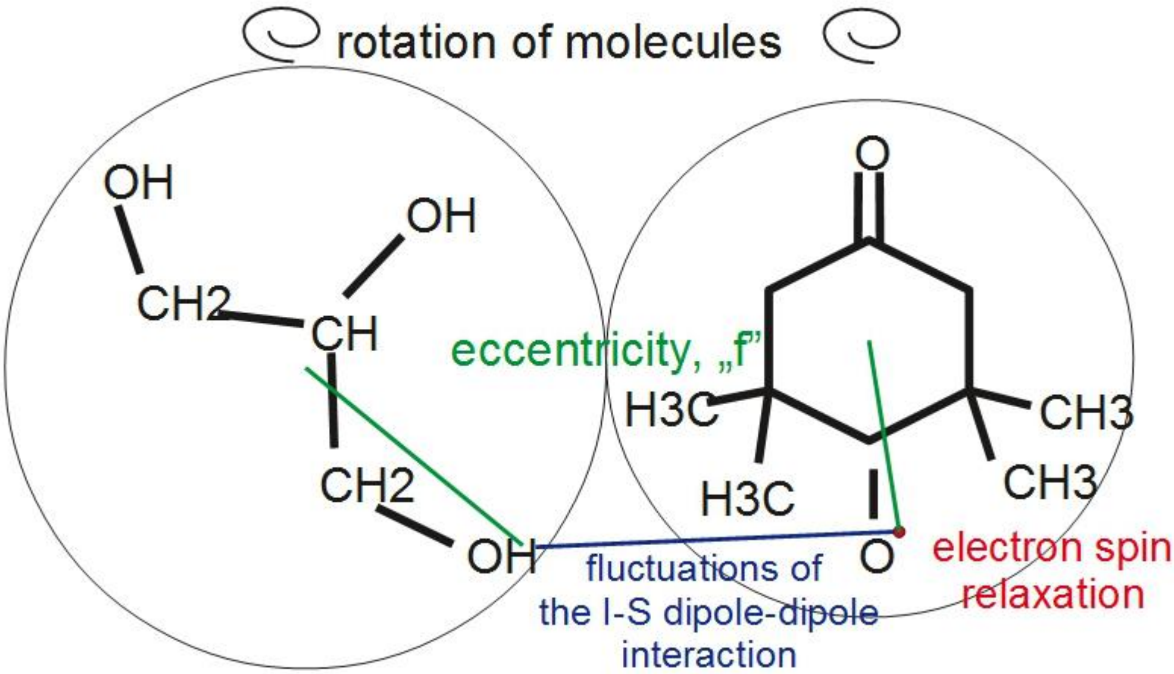

Figure 7.21. A schematic view of the sources of modulations of the proton spin-electron spin dipole-dipole interaction.

As one can see from Fig. 7.21, the role of the rotational dynamics is twofold. First, the rotational motion contributes to the modulations of the proton spin-electron spin dipole-dipole interaction through the eccentricity effects. The rotational corelation time, τ_R, describes the combined effect of the rotation of solvent and solute molecules on the dipolar coupling. Second, the rotational motion of the paramagnetic molecule leads to fluctuations of the anisotropic part of the hyperfine interaction and hence the electron spin relaxation. The electron spin relaxation becomes an important source of the modulations of the proton spin-electron spin dipolar interaction when the dynamics of the system is relatively slow. Taking into account that the rotational dynamics of the nitroxide radicals is similar to the rotational movement of the solvent molecules (the correlation times describing the two cases are close to each other) only one parameter, τ_R, is used in the analysis.

The relaxation data obtained for lower temperatures (starting from 328 K) have been reproduced by fits performed with the same four adjustable parameters: d_{IS}, τ_{trans}, f and τ_R, however the electron spin relaxation has been taken into account. The values of the hyperfine coupling tensor components have been taken from literature: $A_{xx} = 15.4$ MHz, $A_{yy} = 16.1$ MHz, $A_{zz} = 99.5$ MHz for ^{14}N and $A_{xx} = 22.0$ MHz, $A_{yy} = 23.0$ MHz, $A_{zz} = 142.0$ MHz for ^{15}N [58,66,71].

The theory of ^{1}H spin-lattice relaxation in solutions of nitroxide radicals including the effects of electron spin relaxation has been presented in [31]. Here (and in Section 5) only the underlying concept is outlined. The hyperfine coupling tensor is asymmetrical and its components (listed above) give the isotropic part $A_{iso} = (A_{xx} + A_{yy} + A_{zz})/3$ equal to 44 MHz for ^{15}N and 62 MHz for ^{14}N as used in the analysis. The assymetric part modulated by rotation of the paramagnetic molecule causes the electronic relaxation which contributes to the efective modulations of the proton spin-electron spin dipolar coupling. Thus, the number of the adjustable parameters remains unchanged; the parameters are: d_{IS}, τ_{trans}, f and τ_R.

In the temperature range 328 K - 290 K, the relaxation dispersion profiles for the ^{14}N and ^{15}N cases have been fitted simoultaneously at each temperature. The obtained values of τ_R and D_{12} (listed in Table 7.2) are compared in Figs. 7.14 and 7.15 (blue squares) with literature data yielding good agreement. In this temperature range it was difficult to keep the parameter f temperature independent (the values are presented in Table 7.2). The analysis with electron spin relaxation effects included into ^{1}H relaxation theory has been presented in [31].

At 313 K the low frequency values of the ^{1}H relaxation rates $R_1^{norm}(\omega_H)$ for ^{14}N and ^{15}N cases become comparable and then for even lower temperatures the relaxation rate for the case of ^{15}N exceeds the value for the ^{14}N case (the theoretically predicted relation $R_1^{norm}(\omega_H = 0, ^{14}\mathrm{N}) < R_1^{norm}(\omega_H = 0, ^{15}\mathrm{N})$ is not fulfilled). This situation may be caused by the simplifications of the dynamical model: the eccentricity effects are included into the theory by adding a term described by Cole-Davidson spectral density and it was assumed that the solvent and radical molecules rotate with the same correlation times, τ_R. Another explanation is quadrupole relaxation present for ^{14}N nuclei ($S = 1$) and not present for ^{15}N ($S = 1/2$) – this effect is not included into the theoretical description. To somewhat mitigate the low frequency discrepancies between the theoretical predictions and the experimental data for 313 K and

306 K slight differences in the parameters, d_{IS}, τ_{trans}, f and τ_R for ^{14}N and ^{15}N cases have been allowed. The obtained values are collected in Table 7.2 and shown in Figs. 7.14 and 7.15 (τ_R and D_{12}, respectively).

In Fig. 7.22 the predictions with neglected electron spin relaxation are presented and compared with the fits performed at 306 K. One can clearly see that the electron spin relaxation leads to a very considerable reduction of the relaxation rate $R_1^{norm}(\omega_H)$ at low frequencies. The contribution of the electron spin relaxation makes the effective fluctuations of the dipolar interaction faster and this, in consequence, leads to a slower proton relaxation at low frequencies.

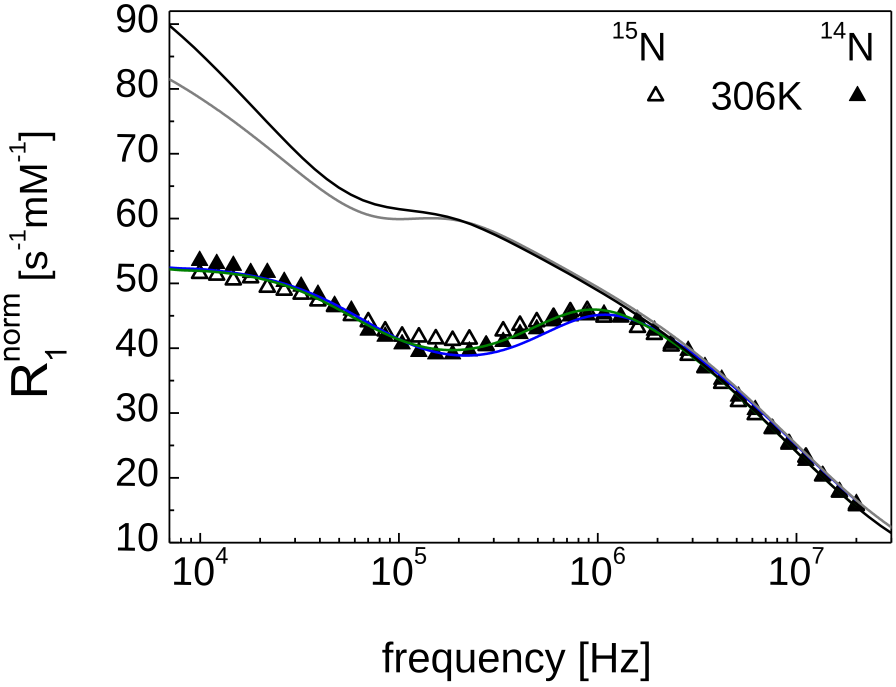

Figure 7.22. ^{1}H spin-lattice relaxation dispersion, $R_1^{norm}(\omega_H)$, for 4-oxo-TEMPO-d$_{16}$-^{15}N and 4-oxo-TEMPO-d$_{16}$-^{14}N (open and solid symbols, respectively) in glycerol solution at 306 K (Ref. [31]). Solid lines (green and blue) corresponding fits (for ^{15}N and ^{14}N, respectively). Black and grey lines - predictions for the cases of ^{15}N and ^{14}N according to Eqs. 73 and 74, respectively, neglecting electron spin relaxation. Adopted with permission from D. Kruk et al., J. Chem. Phys. 138, 124506 (2013), Copyright 2013, AIP Publishing LLC.

The examples for 313 K and 306 K show that the differences in the parameters d_{IS}, τ_{trans}, f and τ_R obtained from the analysis performed separately for the ^{15}N and ^{14}N cases are small, therefore it has been decided for the lowest temperatures (300 K, 295 K and 290 K) to come back to the analysis of both cases with the same set of parameters. The strategy has been, however, modified. The fits are not performed simultaneously, but first the relaxation dispersion profiles for the ^{15}N case have been fitted and then the obtained parameters have been used to reproduce the relaxation data for the ^{14}N case, at the cost of somewhat worse agreement at low frequencies for the last case. The obtained parameters are included into Table 7.2 and figures 7.14 and 7.15.

In analogy to Fig. 7.19 in Fig. 7.23 a decomposition of the overall relaxation dispersion profile at 300 K (when the electron spin relaxation is taken into account) into individual terms (Eqs. 73 and 74) is shown.

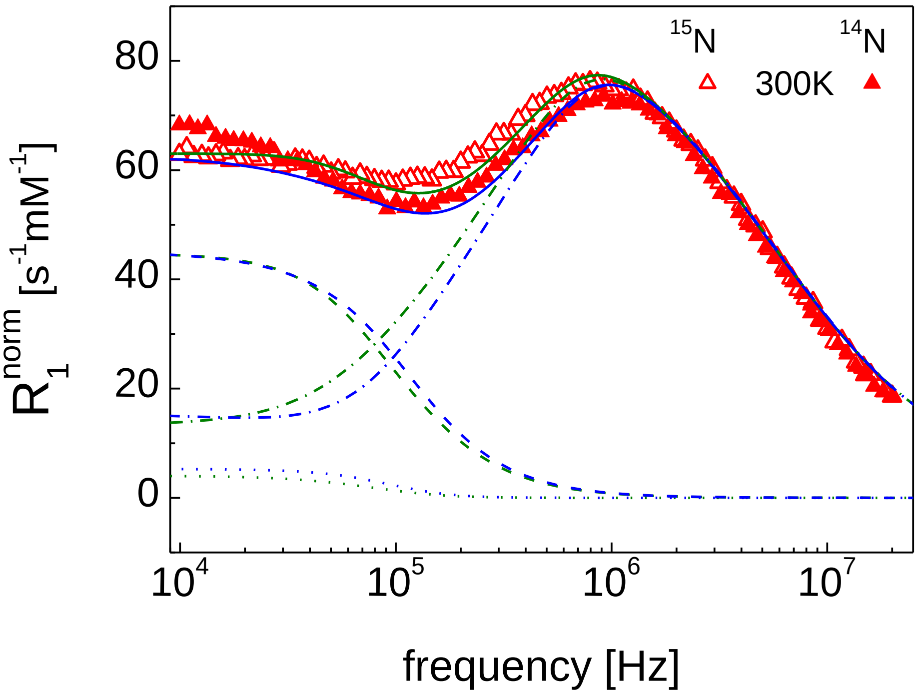

Figure 7.23. ^{1}*H spin-lattice relaxation dispersion,* $R_1^{norm}(\omega_H)$, *for 4-oxo-TEMPO-d*$_{16}$-^{15}*N and 4-oxo-TEMPO-d*$_{16}$-^{14}*N (open and solid symbols, respectively) in glycerol solution at 300 K (Ref. [31]). Solid lines (green and blue) – corresponding fits (according to Eqs. 73 and 74 for* ^{15}*N and* ^{14}*N, respectively); dashed dotted green line -* $K_{DD}R_1^{15,I}(\omega_H, R^e)$ *from Eq. 73; dashed green line -* $K_{DD}R_1^{15,III}(\omega_H, R^e)$ *from Eq. 73 ; dotted green line -* $K_{DD}R_1^{15,II}(\omega_H, R^e)$ *from Eq. 73; dashed - dotted blue line -* $K_{DD}R_1^{14,I}(\omega_H, R^e)$ *from Eq. 74; dashed blue line -* $K_{DD}\left(R_1^{14,III}(\omega_H, R^e)+R_1^{14,IV}(\omega_H, R^e)\right)$ *from Eq. 74; dotted blue line -* $K_{DD}R_1^{14,II}(\omega_H, R^e)$ *from Eq. 74.*

The notation $K_{DD}R_1^{15,I}\left(\omega_H, R^e\right)$ in the caption of Fig. 7.23 means that the nuclear spectral density characterizing the fluctuations of the proton spin – electron spin dipole-dipole interaction, $J^R\left(\omega_H\right)$, includes the electron spin relaxation according to theory presented in [31].

The figure shows that, as already explained in Section 5, the relaxation maximum is created by the term $K_{DD}R_1^{15,I}\left(\omega_H, R^e\right) = K_{DD}\frac{3}{2}\left[1+\left(a^2-b^2\right)^2\right]J^R\left(\omega_H\right)$ for the case of ^{15}N and $K_{DD}R_1^{14,I}\left(\omega_H, R^e\right) = K_{DD}\left[1+\frac{\left(a^2-b^2\right)^2}{2}+\frac{\left(c^2-d^2\right)^2}{2}+\frac{\left(e^2-f^2\right)^2}{2}+\frac{\left(g^2-h^2\right)^2}{2}\right]J^R\left(\omega_H\right)$ for the case of ^{14}N. The maximum stems from the competition between the prefactors which increase with increasing frequency (from 3/2 to 3 for ^{15}N and from 11/9 to 3 for ^{14}N) and the spectral density $J^R\left(\omega_H\right)$ which decays with increasing frequency.

Before finishing the discussion of the relaxation data for the glycerol solutions it is worth to focus for a while on the subject of the rotational contribution to the modulations of the proton spin-electron spin dipolar coupling as for lower temperatures the role of the rotational dynamics becomes more significant.

In Fig. 7.24 the unsuccessful attempt to fit the relaxation data at 318 K without the rotational part (setting $f = 0$) is shown.

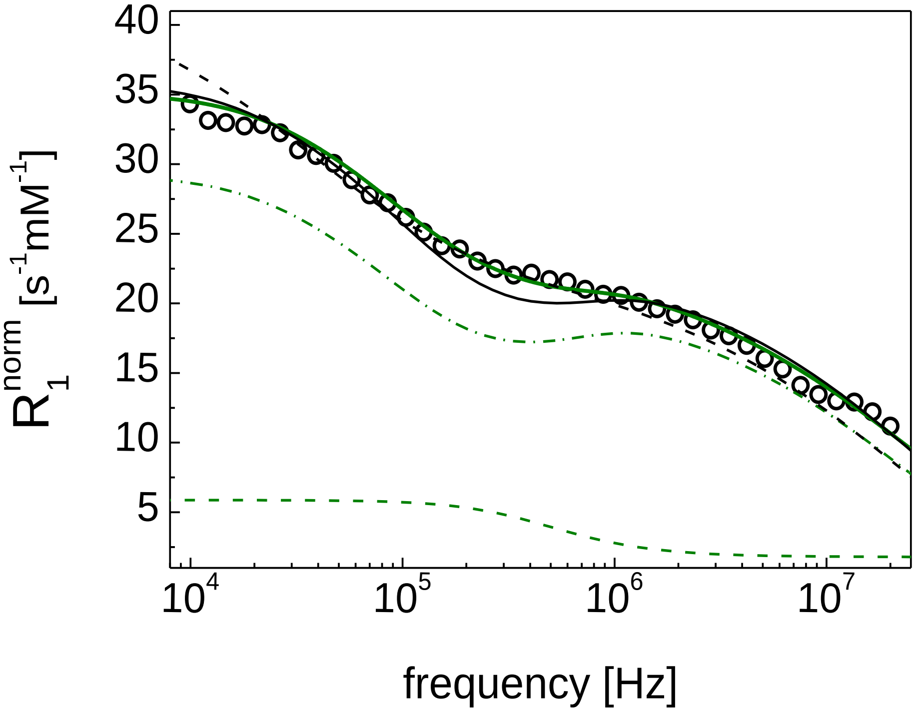

Figure 7.24. ^{1}*H spin-lattice relaxation dispersion,* $R_1^{norm}(\omega_H)$*, for 4-oxo-TEMPO-d*$_{16}$*-*^{15}*N in glycerol solution at 318 K (Ref. [31]). Solid green line – corresponding fit (according to Eq. 73); dashed dotted line – translational contribution to* $R_1^{norm}(\omega_H)$*; dashed line – rotational contribution to* $R_1^{norm}(\omega_H)$*; solid black line – result of fitting the data setting* $f=0$*, obtained parameters:* $\tau_{trans}=1.17*10^{-8}\,s$*,* $d_{IS}=3.40\,Å$*; dashed black line – result of fitting the data setting* $f=0$ *and neglecting the electron spin relaxation, obtained parameters:* $\tau_{trans}=1.52*10^{-8}\,s$*,* $d_{IS}=3.77\,Å$*.*

Eventually, in Fig. 7.25 the rotational contribution to the overall relaxation is shown for the lowest temperature of 290 K. The role of this term is apparently significant.

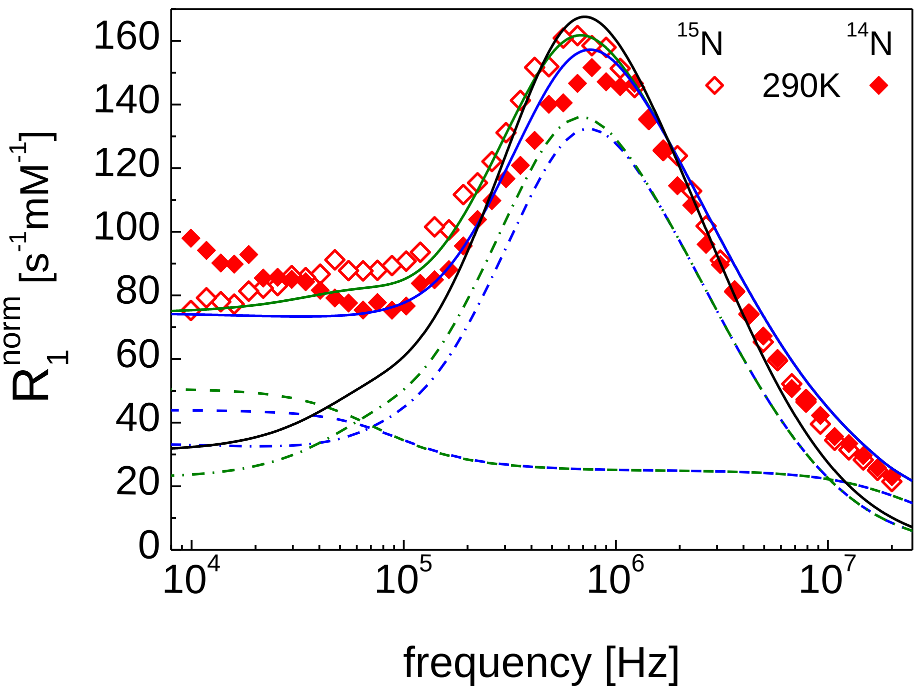

Figure 7.25. ^{1}H spin-lattice relaxation dispersion, $R_1^{norm}(\omega_H)$, for 4-oxo-TEMPO-d$_{16}$-^{15}N and 4-oxo-TEMPO-d$_{16}$-^{14}N (open and solid symbols, respectively) in glycerol solution at 290 K (Ref. [31]). Solid lines (green and blue) – corresponding fits (according to Eqs. 73 and 74, for ^{15}N and ^{14}N, respectively); dashed dotted lines – translational contribution to $R_1^{norm}(\omega_H)$; dashed lines – rotational contribution to $R_1^{norm}(\omega_H)$; solid black line – result of fitting the data (^{15}N) setting $f = 0$, obtained parameters: $\tau_{trans} = 1.40*10^{-7}$ s, $d_{IS} = 3.35\,Å$.

To test whether the features of the proton relaxation dispersion profiles are universal and depend only on dynamical parameters (and not on the solvent) analogous studies have been performed for propylene glycol solutions.

7.3. Propylene glycol solutions of 4-oxo-TEMPO-d$_{16}$-$^{15(14)}$N

^{1}H spin-lattice relaxation dispersion profiles for pure propylene glycol are shown in Fig.7.26.

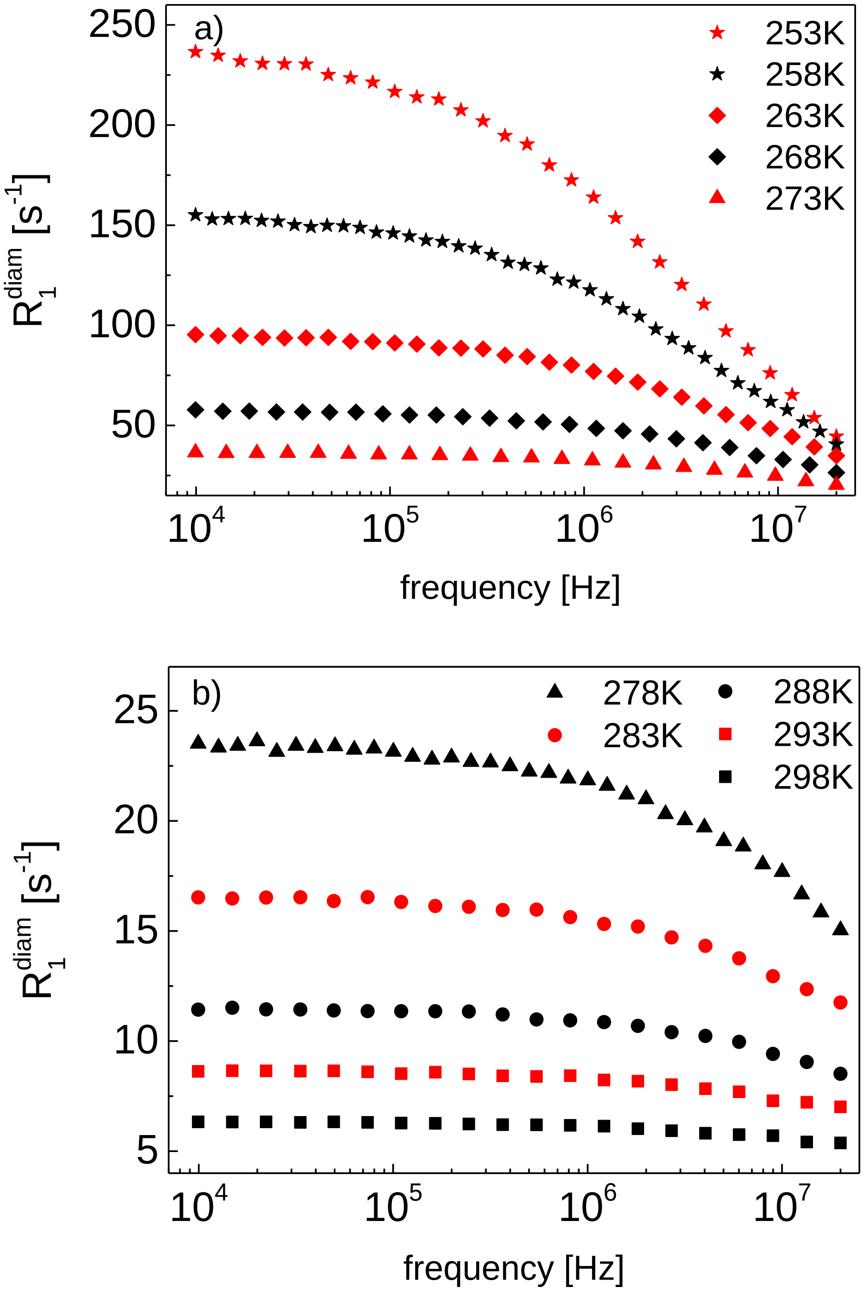

Figure 7.26. ^{1}H spin-lattice relaxation dispersion, $R_1^{diam}(\omega_H)$, for pure propylene glycol (Ref. [57]). Adopted with permission from D. Kruk et al., J. Chem. Phys. 139, 244502 (2013), Copyright 2013, AIP Publishing LLC.

The relaxation is also (in analogy to decalin and glycerol) single exponential (Fig. 7.27 shows illustrative time dependences of the proton magnetization measured at 253 K and 298 K for the highest and lowest frequencies – 20 MHz and 10 kHz).

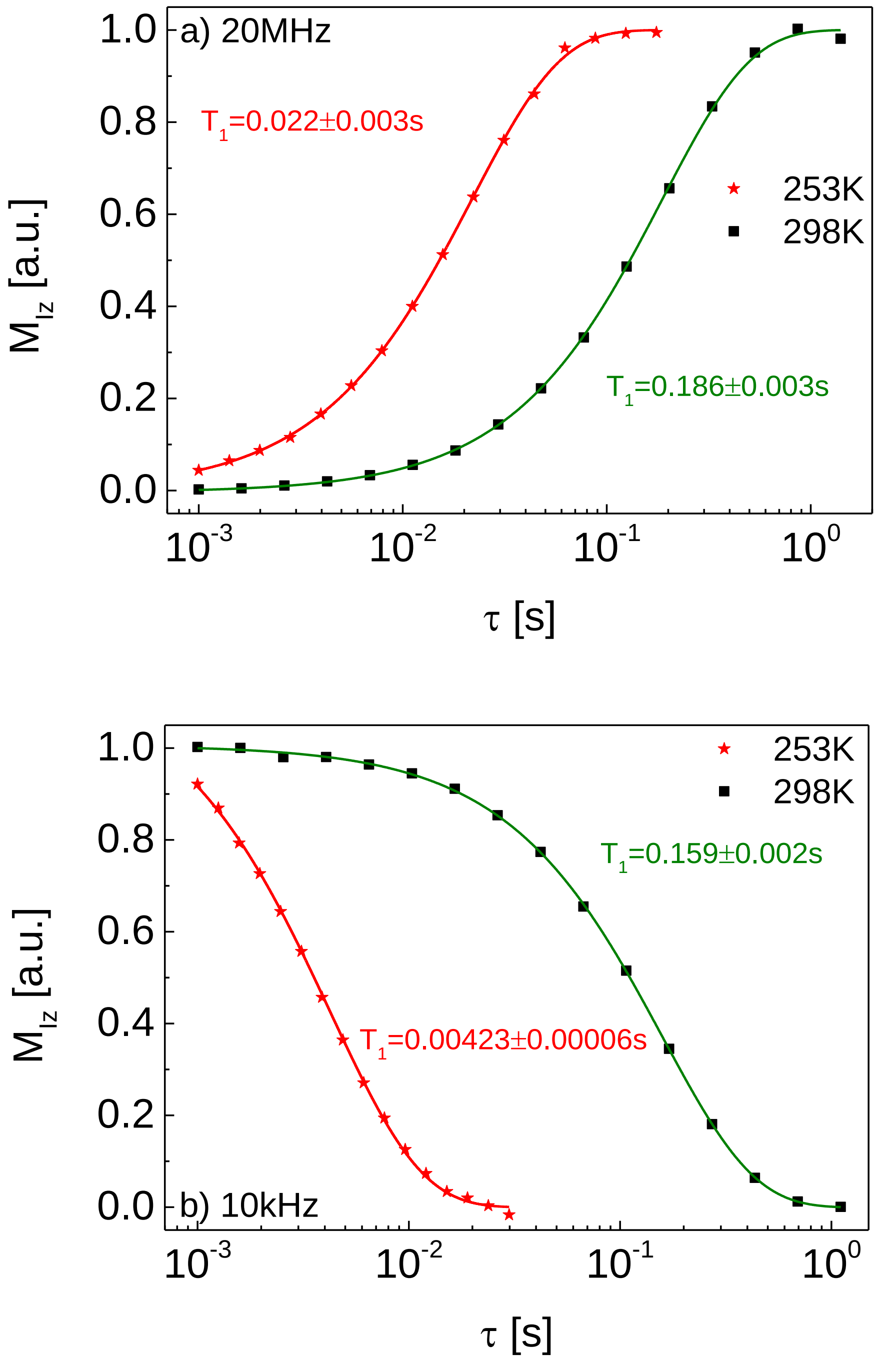

Figure 7.27. ^{1}H magnetization (in arbitrary units) versus time for pure propylene glycol obtained by a) NP sequence at 20 MHz and by b) PP sequence at 10 kHz. Solid red and green lines show single-exponential fits at 253 K and 298 K, respectively (for both cases).

The ^{1}H relaxation rates for pure propylene glycol have been studied in Refs. [72] and [73] (again the data presented in Refs. [72] and [73] have been collected at different tempratures than needed for the current analysis, therefore the ^{1}H relaxation dispersion profiles presented in this section have been measured as a reference for the experiments on the solutions of nitroxide radicals).

^{1}H spin-lattice relaxation dispersion profiles for propylene glycol solutions of 4-oxo-TEMPO-d$_{16}$-^{15}N and 4-oxo-TEMPO-d$_{16}$-^{14}N are shown in Fig. 7.28. As it was in the case of decalin and glycerol the ^{1}H relaxation is also single exponential (see Fig. 7.29 a), b), c) and d)).

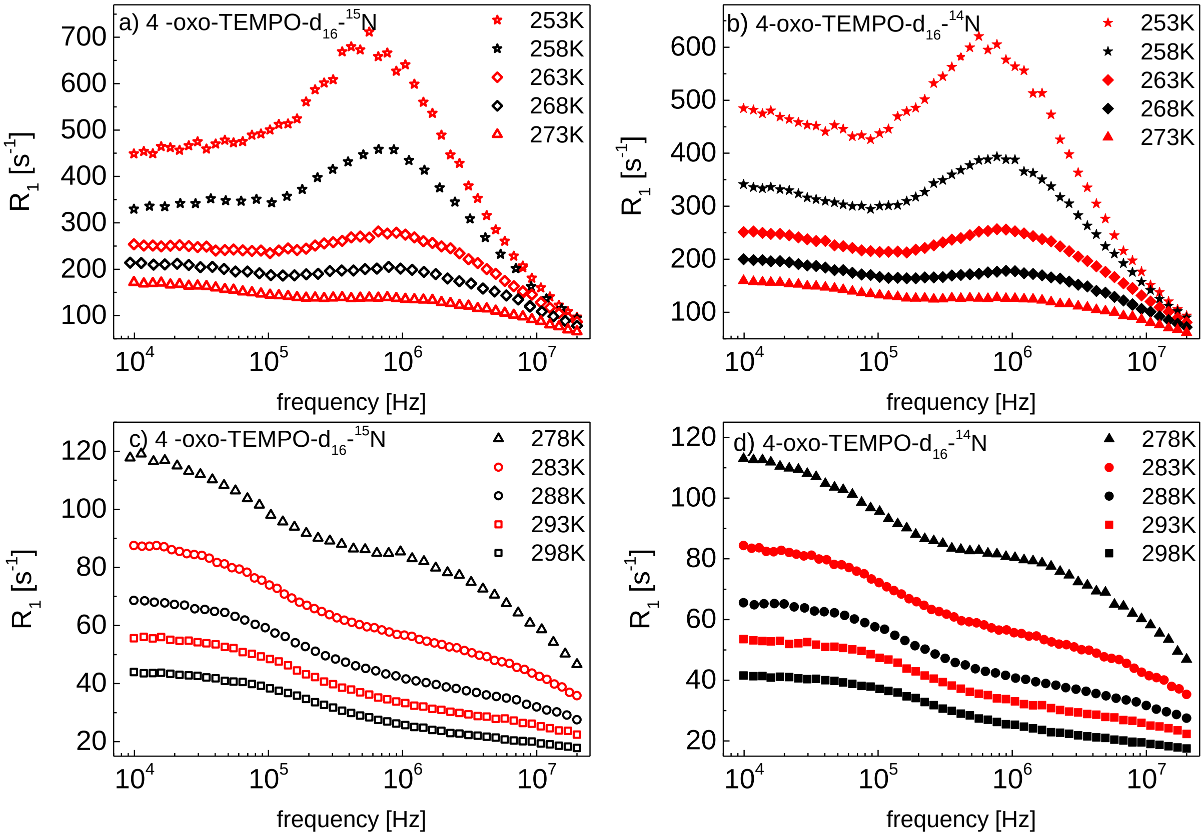

Figure 7.28. ^{1}H spin-lattice relaxation dispersion, $R_1(\omega_H)$, for propylene glycol solutions of a), c) 4-oxo-TEMPO-d$_{16}$-^{15}N and b), d) 4-oxo-TEMPO-d$_{16}$-^{14}N for 5 mM concentration of radicals (Ref. [57]). Adopted with permission from D. Kruk et al., J. Chem. Phys. 139, 244502 (2013), Copyright 2013, AIP Publishing LLC.

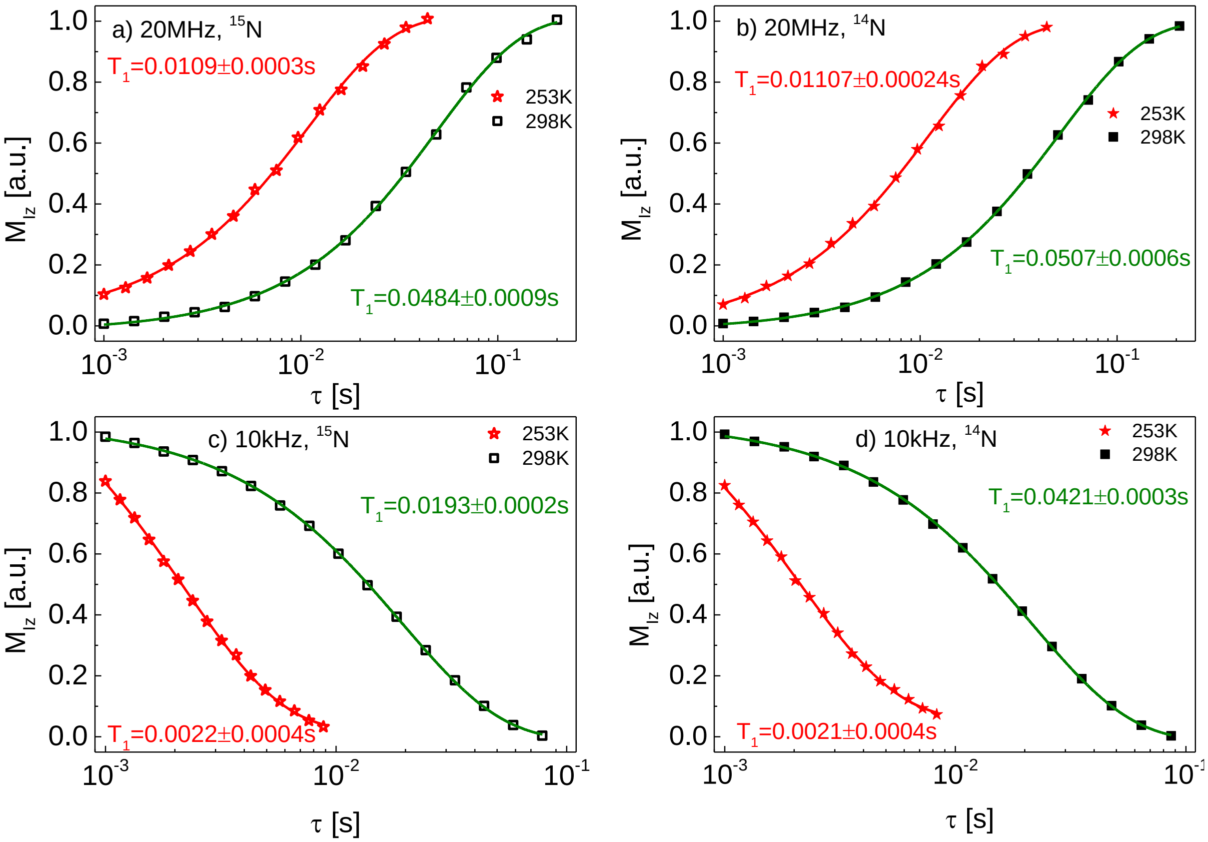

Figure 7.29. ^{1}H magnetization (in arbitrary units) versus time for 5 mM propylene glycol solutions of 4-oxo-TEMPO-d$_{16}$-^{15}N (left) and 4-oxo-TEMPO-d$_{16}$-^{14}N (right) obtained by a), b) NP sequence at 20 MHz and c), d) PP sequence at 10 kHz. Solid red and green lines show the single-exponential fits at 253 K and 298 K, respectively.

$R_1^{par}(\omega_H)$ have been determined in the same way as previously, by subtracting the diamagnetic contribution, $R_1^{diam}(\omega_H)$, (shown in Fig. 7.26) from the total relaxation profile, $R_1(\omega_H)$. Then the $R_1^{par}(\omega_H)$ relaxation rates were normalized to 1 mM concentration of the radicals. The normalized relaxation rates, $R_1^{norm}(\omega_H)$, are shown in Fig. 7.30 with corresponding theoretical fits.

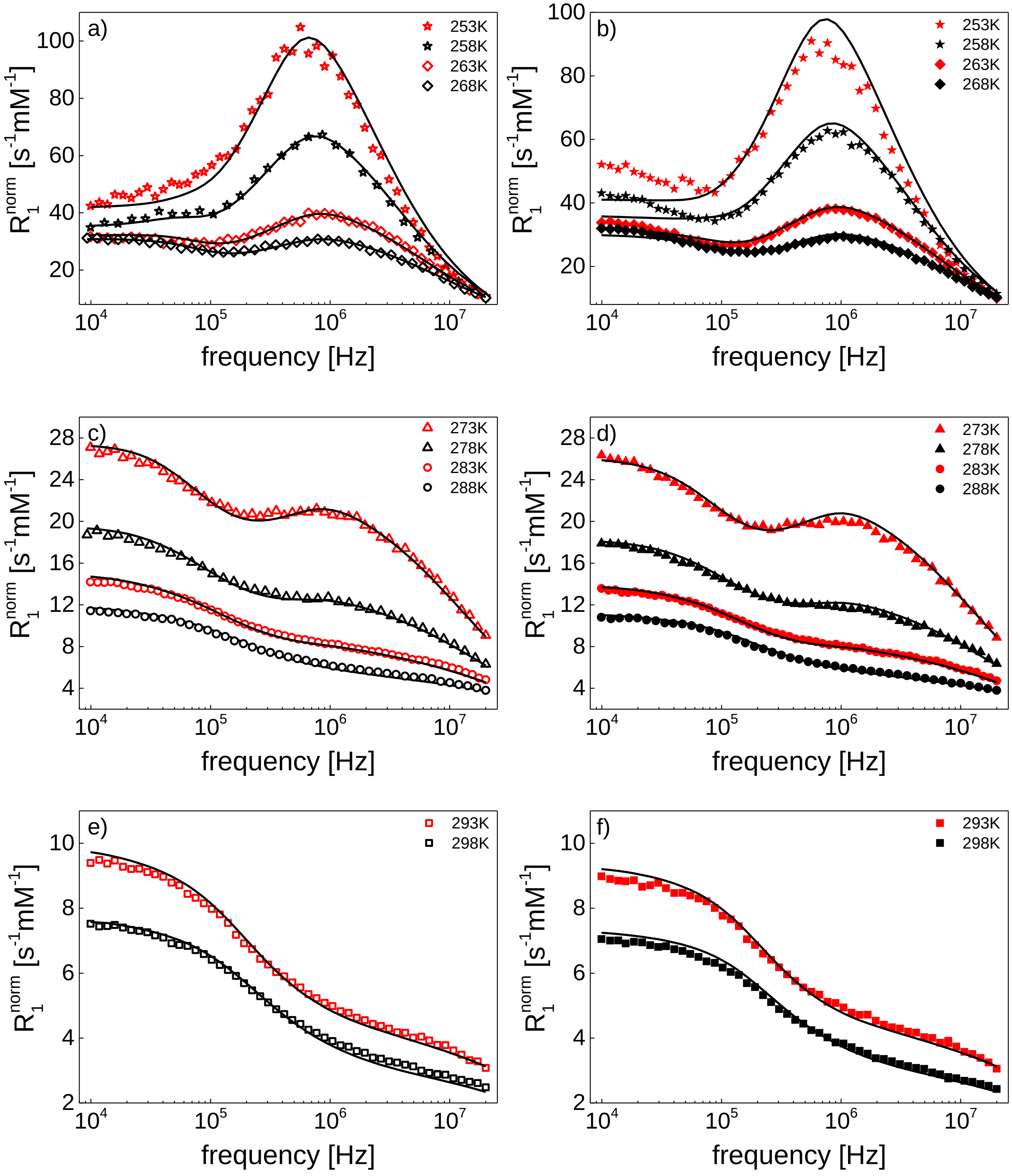

Figure 7.30. ^{1}H relaxation dispersion profiles, $R_1^{norm}(\omega_H)$, for 1 mM propylene glycol solutions of a), c), e) 4-oxo-TEMPO-d_{16}-^{15}N and b), d), f) 4-oxo-TEMPO-d_{16}-^{14}N with corresponding fits in terms of Eq. 73 and 74, respectively (Ref. [57]). Adopted with permission from D. Kruk et al., J. Chem. Phys. 139, 244502 (2013), Copyright 2013, AIP Publishing LLC.

The rotational correlation time, τ_R at the highest temperature (298 K) is of the order of $2*10^{-10}$ s. For correlation times of this order the rotational contribution to the overall relaxation rate, $R_1^{norm}(\omega_H)$, is not negligible (as it has been shown in the previous section for glycerol). This is confirmed by Fig. 7.31 in which the result of the attempt to reproduce the $R_1^{norm}(\omega_H)$ relaxation dispersion profile assuming no rotational contribution ($f=0$) are presented. Significant discrepancies between the fits and the experimental data are observed at low as well as at intermediate frequencies.

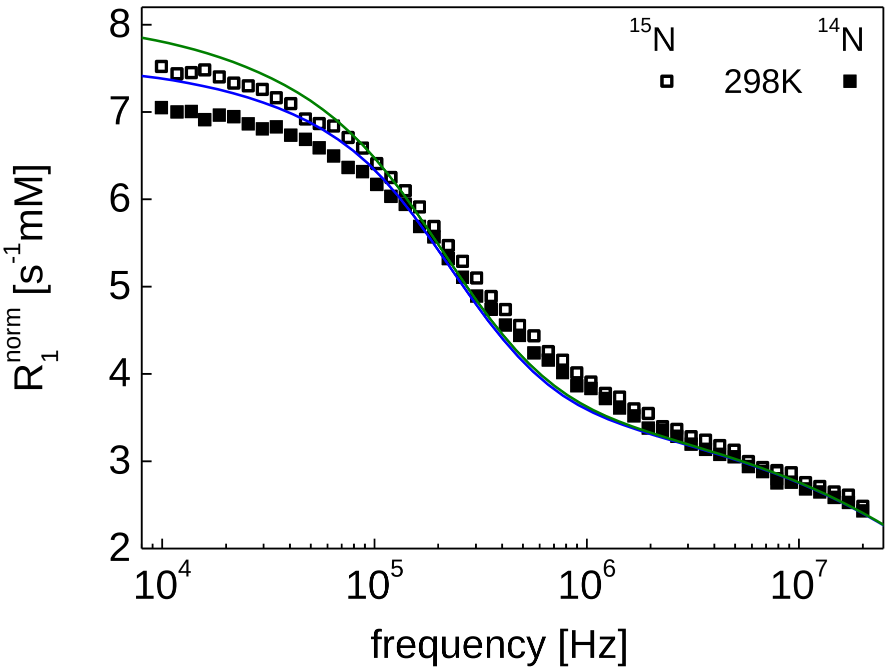

Figure 7.31. ^{1}H spin-lattice relaxation dispersion profiles, $R_1^{norm}(\omega_H)$, for 1 mM propylene glycol solutions of 4-oxo-TEMPO-d_{16}-^{15}N (open symbols) and 4-oxo-TEMPO-d_{16}-^{14}N (closed symbols) at 298 K (Ref. [57]) with corresponding fits ($f=0$). The translational correlation time and the distance of closest approach are in both cases: $\tau_{trans}=3.53*10^{-9}$ s, $d_{IS}=4.32Å$.

The data sets for all temperatures have been fitted with five adjustable parameters: d_{IS}, τ_{trans}, f, τ_R and β. Although in Ref. [57] d_{IS}, x, f, τ_R and β have been chosen as the adjustable parameters, both fitting strategies are fully equivalent because of the relationship: $x=\tau_{trans}/\tau_R$. Therefore, for consistency reasons it has been decided in this thesis to refer to

d_{IS}, τ_{trans}, f, τ_R and β as the adjustable parameters for all cases.

The components of the anisotropic hyperfine coupling have been fixed to the values obtained in ESR experiments performed for the solutions of 4-oxo-TEMPO-d_{16}-$^{15(14)}$N in propylene glycol ($A_{xx} = 10.6$ MHz, $A_{yy} = 10.6$ MHz, $A_{zz} = 107.3$ MHz for ^{14}N and $A_{xx} = 14.85$ MHz, $A_{yy} = 14.85$ MHz, $A_{zz} = 150.2$ MHz for ^{15}N [57]). The analysis has started from the highest temperature of 298 K. Down to 273 K the proton relaxation data for both cases (^{14}N and ^{15}N) have been fitted simultaneously. As expected, at low temperatures (from 288 K) the electron spin relaxation has become significant.

Three of the five adjustable parameters listed above should be temperature independent: d_{IS}, f and β. After a preliminary five-parameters analysis performed in the temperature range of 298 K-253 K, it has been concluded that the best quality of the fits can be obtained when the average values of d_{IS}, f, and β are as follows: $d_{IS} = 4.35$ Å, $f = 1.3$, and $\beta = 0.45$. The stretching parameter is small as already indicated in Ref. [72].

Finally the parameters d_{IS}, f, and β have been fixed to the values given above and the ^{1}H relaxation data for the ^{15}N and ^{14}N cases have been fitted simultaneously with two adjustable parameters: the rotational correlation time, τ_R, and the translational correlation time, τ_{trans}. The obtained parameters are listed in Table 7.3 and the rotational correlation times are shown in Fig. 7.32. Using the expression $D_{12} = d_{IS}^2 / \tau_{trans}$, the values of the relative diffusion coefficient have been calculated and compared with literature data in Fig. 7.33. It is particularly worth mentioning that for propylene glycol solutions the rotational correlation time has been determined also by means of ESR in Ref. [57]. The ratio between the translational and rotational correlation times slightly changes with temperature and its value oscillates around $\tau_{trans} / \tau_R \cong 30$.

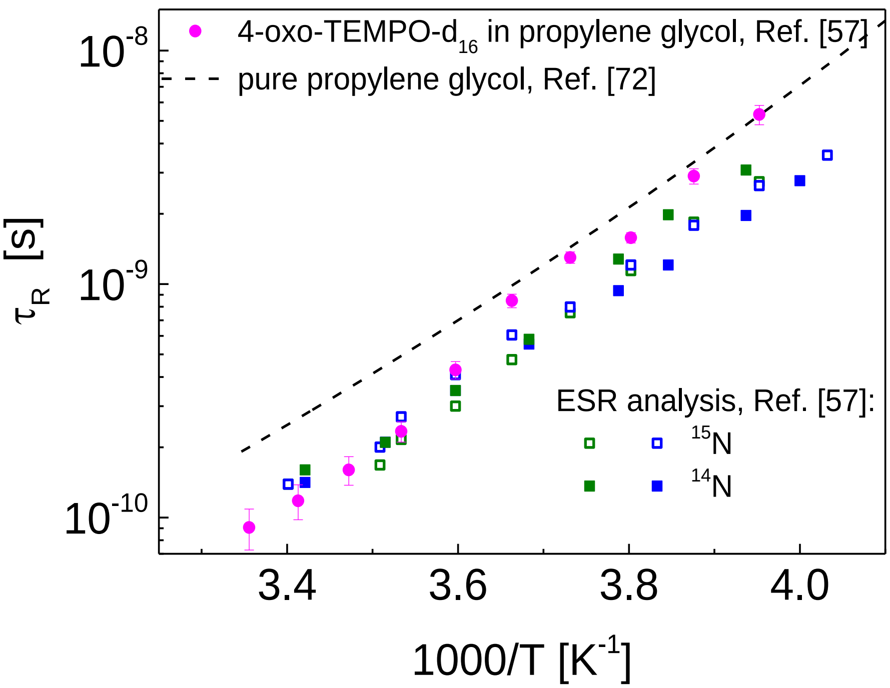

Figure 7.32. Rotational correlation times, τ_R, for propylene glycol solutions of 4-oxo-TEMPO-d$_{16}$-^{15}N and 4-oxo-TEMPO-d$_{16}$-^{14}N (one value for both ^{15}N and ^{14}N cases) obtained from the current analysis of ^{1}H spin-lattice relaxation dispersion data (described in Ref. [57]) compared with rotational correlation times for pure propylene glycol and for propylene glycol solution of -oxo-TEMPO-d$_{16}$-^{15}N and 4-oxo-TEMPO-d$_{16}$-^{14}N (from literature, Refs. [57,72]). Reprinted with permission from D. Kruk et al., J. Chem. Phys. 139, 244502 (2013), Copyright 2013, AIP Publishing LLC.

Analogously to the situation with glycerol, at some point it was not possible to fully reproduce the data with one set of parameters due to the low field values of $R_1^{norm}(\omega_H)$ for ^{14}N. Therefore, the profile obtained for the case of ^{15}N has been analysed and the obtained set of parameters has been used to reproduce the relaxation profile for the ^{14}N case. Due to large discrepancies in the low field which have an impact on the accuracy of the parameters, two values of errors (separately for ^{15}N and ^{14}N) are given in Table 7.3.

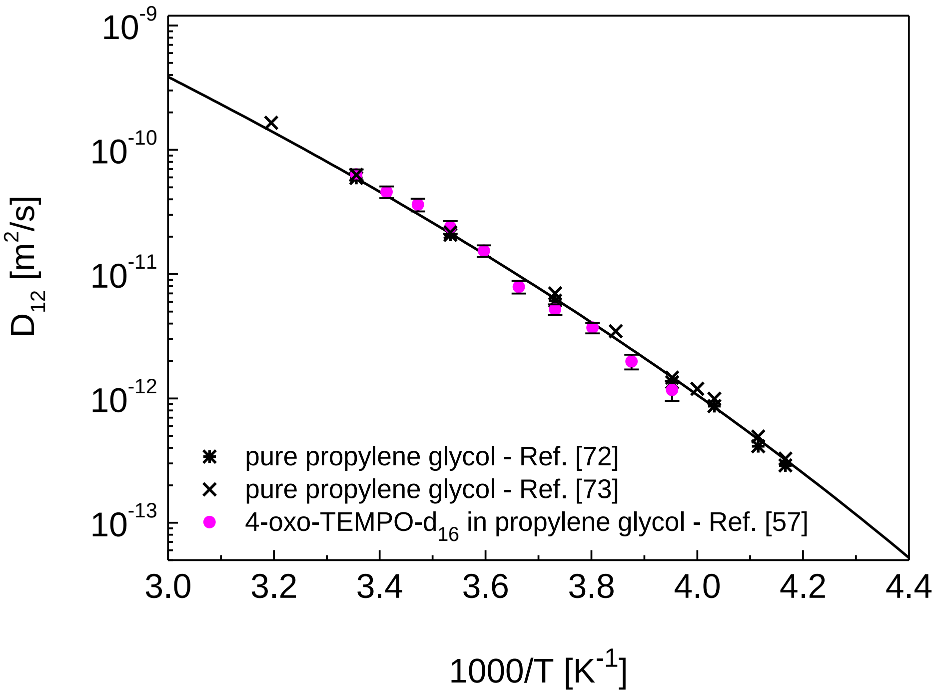

Figure 7.33. Relative diffusion coefficient, D_{12}*, for propylene glycol solution of 4-oxo-TEMPO-*d_{16} *(*^{15}*N,* ^{14}*N) obtained from the current analysis of the* ^{1}*H spin-lattice relaxation dispersion profiles (Ref. [57]) compared with literature values, Refs. [72,73]. Reprinted with permission from D. Kruk et al., J. Chem. Phys. 139, 244502 (2013), Copyright 2013, AIP Publishing LLC.*

T [K]		τ_R [s]		τ_{trans} [s]		d_{IS} [Å]	f	$x = \frac{\tau_{trans}}{\tau_R}$	D_{12} [m^2/s]	
298		$9.07*10^{-11}$	(20%)	$2.99*10^{-9}$	(9.3%)	4.35	1.3	33	$6.32*10^{-11}$	(10%)
293		$1.18*10^{-10}$	(17%)	$4.13*10^{-9}$	(10%)	4.35	1.3	35	$4.58*10^{-11}$	(11%)
288		$1.60*10^{-10}$	(14%)	$5.23*10^{-9}$	(11%)	4.35	1.3	33	$3.62*10^{-11}$	(12%)
283		$2.34*10^{-10}$	(10%)	$7.93*10^{-9}$	(11%)	4.35	1.3	34	$2.39*10^{-11}$	(12%)
278		$4.29*10^{-10}$	(8.6%)	$1.23*10^{-8}$	(10%)	4.35	1.3	29	$1.54*10^{-11}$	(11%)
273		$8.49*10^{-10}$	(6.7%)	$2.39*10^{-8}$	(9.8%)	4.35	1.3	28	$7.90*10^{-12}$	(11%)
268	^{15}N ^{14}N	$1.30*10^{-9}$	(5.3%) (5.6%)	$3.64*10^{-8}$	(8.6%) (9.1%)	4.35	1.3	28	$5.20*10^{-12}$	(9.5%) (10%)
263	^{15}N ^{14}N	$1.58*10^{-9}$	(5.0%) (5.5%)	$5.12*10^{-8}$	(8.0%) (8.9%)	4.35	1.3	32	$3.70*10^{-12}$	(8.9%) (9.8%)
258	^{15}N ^{14}N	$2.90*10^{-9}$	(7.2%) (7.5%)	$9.57*10^{-8}$	(9.9%) (13%)	4.35	1.3	33	$1.98*10^{-12}$	(11%) (14%)
253	^{15}N ^{14}N	$5.32*10^{-9}$	(6.5%) (9.5%)	$1.62*10^{-7}$	(12%) (18%)	4.35	1.3	30.5	$1.17*10^{-12}$	(13%) (18%)

Table 7.3. Rotational and translational parameters for propylene glycol solutions of 4-oxo-TEMPO-d$_{16}$ (^{14}N and ^{15}N), Ref. [57]. The accuracy of the parameters is given in %. Red line indicates the temperature for which (and below) electron spin relaxation has been included into the analysis. Adopted with permission from D. Kruk et al., J. Chem. Phys. 139, 244502 (2013), Copyright 2013, AIP Publishing LLC.

To reveal the role of the individual terms present in Eqs. 73 and 74 in Fig. 7.34 the relaxation dispersion profiles for 288 K have been decomposed analogously to decalin and glycerol (Figs. 7.10, 7.11 and 7.19).

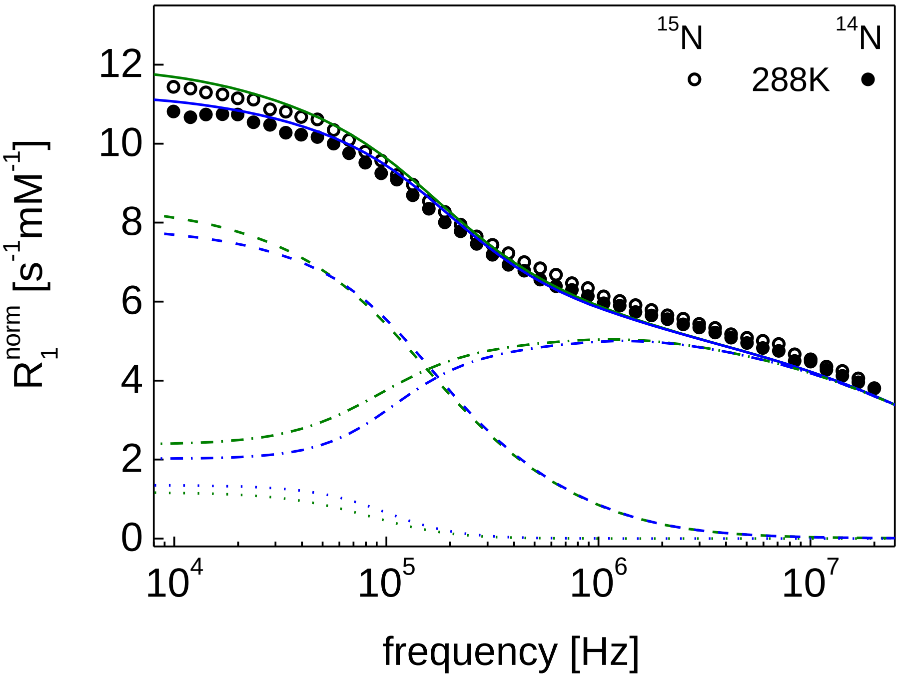

Figure 7.34. ^{1}*H spin-lattice relaxation dispersion profiles,* $R_1^{norm}(\omega_H)$*, for 4-oxo-TEMPO-d*$_{16}$*-*^{15}*N and 4-oxo-TEMPO-d*$_{16}$*-*^{14}*N (open and solid symbols, respectively) with corresponding fits (green and blue solid lines, according to Eqs. 73 and 74, respectively) at 288 K (Ref. [57]). Dashed – dotted green line -* $K_{DD}R_1^{15,I}\left(\omega_H, R^e\right)$ *from Eq. 73; dashed green line -* $K_{DD}R_1^{15,III}\left(\omega_H, R^e\right)$ *from Eq. 73; dotted green line -* $K_{DD}R_1^{15,II}\left(\omega_H, R^e\right)$ *from Eq. 73. Dashed blue line –* $K_{DD}\left(R_1^{14,III}\left(\omega_H, R^e\right)+R_1^{14,IV}\left(\omega_H, R^e\right)\right)$ *from Eq. 74; dashed-dotted blue line –* $K_{DD}R_1^{14,I}\left(\omega_H, R^e\right)$ *from Eq. 74; dotted blue line* $K_{DD}R_1^{14,II}\left(\omega_H, R^e\right)$ *from Eq. 74.*

Already for 288 K the electron spin relaxation is relevant. It becomes progresively more important at lower temperatures – an example for 273 K is shown in Fig. 7.35.

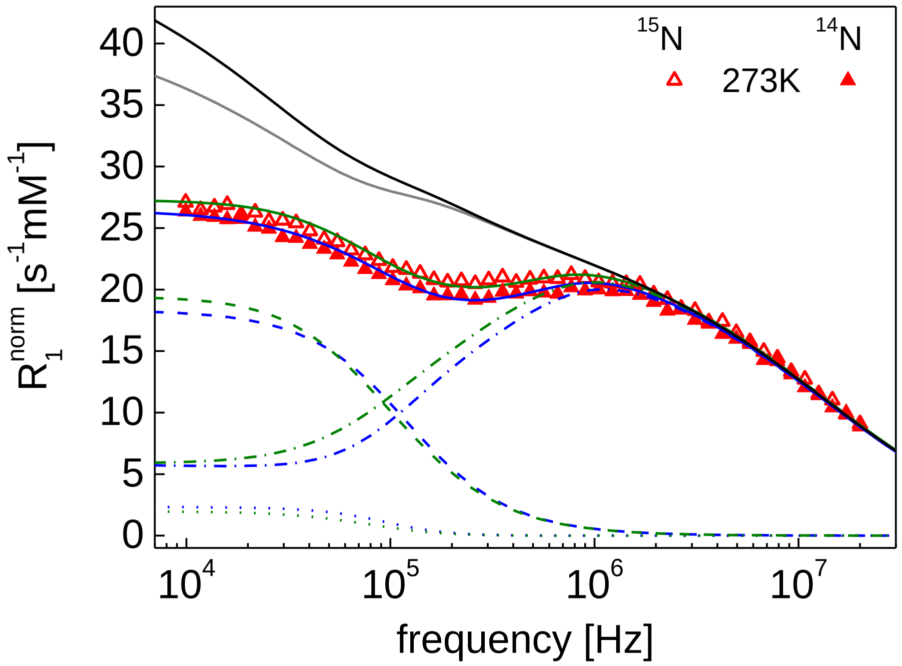

Figure 7.35. ^{1}H spin-lattice relaxation dispersion profiles, $R_1^{norm}(\omega_H)$, for 4-oxo-TEMPO-d$_{16}$-^{15}N and 4-oxo-TEMPO-d$_{16}$-^{14}N (open and solid symbols, respectively) with corresponding fits (green and blue solid lines, according to Eqs. 73 and 74, respectively) 273 K (Ref. [57]). Dashed-dotted green line - $K_{DD}R_1^{15,I}\left(\omega_H, R^e\right)$ from Eq. 73; dashed green line - $K_{DD}R_1^{15,III}\left(\omega_H, R^e\right)$ from Eq. 73; dotted green line - $K_{DD}R_1^{15,II}\left(\omega_H, R^e\right)$ from Eq. 73. Dashed blue line $-K_{DD}\left(R_1^{14,III}\left(\omega_H, R^e\right)+R_1^{14,IV}\left(\omega_H, R^e\right)\right)$ from Eq. 74; dashed-dotted blue line $-$ $K_{DD}R_1^{14,I}\left(\omega_H, R^e\right)$ from Eq. 74; dotted blue line $K_{DD}R_1^{14,II}\left(\omega_H, R^e\right)$ from Eq. 74. Black and grey lines - predictions for case of ^{15}N and ^{14}N according to Eqs. 73 and 74 respectively with neglected electron spin relaxation.

The low frequency reduction of the relaxation rate, $R_1^{norm}(\omega_H)$, is already for 273 K very significant and the effects of the electron spin relaxation becomes crucial at lower temperature (slower dynamics) as shown in Fig. 7.36 for 253 K.

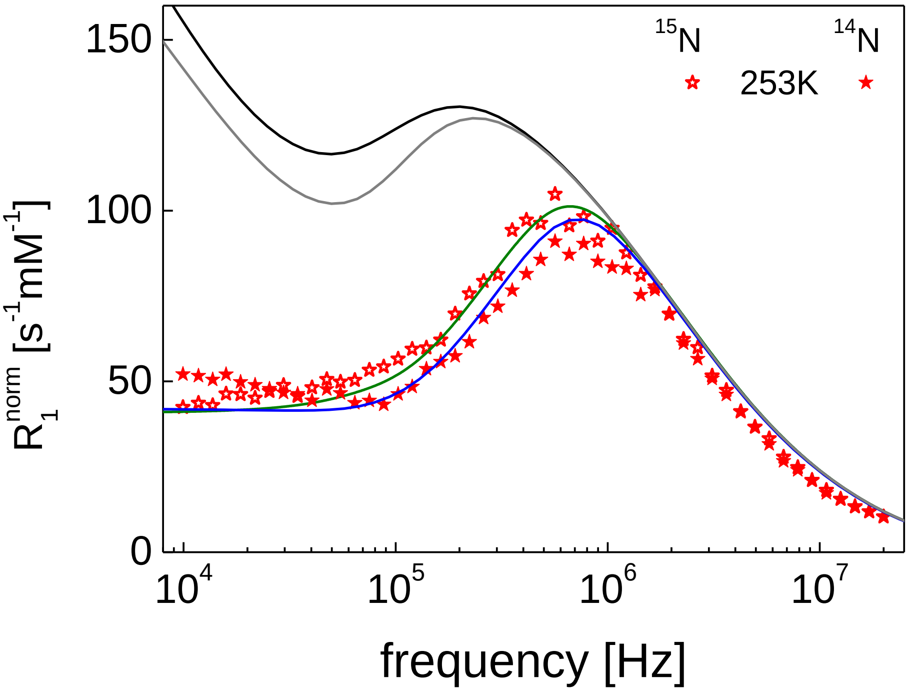

Figure 7.36. ^{1}*H spin-lattice relaxation dispersion profiles,* $R_1^{norm}(\omega_H)$*, for 4-oxo-TEMPO-d*$_{16}$*-*^{15}*N and 4-oxo-TEMPO-d*$_{16}$*-*^{14}*N (open and solid symbols, respectively) dissolved in propylene glycol with corresponding fits at 253 K (Ref. [57]). Black and grey lines - predictions for case of* ^{15}*N and* ^{14}*N according to Eqs. 73 and 74, respectively with neglected electron spin relaxation.*

This is a good moment to remind the origin of the relaxation maximum. As already explained, it results from the competition between the spectral density (which decays with increasing frequency) and pre-factor ($\frac{3}{2}\left[1+\left(a^2-b^2\right)^2\right]$ for ^{15}N and $\left[1+\frac{\left(a^2-b^2\right)^2}{2}+\frac{\left(c^2-d^2\right)^2}{2}+\frac{\left(e^2-f^2\right)^2}{2}+\frac{\left(g^2-h^2\right)}{2}\right]$ for ^{14}N) which increases with frequency. One can see from Fig. 7.36 that the relaxation maximum appears independently of whether the electron spin relaxation is present or not. Nevertheless, in the presence of the electron spin relaxation its position is shifted towards higher frequencies as the effective correlation time of the modulations of the proton spin – electron spin dipole-dipole coupling becomes shorter (due to the contribution of the electron spin relaxation).

Eventually, in analogy to the case of glycerol, in Fig. 7.37 the contribution to the overall relaxation associated with the rotational modulations of the proton spin-electron spin dipolar coupling ($f \neq 0$, eccentricity effect) is shown for the propylene-glycol solution at 273 K. The role of the eccentricity effects is undoubtedly relevant.

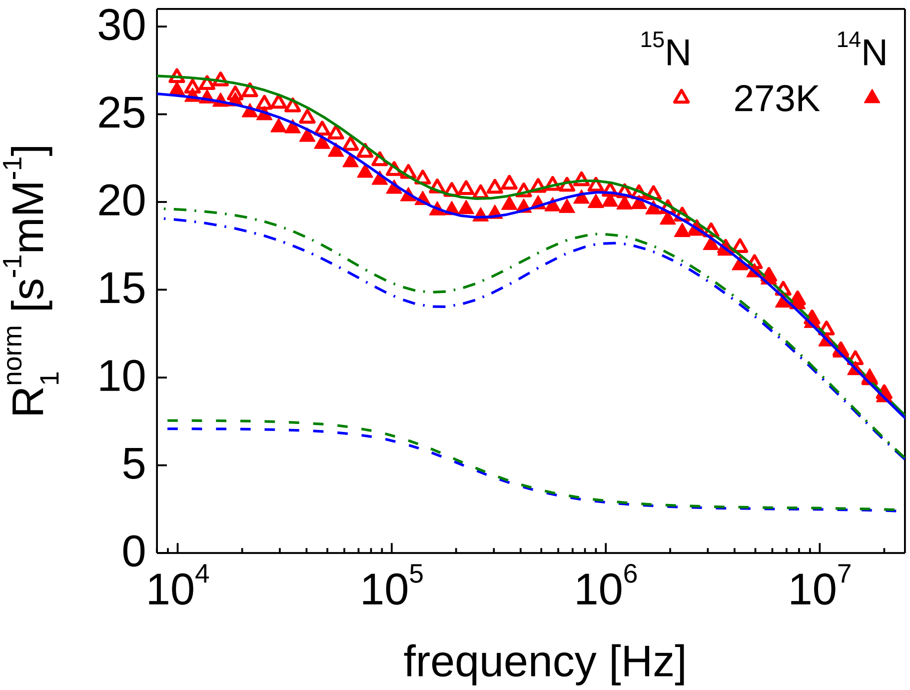

Figure 7.37. *^{1}H spin-lattice relaxation dispersion profiles,* $R_1^{norm}(\omega_H)$, *for 4-oxo-TEMPO-d$_{16}$-^{15}N and 4-oxo-TEMPO-d$_{16}$-^{14}N (open and solid symbols, respectively) dissolved in propylene glycol with corresponding fits (Ref. [57]) decomposed into rotational (dashed lines) and translational (dashed-dotted lines) contributions at 273 K.*

^{1}H relaxation dispersion measurements presented in this Section for pure solvent are a result of joint work of the author and Roman Meier (who collected most of the NMRD profiles for pure glycerol). The experiments for the paramagnetic solutions have been performed by the author, as said in the Introduction.

8. Summary

In the thesis a large set of ^{1}H spin-lattice relaxation dispersion data for solutions of nitroxide radicals containing ^{14}N and ^{15}N isotopes is presented. By using different solvents (decalin, glycerol, propylene glycol) and performing the experiments for different temperatures, a broad range of the timescales of the rotational and translational dynamics of the solvent and solute molecules has been covered. The following observations have been made:

- The relaxation data for solutions of nitroxide radicals (collected in the frequency range of 10 kHz – 20 MHz) show a significant dispersion even when the dynamics is so fast that the corresponding data for pure solvents are (almost) frequency independent ($D_{12} = 1*10^{-9}$ m/s^{2}).
- At low frequencies the ^{1}H spin lattice relaxation rates for solutions of ^{15}N containing radicals differ from the relaxation rates for the case of ^{14}N containing radicals. This effect evolves with temperature (*i.e.* the time scale of the translational and rotational dynamics). For relatively high temperatures (corresponding to the translation diffusion coefficient of about $1*10^{-9}$ m/s^{2}) the ^{1}H spin-lattice relaxation rate for the case of ^{14}N containing radicals is somewhat smaller than for the ^{15}N case. This effect becomes more pronounced for slower dynamics, but when the diffusion coefficient reaches a value of about $5*10^{-12}$ m/s^{2} the relaxation rates become close again and then the relationship gets inverted (the ^{1}H spin-lattice relaxation rate for the ^{14}N cases becomes larger than for solutions of ^{15}N containing radicals).
- For slower dynamics the relaxation dispersion data show (in both cases: for ^{14}N and ^{15}N) a maximum at intermediate frequencies (about 200 kHz – 3 MHz).

These effects are explained and the ^{1}H spin-lattice relaxation dispersion is quantitatively analyzed by means of a comprehensive theory of paramagnetic relaxation enhancement in solutions of nitroxide radicals [31,32,57]. The main elements of the theory are outlined in the thesis. The relaxation scenario is as follows. The mechanism of the ^{1}H spin-lattice relaxation is provided by dipole-dipole interactions between protons of the solvent molecules and unpaired electrons of the radical molecules. The dipole-dipole coupling fluctuates in time due to relative translational dynamics of the solvent and solute molecules, their rotational dynamics and electron spin relaxation. The source of the electron spin relaxation is provided by the anisotropic part of the electron – nitrogen hyperfine coupling modulated by rotational dynamics of the paramagnetic molecules, while the isotropic part of the hyperfine coupling affects the energy level structure of the electron spin. The electron spin relaxation is described by means of the Redfield relaxation theory. In consequence the approach is valid when the condition $\omega_{aniso}\tau_R < 1$ is fulfilled (ω_{aniso} is the amplitude of the anisotropic part of the hyperfine interaction in angular frequency units). In consequence, the upper limit of the rotational correlation time yields $\tau_R = (2-3)*10^{-9}$ s. For fast dynamics the role of the electron spin relaxation is less significant and for the rotational correlation time of the order of $\tau_R \cong 1*10^{-10}$ s it becomes negligible. The theory consists of three steps. First, it has been formulated for the simpler case of ^{15}N (the ^{15}N spin yields $P = 1/2$) in [15,32], neglecting the electron spin relaxation. Next it has been complemented by a counterpart dedicated to the more complex case of ^{14}N containing radicals ($P = 1$) [32]. Eventually, the approach has been generalized by including the electron spin relaxation for both cases [31]. The relative translational diffusion of the interacting molecules have been described by the force-free-hard sphere model [26,27]. The rotational dynamics modulates the proton-electron dipole-dipole coupling directly, through the eccentricity effect, and, indirectly, through the electron spin relaxation rates. The rotational dynamics has been described by a Cole-Davidson spectral density.

Numerous simulations have been performed in the thesis, to explain the influence of the dynamical and electron spin parameters on the ^{1}H spin-lattice relaxation in different frequency ranges. The theory has been used for the analysis of the experimental data. In this way translational diffusion coefficients and rotational correlation times have been determined. The values of these parameters have been compared with values obtained by other methods (taken from literature). The agreement is very good and the analysis of the ^{14}N and ^{15}N systems is consistent and it explains the features of the ^{1}H spin-lattice relaxation dispersion profiles outlined above.

- The significant relaxation dispersion observed for the paramagnetic solutions even for fast dynamics is caused by the presence of spectral densities taken at the electron spin frequency (which is by factor 657 larger than the proton frequency) in the equations describing the ^{1}H spin-lattice relaxation. This means that by introducing paramagnetic molecules to diamagnetic liquids one can probe a much faster dynamical processes than for pure diamagnetic liquids.

- The behavior of the ^{1}H spin-lattice relaxation rates for solutions of ^{14}N and ^{15}N containing radicals can be explained by means of the theory as a result of the isotropic part of the hyperfine coupling (this explains why the low frequency relaxation rates for the ^{14}N case are lower than for the ^{15}N case) and the electron spin relaxation (anisotropic part of the hyperfine coupling). The last factor explains why for slower dynamics the ratio between the relaxation rates deviates from the value predicted in the absence of the electron spin relaxation), but some deviations from the experimental data are observed. They might be caused by simplifications of the motional models. It is also possible that interference effects between the hyperfine coupling and the quadrupolar coupling of ^{14}N (which is not included into presented approach) gives a relevant contribution to the electron spin relaxation.
- The relaxation maximum is caused by an interplay (competition) between spectral densities decaying with increasing frequency and pre-factors in the relaxation formulae which increase with increasing frequency.

9. Further Perspectives

The intensity of NMR signals can be enhanced through Dynamic Nuclear Polarization (DNP) effects in which the large electron spin polarization is transferred to neighbouring nuclei [47,74-77]. In most cases monomeric paramagnetic centers (e.g. nitroxide radicals or metal ions) are used as a source of the polarization. Molecules containing two paramagnetic centers are very promising candidates for increasing the efficiency of the polarization transfer. The electron spin and nuclear spin relaxation rates are very important factors determining the obtained enhancement of the NMR signal.

From this perspective, the theory of electronic and nuclear relaxation in solutions of monomeric nitroxide radicals is a very good starting point for theoretical modeling of relaxation processes in systems containing biradicals. A well-known example of biradicals is TOTAPOL (1-(TEMPO-4-oxy)-3-(TEMPO-4-amino)propan-2-ol, Fig. 9.1). The linker between the two TEMPO molecules containing unpaired electrons is rather short (the analysis of the powder PER line shapes shows that the electron-electron distance is about 12.8 Å [78]) that leads to strong interactions between the paramagnetic centres. Thus, the Hamiltonian of the spin system has to include a term describing the dipole-dipole interaction of the two electron spins.

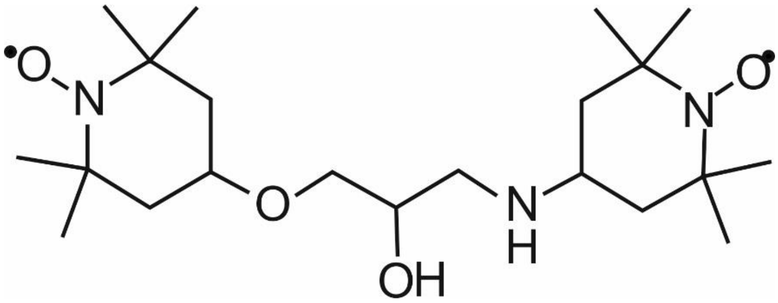

Figure 9.1. Structure of TOTAPOL.

In Fig. 9.2 an example of ^{1}H spin-lattice relaxation dispersion data for propylene-glycol solutions of TOTAPOL (biradical) and 4-oxo-TEMPO-d_{16}-^{14}N (monomeric nitroxide radical) is shown. The data have been normalized to the same concentration of paramagnetic centres – 10 mM. As TOTAPOL has two unpaired electrons the concentration of the TOTAPOL molecules is twice smaller than that of 4-oxo-TEMPO-d_{16}-^{14}N . The results agree at high magnetic field as expected (the electron Zeeman interactions dominate all other interactions within the spin system), but they considerably differ at low and intermediate fields. The ^{1}H relaxation rates for the TOTAPOL solution is smaller as a result of a faster modulations of the proton spin-electron spin dipole-dipole coupling caused by faster electron spin relaxation resulted from the strong dipolar coupling between the electron spins.

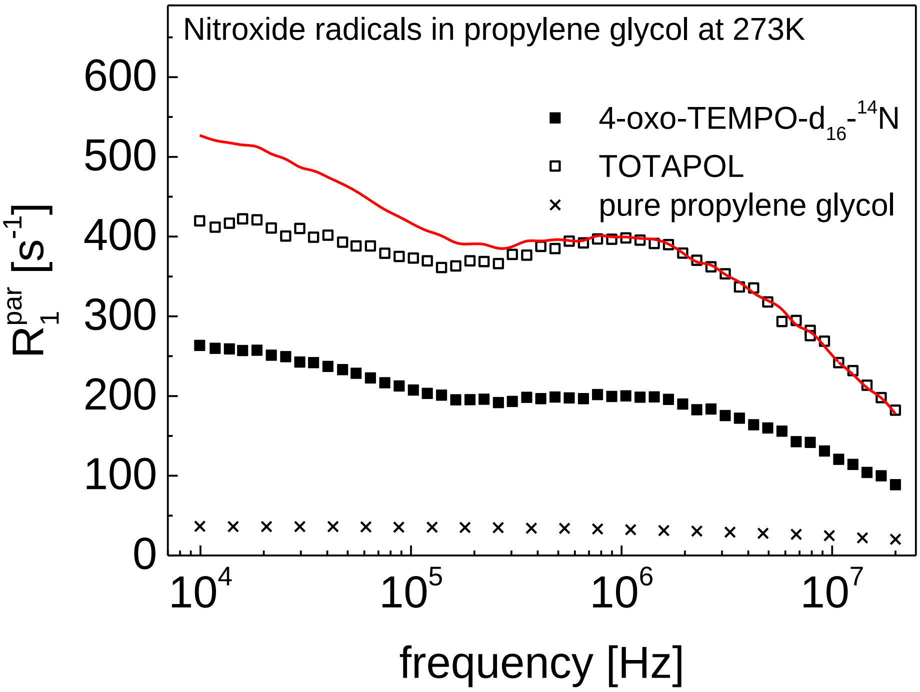

Figure 9.2. Experimental ^{1}H spin-lattice relaxation dispersion profiles for 10 mM propylene glycol solutions of TOTAPOL (open squares) and of 4-oxo-TEMPO-d_{16}-^{14}N (solid squares). Solid red line - the relaxation profile for 4-oxo-TEMPO-d_{16}-^{14}N normalized to the same electron spin S concentration as it is for TOTAPOL;

References

1. J. McConnell, *The theory of nuclear magnetic relaxation in liquids*, Cambridge University Press, Cambridge (1987).
2. D. Kruk, *Theory of Evolution and Relaxation of Multi-spin Systems*, Arima Publishing, Bury St Edmunds (2007).
3. R. Freeman. *Spin Choreography, Basic Steps in High Resolution NMR*, Oxford University Press, Oxford, New York, Tokyo (1998).
4. C. P. Slichter. *Principles of Magnetic Resonance*. Springer-Verlag Berlin Heidelberg, New York (1978).
5. J. Kowalewski and L. Mäller, *Nuclear Spin Relaxation in Liquids: Theory, Experiments, and Applications*, Taylor & Francis, New York (2006).
6. E. L. Hahn, Spin echoes. *Phys. Rev.* **80**(4), 580-594 (1950).
7. J. McConnell, Theory of nuclear magnetic relaxation by dipolar interaction. *Physica A* **135**(1), 38-62 (1986).
8. J. H. Jeans, *The Mathematical Theory of Electricity and Magnetism*, Cambridge University Press, Cambridge (1933).
9. A. Abragam, *The principles of nuclear magnetism*, Oxford University Press, Oxford (1961).
10. M. H. Levitt, *Spin Dynamics*, Chichester, Wiley (2001).
11. J. W. Hennel and J. Klimowski, *Fundamentals of Nuclear Magnetic Resonance in One and Two Dimensions*, Clarendon Press, Oxford (1994).
12. R. R. Sharp, Nuclear-spin relaxation in paramagnetic solutions when the electronic zero-field splitting and zeeman interactions are of arbitrary magnitude, *J. Magn. Reson.* **100**, 491-516 (1992).
13. J. H. Freed, Dynamic effects of pair correlation functions on spin relaxation by translational diffusion in liquids: II. Finite jumps and independent T_1 processes, *J. Chem. Phys.* **68**, 4034-4037 (1978).
14. H. A. Buckmaster, Tables of angular momentum transformation matrix elements dJ/M, M(beta) (j=2,4,6), *Can. J. Phys.* **42**, 386-391 (1964).
15. E. Belorizky, D. G. Gillies, W Gorecki, K. Lang, F. Noack, C. Roux, J. Struppe, L. H. Sutcliffe, J. P. Travers, and X. Wu. Translational diffusion constants and intermolecular relaxation in paramagnetic solutions with hyperfine coupling on the electronic site. *J. Phys. Chem. A* **102**, 3674-3680 (1998).
16. I. Bertini, F. Briganti, C. Luchinat, M. Mancini, and G. J. Spina. The electron-nucleus dipolar coupling in slow rotating systems. 2. the effect of g anisotropy and hyperfine coupling when s=1/2 and i=3/2. *J. Magn. Reson.* **63**, 41–55 (1985).
17. I. Bertini, C. Luchinat, and G. Parigi, *Solution NMR of Paramagnetic Molecules*, Elsevier, Amsterdam (2001).
18. L. Barci, I. Bertini, and C. Luchinat, *Nuclear and Electron Relaxation*, VCH, Weinheim, (1991).
19. D. Canet. Introduction: General theory of nuclear relaxation, *Adv. Inorg. Chem.* **57**, 3–40 (2005).

20. J. Kowalewski, D. Kruk, and G. Parigi, NMR relaxation in solution of paramagnetic compexes: Recent theoretical progress for S>=1, *Adv. Inorg. Chem.* **57**, 41-104 (2005).
21. N. Bloembergen, E. M. Purcell, and R. V. Pound, Relaxation effects in nuclear magnetic resonance absorption, *Phys. Rev.* **73**, 679-712 (1948).
22. R. Kohlrausch, Theorie des elektrischen Rückstandes in der Leidner Flasche, *Ann. Phys. Chem. (Poggendorff)* **91**, 179-213 (1854).
23. C. J. F. Böttcher and P. Bordewijk. *Theory of Electric Polarization*, volume 2. Elsevier, Amsterdam (1973).
24. L. W. Wang and H.-J. Fecht, A kinetic model for liquids: Relaxation in liquids, origin of the Vogel-Tammann-Fulcher equation, and the essence of fragility, *J. Appl. Phys.* **104**, 113538 (2008).
25. J. P. Albrand, M. C. Taieb, P. H. Fries, and E. Belorizky, NMR study of spectral densities over a large frequency range for intermolecular relaxation in liquids: Pair correlation effects. *J. Chem. Phys.* **78**, 5809-5815 (1983).
26. J. P. Albrand, M. C. Taieb, P. H. Fries, and E. Belorizky, Effects of eccentricity on nuclear magnetic relaxation by intermolecular dipole-dipole interactions: ^{13}C relaxation of neopentane, *J.Chem. Phys.* **75**, 2141 (1981).
27. Y. Ayant, E. Belorizky, P. Fries, and J. Rosset. Effet des interactions dipolaires magnétiques intermoléculaires sur la relaxation nucléaire de molécules polyatomiques dans les liquides. *J. Phys.* **38**(3), 325-337 (1977).
28. Y. Ayant, E. Belorizky, J. Alizon, and J. Gallice, Calcul des densités spectrales résultant d'un mouvement aléatoire de translation en relaxation par interaction dipolaire magnétique dans les liquides. *J. Phys.* **36**(10), 991-1004 (1975).
29. L. P. Hwang and J. H. Freed. Dynamic effects of pair correlation functions on spin relaxation by translational diffusion in liquids. *J. Chem. Phys.* **63**, 4017 (1975).
30. P. H. Fries, J. P. Albrand, M. C. Taieb, E. Belorizky, and M. Minier, Frequency dependence of the effects of eccentricity on nuclear magnetic relaxation in liquids. ^{13}C relaxation of neopentane due to free radicals. *J. Magn. Reson.* **54**, 177-189 (1983).
31. D. Kruk, A. Korpała, A. Kubica, J. Kowalewski, E. A. Rössler, and J. Moscicki, ^{1}H relaxation dispersion in solutions of nitroxide radicals: Influence of electron spin relaxation, *J. Chem. Phys.* **138**, 124506 (2013).
32. D. Kruk, A. Korpała, J. Kowalewski, E. A. Rössler, and J. Moscicki, ^{1}H relaxation dispersion in solutions of nitroxide radicals: Effects of hyperfine interactions with ^{14}N and ^{15}N nuclei. *J. Chem. Phys.* **137**, 044512 (2012).
33. D. Kruk, A. Korpała, E. A. Rössler, K. A. Earle, W. Medycki, and J. Moscicki, ^{1}H NMR relaxation in glycerol solutions of nitroxide radicals: Effects of translational and rotational dynamics, *J. Chem. Phys.* **136**, 114504 (2012).
34. D. Kruk, R. Meier, and E. Rössler, Translational and rotational diffusion of glycerol by means of field cycling ^{1}H NMR relaxometry, *J. Phys. Chem. B* **115**, 951-957 (2011).
35. R. Meier, D. Kruk, J. Gmeiner, and E. A. Rössler, Intermolecular relaxation in glycerol as revealed by field cycling ^{1}H NMR relaxometry dilution experiments. *J.*

Chem. Phys. **136**, 034508 (2012).

36. N. Bloembergen, Proton relaxation times in paramagnetic solutions, *J. Chem. Phys.* **27**, 572-573 (1957).
37. R. K. Wangsness and F. Bloch, The dynamic theory of nuclear induction, *Phys. Rev.* **89**, 728-739 (1953).
38. F. Bloch, Dynamical theory of nuclear induction. 2., *Phys. Rev.* **102**, 104-135 (1956).
39. I. Solomon, Relaxation processes in a system of two spins, *Phys. Rev.* **99**, 559-566 (1955).
40. N. Bloembergen and L. O. Morgan, Proton relaxation times in paramagnetic solutions. Effects of electron spin relaxation, *J. Chem. Phys.* **34**, 842-850 (1961).
41. R. Kimmich, *NMR Tomography, Diffusiometry, Relaxometry*, Springer, Berlin (1997).
42. D. Kruk, T. Nilsson, and J. Kowalewski, Outher-sphere nuclear spin relaxation in paramagnetic systems: a low-field theory, *Mol. Phys.* **99**, 1435-1445 (2001).
43. D. Kruk and O. Lips, Field-dependent nuclear relaxation of spins 1/2 induced by dipole-dipole coupling to quadrupole spins: LaF_3 crystals as an example, *J. Magn. Reson.* **179**, 250-262 (2006).
44. L. T. Muss and P. W. Atkins (Eds.), *Electron spin relaxation in liquids*, Plenum Press, New York (1972).
45. R. Kubo, Stochastic Liouville equations, *J. Math. Phys.* **4**, 174-183 (1963).
46. K. Blum, *Density matrix theory and applications*, Plenum Press, New York (1989).
47. M. Bennati, C. Luchinat, G. Parigi, and M.-T. Türke. Water ^{1}H relaxation dispersion analysis on a nitroxide radical provides information on the maximal signal engancement in Overhauser dynamic nuclear polarization experiments. Phys. Chem. Chem. Phys. **12**, 5902-5910 (2010).
48. R. Kimmich and E. Anoardo, Field-cycling NMR relaxometry, Progr. NMR Spectrosc. **44**, 257-320 (2004).
49. D. Kruk, T. Nilsson, and J. Kowalewski, Nuclear spin relaxation in paramagnetic systems with zero-field splitting and arbitrary electron spin, *Phys. Chem. Chem. Phys.* **3**, 4907-4917 (2001).
50. S. Rast, P. H. Fries, and E. Belorizky, Static zero field splitting effects on the electronic relaxation of paramagnetic metal ion complexes in solution, *J. Chem. Phys.* **113**, 8724-8735 (2000).
51. T. Nilsson and J. Kowalewski, Slow-motion theory of nuclear spin relaxation in paramagnetic low-symmetry complexes: A generalization to high electron spin, *J. Magn. Reson.* **146**, 345-358 (2000).
52. N. Schaefle and R. Sharp, Electron spin relaxation due to reorientation of a permanent zero field splitting tensor, *J. Chem. Phys.* **121**, 5387-5394 (2004).
53. P. H. Fries and E. Belorizky, Relaxation theory of the electronic spin of a complexed paramagnetic metal ion in solution beyond the Redfield limit, *J. Chem. Phys.* **126**, 204503 (2007).
54. E. Belorizky, P. H. Fries, L. Helm, J. Kowalewski, D. Kruk, R. R. Sharp, and P. O. Westlund, Comparison of different methods for calculating the paramagnetic

relaxation enhancement of nuclear spins as a function of the magnetic field, *J. Chem. Phys.* **128**, 052315 (2008).

55. D. Kruk and J. Kowalewski, General treatment of paramagnetic relaxation enhancement associated with translational diffusion, *J. Chem. Phys.* **130**, 174104 (2009).
56. D. Kruk, J. Kowalewski, D. S. Tipikin, J. H. Freed, M. Moscicki, A. Mielczarek and M. Port, Joint analysis of ESR lineshapes and ^{1}H NMRD profiles of DOTA-Gd derivatives by means of the slow motion theory, *J. Chem. Phys.* **134**, 024508 (2011).
57. D. Kruk, S. K. Hoffman, J. Goslar, S. Lijewski, A. Kubica-Misztal, A. Korpała, I. Ogłodek, J. Kowalewski, E. A. Rössler, and J. Mościcki, ESR lineshape and ^{1}H spin-lattice relaxation dispersion in propylene glycol solutions of nitroxide radicals – joint analysis, *J. Chem. Phys.* **139**, 244502 (2013).
58. J. S. Hwang, R. P. Mason, L. Hwang, and J. H. Freed, Electron spin resonance studies of anisotropic rotational reorientation and low tumbling in liquid and frozen media. iii. Predeuterated 2,2,6,6-tetramethyl-4-piperidone-N-oxide and an analysis of fluctuating torques, *J. Phys. Chem.* **79**, 489-511 (1975).
59. D. Kruk and J. Kowalewski, Nuclear spin relaxation in solution of paramagnetic complexes with large transient zerio-field splitting, *Mol. Phys.* **101**, 2861-2874 (2003).
60. W. M. Hayness, *Handbook of Chemistry and Physics*, Boca Raton, Florida: CRC Press. p. 3-134 (2010).
61. J. Wuttke, J. Hernandez, G. Li, G. Coddens, H. Z. Cummins, F. Fujara, W. Petry, and H. Sillescu, Neutron and light scattering study of supercooled glycerol, *Phys. Rev. Lett.* **72**, **19**, 3052-3055 (1994).
62. C. K. Zeberg-Mikkelsen, A. Baylaucq, M. Barrouhou, and C. Boned, The effect of stereoisomerism on dynamic viscosity: A study of cis-decalin and trans-decalin versus pressure and temperature, *Phys. Chem. Chem. Phys.* **5**, 1547-1551 (2003).
63. J. B. Segur and H. E. Oberstar, Viscosity of glycerol and its aqueous solutions, *Ind. Eng. Chem.* **43**, 2117-2120 (1951).
64. J. George and N. V. Sastry, Densities, dynamic viscosities, speeds of sound, and relatice permittivities for water + alkanediols (propane-1,2- and -1,3-diol and butane-1,2-, -1,3-, -1,4-, and -2,3-diol) at different temperatures, *J. Chem. Eng. Data* **48**, 1529-1539 (2003).
65. D. Kruk, A. Korpała, S. Mehdizadeh Taheri, A. Kozłowski, S. Förster, and E. A. Rössler, ^{1}H relaxation enhancement induced by nanoparticles in solutions: Influence of magnetic properties and diffusion, *J. Chem. Phys.* **140**, 174504 (2014).
66. H. Sato, S. E. Bottle, J. P. Blinco, A. S. Micallef, G. R. eaton, and S. S. Eaton, Electron spin-lattice relaxation of nitroxyl radicals in temperature ranges that span glassy solutions to low-viscosity liquids, *J. Magn. Reson.* **191**, 66-77 (2008).
67. H. Sato, V. Kathirvelu, A. Fielding, A. P. Blinco, A. S. Micallef, S. E. Bottle, S. S. Eaton, and G. R. Eaton, Impact of molecular size on electron spin relaxation rates of nitroxyl radicals in glassy solvents between 100 and 300 K, *Mol. Phys.* **105**, 2137-2151 (2007).
68. J. Fischer and A. Weiss, Transport Properties of Liquids. V. Self Diffusion,

Viscosity, and Mass Density of Ellipsoidal Shaped Molecules in the Pure Liquid Phase, *Ber. Bunsenges. Phys. Chem.* **90**, 896-905 (1986).

69. B. Chen, E. E. Sigmund, and W. P. Halperin, Stokes-Einstein relation in supercooled aqueous solutions of glycerol, *Phys. Rev. Lett.* **96**, 145502 (2006).
70. D. Kruk, A. Herrmann, and E. A. Rössler, Field-cycling NMR relaxometry of viscous liquids and polymers, *Progr. NMR Spectrosc.* **63**, 33-64 (2012).
71. A. M. F. Benial, M. Kumara Dhas, and A. Jawahar, Rotational Correlation time studies on nitroxyl radicals using 300 MHz ESR spectrometer in high viscous liquid, *Appl. Magn. Reson.* **40**, 311-319 (2011).
72. R. Meier, R. Kahlau, D. Kruk, and E. A. Rössler, Comparative studies of the dynamics in viscous liquids by means of dielectric spectroscopy and field cycling NMR, *J. Phys. Chem. A* **114**, 7874-7855 (2010).
73. R. Meier, E. Schneider, and E. A. Rössler, Change of translational-rotational coupling in liquids revealed by field-cycling ^{1}H NMR, *J. Chem. Phys.* **142**, 034503 (2015).
74. Y. Hovav, A. Feintuch, and S. Vega, Dynamic nuclear polarization assisted spin diffusion for the solid case, *J. Chem. Phys.* **134**, 074509 (2011).
75. P. Höfer, G. Parigi, C. Luchinat, P. Carl, G. guthausen, M. Reese, T. Carlomango, C. Griedenger, and M. Bennati, Field dependent dynamic nuclear polarization with radicals in aqueous solution, *J. Am. Chem. Soc.* **130**, 3254-3255 (2008).
76. B. D. Armstrong and S. Han, Overhauser dynamic nuclear polarization to study local water dynamics, *J. Am. Chem. Soc.* **131**, 4641-4647 (2009).
77. M.-T. Türke, G. Parigi, C. Luchinat, and M. Bennati, Overhauser DNP with ^{15}N labelled Frémy salt at 0.35 Tesla, *Phys. Chem. Chem. Phys.* **14**, 502-510 (2012).
78. Ch. Song, K.-N. Hu, Ch.-G. Joo, T. M. Swager, and R. G. Griffin, Totapol: a biradical polarizing agent for dynamic nuclear polarization experiments in aqueous media, *J. Am. Chem. Soc.* **128**(35), 11385-11390 (2006).
79. D. M. Bates and D. G. Watts, *Nonlinear regression analysis & its application,* John Wiles & Sons, Inc (1988).
80. A. R. Gallant, *Nonlinear statistical models*, Wiley Series in Probability and Mathematical Statistics **310**, John Wiley & Sons, Inc (2009).

Appendix

A.1 Program code

Code of the main body of the fitting program:

```
clc;
tic

load 'dane\prop\n14_298.txt';
x=n14_298(:,1)';
w=x;
y=n14_298(:,2)';
semilogx(w,y,'ro','Linewidth',2); hold on

x0=[7.0e0  30.0 0.00 0.67 4.5e0];

lb=[3.10e-1 34.0 0.00 0.44999 3.0e0];
ub=[5.70e-1 35.0 2.00 0.45001 7.5e0];

[pout,resnorm,residual,exitflag,output,lambda,J] =
lsqcurvefit(@funkcja_relaksacji_14N,x0,w,y,lb,ub);

p=pout;
disp('tauR0'); disp(p(1)*1e-10);
disp('x'); disp(p(2));
disp('f'); disp(p(3));
disp('\beta'); disp(p(4));
disp('d_{IS}'); disp(p(5));


sigma=sqrt((1/(length(y)-5))*resnorm*diag(full(inv(J'*J))));

for i=1:8
    sigma(i)=100*sigma(i)*pout(i).^(-1);
end

w=logspace(3,9,100);
[R1,J_trans,J_rot,J_1t,J_2t,J_3t,J_4t]= funkcja_relaksacji_14N
(p,w);
semilogx(w,R1,'k-','Linewidth',2); hold on
semilogx(w,J_trans,'g.','Linewidth',2);
semilogx(w,J_rot,'b-','Linewidth',2);

toc

T=[w;R1];
f2=fopen('relaksacja14N.txt','w');
fprintf(f2,'\n%d\t%d', T);
fclose(f2);
```

Relaxation functions (Eqs. 73 and 74, respectively) defined in MATLAB:

```
function [R1,J_trans,J_rot,J_1t,J_2t,J_3t,J_4t,stala,J_1]=
funkcja_relaksacji_15N (p,w)

%%%%%%%%%%%%%%%%%%%%%%%%%%%%%%%%%%%%%%%%%%%%%%%%%%%%%%%%%%%%%%%%%%%%
%%%             parameters
%%%%%%%%%%%%%%%%%%%%%%%%%%%%%%%%%%%%%%%%%%%%%%%%%%%%%%%%%%%%%%%%%%%%
p(1)=p(1)*1e-10;
%tauR=p(1);
%x=p(2);
%fcd=p(3);
%beta=p(4);
%dIS=p(5);

%%%%%%%%%%%%%%%%%%%%%%%%%%%%%%%%%%%%%%%%%%%%%%%%%%%%%%%%%%%%%%%%%%%%
%%% hyperfine coupling
%%%%%%%%%%%%%%%%%%%%%%%%%%%%%%%%%%%%%%%%%%%%%%%%%%%%%%%%%%%%%%%%%%%%
Axx=44e6; %Hz
Ayy=44e6;
Azz=44e6;

A=(Axx+Ayy+Azz)/3;
A=A*2*pi;
DeltaA=Azz-(1/2)*(Axx+Ayy);
DeltaA=sqrt(2/3)*DeltaA;
deltaA=(1/2)*(Axx-Ayy);

%%%%%%%%%%%%%%%%%%%%%%%%%%%%%%%%%%%%%%%%%%%%%%%%%%%%%%%%%%%%%%%%%%%%
R1=zeros;
J_trans=zeros;
J_rot=zeros;
wp=2*pi*w;

%%%%%%% constants %%%%%%%%%%%%%%%%%%%%%%%%%%%%%%%%%%%%%%%%%%%%%%%%%%
gammaI=2.67522212e8;
gammaS=1.760859794e11;
mi0= 12.566370614e-7;
Na=6.02214199e23;
Ni=1.0;
Ni=Ni*Na;
hbar=1.054571596e-34;
dIS=p(5)*1e-10;
Kdd=(1/10)*((4*pi)/3)*((mi0*gammaI*gammaS*hbar/(4*pi)).^2)*(Ni/(dIS.
^3));

%%%%%%%%%%%%%%%%%%%%%%%%%%%%%%%%%%%%%%%%%%%%%%%%%%%%%%%%%%%%%%%%%%%%

wH=2*pi*w;
wS=657*wH;


%%%%%%%%%%%%%%%%%%%%%%%%%%%%%%%%%%%%%%%%%%%%%%%%%%%%%%%%%%%%%%%%%%%%
%%%              constants
%%%%%%%%%%%%%%%%%%%%%%%%%%%%%%%%%%%%%%%%%%%%%%%%%%%%%%%%%%%%%%%%%%%%
c1=sqrt(0.5*(1+(wS./sqrt(A.^2+wS.^2))));
c2=sqrt(0.5*(1-(wS./sqrt(A.^2+wS.^2))));
```

```
%%%%%%%%%%%%%%%%%%%%%%%%%%%%%%%%%%%%%%%%%%%%%%%%%%%%%%%%%%%%%%%%%%%%
%%%%%%%%%%%%%%%%%%%%%%%%%%%%%%%%%%%%%%%%%%%%%%%%%%%%%%%%%%%%%%%%%%%%
%%%               frequencies
%%%%%%%%%%%%%%%%%%%%%%%%%%%%%%%%%%%%%%%%%%%%%%%%%%%%%%%%%%%%%%%%%%%%
w12=wS./2+A/2-0.5*sqrt(A.^2+wS.^2);
w21=-w12;
w13=wS./2+A/2+0.5*sqrt(A.^2+wS.^2);
w31=-w13;
w23=sqrt(A.^2+wS.^2);
w32=-w23;
w24=wS./2-A./2+0.5*sqrt(A.^2+wS.^2);
w42=-w24;
w34=wS./2-A./2-0.5*sqrt(A.^2+wS.^2);
w43=-w34;
%%%%%%%%%%%%%%%%%%%%%%%%%%%%%%%%%%%%%%%%%%%%%%%%%%%%%%%%%%%%%%%%%%%%



%%%%%%%%%%%%%%%%%%%%%%%%%%%%%%%%%%%%%%%%%%%%%%%%%%%%%%%%%%%%%%%%%%%%
%%%        total spectral densities - function
%%%%%%%%%%%%%%%%%%%%%%%%%%%%%%%%%%%%%%%%%%%%%%%%%%%%%%%%%%%%%%%%%%%%
[J_1,J_1_trans,J_1_rot]=J_gest_2(p,wH);
[J_2,J_2_trans,J_2_rot]=J_gest_2(p,w23-wH);
[J_3,J_3_trans,J_3_rot]=J_gest_2(p,w23+wH);
[J_4,J_4_trans,J_4_rot]=J_gest_2(p,w32-wH);
[J_5,J_5_trans,J_5_rot]=J_gest_2(p,w32+wH);
[J_6,J_6_trans,J_6_rot]=J_gest_2(p,w31-wH);
[J_7,J_7_trans,J_7_rot]=J_gest_2(p,w31+wH);
[J_8,J_8_trans,J_8_rot]=J_gest_2(p,w13+wH);
[J_9,J_9_trans,J_9_rot]=J_gest_2(p,w13-wH);
[J_10,J_10_trans,J_10_rot]=J_gest_2(p,w24+wH);
[J_11,J_11_trans,J_11_rot]=J_gest_2(p,w24-wH);
[J_12,J_12_trans,J_12_rot]=J_gest_2(p,w42-wH);
[J_13,J_13_trans,J_13_rot]=J_gest_2(p,w42+wH);
[J_14,J_14_trans,J_14_rot]=J_gest_2(p,w21-wH);
[J_15,J_15_trans,J_15_rot]=J_gest_2(p,w21+wH);
[J_16,J_16_trans,J_16_rot]=J_gest_2(p,w43-wH);
[J_17,J_17_trans,J_17_rot]=J_gest_2(p,w43+wH);
[J_18,J_18_trans,J_18_rot]=J_gest_2(p,w12+wH);
[J_19,J_19_trans,J_19_rot]=J_gest_2(p,w12-wH);
[J_20,J_20_trans,J_20_rot]=J_gest_2(p,w34+wH);
[J_21,J_21_trans,J_21_rot]=J_gest_2(p,w34-wH);
%%%%%%%%%%%%%%%%%%%%%%%%%%%%%%%%%%%%%%%%%%%%%%%%%%%%%%%%%%%%%%%%%%%%



%%%%%%%%%%%%%%%%%%%%%%%%%%%%%%%%%%%%%%%%%%%%%%%%%%%%%%%%%%%%%%%%%%%%
%%%             total spectral densities
%%%%%%%%%%%%%%%%%%%%%%%%%%%%%%%%%%%%%%%%%%%%%%%%%%%%%%%%%%%%%%%%%%%%
stala=(1+(c1.^2-c2.^2).^2);
J_1t=(1+(c1.^2-c2.^2).^2).*J_1;
J_2t=(c1.^2).*(c2.^2).*(J_2+J_3+J_4+J_5);
J_3t=(1/6)*(c1.^2).*(6*J_6+J_7+6*J_8+J_9+6*J_10+J_11+6*J_12+J_13);
J_4t=(1/6)*(c2.^2).*(6*J_14+J_15+6*J_16+J_17+6*J_18+J_19+6*J_20+J_21
);
%%%%%%%%%%%%%%%%%%%%%%%%%%%%%%%%%%%%%%%%%%%%%%%%%%%%%%%%%%%%%%%%%%%%
```

```
%%%%%%%%%%%%%%%%%%%%%%%%%%%%%%%%%%%%%%%%%%%%%%%%%%%%%%%%%%%%%%%%%%%%
%%%             translational spectral densities
%%%%%%%%%%%%%%%%%%%%%%%%%%%%%%%%%%%%%%%%%%%%%%%%%%%%%%%%%%%%%%%%%%%%
J_1trans=(1+(c1.^2-c2.^2).^2).*J_1_trans;
J_2trans=(c1.^2).*(c2.^2).*(J_2_trans+J_3_trans+J_4_trans+J_5_trans)
;
J_3trans=(1/6)*(c1.^2).*(6*J_6_trans+J_7_trans+6*J_8_trans+J_9_trans
+...
6*J_10_trans+J_11_trans+6*J_12_trans+J_13_trans);
J_4trans=(1/6)*(c2.^2).*(6*J_14_trans+J_15_trans+6*J_16_trans+...
J_17_trans+6*J_18_trans+J_19_trans+6*J_20_trans+J_21_trans);
%%%%%%%%%%%%%%%%%%%%%%%%%%%%%%%%%%%%%%%%%%%%%%%%%%%%%%%%%%%%%%%%%%%%


%%%%%%%%%%%%%%%%%%%%%%%%%%%%%%%%%%%%%%%%%%%%%%%%%%%%%%%%%%%%%%%%%%%%
%%%             rotational spectral densities
%%%%%%%%%%%%%%%%%%%%%%%%%%%%%%%%%%%%%%%%%%%%%%%%%%%%%%%%%%%%%%%%%%%%
J_1rot=(1+(c1.^2-c2.^2).^2).*J_1_rot;
J_2rot=(c1.^2).*(c2.^2).*(J_2_rot+J_3_rot+J_4_rot+J_5_rot);
J_3rot=(1/6)*(c1.^2).*(6*J_6_rot+J_7_rot+6*J_8_rot+J_9_rot+6*J_10_ro
t+...
J_11_rot+6*J_12_rot+J_13_rot);
J_4rot=(1/6)*(c2.^2).*(6*J_14_rot+J_15_rot+6*J_16_rot+J_17_rot+...
6*J_18_rot+J_19_rot+6*J_20_rot+J_21_rot);
%%%%%%%%%%%%%%%%%%%%%%%%%%%%%%%%%%%%%%%%%%%%%%%%%%%%%%%%%%%%%%%%%%%%


%%%%%%%%%%%%%%%%%%%%%%%%%%%%%%%%%%%%%%%%%%%%%%%%%%%%%%%%%%%%%%%%%%%%
%%%          total relaxation rate
%%%%%%%%%%%%%%%%%%%%%%%%%%%%%%%%%%%%%%%%%%%%%%%%%%%%%%%%%%%%%%%%%%%%
R1=Kdd*0.5*3*(J_1t+J_2t+J_3t+J_4t);
J_trans=Kdd*0.5*3*(J_1trans+J_2trans+J_3trans+J_4trans);
J_rot=Kdd*0.5*3*(J_1rot+J_2rot+J_3rot+J_4rot);
%%%%%%%%%%%%%%%%%%%%%%%%%%%%%%%%%%%%%%%%%%%%%%%%%%%%%%%%%%%%%%%%%%%%


J_1t=Kdd*0.5*3*J_1t;
J_2t=Kdd*0.5*3*J_2t;
J_3t=Kdd*0.5*3*J_3t;
J_4t=Kdd*0.5*3*J_4t;
```

```
function
[R1,J_trans,J_rot,J_1tot,J_2tot,J_3tot,J_4tot,J_5tot,J_6tot] =
funkcja_relaksacji_14N (p,w)

%%%%%%%%%%%%%%%%%%%%%%%%%%%%%%%%%%%%%%%%%%%%%%%%%%%%%%%%%%%%%%%%%%%%
%%%            przypisanie wartości zmiennym
%%%%%%%%%%%%%%%%%%%%%%%%%%%%%%%%%%%%%%%%%%%%%%%%%%%%%%%%%%%%%%%%%%%%
p(1)=p(1)*1e-10;
%tauR=p(1);
%x=p(2);
%fcd=p(3);
%beta=p(4);
dIS=p(5)*1e-10;

Axx=63e6; %Hz
Ayy=63e6;
Azz=63e6;

A=(Axx+Ayy+Azz)/3;
A=A*2*pi;
DeltaA=Azz-(1/2)*(Axx+Ayy);
DeltaA=sqrt(2/3)*DeltaA;
deltaA=(1/2)*(Axx-Ayy);
R1=zeros;
J_trans=zeros;
J_rot=zeros;


%%%%%%%%%%%%%%%%%%%%%%%%%%%%%%%%%%%%%%%%%%%%%%%%%%%%%%%%%%%%%%%%%%%%
%%%     physical constants
%%%%%%%%%%%%%%%%%%%%%%%%%%%%%%%%%%%%%%%%%%%%%%%%%%%%%%%%%%%%%%%%%%%%
gammaI=2.67522212e8;
gammaS=1.760859794e11;
mi0= 12.566370614e-7;
Na=6.02214199e23;
Ni=1.0;
Ni=Ni*Na;
hbar=1.054571596e-34;  %stała Plancka
Kdd=(1/10)*((4*pi)/3)*((mi0*gammaI*gammaS*hbar/(4*pi)).^2)*(Ni/(dIS.
^3));

%%%%%%%%%%%%%%%%%%%%%%%%%%%%%%%%%%%%%%%%%%%%%%%%%%%%%%%%%%%%%%%%%%%%


wH=2*pi*w;
wS=657*wH;


%%%%%%%%%%%%%%%%%%%%%%%%%%%%%%%%%%%%%%%%%%%%%%%%%%%%%%%%%%%%%%%%%%%%
%%%                       alpha, beta etc.
%%%%%%%%%%%%%%%%%%%%%%%%%%%%%%%%%%%%%%%%%%%%%%%%%%%%%%%%%%%%%%%%%%%%
alpha=(A+2*wS+sqrt(9*A.^2+4*A*wS+4*wS.^2))./(2*sqrt(2)*A);
beta=(A+2*wS-sqrt(9*A.^2+4*A*wS+4*wS.^2))./(2*sqrt(2)*A);
gamma=(A-2*wS-sqrt(9*A.^2-4*A*wS+4*wS.^2))./(2*sqrt(2)*A);
delta=(A-2*wS+sqrt(9*A.^2-4*A*wS+4*wS.^2))./(2*sqrt(2)*A);
%%%%%%%%%%%%%%%%%%%%%%%%%%%%%%%%%%%%%%%%%%%%%%%%%%%%%%%%%%%%%%%%%%%%
```

```
%%%%%%%%%%%%%%%%%%%%%%%%%%%%%%%%%%%%%%%%%%%%%%%%%%%%%%%%%%%%%%%%%%%%
%%%                   normalized factors
%%%%%%%%%%%%%%%%%%%%%%%%%%%%%%%%%%%%%%%%%%%%%%%%%%%%%%%%%%%%%%%%%%%%

la=sqrt(1+beta.*beta);
lb=sqrt(1+beta.*beta);
lc=sqrt(1+alpha.*alpha);
ld=sqrt(1+alpha.*alpha);
le=sqrt(1+delta.*delta);
lf=sqrt(1+delta.*delta);
lg=sqrt(1+gamma.*gamma);
lh=sqrt(1+gamma.*gamma);
%%%%%%%%%%%%%%%%%%%%%%%%%%%%%%%%%%%%%%%%%%%%%%%%%%%%%%%%%%%%%%%%%%%%


%%%%%%%%%%%%%%%%%%%%%%%%%%%%%%%%%%%%%%%%%%%%%%%%%%%%%%%%%%%%%%%%%%%%
%%%                         factors
%%%%%%%%%%%%%%%%%%%%%%%%%%%%%%%%%%%%%%%%%%%%%%%%%%%%%%%%%%%%%%%%%%%%
a=la.^(-1);
b=beta./lb;
c=lc.^(-1);
d=alpha./ld;
e=le.^(-1);
f=delta./lf;
g=lg.^(-1);
h=gamma./lh;
%%%%%%%%%%%%%%%%%%%%%%%%%%%%%%%%%%%%%%%%%%%%%%%%%%%%%%%%%%%%%%%%%%%%

%%%%%%%%%%%%%%%%%%%%%%%%%%%%%%%%%%%%%%%%%%%%%%%%%%%%%%%%%%%%%%%%%%%%
%%%              transition frequencies
%%%%%%%%%%%%%%%%%%%%%%%%%%%%%%%%%%%%%%%%%%%%%%%%%%%%%%%%%%%%%%%%%%%%
w23=sqrt(wS.^2+wS.*A+(9/4)*A^2);
w45=sqrt(wS.^2-wS.*A+(9/4)*A^2);
w12=wS./2+3*A/4-(0.5)*sqrt(wS.^2+wS.*A+(9/4)*A^2);
w13=wS./2+3*A/4+0.5*sqrt(wS.^2+wS.*A+(9/4)*A^2);
w46=wS./2-3*A/4+0.5*sqrt(wS.^2-wS.*A+(9/4)*A^2);
w56=wS./2-3*A/4-0.5*sqrt(wS.^2-wS.*A+(9/4)*A^2);
w24=0.5*sqrt(wS.^2+wS.*A+(9/4)*A^2)-0.5*sqrt(wS.^2-wS.*A+(9/4)*A^2);
w25=0.5*sqrt(wS.^2+wS.*A+(9/4)*A^2)+0.5*sqrt(wS.^2-wS.*A+(9/4)*A^2);
w34=-w25;
w35=-w24;
%%%%%%%%%%%%%%%%%%%%%%%%%%%%%%%%%%%%%%%%%%%%%%%%%%%%%%%%%%%%%%%%%%%%


%%%%%%%%%%%%%%%%%%%%%%%%%%%%%%%%%%%%%%%%%%%%%%%%%%%%%%%%%%%%%%%%%%%%
%%%        spectral densities
%%%%%%%%%%%%%%%%%%%%%%%%%%%%%%%%%%%%%%%%%%%%%%%%%%%%%%%%%%%%%%%%%%%%
[J_1,J_1_trans,J_1_rot]=J_gest_2(p,wH);
[J_2,J_2_trans,J_2_rot]=J_gest_2(p,w23-wH);
[J_3,J_3_trans,J_3_rot]=J_gest_2(p,w23+wH);
[J_4,J_4_trans,J_4_rot]=J_gest_2(p,w45-wH);
[J_5,J_5_trans,J_5_rot]=J_gest_2(p,w45+wH);
[J_6,J_6_trans,J_6_rot]=J_gest_2(p,w12+wH);
[J_7,J_7_trans,J_7_rot]=J_gest_2(p,w12-wH);
[J_8,J_8_trans,J_8_rot]=J_gest_2(p,w13+wH);
```

```
[J_9,J_9_trans,J_9_rot]=J_gest_2(p,w13-wH);
[J_10,J_10_trans,J_10_rot]=J_gest_2(p,w46+wH);
[J_11,J_11_trans,J_11_rot]=J_gest_2(p,w46-wH);
[J_12,J_12_trans,J_12_rot]=J_gest_2(p,w56+wH);
[J_13,J_13_trans,J_13_rot]=J_gest_2(p,w56-wH);
[J_14,J_14_trans,J_14_rot]=J_gest_2(p,w24+wH);
[J_15,J_15_trans,J_15_rot]=J_gest_2(p,w24-wH);
[J_16,J_16_trans,J_16_rot]=J_gest_2(p,w25+wH);
[J_17,J_17_trans,J_17_rot]=J_gest_2(p,w25-wH);
[J_18,J_18_trans,J_18_rot]=J_gest_2(p,w34+wH);
[J_19,J_19_trans,J_19_rot]=J_gest_2(p,w34-wH);
[J_20,J_20_trans,J_20_rot]=J_gest_2(p,w35+wH);
[J_21,J_21_trans,J_21_rot]=J_gest_2(p,w35-wH);
%%%%%%%%%%%%%%%%%%%%%%%%%%%%%%%%%%%%%%%%%%%%%%%%%%%%%%%%%%%%%%%%%%%%


%%%%%%%%%%%%%%%%%%%%%%%%%%%%%%%%%%%%%%%%%%%%%%%%%%%%%%%%%%%%%%%%%%%%
%%%     spectral densities with factors
%%%%%%%%%%%%%%%%%%%%%%%%%%%%%%%%%%%%%%%%%%%%%%%%%%%%%%%%%%%%%%%%%%%%
J_1t=(1+0.5*(a.^2-b.^2).^2+0.5*(c.^2-d.^2).^2+0.5*(e.^2-f.^2).^2+...
0.5*(g.^2-h.^2).^2).*J_1;
J_2t=((a.*c-b.*d).^2/2).*J_2;
J_3t=((a.*c-b.*d).^2/2).*J_3;
J_4t=((e.*g-f.*h).^2/2).*J_4;
J_5t=((e.*g-f.*h).^2/2).*J_5;
J_6t=2*(b.^2).*J_6;
J_7t=(1/3)*(b.^2).*J_7;
J_8t=2*(d.^2).*J_8;
J_9t=(1/3)*(d.^2).*J_9;
J_10t=2*(e.^2).*J_10;
J_11t=(1/3)*(e.^2).*J_11;
J_12t=2*(g.^2).*J_12;
J_13t=(1/3)*(g.^2).*J_13;
J_14t=2*((a.*f).^2).*J_14;
J_15t=(1/3)*((a.*f).^2).*J_15;
J_16t=2*((a.*h).^2).*J_16;
J_17t=(1/3)*((a.*h).^2).*J_17;
J_18t=2*((c.*f).^2).*J_18;
J_19t=(1/3)*((c.*f).^2).*J_19;
J_20t=2*((c.*h).^2).*J_20;
J_21t=(1/3)*((c.*h).^2).*J_21;
%%%%%%%%%%%%%%%%%%%%%%%%%%%%%%%%%%%%%%%%%%%%%%%%%%%%%%%%%%%%%%%%%%%%



%%%%%%%%%%%%%%%%%%%%%%%%%%%%%%%%%%%%%%%%%%%%%%%%%%%%%%%%%%%%%%%%%%%%
%%%             translational spectral densities
%%%%%%%%%%%%%%%%%%%%%%%%%%%%%%%%%%%%%%%%%%%%%%%%%%%%%%%%%%%%%%%%%%%%
J_1trans=(1+0.5*(a.^2-b.^2).^2+0.5*(c.^2-d.^2).^2+0.5*(e.^2-
f.^2).^2+...
0.5*(g.^2-h.^2).^2).*J_1_trans;
J_2trans=((a.*c-b.*d).^2/2).*J_2_trans;
J_3trans=((a.*c-b.*d).^2/2).*J_3_trans;
J_4trans=((e.*g-f.*h).^2/2).*J_4_trans;
J_5trans=((e.*g-f.*h).^2/2).*J_5_trans;
J_6trans=2*(b.^2).*J_6_trans;
J_7trans=(1/3)*(b.^2).*J_7_trans;
J_8trans=2*(d.^2).*J_8_trans;
```

```
J_9trans=(1/3)*(d.^2).*J_9_trans;
J_10trans=2*(e.^2).*J_10_trans;
J_11trans=(1/3)*(e.^2).*J_11_trans;
J_12trans=2*(g.^2).*J_12_trans;
J_13trans=(1/3)*(g.^2).*J_13_trans;
J_14trans=2*((a.*f).^2).*J_14_trans;
J_15trans=(1/3)*((a.*f).^2).*J_15_trans;
J_16trans=2*((a.*h).^2).*J_16_trans;
J_17trans=(1/3)*((a.*h).^2).*J_17_trans;
J_18trans=2*((c.*f).^2).*J_18_trans;
J_19trans=(1/3)*((c.*f).^2).*J_19_trans;
J_20trans=2*((c.*h).^2).*J_20_trans;
J_21trans=(1/3)*((c.*h).^2).*J_21_trans;
%%%%%%%%%%%%%%%%%%%%%%%%%%%%%%%%%%%%%%%%%%%%%%%%%%%%%%%%%%%%%%%%%%%%


%%%%%%%%%%%%%%%%%%%%%%%%%%%%%%%%%%%%%%%%%%%%%%%%%%%%%%%%%%%%%%%%%%%%
%%%             rotational spectral densities
%%%%%%%%%%%%%%%%%%%%%%%%%%%%%%%%%%%%%%%%%%%%%%%%%%%%%%%%%%%%%%%%%%%%
J_1rot=(1+0.5*(a.^2-b.^2).^2+0.5*(c.^2-d.^2).^2+0.5*(e.^2-
f.^2).^2+...
0.5*(g.^2-h.^2).^2).*J_1_rot;
J_2rot=((a.*c-b.*d).^2/2).*J_2_rot;
J_3rot=((a.*c-b.*d).^2/2).*J_3_rot;
J_4rot=((e.*g-f.*h).^2/2).*J_4_rot;
J_5rot=((e.*g-f.*h).^2/2).*J_5_rot;
J_6rot=2*(b.^2).*J_6_rot;
J_7rot=(1/3)*(b.^2).*J_7_rot;
J_8rot=2*(d.^2).*J_8_rot;
J_9rot=(1/3)*(d.^2).*J_9_rot;
J_10rot=2*(e.^2).*J_10_rot;
J_11rot=(1/3)*(e.^2).*J_11_rot;
J_12rot=2*(g.^2).*J_12_rot;
J_13rot=(1/3)*(g.^2).*J_13_rot;
J_14rot=2*((a.*f).^2).*J_14_rot;
J_15rot=(1/3)*((a.*f).^2).*J_15_rot;
J_16rot=2*((a.*h).^2).*J_16_rot;
J_17rot=(1/3)*((a.*h).^2).*J_17_rot;
J_18rot=2*((c.*f).^2).*J_18_rot;
J_19rot=(1/3)*((c.*f).^2).*J_19_rot;
J_20rot=2*((c.*h).^2).*J_20_rot;
J_21rot=(1/3)*((c.*h).^2).*J_21_rot;

%%%%%%%%%%%%%%%%%%%%%%%%%%%%%%%%%%%%%%%%%%%%%%%%%%%%%%%%%%%%%%%%%%%%
%%%          relaxation rate
%%%%%%%%%%%%%%%%%%%%%%%%%%%%%%%%%%%%%%%%%%%%%%%%%%%%%%%%%%%%%%%%%%%%
R1=Kdd*(J_1t+J_2t+J_3t+J_4t+J_5t+J_6t+J_7t+J_8t+J_9t+J_10t+J_11t+...
J_12t+J_13t+J_14t+J_15t+J_16t+J_17t+J_18t+J_19t+J_20t+J_21t);
J_trans=Kdd*(J_1trans+J_2trans+J_3trans+J_4trans+J_5trans+J_6trans+.
..
J_7trans+J_8trans+J_9trans+J_10trans+J_11trans+J_12trans+J_13trans+.
..
J_14trans+J_15trans+J_16trans+J_17trans+J_18trans+J_19trans+...
J_20trans+J_21trans);
J_rot=Kdd*(J_1rot+J_2rot+J_3rot+J_4rot+J_5rot+J_6rot+...
J_7rot+J_8rot+J_9rot+J_10rot+J_11rot+J_12rot+J_13rot+...
J_14rot+J_15rot+J_16rot+J_17rot+J_18rot+J_19rot+J_20rot+J_21rot);
%%%%%%%%%%%%%%%%%%%%%%%%%%%%%%%%%%%%%%%%%%%%%%%%%%%%%%%%%%%%%%%%%%%%
```

```
J_1tot=Kdd*J_1t;
J_2tot=Kdd*(J_2t+J_3t+J_4t+J_5t);
J_3tot=Kdd*(J_6t+J_7t+J_8t+J_9t);
J_4tot=Kdd*(J_10t+J_11t+J_12t+J_13t);
J_5tot=Kdd*(J_14t+J_15t+J_16t+J_17t);
J_6tot=Kdd*(J_18t+J_19t+J_20t+J_21t);
```

Generalized spectral density defined in a separate file (Eq. 39):

```
function [J,J_trans,J_rot] = J_gest_2 (p,w)

J=zeros;
J_trans=zeros;
J_rot=zeros;
%%%%%%%%%%%%%%%%%%%%%%%%%%%%%%%%%%%%%%%%%%%

tauR=p(1);
x=p(2);
fcd=p(3);
beta=p(4);
tau=x.*tauR;


for i=1:length(w)
 fun = @(u)u.^4.*tau./((81.+9*u.^2.-
2*u.^4.+u.^6).*(u.^4.+(tau.*w(i)).^2));
 Ji(i)=(72*(3/(4*pi)))*quadgk(fun,0,inf);
end

for i=1:length(w)
 Jcd(i)= fcd.*(sin(beta*atan(w(i).*tauR./beta)))...
          /(w(i).*(1+(w(i).*tauR./beta).^2).^(beta/2));
end

for i=1:length(w)
 J(i)=Ji(i)+Jcd(i);
end

  J_rot=Jcd;
  J_trans=Ji;
end
```

Proton relaxation function including electron spin relaxation for ^{15}N and ^{14}N, respectively:

```
function [Rtotale,Rtrans,Rrot,R0e,R1e,R2e,R3e,R0e_trans,R0e_rot]=
funkcja_relaksacji_15N_1e (p,w)


%%%%%%%%%%%%%%%%%%%%%%%%%%%%%%%%%%%%%%%%%%%%%%%%%%%%%%%%%%%%%%%%%%%%%%
tauR=p(1)*1e-10;
x=p(2);
f=p(3);
beta=p(4);
%dIS=p(5);
tau=x*tauR;
```

```
tauRe=tauR;
%tauRe=p(6);

%%%%%%%%%%%%%%%%%%%%%%%%%%%%%%%%%%%%%%%%%%%%%%%%%%%%%%%%%%%%%%%%%%%%
%%% hyperfine coupling
%%%%%%%%%%%%%%%%%%%%%%%%%%%%%%%%%%%%%%%%%%%%%%%%%%%%%%%%%%%%%%%%%%%%
Axx=22e6;
Ayy=23e6;
Azz=142e6;
A=(Axx+Ayy+Azz)/3;
A=A*2*pi;
Axx=Axx*2*pi;
Ayy=Ayy*2*pi;
Azz=Azz*2*pi;
DeltaA=Azz-(1/2)*(Axx+Ayy);
DeltaA=2/3*DeltaA*DeltaA+0.5*(Axx-Ayy).^2;
w=2*pi*w;
wS=657*w;

%%%%%%%%%%%%%%%%%%%%%%%%%%%%%%%%%%%%%%%%%%%%%%%%%%%%%%%%%%%%%%%%%%%%
%%%         physical constants
%%%%%%%%%%%%%%%%%%%%%%%%%%%%%%%%%%%%%%%%%%%%%%%%%%%%%%%%%%%%%%%%%%%%
gammaI=2.67522212e8;
gammaS=1.760859794e11;
mi0= 12.566370614e-7;
Na=6.02214199e23;
Ni=1.0;
Ni=Ni*Na;
hbar=1.054571596e-34;
dIS=p(5)*1e-10;
Kdd=(1/10)*((mi0*gammaI*gammaS*hbar/(4*pi)).^2)*(Ni/(dIS.^3));
%%%%%%%%%%%%%%%%%%%%%%%%%%%%%%%%%%%%%%%%%%%%%%%%%%%%%%%%%%%%%%%%%%%%



%%%%%%%%%%%%%%%%%%%%%%%%%%%%%%%%%%%%%%%%%%%%%%%%%%%%%%%%%%%%%%%%%%%%
%%%              eigenvectors coefficients
%%%%%%%%%%%%%%%%%%%%%%%%%%%%%%%%%%%%%%%%%%%%%%%%%%%%%%%%%%%%%%%%%%%%
c1=sqrt(0.5*(1+(wS./sqrt(A.^2+wS.^2))));
c2=sqrt(0.5*(1-(wS./sqrt(A.^2+wS.^2))));
%%%%%%%%%%%%%%%%%%%%%%%%%%%%%%%%%%%%%%%%%%%%%%%%%%%%%%%%%%%%%%%%%%%%



%%%%%%%%%%%%%%%%%%%%%%%%%%%%%%%%%%%%%%%%%%%%%%%%%%%%%%%%%%%%%%%%%%%%
%%%               transition frequencies
%%%%%%%%%%%%%%%%%%%%%%%%%%%%%%%%%%%%%%%%%%%%%%%%%%%%%%%%%%%%%%%%%%%%
w12=wS./2+A/2-0.5*sqrt(A.^2+wS.^2);
w21=-w12;
w13=wS./2+A/2+0.5*sqrt(A.^2+wS.^2);
w31=-w13;
w23=sqrt(A.^2+wS.^2);
w32=-w23;
w24=wS./2-A./2+0.5*sqrt(A.^2+wS.^2);
w42=-w24;
w34=wS./2-A./2-0.5*sqrt(A.^2+wS.^2);
w43=-w34;
w14=wS;
```

```
%%%%%%%%%%%%%%%%%%%%%%%%%%%%%%%%%%%%%%%%%%%%%%%%%%%%%%%%%%%%%%%%%%%%%%%%%%%


%%%%%%%%%%%%%%%%%%%%%%%%%%%%%%%%%%%%%%%%%%%%%%%%%%%%%%%%%%%%%%%%%%%%%%%%%%%
%%%   electron relaxation rates
%%%%%%%%%%%%%%%%%%%%%%%%%%%%%%%%%%%%%%%%%%%%%%%%%%%%%%%%%%%%%%%%%%%%%%%%%%%
R1212=(1/24)*(((c1+c2).^2+1).^2).*Jrotb(tauRe,beta,w*1e-10);
R1212=R1212+(1/8)*((c1+c2).^2).*Jrotb(tauRe,beta,w12);
R1212=R1212+(1/16)*((c1-c2).^2).*Jrotb(tauRe,beta,w13);
R1212=R1212+(1/4)*Jrotb(tauRe,beta,w14);
R1212=R1212+(1/24)*((c1.^2-c2.^2).^2).*Jrotb(tauRe,beta,w23);
R1212=R1212+(1/16)*((c1+c2).^2).*Jrotb(tauRe,beta,w24);
R1212=R1212*DeltaA;

R1313=(1/24)*(((c1-c2).^2+1).^2).*Jrotb(tauRe,beta,w*1e-10);
R1313=R1313+(1/8)*((c1-c2).^2).*Jrotb(tauRe,beta,w13);
R1313=R1313+(1/16)*((c1+c2).^2).*Jrotb(tauRe,beta,w12);
R1313=R1313+(1/4)*Jrotb(tauRe,beta,w14);
R1313=R1313+(1/24)*((c1.^2-c2.^2).^2).*Jrotb(tauRe,beta,w23);
R1313=R1313+(1/16)*((c1-c2).^2).*Jrotb(tauRe,beta,w34);
R1313=R1313*DeltaA;

R2424=(1/24)*(((c1+c2).^2+1).^2).*Jrotb(tauRe,beta,w*1e-10);
R2424=R2424+(1/8)*((c1+c2).^2).*Jrotb(tauRe,beta,w24);
R2424=R2424+(1/16)*((c1+c2).^2).*Jrotb(tauRe,beta,w12);
R2424=R2424+(1/4)*Jrotb(tauRe,beta,w14);
R2424=R2424+(1/24)*((c1.^2+c2.^2).^2).*Jrotb(tauRe,beta,w23);
R2424=R2424+(1/16)*((c1-c2).^2).*Jrotb(tauRe,beta,w34);
R2424=R2424*DeltaA;

R3434=(1/24)*(((c1-c2).^2+1).^2).*Jrotb(tauRe,beta,w*1e-10);
R3434=R3434+(1/8)*((c1-c2).^2).*Jrotb(tauRe,beta,w34);
R3434=R3434+(1/16)*((c1-c2).^2).*Jrotb(tauRe,beta,w13);
R3434=R3434+(1/4)*Jrotb(tauRe,beta,w14);
R3434=R3434+(1/24)*((c1.^2-c2.^2).^2).*Jrotb(tauRe,beta,w23);
R3434=R3434+(1/16)*((c1+c2).^2).*Jrotb(tauRe,beta,w24);
R3434=R3434*DeltaA;

R2323=(1/24)*(((c1+c2).^2+(c1-c2).^2).^2).*Jrotb(tauRe,beta,w*1e-
10);
R2323=R2323+(1/16)*((c1+c2).^2).*Jrotb(tauRe,beta,w24);
R2323=R2323+(1/16)*((c1+c2).^2).*Jrotb(tauRe,beta,w12);
R2323=R2323+(1/16)*((c1-c2).^2).*Jrotb(tauRe,beta,w13);
R2323=R2323+(1/12)*((c1.^2-c2.^2).^2).*Jrotb(tauRe,beta,w23);
R2323=R2323+(1/16)*((c1-c2).^2).*Jrotb(tauRe,beta,w34);

R1122=DeltaA*(1/8)*((c1+c2).^2).*Jrotb(tauRe,beta,w12);
R1133=DeltaA*(1/8)*((c1-c2).^2).*Jrotb(tauRe,beta,w13);
R1144=DeltaA*(1/2)*Jrotb(tauRe,beta,w14);
R2233=DeltaA*(1/12)*((c1.^2-c2.^2).^2).*Jrotb(tauRe,beta,w23);
R2244=DeltaA*(1/8)*((c1+c2).^2).*Jrotb(tauRe,beta,w24);
R3344=DeltaA*(1/8)*((c1-c2).^2).*Jrotb(tauRe,beta,w34);
R1111=-R1122-R1133-R1144;
R2222=-R1122-R2233-R2244;
R3333=-R1133-R2233-R3344;
R4444=-R1144-R2244-R3344;
```

```
%%%%%%%%%%%%%%%%%%%%%%%%%%%%%%%%%%%%%%%%%%%%%%%%%%%%%%%%%%%%%%%%%%%%%
%%%        spectral densities
%%%%%%%%%%%%%%%%%%%%%%%%%%%%%%%%%%%%%%%%%%%%%%%%%%%%%%%%%%%%%%%%%%%%%
R0e=3*J_gwI(p,w);
R0e=R0e+3*(1+(c1.^2-c2.^2).^2).*Jrotb(tauR,beta,w)*f*(pi*20/3);
R0e=(0.5)*R0e*Kdd;
R0e_trans=(0.5)*Kdd*3*J_gwI(p,w);
R0e_rot=(0.5)*Kdd.*3*(1+(c1.^2-
c2.^2).^2).*Jrotb(tauR,beta,w)*f*(pi*20/3);

R1e=12*(c1.^2).*(c2.^2).*(Jtranse(tau,w23,R2323)+f*Jrotb(tauR,beta,w
23)*(pi*20/3));
R1e=(0.5)*Kdd*R1e;
R1e_trans=(0.5)*Kdd*12*(c1.^2).*(c2.^2).*(Jtranse(tau,w23,R2323));
R1e_rot=(0.5)*Kdd.*12*(c1.^2).*(c2.^2).*f.*Jrotb(tauR,beta,w23)*(pi*
20/3);


R2e=6*(c1.^2).*(Jtranse(tau,w13+w,R1313)+f*Jrotb(tauR,beta,w13+w)*(p
i*20/3));
R2e=R2e+6*(c1.^2).*(Jtranse(tau,w24+w,R2424)+f*Jrotb(tauR,beta,w24+w
)*(pi*20/3));
R2e=R2e+6*(c2.^2).*(Jtranse(tau,w12+w,R1212)+f*Jrotb(tauR,beta,w12+w
)*(pi*20/3));
R2e=R2e+6*(c2.^2).*(Jtranse(tau,w34+w,R3434)+f*Jrotb(tauR,beta,w34+w
)*(pi*20/3));
R2e=(0.5)*Kdd*R2e;

R2e_trans=6*(c1.^2).*(Jtranse(tau,w13+w,R1313));
R2e_trans=R2e_trans+6*(c1.^2).*(Jtranse(tau,w24+w,R2424));
R2e_trans=R2e_trans+6*(c2.^2).*(Jtranse(tau,w12+w,R1212));
R2e_trans=R2e_trans+6*(c2.^2).*(Jtranse(tau,w34+w,R3434));
R2e_trans=(0.5)*Kdd*R2e_trans;

R2e_rot=6*(c1.^2).*(f*Jrotb(tauR,beta,w13+w)*(pi*20/3));
R2e_rot=R2e_rot+6*(c1.^2).*(f*Jrotb(tauR,beta,w24+w)*(pi*20/3));
R2e_rot=R2e_rot+6*(c2.^2).*(f*Jrotb(tauR,beta,w12+w)*(pi*20/3));
R2e_rot=R2e_rot+6*(c2.^2).*(f*Jrotb(tauR,beta,w34+w)*(pi*20/3));
R2e_rot=(0.5)*Kdd*R2e_rot;



R3e=(c1.^2).*(Jtranse(tau,w13-w,R1313)+f*Jrotb(tauR,beta,w13-
w)*(pi*20/3));
R3e=R3e+(c1.^2).*(Jtranse(tau,w24-w,R2424)+f*Jrotb(tauR,beta,w24-
w)*(pi*20/3));
R3e=R3e+(c2.^2).*(Jtranse(tau,w12-w,R1212)+f*Jrotb(tauR,beta,w12-
w)*(pi*20/3));
R3e=R3e+(c2.^2).*(Jtranse(tau,w34-w,R3434)+f*Jrotb(tauR,beta,w34-
w)*(pi*20/3));
R3e=(0.5)*R3e*Kdd;

R3e_trans=(c1.^2).*(Jtranse(tau,w13-w,R1313));
R3e_trans=R3e_trans+(c1.^2).*(Jtranse(tau,w24-w,R2424));
R3e_trans=R3e_trans+(c2.^2).*(Jtranse(tau,w12-w,R1212));
R3e_trans=R3e_trans+(c2.^2).*(Jtranse(tau,w34-w,R3434));
R3e_trans=(0.5)*R3e_trans*Kdd;
```

```
R3e_rot=(c1.^2).*(f*Jrotb(tauR,beta,w13-w)*(pi*20/3));
R3e_rot=R3e_rot+(c1.^2).*(f*Jrotb(tauR,beta,w24-w)*(pi*20/3));
R3e_rot=R3e_rot+(c2.^2).*(f*Jrotb(tauR,beta,w12-w)*(pi*20/3));
R3e_rot=R3e_rot+(c2.^2).*(f*Jrotb(tauR,beta,w34-w)*(pi*20/3));
R3e_rot=(0.5)*R3e_rot*Kdd;

Rtotale=R0e+R1e+R2e+R3e;
Rtrans=R0e_trans+R1e_trans+R2e_trans+R3e_trans;
Rrot=R0e_rot+R1e_rot+R2e_rot+R3e_rot;
function [R1,R1_trans, R1_rot,R0e,R1e,R2e,R3e,R4e,R5e] =
funkcja_relaksacji_14N_1e (p,w)


%%%%%%%%%%%%%%%%%%%%%%%%%%%%%%%%%%%%%%%%%%%%%%%%%%%%%%%%%%%%%%%%%%%%
tauR=p(1);
x=p(2);
fac=p(3);
beta=p(4);
dIS=p(5)*1e-10;
tau=x*tauR;
tauRe=tauR;
%tauRe=p(9);

w=2*pi*w;
wS=657*w;

%%%%%%%%%%%%%%%%%%%%%%%%%%%%%%%%%%%%%%%%%%%%%%%%%%%%%%%%%%%%%%%%%%%%
%%% hyperfine coupling
%%%%%%%%%%%%%%%%%%%%%%%%%%%%%%%%%%%%%%%%%%%%%%%%%%%%%%%%%%%%%%%%%%%%
Axx=15.4e6;
Ayy=16.1e6;
Azz=99.5e6;
A=(Axx+Ayy+Azz)/3;
A=A*2*pi;
Axx=Axx*2*pi;
Ayy=Ayy*2*pi;
Azz=Azz*2*pi;
DeltaA=Azz-(1/2)*(Axx+Ayy);
DeltaA=2/3*DeltaA*DeltaA+0.5*(Axx-Ayy).^2;

%%%%%%%%%%%%%%%%%%%%%%%%%%%%%%%%%%%%%%%%%%%%%%%%%%%%%%%%%%%%%%%%%%%%
R1=zeros;
J_trans=zeros;
J_rot=zeros;
%%%%%%%%%%%%%%%%%%%%%%%%%%%%%%%%%%%%%%%%%%%%%%%%%%%%%%%%%%%%%%%%%%%%
%%%     constants
%%%%%%%%%%%%%%%%%%%%%%%%%%%%%%%%%%%%%%%%%%%%%%%%%%%%%%%%%%%%%%%%%%%%
gammaI=2.67522212e8;
gammaS=1.760859794e11;
mi0= 12.566370614e-7;
Na=6.02214199e23;
Ni=1.0;
Ni=Ni*Na;
hbar=1.054571596e-34;
Kdd=(1/10)*((mi0*gammaI*gammaS*hbar/(4*pi)).^2)*(Ni/(dIS.^3));

%%%%%%%%%%%%%%%%%%%%%%%%%%%%%%%%%%%%%%%%%%%%%%%%%%%%%%%%%%%%%%%%%%%%
```

```
%%%%%%%%%%%%%%%%%%%%%%%%%%%%%%%%%%%%%%%%%%%%%%%%%%%%%%%%%%%%%%%%%%%%
%%%                      alpha, beta etc..
%%%%%%%%%%%%%%%%%%%%%%%%%%%%%%%%%%%%%%%%%%%%%%%%%%%%%%%%%%%%%%%%%%%%
alpha=(A+2*wS+sqrt(9*A.^2+4*A*wS+4*wS.^2))./(2*sqrt(2)*A);
betab=(A+2*wS-sqrt(9*A.^2+4*A*wS+4*wS.^2))./(2*sqrt(2)*A);
gamma=(A-2*wS-sqrt(9*A.^2-4*A*wS+4*wS.^2))./(2*sqrt(2)*A);
delta=(A-2*wS+sqrt(9*A.^2-4*A*wS+4*wS.^2))./(2*sqrt(2)*A);
%%%%%%%%%%%%%%%%%%%%%%%%%%%%%%%%%%%%%%%%%%%%%%%%%%%%%%%%%%%%%%%%%%%%

%%%%%%%%%%%%%%%%%%%%%%%%%%%%%%%%%%%%%%%%%%%%%%%%%%%%%%%%%%%%%%%%%%%%
%%%                   normalized factors
%%%%%%%%%%%%%%%%%%%%%%%%%%%%%%%%%%%%%%%%%%%%%%%%%%%%%%%%%%%%%%%%%%%%
la=sqrt(1+betab.*betab);
lb=sqrt(1+betab.*betab);
lc=sqrt(1+alpha.*alpha);
ld=sqrt(1+alpha.*alpha);
le=sqrt(1+delta.*delta);
lf=sqrt(1+delta.*delta);
lg=sqrt(1+gamma.*gamma);
lh=sqrt(1+gamma.*gamma);
%%%%%%%%%%%%%%%%%%%%%%%%%%%%%%%%%%%%%%%%%%%%%%%%%%%%%%%%%%%%%%%%%%%%



%%%%%%%%%%%%%%%%%%%%%%%%%%%%%%%%%%%%%%%%%%%%%%%%%%%%%%%%%%%%%%%%%%%%
%%%                         factors
%%%%%%%%%%%%%%%%%%%%%%%%%%%%%%%%%%%%%%%%%%%%%%%%%%%%%%%%%%%%%%%%%%%%
a=la.^(-1);
b=betab./lb;
c=lc.^(-1);
d=alpha./ld;
e=le.^(-1);
f=delta./lf;
g=lg.^(-1);
h=gamma./lh;
%%%%%%%%%%%%%%%%%%%%%%%%%%%%%%%%%%%%%%%%%%%%%%%%%%%%%%%%%%%%%%%%%%%%

%%%%%%%%%%%%%%%%%%%%%%%%%%%%%%%%%%%%%%%%%%%%%%%%%%%%%%%%%%%%%%%%%%%%
%%%              frequencies
%%%%%%%%%%%%%%%%%%%%%%%%%%%%%%%%%%%%%%%%%%%%%%%%%%%%%%%%%%%%%%%%%%%%
E1=wS./2+A/2;
E2=0.5*sqrt(wS.^2+wS.*A+(9/4)*A^2)-A/4;
E3=-0.5*sqrt(wS.^2+wS.*A+(9/4)*A^2)-A/4;
E4=0.5*sqrt(wS.^2-wS.*A+(9/4)*A^2)-A/4;
E5=-0.5*sqrt(wS.^2-wS.*A+(9/4)*A^2)-A/4;
E6=-wS./2+A/2;
w23=sqrt(wS.^2+wS.*A+(9/4)*A^2);
w45=sqrt(wS.^2-wS.*A+(9/4)*A^2);
w12=wS./2+3*A/4-(0.5)*sqrt(wS.^2+wS.*A+(9/4)*A^2);
w13=wS./2+3*A/4+0.5*sqrt(wS.^2+wS.*A+(9/4)*A^2);
w46=wS./2-3*A/4+0.5*sqrt(wS.^2-wS.*A+(9/4)*A^2);
w56=wS./2-3*A/4-0.5*sqrt(wS.^2-wS.*A+(9/4)*A^2);
w24=0.5*sqrt(wS.^2+wS.*A+(9/4)*A^2)-0.5*sqrt(wS.^2-wS.*A+(9/4)*A^2);
w25=0.5*sqrt(wS.^2+wS.*A+(9/4)*A^2)+0.5*sqrt(wS.^2-wS.*A+(9/4)*A^2);
w34=-w25;
w35=-w24;
w14=wS./2+3*A/4-0.5*sqrt(wS.^2-wS.*A+(9/4)*A^2);
w15=wS./2+3*A/4+0.5*sqrt(wS.^2-wS.*A+(9/4)*A^2);
```

```
w26=E2-E6;
w36=E3-E6;
%%%%%%%%%%%%%%%%%%%%%%%%%%%%%%%%%%%%%%%%%%%%%%%%%%%%%%%%%%%%%%%%%%%%


%%%%%%%%%%%%%%%%%%%%%%%%%%%%%%%%%%%%%%%%%%%%%%%%%%%%%%%%%%%%%%%%%%%%
%%% electron relaxation rates
%%%%%%%%%%%%%%%%%%%%%%%%%%%%%%%%%%%%%%%%%%%%%%%%%%%%%%%%%%%%%%%%%%%%
R1212=(1/6)*((1+b.*(b+a.*sqrt(2))).^2).*Jrotb(tauRe,beta,w*1e-10);
R1212=R1212+(1/4)*(a+b*sqrt(2)).^2.*Jrotb(tauRe,beta,w12);
R1212=R1212+(1/8)*(c+d*sqrt(2)).^2.*Jrotb(tauRe,beta,w13);
R1212=R1212+(1/2)*f.^2.*Jrotb(tauRe,beta,w14);
R1212=R1212+(1/2)*h.^2.*Jrotb(tauRe,beta,w15);
R1212=R1212+(1/12)*((a.*d+b.*c+b.*d.*sqrt(2)).^2).*Jrotb(tauRe,beta,
w23);
R1212=R1212+(1/8)*(b.*f-a.*e).^2.*Jrotb(tauRe,beta,w24);
R1212=R1212+(1/8)*(b.*h-a.*g).^2.*Jrotb(tauRe,beta,w25);
R1212=R1212+(1/2)*a.^2.*Jrotb(tauRe,beta,w26);
R1212=R1212*DeltaA;


R1313=(1/6)*(1+d.*(d+c.*sqrt(2))).^2.*Jrotb(tauRe,beta,w*1e-10);
R1313=R1313+(1/8)*(a+b.*sqrt(2)).^2.*Jrotb(tauRe,beta,w12);
R1313=R1313+(1/4)*(c+d.*sqrt(2)).^2.*Jrotb(tauRe,beta,w13);
R1313=R1313+(1/2)*f.^2.*Jrotb(tauR,beta,w14);
R1313=R1313+(1/2)*h.^2.*Jrotb(tauR,beta,w15);
R1313=R1313+(1/12)*(a.*d+b.*c+b.*d.*sqrt(2)).^2.*Jrotb(tauRe,beta,w2
3);
R1313=R1313+(1/8)*(d.*f-c.*e).^2.*Jrotb(tauRe,beta,w34);
R1313=R1313+(1/8)*(d.*h-c.*g).^2.*Jrotb(tauRe,beta,w35);
R1313=R1313+(1/2)*c.^2.*Jrotb(tauRe,beta,w36);
R1313=R1313*DeltaA;

R2323=(1/6)*(b.*(b+a*sqrt(2))-
d.*(d+c*sqrt(2))).^2.*Jrotb(tauRe,beta,w*1e-10);
R2323=R2323+(1/8)*(a+b.*sqrt(2)).^2.*Jrotb(tauRe,beta,w12);
R2323=R2323+(1/6)*(a.*d+b.*c+b.*d.*sqrt(2)).^2.*Jrotb(tauRe,beta,w23
);
R2323=R2323+(1/8)*(b.*f-a.*e).^2.*Jrotb(tauR,beta,w24);
R2323=R2323+(1/8)*(b.*h-a.*g).^2.*Jrotb(tauR,beta,w25);
R2323=R2323+(1/2)*a.^2.*Jrotb(tauRe,beta,w26);
R2323=R2323+(1/8)*(c+d.*sqrt(2)).*Jrotb(tauR,beta,w13);
R2323=R2323+(1/8)*(d.*f-c.*e).^2.*Jrotb(tauR,beta,w34);
R2323=R2323+(1/8)*(d.*h-c.*g).^2.*Jrotb(tauR,beta,w35);
R2323=R2323+(1/2)*c.^2.*Jrotb(tauR,beta,w36);
R2323=R2323*DeltaA;

R2424=(1/6)*(b.*(b+a*sqrt(2))-
e.*(e+f.*sqrt(2))).^2.*Jrotb(tauRe,beta,w*1e-10);
R2424=R2424+(1/8)*(a+b.*sqrt(2)).^2.*Jrotb(tauRe,beta,w12);
R2424=R2424+(1/6)*(a.*d+b.*c+b.*d.*sqrt(2)).^2.*Jrotb(tauRe,beta,w23
);
R2424=R2424+(1/4)*(b.*f-a.*e).^2.*Jrotb(tauRe,beta,w24);
R2424=R2424+(1/8)*(b.*h-a.*g).^2.*Jrotb(tauRe,beta,w25);
R2424=R2424+(1/2)*a.^2.*Jrotb(tauRe,beta,w26);
R2424=R2424+(1/2)*f.^2.*Jrotb(tauRe,beta,w14);
R2424=R2424+(1/8)*(d.*f-c.*e).*Jrotb(tauRe,beta,w34);
```

```
R2424=R2424+(1/12)*(e.*h+f.*g+e.*g.*sqrt(2)).^2.*Jrotb(tauR,beta,w45
);
R2424=R2424+(1/8)*(f+e.*sqrt(2)).^2.*Jrotb(tauRe,beta,w46);
R2424=R2424*DeltaA;

R2525=(1/6)*(b.*(b+a.*sqrt(2))-
g.*(g+h.*sqrt(2))).^2.*Jrotb(tauRe,beta,w*1e-10);
R2525=R2525+(1/8)*(a+b.*sqrt(2)).^2.*Jrotb(tauRe,beta,w12);
R2525=R2525+(1/12)*(a.*d+b.*c+b.*d.*sqrt(2)).^2.*Jrotb(tauRe,beta,w2
3);
R2525=R2525+(1/8)*(b.*f-a.*e).^2.*Jrotb(tauRe,beta,w24);
R2525=R2525+(1/4)*(b.*h-a.*g).^2.*Jrotb(tauRe,beta,w25);
R2525=R2525+(1/2)*a.^2.*Jrotb(tauRe,beta,w26);
R2525=R2525+(1/2)*h.^2.*Jrotb(tauRe,beta,w15);
R2525=R2525+(1/8)*(d.*h-c.*g).^2.*Jrotb(tauRe,beta,w35);
R2525=R2525+(1/12)*(e.*h+f.*g+e.*g.*sqrt(2)).*Jrotb(tauRe,beta,w45);
R2525=R2525+(1/8)*(h+g.*sqrt(2)).*Jrotb(tauRe,beta,w56);
R2525=R2525*DeltaA;


R3434=(1/6)*(d.*(d+c.*sqrt(2))-
e.*(e+f.*sqrt(2))).^2.*Jrotb(tauRe,beta,w*1e-10);
R3434=R3434+(1/8)*(c+d.*sqrt(2)).^2.*Jrotb(tauRe,beta,w13);
R3434=R3434+(1/12)*(a.*d+b.*c+b.*d*sqrt(2)).^2.*Jrotb(tauRe,beta,w23
);
R3434=R3434+(1/4)*(d.*f-c.*e).^2.*Jrotb(tauRe,beta,w34);
R3434=R3434+(1/8)*(d.*h-c.*g).^2.*Jrotb(tauRe,beta,w35);
R3434=R3434+(1/2)*c.^2.*Jrotb(tauRe,beta,w36);
R3434=R3434+(1/2)*f.^2.*Jrotb(tauRe,beta,w14);
R3434=R3434+(1/8)*(b.*f-a.*e).^2.*Jrotb(tauRe,beta,w24);
R3434=R3434+(1/12)*(e.*h+f.*g+e.*g.*sqrt(2)).^2.*Jrotb(tauRe,beta,w4
5);
R3434=R3434+(1/8)*(c+d.*sqrt(2)).^2.*Jrotb(tauRe,beta,w46);
R3434=R3434*DeltaA;


R3535=(1/6)*(d.*(d+c.*sqrt(2))-
g.*(g+f.*sqrt(2))).^2.*Jrotb(tauRe,beta,w*1e-10);
R3535=R3535+(1/8)*(c+d.*sqrt(2)).*Jrotb(tauRe,beta,w13);
R3535=R3535+(1/12)*(a.*d+b.*c+b.*d.*sqrt(2)).^2.*Jrotb(tauRe,beta,w2
3);
R3535=R3535+(1/8)*(d.*f-c.*e).^2.*Jrotb(tauRe,beta,w34);
R3535=R3535+(1/4)*(d.*h-c.*g).^2.*Jrotb(tauRe,beta,w35);
R3535=R3535+(1/2)*c.^2.*Jrotb(tauRe,beta,w36);
R3535=R3535+(1/2)*h.^2.*Jrotb(tauRe,beta,w15);
R3535=R3535+(1/8)*(b.*h-a.*g).^2.*Jrotb(tauRe,beta,w25);
R3535=R3535+(1/12)*(e.*h+f.*g+e.*g.*sqrt(2)).*Jrotb(tauRe,beta,w45);
R3535=R3535+(1/8)*(h+g.*sqrt(2)).^2.*Jrotb(tauRe,beta,w56);
R3535=R3535*DeltaA;


R4545=(1/6)*(e.*(e+f.*sqrt(2))-
g.*(g+h.*sqrt(2))).^2.*Jrotb(tauRe,beta,w*1e-10);
R4545=R4545+(1/2)*f.^2.*Jrotb(tauRe,beta,w14);
R4545=R4545+(1/6)*(e.*h+f.*g+e.*g.*sqrt(2)).^2.*Jrotb(tauRe,beta,w45
);
R4545=R4545+(1/8)*(b.*f-a.*e).^2.*Jrotb(tauRe,beta,w24);
R4545=R4545+(1/8)*(d.*f-c.*e).^2.*Jrotb(tauRe,beta,w34);
```

```
R4545=R4545+(1/8)*(f+e.*sqrt(2)).^2.*Jrotb(tauRe,beta,w46);
R4545=R4545+(1/2)*h.^2.*Jrotb(tauRe,beta,w15);
R4545=R4545+(1/8)*(b.*h-a.*g).^2.*Jrotb(tauRe,beta,w25);
R4545=R4545+(1/8)*(d.*h-c.*g).^2.*Jrotb(tauRe,beta,w35);
R4545=R4545+(1/2)*(h+g.*sqrt(2)).*Jrotb(tauRe,beta,w56);
R4545=R4545*DeltaA;


R4646=(1/6)*(1+e.*(e+f.*sqrt(2))).^2.*Jrotb(tauRe,beta,w*1e-10);
R4646=R4646+(1/2)*f.^2.*Jrotb(tauRe,beta,w14);
R4646=R4646+(1/8)*(b.*f-a.*e).^2.*Jrotb(tauRe,beta,w24);
R4646=R4646+(1/8)*(d.*f-c.*e).^2.*Jrotb(tauRe,beta,w34);
R4646=R4646+(1/12)*(e.*h+f.*g+e.*g.*sqrt(2)).^2.*Jrotb(tauRe,beta,w4
5);
R4646=R4646+(1/4)*(f+e.*sqrt(2)).*Jrotb(tauRe,beta,w46);
R4646=R4646+(1/2)*a.^2.*Jrotb(tauRe,beta,w26);
R4646=R4646+(1/2)*c.^2.*Jrotb(tauRe,beta,w36);
R4646=R4646+(1/8)*(h+g.*sqrt(2)).^2.*Jrotb(tauRe,beta,w56);
R4646=R4646*DeltaA;

R5656=(1/6)*(1+g.*(g+h.*sqrt(2))).^2.*Jrotb(tauRe,beta,w*1e-10);
R5656=R5656+(1/2)*h.^2.*Jrotb(tauRe,beta,w15);
R5656=R5656+(1/8)*(b.*h-a.*g).^2.*Jrotb(tauRe,beta,w25);
R5656=R5656+(1/8)*(d.*h-c.*g).^2.*Jrotb(tauRe,beta,w35);
R5656=R5656+(1/12)*(e.*h+f.*g+e.*g.*sqrt(2)).*Jrotb(tauRe,beta,w45);
R5656=R5656+(1/4)*(h+g.*sqrt(2)).^2.*Jrotb(tauRe,beta,w56);
R5656=R5656+(1/2)*a.^2.*Jrotb(tauRe,beta,w26);
R5656=R5656+(1/2)*c.^2.*Jrotb(tauRe,beta,w36);
R5656=R5656+(1/8)*(f+e.*sqrt(2)).*Jrotb(tauRe,beta,w46);
R5656=R5656*DeltaA;

%%%%%%%%%%%%%%%%%%%%%%%%%%%%%%%%%%%%%%%%%%%%%%%%%%%%%%%%%%%%%%%%%

R0e=J_gwI14(p,w);
R0e=R0e+(1+0.5*(a.^2-b.^2).^2+0.5*(c.^2-d.^2).^2+0.5*(e.^2-
f.^2).^2+0.5*(g.^2-h.^2).^2).*Jrotb(tauR,beta,w)*fac*(pi*20/3);
R0e=R0e*Kdd;

R0e_trans=J_gwI14(p,w);
R0e_trans=R0e_trans*Kdd;

R0e_rot=(1+0.5*(a.^2-b.^2).^2+0.5*(c.^2-d.^2).^2+0.5*(e.^2-
f.^2).^2+0.5*(g.^2-h.^2).^2).*Jrotb(tauR,beta,w)*fac*(pi*20/3);
R0e_rot=R0e_rot*Kdd;

R1e=((a.*c-
b.*d).^2/2).*(Jtranse(tau,w23+w,R2323)+Jrotb(tauR,beta,w23)*fac*(pi*
20/3));
R1e=R1e+((a.*c-b.*d).^2/2).*(Jtranse(tau,w23-
w,R2323)+Jrotb(tauR,beta,w23)*fac*(pi*20/3));
R1e=R1e+((e.*g-
f.*h).^2/2).*(Jtranse(tau,w45+w,R4545)+Jrotb(tauR,beta,w45)*fac*(pi*
20/3));
R1e=R1e+((e.*g-f.*h).^2/2).*(Jtranse(tau,w45-
w,R4545)+Jrotb(tauR,beta,w45)*fac*(pi*20/3));
R1e=R1e*Kdd;

R1e_trans=((a.*c-b.*d).^2/2).*(Jtranse(tau,w23+w,R2323));
```

```
R1e_trans=R1e_trans+((a.*c-b.*d).^2/2).*(Jtranse(tau,w23-w,R2323));
R1e_trans=R1e_trans+((e.*g-f.*h).^2/2).*(Jtranse(tau,w45+w,R4545));
R1e_trans=R1e_trans+((e.*g-f.*h).^2/2).*(Jtranse(tau,w45-w,R4545));
R1e_trans=R1e_trans*Kdd;

R1e_rot=((a.*c-b.*d).^2/2).*(Jrotb(tauR,beta,w23)*fac*(pi*20/3));
R1e_rot=R1e_rot+((a.*c-
b.*d).^2/2).*(Jrotb(tauR,beta,w23)*fac*(pi*20/3));
R1e_rot=R1e_rot+((e.*g-
f.*h).^2/2).*(Jrotb(tauR,beta,w45)*fac*(pi*20/3));
R1e_rot=R1e_rot+((e.*g-
f.*h).^2/2).*(Jrotb(tauR,beta,w45)*fac*(pi*20/3));
R1e_rot=R1e_rot*Kdd;

R2e=2*(b.^2).*(Jtranse(tau,w12+w,R1212)+Jrotb(tauR,beta,w12)*fac*(pi
*20/3));
R2e=R2e+(1/3)*(b.^2).*(Jtranse(tau,w12-
w,R1212)+Jrotb(tauR,beta,w12)*fac*(pi*20/3));
R2e=R2e+2*(d.^2).*(Jtranse(tau,w13+w,R1313)+Jrotb(tauR,beta,w13)*fac
*(pi*20/3));
R2e=R2e+(1/3)*(d.^2).*(Jtranse(tau,w13-
w,R1313)+Jrotb(tauR,beta,w13)*fac*(pi*20/3));
R2e=R2e*Kdd;

R2e_rot=2*(b.^2).*(Jrotb(tauR,beta,w12)*fac*(pi*20/3));
R2e_rot=R2e_rot+(1/3)*(b.^2).*(Jrotb(tauR,beta,w12)*fac*(pi*20/3));
R2e_rot=R2e_rot+2*(d.^2).*(Jrotb(tauR,beta,w13)*fac*(pi*20/3));
R2e_rot=R2e_rot+(1/3)*(d.^2).*(Jrotb(tauR,beta,w13)*fac*(pi*20/3));
R2e_rot=R2e_rot*Kdd;

R2e_trans=2*(b.^2).*(Jtranse(tau,w12+w,R1212));
R2e_trans=R2e_trans+(1/3)*(b.^2).*(Jtranse(tau,w12-w,R1212));
R2e_trans=R2e_trans+2*(d.^2).*(Jtranse(tau,w13+w,R1313));
R2e_trans=R2e_trans+(1/3)*(d.^2).*(Jtranse(tau,w13-w,R1313));
R2e_trans=R2e_trans*Kdd;

R3e=2*(e.^2).*(Jtranse(tau,w46+w,R4646)+Jrotb(tauR,beta,w46)*fac*(pi
*20/3));
R3e=R3e+(1/3)*(e.^2).*(Jtranse(tau,w46-
w,R4646)+Jrotb(tauR,beta,w46)*fac*(pi*20/3));
R3e=R3e+2*(g.^2).*(Jtranse(tau,w56+w,R5656)+Jrotb(tauR,beta,w56)*fac
*(pi*20/3));
R3e=R3e+(1/3)*(g.^2).*(Jtranse(tau,w56-
w,R5656)+Jrotb(tauR,beta,w56)*fac*(pi*20/3));
R3e=R3e*Kdd;

R3e_trans=2*(e.^2).*(Jtranse(tau,w46+w,R4646));
R3e_trans=R3e_trans+(1/3)*(e.^2).*(Jtranse(tau,w46-w,R4646));
R3e_trans=R3e_trans+2*(g.^2).*(Jtranse(tau,w56+w,R5656));
R3e_trans=R3e_trans+(1/3)*(g.^2).*(Jtranse(tau,w56-w,R5656));
R3e_trans=R3e_trans*Kdd;

R3e_rot=2*(e.^2).*(Jrotb(tauR,beta,w46)*fac*(pi*20/3));
R3e_rot=R3e_rot+(1/3)*(e.^2).*(Jrotb(tauR,beta,w46)*fac*(pi*20/3));
R3e_rot=R3e_rot+2*(g.^2).*(Jrotb(tauR,beta,w56)*fac*(pi*20/3));
R3e_rot=R3e_rot+(1/3)*(g.^2).*(Jrotb(tauR,beta,w56)*fac*(pi*20/3));
R3e_rot=R3e_rot*Kdd;
```

```
R4e=2*((a.*f).^2).*(Jtranse(tau,w24+w,R2424)+Jrotb(tauR,beta,w24)*fac*(pi*20/3));
R4e=R4e+(1/3)*((a.*f).^2).*(Jtranse(tau,w24-w,R2424)+Jrotb(tauR,beta,w24)*fac*(pi*20/3));
R4e=R4e+2*((a.*h).^2).*(Jtranse(tau,w25+w,R2525)+Jrotb(tauR,beta,w25)*fac*(pi*20/3));
R4e=R4e+(1/3)*((a.*h).^2).*(Jtranse(tau,w25-w,R2525)+Jrotb(tauR,beta,w25)*fac*(pi*20/3));
R4e=R4e*Kdd;

R4e_trans=2*((a.*f).^2).*(Jtranse(tau,w24+w,R2424));
R4e_trans=R4e_trans+(1/3)*((a.*f).^2).*(Jtranse(tau,w24-w,R2424));
R4e_trans=R4e_trans+2*((a.*h).^2).*(Jtranse(tau,w25+w,R2525));
R4e_trans=R4e_trans+(1/3)*((a.*h).^2).*(Jtranse(tau,w25-w,R2525));
R4e_trans=R4e_trans*Kdd;

R4e_rot=2*((a.*f).^2).*(Jrotb(tauR,beta,w24)*fac*(pi*20/3));
R4e_rot=R4e_rot+(1/3)*((a.*f).^2).*(Jrotb(tauR,beta,w24)*fac*(pi*20/3));
R4e_rot=R4e_rot+2*((a.*h).^2).*(Jrotb(tauR,beta,w25)*fac*(pi*20/3));
R4e_rot=R4e_rot+(1/3)*((a.*h).^2).*(Jrotb(tauR,beta,w25)*fac*(pi*20/3));
R4e_rot=R4e_rot*Kdd;

R5e=2*((c.*f).^2).*(Jtranse(tau,w34+w,R3434)+Jrotb(tauR,beta,w34)*fac*(pi*20/3));
R5e=R5e+(1/3)*((c.*f).^2).*(Jtranse(tau,w34-w,R3434)+Jrotb(tauR,beta,w34)*fac*(pi*20/3));
R5e=R5e+2*((c.*h).^2).*(Jtranse(tau,w35+w,R3535)+Jrotb(tauR,beta,w35)*fac*(pi*20/3));
R5e=R5e+(1/3)*((c.*h).^2).*(Jtranse(tau,w35-w,R3535)+Jrotb(tauR,beta,w35)*fac*(pi*20/3));
R5e=R5e*Kdd;

R5e_trans=2*((c.*f).^2).*(Jtranse(tau,w34+w,R3434));
R5e_trans=R5e_trans+(1/3)*((c.*f).^2).*(Jtranse(tau,w34-w,R3434));
R5e_trans=R5e_trans+2*((c.*h).^2).*(Jtranse(tau,w35+w,R3535));
R5e_trans=R5e_trans+(1/3)*((c.*h).^2).*(Jtranse(tau,w35-w,R3535));
R5e_trans=R5e_trans*Kdd;

R5e_rot=2*((c.*f).^2).*(Jrotb(tauR,beta,w34)*fac*(pi*20/3));
R5e_rot=R5e_rot+(1/3)*((c.*f).^2).*(Jrotb(tauR,beta,w34)*fac*(pi*20/3));
R5e_rot=R5e_rot+2*((c.*h).^2).*(Jrotb(tauR,beta,w35)*fac*(pi*20/3));
R5e_rot=R5e_rot+(1/3)*((c.*h).^2).*(Jrotb(tauR,beta,w35)*fac*(pi*20/3));
R5e_rot=R5e_rot*Kdd;

R1=R0e+R1e+R2e+R3e+R4e+R5e;
R1_trans=R0e_trans+R1e_trans+R2e_trans+R3e_trans+R4e_trans+R5e_trans;
R1_rot=R0e_rot+R1e_rot+R2e_rot+R3e_rot+R4e_rot+R5e_rot;
%%%%%%%%%%%%%%%%%%%%%%%%%%%%%%%%%%%%%%%%%%%%%%%%%%%%%%%%%%%%
```

Spectral density dependent on proton Larmor frequency (Eq. 82) for ^{15}N:

```
function [calka] = J_gwI (p,w)

for i=1:length(w)
    calka(i)=quadgk(@(u)macierzodw15N(p,w(i),u),0,inf);
end

end



function [wynik,R1111,R2222,R3333,R4444] = macierzodw15N (p,w,u)

tauR=p(1)*1e-10;
x=p(2);
tau=x*tauR;
beta=p(4);

Axx=22e6;
Ayy=23e6;
Azz=142e6;
A=(Axx+Ayy+Azz)/3;
A=A*2*pi;
Axx=Axx*2*pi;
Ayy=Ayy*2*pi;
Azz=Azz*2*pi;


DeltaA=Azz-(1/2)*(Axx+Ayy);
DeltaA=2/3*DeltaA*DeltaA+0.5*(Axx-Ayy).^2;

wS=657*w;
tauRe=tauR;

c1=sqrt(0.5*(1+(wS./sqrt(A.^2+wS.^2))));
c2=sqrt(0.5*(1-(wS./sqrt(A.^2+wS.^2))));
w12=wS./2+A/2-0.5*sqrt(A.^2+wS.^2);
w21=-w12;
w13=wS./2+A/2+0.5*sqrt(A.^2+wS.^2);
w31=-w13;
w23=sqrt(A.^2+wS.^2);
w32=-w23;
w24=wS./2-A./2+0.5*sqrt(A.^2+wS.^2);
w42=-w24;
w34=wS./2-A./2-0.5*sqrt(A.^2+wS.^2);
w43=-w34;
w14=wS;
%%%%%%%%%%%%%%%%%%%%%%%%%%%%%%%%%%%%%%%%%%%%%%%%%%%%%%%%%%%%%%%%%%%%%

R1122=(1/16)*(c1+c2).^2*Jrotb(tauRe,beta,w12);
R1122=-2*R1122*DeltaA;


R1133=(1/16)*(c1-c2).^2*Jrotb(tauRe,beta,w13);
R1133=-2*R1133*DeltaA;
```

```
R1144=(1/4)*Jrotb(tauRe,beta,w14);
R1144=-2*R1144*DeltaA;

R2233=(1/24)*(c1.^2-c2.^2).^2*Jrotb(tauRe,beta,w23);
R2233=-2*R2233*DeltaA;

R2244=(1/16)*(c1+c2).^2*Jrotb(tauRe,beta,w24);
R2244=-2*R2244*DeltaA;

R3344=(1/16)*(c1-c2).^2*Jrotb(tauRe,beta,w34);
R3344=-2*R3344*DeltaA;

R1111=-R1122-R1133-R1144;
R2222=-R1122-R2233-R2244;
R3333=-R1133-R2233-R3344;
R4444=-R1144-R2244-R3344;




for k=1:length(u)

X1111(k)=(u(k).^2)./tau+R1111+w*1i;
X2222(k)=(u(k).^2)./tau+R2222+w*1i;
X3333(k)=(u(k).^2)./tau+R3333+w*1i;
X4444(k)=(u(k).^2)./tau+R4444+w*1i;

M=[X1111(k) R1122 R1133 R1144;
   R1122 X2222(k) R2233 R2244;
   R1133 R2233 X3333(k) R3344;
   R1144 R2244 R3344 X4444(k);];
Modw=inv(M);

v1=[1 c1.^2-c2.^2 c2.^2-c1.^2 -1];
v2=v1';
Mwynik(k)=(1/2)*v1*Modw*v2;
MwynikRe(k)=real(Mwynik(k));

wynik(k)=(72).*(u(k).^2./...
    (81.+9*u(k).^2.-2*u(k).^4.+u(k).^6)).*(MwynikRe(k));

end
end
```

Translational spectral density:

```
function [sum] = Jtranse(tau,w,Rxx)

J=zeros;
Ji=zeros;

for i=1:length(w)
par(i)=tau.*Rxx(i);
end
```

```
for i=1:length(w)
sum(i)=0;
end

for i=1:length(w)
umin=1.0d-4;
umax=1.0d3;
nstep=5000.0d0;
step=(umax-umin)/nstep;
u=umin;
while (u <= umax)

help1(i)=(u.^2)/(81.+9.0*u.^2-2*u.^4+u.^6);
help1(i)=help1(i)*72.0;
Jouter(i)=help1(i)*(u.*u+par(i))./((u.*u+par(i)).^2+(w(i)*tau).^2);
sum(i)=sum(i)+Jouter(i)*step*tau;
u=u+step;

end
end
end
```

Rotational spectral density:

```
function [J] = Jrotb (tauR,beta,w)
for i=1:length(w)
    Jcd(i)= (sin(beta*atan(w(i).*tauR./beta)))/...
    (w(i).*(1+(w(i).*tauR./beta).^2).^(beta/2));
end

J=(1/5)*Jcd;
end
```

Spectral density dependent on proton Larmor frequency for ^{14}N (Eq. 84):

```
function [calka] = J_gwI14 (p,w)

for i=1:length(w)
    calka(i)=quadgk(@(u)macierzodw14(p,w(i),u),0,inf);
end
end


function [wynik,R1111,R2222,R3333,R4444] = macierzodw14 (p,w,u)

tauR=p(1);
x=p(2);
tau=x*tauR;
beta=p(4);
Axx=15.4e6;
Ayy=16.1e6;
Azz=99.5e6;

A=(Axx+Ayy+Azz)/3;
A=A*2*pi;
Axx=Axx*2*pi;
```

```
Ayy=Ayy*2*pi;
Azz=Azz*2*pi;
DeltaA=Azz-(1/2)*(Axx+Ayy);
DeltaA=2/3*DeltaA*DeltaA+0.5*(Axx-Ayy).^2;

wS=657*w;
tauRe=tauR;

betab=(A+2*wS+sqrt(9*A.^2+4*A*wS+4*wS.^2))./(2*sqrt(2)*A);
alpha=(A+2*wS-sqrt(9*A.^2+4*A*wS+4*wS.^2))./(2*sqrt(2)*A);
delta=(A-2*wS-sqrt(9*A.^2-4*A*wS+4*wS.^2))./(2*sqrt(2)*A);
gamma=(A-2*wS+sqrt(9*A.^2-4*A*wS+4*wS.^2))./(2*sqrt(2)*A);


la=sqrt(1+alpha.*alpha);
lb=sqrt(1+alpha.*alpha);
lc=sqrt(1+betab.*betab);
ld=sqrt(1+betab.*betab);
le=sqrt(1+gamma.*gamma);
lf=sqrt(1+gamma.*gamma);
lg=sqrt(1+delta.*delta);
lh=sqrt(1+delta.*delta);


a=la.^(-1);
b=alpha./lb;
c=lc.^(-1);
d=betab./ld;
e=le.^(-1);
f=gamma./lf;
g=lg.^(-1);
h=delta./lh;

E1=wS./2+A/2;
E2=0.5*sqrt(wS.^2+wS.*A+(9/4)*A^2)-A/4;
E3=-0.5*sqrt(wS.^2+wS.*A+(9/4)*A^2)-A/4;
E4=0.5*sqrt(wS.^2-wS.*A+(9/4)*A^2)-A/4;
E5=-0.5*sqrt(wS.^2-wS.*A+(9/4)*A^2)-A/4;
E6=-wS./2+A/2;
w23=E2-E3;
w45=E4-E5;
w12=E1-E2;
w13=E1-E3;
w46=E4-E6;
w56=E5-E6;
w24=E2-E4;
w25=E2-E5;
w34=E3-E4;
w35=E3-E5;
w14=E1-E4;
w15=E1-E5;
w26=E2-E6;
w36=E3-E6;


R1122=(1/4)*(a+b.*sqrt(2)).^2.*Jrotb(tauRe,beta,w12);
R1122=-1*DeltaA*R1122;
```

```
R1133=(1/4)*(c+d.*sqrt(2)).^2.*Jrotb(tauRe,beta,w13);
R1133=-1*DeltaA*R1133;

R1144=f.^2.*Jrotb(tauRe,beta,w14);
R1144=-1*DeltaA*R1144;

R1155=h.^2.*Jrotb(tauRe,beta,w15);
R1155=-1*DeltaA*R1155;

for m=1:length(w)
R1166(m)=0;
End

R2233=(1/6)*(a.*d+c.*b+b.*d.*sqrt(2)).^2.*Jrotb(tauRe,beta,w23);
R2233=-1*DeltaA*R2233;

R2244=(1/4)*(b.*f-a.*e).^2.*Jrotb(tauRe,beta,w24);
R2244=-1*DeltaA*R2244;

R2255=(1/4)*(b.*h-a.*g).^2.*Jrotb(tauRe,beta,w25);
R2255=-1*DeltaA*R2255;

R2266=a.^2.*Jrotb(tauRe,beta,w26);
R2266=-1*DeltaA*R2266;

R3344=(1/4)*(d.*f-c.*e).^2.*Jrotb(tauRe,beta,w34);
R3344=-1*DeltaA*R3344;

R3355=(1/4)*(d.*h-c.*g).^2.*Jrotb(tauRe,beta,w35);
R3355=-1*DeltaA*R3355;

R3366=c.^2.*Jrotb(tauRe,beta,w36);
R3366=-1*DeltaA*R3366;

R4455=(1/6)*(e.*h+f.*g+e.*g*sqrt(2)).*Jrotb(tauRe,beta,w45);
R4455=1*DeltaA*R4455;

R4466=(1/4)*(f+e.*sqrt(2)).*Jrotb(tauRe,beta,w46);
R4466=-1*DeltaA*R4466;

R5566=(1/4)*(h+g.*sqrt(2)).*Jrotb(tauRe,beta,w56);
R5566=1*DeltaA*R5566;

R1111=-R1122-R1133-R1144-R1155-R1166;
R2222=-R1122-R2233-R2244-R2255-R2266;
R3333=-R1133-R2233-R3344-R3355-R3366;
R4444=-R1144-R2244-R3344-R4455-R4466;
R5555=-R1155-R2255-R3355-R4455-R5566;
R6666=-R1166-R2266-R3366-R4466-R5566;


for k=1:length(u)


X1111(k)=(u(k).^2)./tau+R1111+w*1i;
X2222(k)=(u(k).^2)./tau+R2222+w*1i;
X3333(k)=(u(k).^2)./tau+R3333+w*1i;
X4444(k)=(u(k).^2)./tau+R4444+w*1i;
```

```
X5555(k)=(u(k).^2)./tau+R5555+w*1i;
X6666(k)=(u(k).^2)./tau+R6666+w*1i;

M=[X1111(k) R1122 R1133 R1144 R1155 R1166;
   R1122 X2222(k) R2233 R2244 R2255 R2266;
   R1133 R2233 X3333(k) R3344 R3355 R3366;
   R1144 R2244 R3344 X4444(k) R4455 R4466;
   R1155 R2255 R3355 R4455 X5555(k) R5566;
   R1166 R2266 R3366 R4466 R5566 X6666(k);];
Modw=inv(M);


v1=[1/2 0.5*(a.^2-b.^2) 0.5*(c.^2-d.^2) 0.5*(e.^2-f.^2) 0.5*(g.^2-
h.^2) -1/2];
v2=v1';
Mwynik(k)=(2)*v1*Modw*v2;
MwynikRe(k)=real(Mwynik(k));

wynik(k)=(72).*(u(k).^2./...
    (81.+9*u(k).^2.-2*u(k).^4.+u(k).^6)).*(MwynikRe(k));
end
end
```

A.2 Error analysis

The errors of the fitted coefficients have been estimated in the following way. For a dataset of N points ($(x_i, y_i),\ i = 1,...,N$) a function, $f(x, p)$, has been fitted (p is the matrix of the fitted parameters which have been find using the method of least squares). The least square estimator (denoted here as $\hat{\beta}$) is such set of fitted parameters that minimizes the following expression [79,80]:

$$\sum_{i=1}^{N} (y_i - f(x_i, p))^2$$

(A.1)

As one of the outputs the *lsqurvefit* MATLAB function returns the Jacobian matrix. In the next step the variance of residuals is calculated [79,80]:

$$\sigma = \frac{1}{N-k} \sum_{i=1}^{N} (y_i - f(x_i, p))^2$$

(A.2)

Using its values the covariance matrix can be defined [79,80]:

$$\mathrm{cov}(p) = \sigma \left(J^T J\right)^{-1}$$

(A.3)

The pointwise square root of the covariance matrix gives the error estimates of the fitted parameters [79,80]:

$$s_p = (\mathrm{cov}(p))^{1/2}.$$

(A.4)

Values of the error estimates s_p have been used to calculate the percentage errors listed in Tables 7.1, 7.2 and 7.3. The errors, $s(D_{12})$, of the diffusion coefficient have been estimated using the equation:

$$s(D_{12}) = \sqrt{\left(\frac{\partial D_{12}}{\partial d_{IS}} s(d_{IS})\right)^2 + \left(\frac{\partial D_{12}}{\partial \tau_{trans}} s(\tau_{trans})\right)^2}$$

(A.5)

List of figures

List of tables

List of publications of the author

1. D. Kruk, A. Korpała, E. A. Rössler, K. A. Earle, W. Medycki, and J. Moscicki, ^{1}H NMR relaxation in glycerol solutions of nitroxide radicals: Effects of translational and rotational dynamics, *J. Chem. Phys.* **136**, 114504 (2012).
2. D. Kruk, A. Mielczarek, A. Korpała, A. Kozłowski, K. A. Earle, and J. Moscicki, Sensitivity of ^{2}H NMR spectroscopy to motional models: Proteins and highly viscous liquids as examples, *J. Chem. Phys.* **136**, 244509 (2012).
3. D. Kruk, A. Korpała, J. Kowalewski, E. A. Rössler, and J. Moscicki, ^{1}H relaxation dispersion in solutions of nitroxide radicals: Effects of hyperfine interactions with ^{14}N and ^{15}N nuclei. *J. Chem. Phys.* **137**, 044512 (2012).
4. D. Kruk, A. Korpała, A. Kubica, R. Meier, E. A. Rössler, and J. Moscicki, Translational diffusion in paramagnetic liquids by ^{1}H NMR relaxometry: Nitroxide radicals in solution, J. Chem. Phys. **138**, 024506 (2013).
5. D. Kruk, A. Korpała, A. Kubica, J. Kowalewski, E. A. Rössler, and J. Moscicki, ^{1}H relaxation dispersion in solutions of nitroxide radicals: Influence of electron spin relaxation, *J. Chem. Phys.* **138**, 124506 (2013).
6. D. Kruk, S. K. Hoffman, J. Goslar, S. Lijewski, A. Kubica-Misztal, A. Korpała, I. Ogłodek, J. Kowalewski, E. A. Rössler, and J. Mościcki, ESR lineshape and ^{1}H spin-lattice relaxation dispersion in propylene glycol solutions of nitroxide radicals – joint analysis, *J. Chem. Phys.* **139**, 244502 (2013).
7. D. Kruk, A. Korpała, S. Mehdizadeh Taheri, A. Kozłowski, S. Förster, and E. A. Rössler, ^{1}H relaxation enhancement induced by nanoparticles in solutions: Influence of magnetic properties and diffusion, *J. Chem. Phys.* **140**, 174504 (2014).
8. D. Kruk, R. Meier, A. Rachocki, A. Korpała, R. K. Singh, and E. A. Rössler, Determining diffusion coefficients of ionic liquids by means of field cycling nuclear magnetic resonance relaxometry, *J. Chem. Phys.* **140**, 244509 (2014).